GEOLOGICA ULTRAIECTINA

Mededelingen van de
Faculteit Geowetenschappen
Universiteit Utrecht

No. 244

Early Archaean sedimentary basins: depositional environment and hydrothermal systems

Examples from the Barberton and Coppin Gap Greenstone Belts

Sjoukje Tsjitske de Vries

Cover illustration: Black and white banded chert (Buck Ridge Chert, Barberton Greenstone Belt, South Africa) showing fractures and early diagenetic structures.

Faculty of Geosciences
Utrecht University
Budapestlaan 4
3584 CD Utrecht
The Netherlands

http://www.geo.uu.nl/

ISBN: 90-5744-104-7

Early Archaean sedimentary basins: depositional environment and hydrothermal systems

Examples from
the Barberton and Coppin Gap Greenstone Belts

Vroeg Archeïsche sedimentaire bekkens: afzettingsmilieu en hydrothermale systemen

Voorbeelden uit
de Barberton en Coppin Gap Groensteengordels

(met een samenvatting in het Nederlands)

PROEFSCHRIFT

ter verkrijging van de graad van doctor aan de Universiteit Utrecht,
op gezag van de Rector Magnificus Prof. Dr W.H. Gispen,
ingevolge het besluit van het College voor Promoties in het openbaar te
verdedigen op dinsdag 7 september 2004 des middags om 12.45 uur

door
Sjoukje Tsjitske de Vries

geboren op 31 oktober 1975 te Leeuwarden

Promotoren:

Prof. Dr P.L. de Boer
Faculteit Geowetenschappen
Universiteit Utrecht, The Netherlands

Prof. Dr M.J. de Wit
Department of Geological Sciences
University of Cape Town, South Africa

Co-promotor:

Dr W. Nijman
Faculteit Geowetenschappen
Universiteit Utrecht, The Netherlands

Members of the dissertation committee:

Dr C.E.J. de Ronde
Institute of Geological and Nuclear Sciences
Lower Hutt, New Zealand

Prof. Dr J. Smit
Faculteit der Aard- en Levenswetenschappen
Vrije Universiteit Amsterdam, The Netherlands

Prof. Dr J.L.R. Touret
Musée de Minéralogie, Ecole des Mines
Paris, France

Dr F. Westall
Centre Biophysique Moléculaire
Orléans, France

Prof. Dr G.J. van der Zwaan
Faculteit Geowetenschappen
Universiteit Utrecht, The Netherlands

Table of contents

Chapter 1

General introduction

What contribution can basin studies make to the understanding of the Early Earth?

Sedimentary basins are a well-studied topic in geology. Much is known about the settings in which they form, and the different types of basin fills. Less is known about basins early on in

Earth's history, particularly in the early Archaean (i.e. before ~3.3 Ga[1]). Were those basins similar to, or different from basins on the modern Earth?

From ca. 3.3 Ga on, sedimentary sequences such as the Fig Tree and Moodies Groups in the Barberton Greenstone Belt and the Mosquito Creek, Mallina and Lalla Rookh Basin fills in the Pilbara, are very similar to modern-day sedimentary sequences (e.g. descriptions by Eriksson, 1980a,b, 1981, 1982; Krapez and Barley, 1987; Lamb and Paris, 1988; Nocita and Lowe, 1990; Krapez, 1993; Eriksson et al., 1994; Heubeck and Lowe, 1994, 1999; Lowe and Nocita, 1999; Toulkeridis et al., 1999; Smithies et al., 1999, 2001). Older preserved sedimentary sequences are largely volcaniclastic, lack significant arkosic and quartz-arenitic clastics, and many of them are thoroughly silicified. If sedimentary deposits and basins in the early Archaean were different, they may also have been formed differently from those that formed later in Earth's history.

There is quite a number of studies on sediments older than 3.3 Ga. In the Barberton Greenstone Belt (South Africa), the silicified sediments of the Onverwacht Group, including the Middle Marker, Buck Ridge, Footbridge and Msauli Cherts were described by e.g. Lowe and Knauth (1977); Lanier and Lowe (1982); Lowe (1982, 1999a,b; Heinrichs (1984); Paris (1990); Lowe and Fisher Worrell (1999); Ransom et al. (1999); Walsh and Lowe (1999). Paris et al. (1985) focused on silicification, but also drew conclusions about the paleo-environment and early diagenesis of the Onverwacht Group cherts. In the Pilbara (Australia), silicified sediments and volcaniclastic rocks of the Warrawoona Group were described by e.g. Barley et al. (1979); Dunlop and Buick (1981); Buick and Barnes (1984); DiMarco and Lowe (1989a,b); Buick and Dunlop (1990); Barley (1993); Nijman et al. (1998a); Lowe (1983). Authors that focused on other topics than sedimentolog, also interpreted the (silicified) sedimentary sequences in terms of depth or depositional environment (e.g. Kitajima et al., 2001b). Interpretations of the depositional environment of the silicified sediments range from deep-sea to shallow water and locally even subaerial, sometimes for the same unit. In particular, there are controversies about the interpretation of highly silicified units. Detailed sedimentological studies of such silicified sedimentary units are therefore necessary.

So far, most studies of early Archaean deposits have focused on one or two aspects of the rock succession, such as the depositional environment, geochemistry, structural geology, fluid inclusions and the possible development of early life. The different studies were carried out in similar, but often temporally and/or geographically different (parts of) greenstone belts, which makes them more

[1] The terms early, mid and late Archaean are not always applied consistently throughout the literature. There is especially inconsistency in the use of early and mid Archaean. In this study, the terms early, mid and late Archaean are used for the time periods from 3.8-3.3, 3.3-2.7 and 2.7-2.5 Ga respectively.

difficult to combine or compare. As a result, there is only limited insight into the geometry and setting of early Archaean basins.

This study aims at getting better insight into the geometry of early Archaean basins and their relation to syndepositional deformation. Syndepositional extensional deformation has been suggested e.g. for the Coongan Greenstone Belt (Pilbara, Australia) by Zegers et al. (1996), for the North Pole Dome (Pilbara) by Nijman et al. (1998a) and for the Barberton Greenstone Belt (South Africa) by De Vries (1999). This study investigates the extent of this extensional structural control. Furthermore, it aims at getting better insight into the sedimentological and diagenetic processes in the early Archaean sedimentary basins, as well as into the location of hydrothermal systems within those basins. The hydrothermal systems and their effect on the sediments and the temperature distribution in the basins are particularly important in relation to the development of early life.

To achieve these aims, a multidisciplinary approach was chosen for this study (see Method), with emphasis on linking information from different disciplines, applied to the same area. Large-scale mapping, integrating sedimentary, structural and volcanic data was combined with detailed (10-100 metre-scale) mapping, sedimentary logging, geochemistry, and geochronology.

Ultimately, such an integrated study leads to conclusions about scale, shape and setting of the basins, and the conclusions may also contribute to discussions about for example plate tectonics and (crustal) lithosphere development on the early Earth. The shape and fill of sedimentary basins may, for instance, give information about the tectonic regime under which they were formed. The nature of the tectonic regime is still controversial for much of the Archaean (see e.g. De Wit, 1998; Hamilton, 1998; Hofmann et al., 2001; Van Kranendonk et al., 2002 and references therein).

Selection of the areas

Surface exposures of early Archaean (i.e. > 3.3 Ga) rocks on Earth are only known from Canada, Greenland, South Africa and Australia. The greenstone belts in Greenland and Canada have been subject to medium to high-grade metamorphism, which makes them unsuitable for studies regarding the sedimentary environment and related topics. The two remaining granite-greenstone terranes in which >3.3 Ga rocks have been preserved are the Barberton Greenstone Belt in South Africa, and a number of greenstone belts in the East Pilbara, Western Australia.

From those two granite-greenstone terrains, the Buck Ridge volcano-sedimentary complex (BR-vsc, in the Barberton Greenstone Belt) and the Coppin Gap Greenstone Belt, and within the latter in particular the Duffer Formation and the Kittys Gap volcano-sedimentary complex (KG-vsc, East Pilbara) were selected for this study. The BR-vsc includes the oldest sedimentary unit of significant thickness (up to 400m) in the Barberton Greenstone Belt. Contemporaneous sediments in the KG-vsc in the Pilbara are much thinner, but are also amongst the oldest well-preserved sedimentary units in the area. The BR-vsc and KG-vsc are both approximately 3.45 Ga old.

Both study areas have experienced only low-grade metamorphism, and were not significantly disturbed by deformational processes. They are well preserved and well exposed, partly owing to early silicification of parts of the succession.

East Pilbara Granite-Greenstone Terrane, Australia

The Pilbara Granite-Greenstone Terrain is exposed over an area of ~480 km by 230 km in the north of Western Australia. It ranges in age from ~3.72-2.85 Ga, and is unconformably overlain by the

~2.77-2.40 Ga old deposits of the Mount Bruce Supergroup (Van Kranendonk et al., 2002). Van Kranendonk et al. (2002) divided the Pilbara into five lithotectonic elements; the East Pilbara Granite-Greenstone Terrane, the West Pilbara Granite-Greenstone Terrane, the Mallina Basin, the Kurrana Terrane and the Mosquito Creek Basin. Of these five elements, only the East Pilbara Granite-Greenstone Terrane comprises rocks older than 3.3 Ga.

The East Pilbara is characterised by large, ovoid-shaped granitoid complexes that are surrounded by shallow to steeply dipping greenstone belts (consisting of dominantly ultramafic to mafic rocks with minor felsic and sedimentary rocks). The Coppin Gap Greenstone Belt, between the Mt Edgar and Muccan Granitoid Complexes, was selected as the study area. The Coppin Gap Greenstone Belt comprises a tightly folded synclinorium, with a well-developed southern limb and a sheared northern limb. In the southern limb the bedding is oriented roughly east-west, the dips are near-vertical and the limb therefore provides a well-preserved cross-section through part of the early Archaean crust. Regional metamorphism is anchimetamorphic to epimetamorphic (Kisch and Nijman, 2004), except adjacent to the granitoid complexes (cf. Williams, 1999). Nijman et al. (1998b) reported synsedimentary deformation from this greenstone belt. The major part of the rocks in the study area belong to the ~3.49-3.31 Ga (Van Kranendonk et al., 2002) Warrawoona Group.

Barberton Greenstone Belt, South Africa

The Barberton Greenstone Belt (South Africa) is exposed in the eastern part of the ca. 1750 by 1650 km large Kaapvaal Craton. The ~3.5-3.1 Ga Barberton Greenstone Belt covers a surface area of ~130 by 70 km. It is tightly folded, and is surrounded by trondhjemite-tonalite and granodiorite intrusions. The greenstone belt essentially consists of two separate parts that collided about 3.23 Ga, and are now separated by the Saddleback-Inyoka Fault system (e.g. De Ronde and Kamo, 2000).

The lithologies of the Barberton Greenstone Belt are divided into three groups, from old to young, the Onverwacht, Fig Tree and Moodies Groups. The ~3445-3416 Ma study area is located in the southern part of the greenstone belt, and forms part of the upper Onverwacht Group. It comprises the Buck Ridge Chert, which is the most significant sedimentary succession in the Barberton Greenstone Belt below the mid Archaean Fig Tree Group. The rocks experienced anchimetamorphic to epimetamorphic conditions (Kisch and Nijman, 2004).

Method

As stated above, a multi-disciplinary approach was taken for this study. The two selected areas, i.e. the BR-vsc and the Coppin Gap Greenstone Belt, were subjected to a broad research. After selection of the study areas, the regional geological framework was established. Because existing maps were not sufficiently detailed, or had left open certain crucial questions, a significant part of both areas was remapped and/or checked, and additions were made to existing maps. In the Barberton Greenstone Belt, mapping on 1:6000 aerial photographs and field checks covered an area of ~15 by 1.5 km. In the Coppin Gap Greenstone Belt, mapping on 1:12500 and 1:25000 aerial photographs was done in an area of 25 by 5 km, with a small number of additional field checks outside that area.

Within these frameworks, key areas relevant to the aims of the study were selected. In the Pilbara, focus was placed on the Duffer Formation and the KG-vsc, the latter forming the Kittys Gap Chert. In the Barberton Greenstone Belt, focus was placed on the sediments at the top of the BR-vsc, which partly form the Buck Ridge Chert. Within the cherts, metre to 100 metre-scale outcrops were

selected for detailed mapping to establish relationships between hydrothermal systems, sedimentary facies, geometries of the sedimentary bodies etc. On the smallest scale in the field, cm-scale to tens-of-cm-scale outcrops were used to determine mechanisms and styles of silicification. On micrometer-scale, fluid inclusions from within the detailed mapped outcrops were used to characterise the fluids in the ancient hydrothermal system.

Many different techniques have been used in this thesis, including large-scale field mapping and GIS analysis (aerial photographs, satellite and radar images), complemented by petrography, geochronology, geochemistry, sedimentary logging, detailed mapping and fluid-inclusion studies. Since the Archaean rock record is sometimes fragmentary and certain techniques are not always applicable to these ancient, altered rocks anymore, combining the (fragmentary) evidence obtained with different techniques and from different points of view is often the only possibility to come to an interpretation.

Outline of the chapters in this thesis

Chapters 2 and 3 provide the geological framework for the studies in the subsequent chapters. They discuss the tectonic regime during deposition of the Buck Ridge and Kittys Gap volcano-sedimentary sequences (BR-vsc and KG-vsc). Chapters 2 and 3 show that in both study areas, syndepositional extension occurred in the period ~3.45-3.41 Ga. During this extensional phase, a felsic volcanic complex was deposited in both areas (on a mafic to ultramafic substrate), capped by a (now silicified) sedimentary sequence. The sedimentary deposits of the BR-vsc in the Barberton Greenstone Belt are thicker than of those of the KG-vsc in the Coppin Gap Greenstone Belt.

The focus within these two volcano-sedimentary complexes is on the sedimentology of the capping cherts (Chapter 4) and the hydrothermal systems (Chapters 5 and 6) in the top of the complexes. Chapter 4 concludes that the sediments in both areas were deposited in shallow water, around base level. The sequence in the Pilbara was possibly influenced by tidal activity. Chapter 5 explores the hydrothermal activity in the top of both sequences. It is found that hydrothermal systems occur in the vicinity of the syndepositional normal faults (described in Chapters 2 and 3), and that they affected the sediments (Chapter 3) during and/or immediately after deposition. They are interpreted to have vented in shallow water. The nature of the hydrothermal fluids is studied in Chapter 6 by means of a fluid-inclusion study. The fluids were found to have been trapped at a temperature of around 250ºC and a pressure of ~2 kbar, indicating that these fluids were pressurised.

Chapter 7 provides a synthesis of the previous chapters. It aims at integrating the new data and interpretations to come to a more general and refined picture of the early Archaean basins around ~3.4 Ga ago. It combines the data from the previous chapters with data from the literature, and speculates about basin size and shape and mode of basin formation in the early Archaean.

Chapter 2

Structure and stratigraphy of the Buck Ridge volcano-sedimentary complex in the upper Hooggenoeg Formation, Barberton Greenstone Belt, South Africa; a framework for Archaean basin studies

Abstract

This chapter provides a geological framework for basin studies in the ~ 3.45 - 3.42 Ga Buck Ridge volcano-sedimentary complex (BR-vsc) in the upper Hooggenoeg Formation, Barberton Greenstone Belt, South Africa. The complex was deposited in an extensional regime, which is expressed by a number of large, syndepositional normal faults. The syndepositional character of the faults is indicated by thickness variations of rock units across the faults and systematic rotation of the fault blocks. The BR-vsc is a bimodal volcanic complex, consisting mainly of massive and pillow basalts and felsic, quartz-plagioclase porphyritic rocks. The latter become increasingly dominant towards the top of the complex. The basalts and porphyritic rocks are capped by felsic volcaniclastic deposits and other, mostly pervasively silicified, sediments. Deposition of these volcaniclastics and sediments occurred in shallow water. The BR-vsc was intruded by broadly contemporaneous, shallow felsic porphyritic rocks, which often obscure the traces of the normal faults. Extension also created space for the intrusion of approximately bedding-perpendicular felsic and mafic dykes, and black chert veins.

Observations immediately north of the BR-vsc suggest the presence of a fold pattern in that area, with approximately NW-SE trending fold axes. U-Pb dating of a felsic volcanic rock on the northern limb of one of the major inferred folds shows that it has approximately the same age as the felsic volcanic rocks in the BR-vsc. This implies that the BR-vsc, or parts of it, reappear in the area north of the Buck Ridge.

Introduction

Sediments of the ~3.42 Ga Buck Ridge volcano-sedimentary complex (BR-vsc, new name; for details on the nomenclature, see below) in the upper Hooggenoeg Formation are amongst the oldest preserved clastic deposits in the Barberton Greenstone Belt (South Africa). The sediments are well preserved and have experienced little deformation. Therefore, they form a good target for early Archaean basin studies. Knowledge of the geological framework in which these basins were formed, and the timing of the earliest phase of crustal deformation are essential for such basin studies. Synsedimentary deformation is especially important since it directly reflects the tectonic regime experienced by the area during deposition of the sediments and volcanics. Despite the fact that the Barberton Greenstone Belt has been intensively studied, the tectonic regime during deposition of the Buck Ridge volcano-sedimentary complex in the upper Hooggenoeg Formation is still not exactly known. Extensional faults (Viljoen and Viljoen, 1969; Lowe and Fisher Worrell, 1999) as well as compressive features (De Wit, 1982, 1983; De Wit et al., 1987a; Lowe et al., 1985, 1999) have been reported. Some other structural observations in the upper Hooggenoeg Formation, such as the Geluk Disturbed Zone (Lowe et al., 1985, 1999) remained unexplained, and were not attributed to a particular tectonic regime.

Here we present new structural and geochronological data on the upper Hooggenoeg Formation, which allow for a more detailed interpretation of the geological framework in which the earliest sediments in the Barberton Greenstone Belt were deposited. Emphasis lies on the first phase of deformation. Attention will also be paid to the deformation in the area north of the BR-vsc. So far, relatively little is known about the connection between deposits of the BR-vsc and the overlying parts of the stratigraphy.

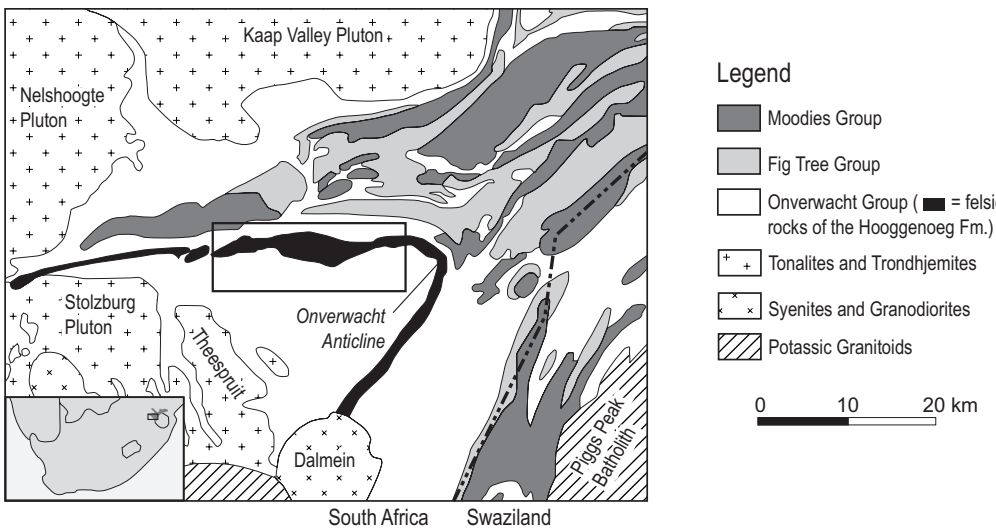

Figure 2.1: Schematic geological map of the southern part of the Barberton Greenstone Belt with surrounding granitoid complexes and its location in South Africa (modified after De Ronde and De Wit, 1994; Kisters et al., 2003). Study area indicated with a rectangle.

Structural geological framework

The Hooggenoeg Formation is exposed in the southern part of the Barberton Greenstone Belt. Structurally, this part of the greenstone belt is dominated by the Onverwacht Anticline. The study area is located on the northern limb of the Onverwacht Anticline (Fig. 2.1), and mainly consists of the uppermost part of the Hooggenoeg Formation. It includes the Buck Ridge (also referred to as Buck Reef, Lowe and Byerly, 1999a) Chert (BRC), which forms the sedimentary top of a bimodal volcanic succession. Together, this bimodal volcanic succession and its sedimentary top are named the BR-vsc. Viljoen and Viljoen (1969) provided one of the first maps and a systematic description of the stratigraphic sequence of the upper Hooggenoeg Formation (Fig. 2.2a). They regarded the Hooggenoeg Formation as an essentially continuous, north-younging stratigraphic succession. Williams and Furnell (1979) suggested the possibility of tectonic discontinuities in the upper Hooggenoeg Formation. De Wit (1982, 1983), De Wit et al. (1987a) and Lowe et al. (1985, 1999) observed deformation in the upper Hooggenoeg Formation that included folding, shearing and rotation.

Compressive deformation is interpreted to have dominated in the southern Barberton Greenstone Belt during deposition of the upper Hooggenoeg Formation (Table 2.1 and references therein). Early extensional deformation in the southern Barberton Greenstone Belt has also been suggested (De Wit,

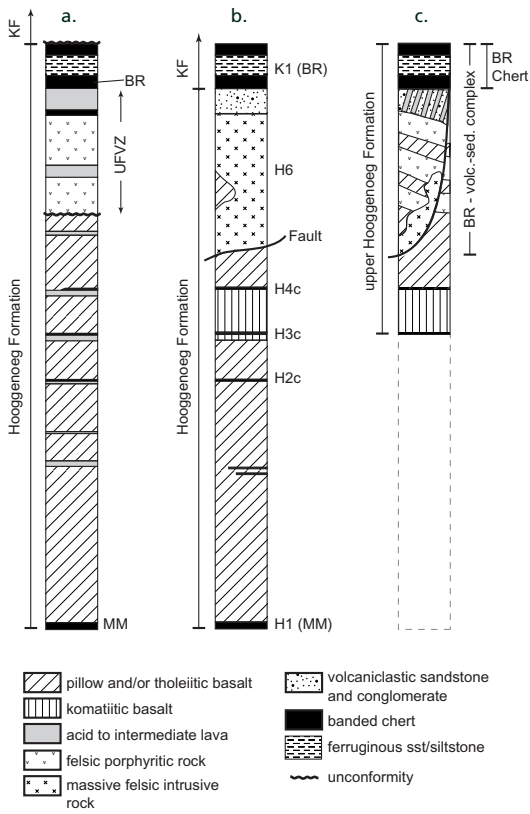

Figure 2.2. Simplified stratigraphic columns of the Hooggenoeg Formation on the northern limb of the Onverwacht Anticline. KF = Kromberg Formation, UFVZ = upper felsic volcanic zone, BR = Buck Ridge (or Reef), MM = Middle Marker. a. Based on the map and description of Viljoen and Viljoen (1969), b. Modified after Lowe and Byerly (1999), c. Terminology used in this article. Sections B and C are from approximately the same location, section A was taken slightly more west. Due to syndepositional faulting, both thickness and composition of the felsic volcaniclastic sequence vary considerably along strike (see text and Fig. 2.3). This partly explains the relatively thin felsic zone and the absence of volcaniclastic rocks in section A.

phase	nature	timing	description	ref.
D0	extension	? ~3486 Ma	normal faulting, decollement	1
		~3.48-3.46 Ga	carbonate extension veins, shearing	2
D1	compression	3445-3416 Ma	recumbent nappes, downward facing sequences	3
D2	compression	3229-3227 Ma	SE to NW thrusting, tight isoclinal folding	3
D3	compression	3226-3084 Ma	NW vergent thrusting, folding	3
D4	extension	<3084 Ma	folding, strike-slip faulting	3

Table 2.1: Current deformation scheme for the southern part of the Barberton Greenstone Belt (1 = De Wit, 1986; 2 = Zegers et al., 1998 and references therein; 3 = De Ronde and De Wit, 1994).

1982; De Wit, 1986), but evidence remained sparse and the timing not well constrained. Lowe et al. (1999) proposed a deformation scheme in which D1 is expressed by a zone of shearing and block rotation that was observed in the upper Hooggenoeg Formation. They suggested that the lower contact of the zone might have formed as a south-dipping thrust or reverse fault. The observations were not placed in a regional framework or attributed to a particular tectonic regime. In most articles, attention is focussed on the compressive phases D2 and D3 (Table 2.1).

Nomenclature

Opinions differ about whether the BRC belongs to the Hooggenoeg Formation or to the Kromberg Formation. To avoid confusion what is meant when these formations are mentioned in this chapter, the different views are summarised in this section.

The BRC was originally placed in the top of the Hooggenoeg Formation (Viljoen and Viljoen, 1969). All other workers adopted this interpretation until Byerly et al. (1996) interpreted the BRC as the basal unit of the Kromberg Formation. They regarded the BRC to be the equivalent of several thin cherts in the Kromberg Formation on the southern limb of the Onverwacht Anticline. Since then, there is debate in which formation the BRC should be placed. Brandl and De Wit (1997) regard it as the uppermost unit of the Hooggenoeg Formation, whereas Lowe and Byerly (1999a) interpret it as the base of the Kromberg Formation.

Our observations concern the northern limb of the Onverwacht Anticline. There, the contact of the BRC with the underlying layers is generally transitional (cf. Viljoen and Viljoen, 1969; Lowe and Fisher Worrell, 1999). Local unconformities are present (see below), but there is no regional unconformity at the base of the BRC. Therefore, we consider the BRC to form the top of the Hooggenoeg Formation (cf. Viljoen and Viljoen, 1969).

Because of the transitional contact of the BRC with the underlying rocks, and because further west cherts identical to those of the BRC occur lower in the sequence, the BRC should be regarded in conjunction with the underlying felsic volcanics. To accommodate this, a new term is introduced that links the sequence of basalts, felsic volcanics and intercalated cherts: the Buck Ridge volcano-sedimentary complex (BR-vsc). The BRC forms the silicified, uppermost part of this complex. The base of the BRC is taken where the uppermost felsic volcanic rocks of the BR-vsc grade into to pervasively silicified, black and white banded sediments (see also section on Stratigraphy).

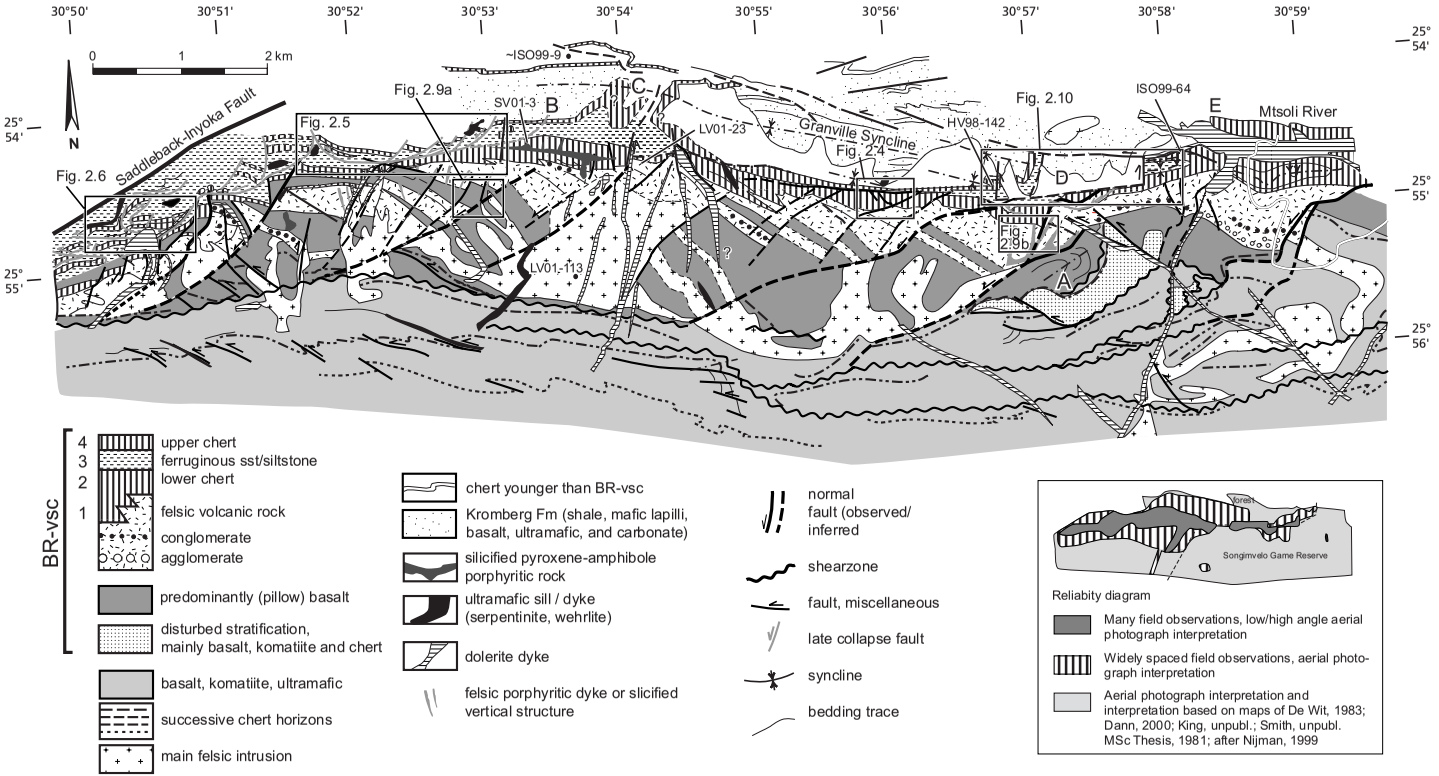

Figure 2.3: Geological map of the study area (locality indicated in Figure 2.1). The orientation of bedding is near vertical, therefore the map also represents a cross section through the upper part of the Hooggenoeg Formation.

Internal structure of the Buck Ridge volcano-sedimentary complex

Structure

The most prominent structural feature on the map in Fig. 2.3 is an array of northeast-striking faults that cut the sediments and the underlying bimodal volcanic deposits of the BR-vsc. The fault array extends at least 15 km, along almost the entire length of the northern limb of the Onverwacht Anticline. The major faults have a spacing of ~ 4 km. Systematic thickness differences of rock units across the faults are largest in the felsic volcanic rocks just below the silicified sediments. Upward in the sedimentary sequence, the thickness differences across the faults gradually decrease. The thickness differences (e.g. Fig. 2.4) indicate that the faults originated as syndepositional, west-block-down normal faults that have since been rotated along with the bedding into a vertical position. In the

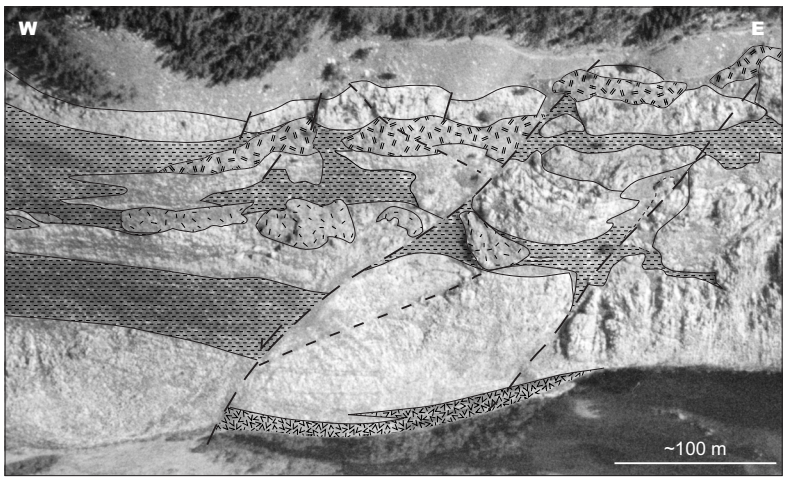

Figure 2.4: Oblique aerial photograph of west-block-down normal fault in the sedimentary sequence of the BR-vsc. Note the thickness difference of the iron-oxide-rich unit on both sides of the fault. Location indicated in Fig. 2.3.

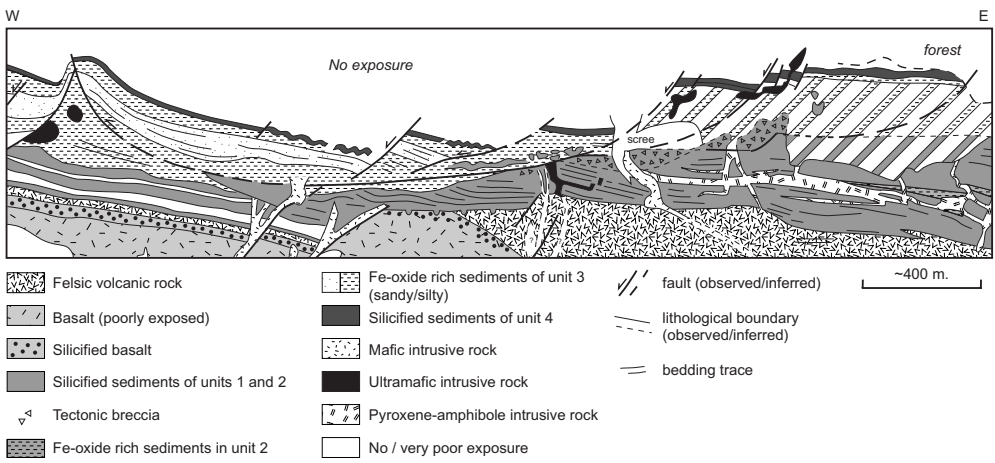

Figure 2.5: Gravitational collapse of the upper sedimentary units of the BR-vsc. Location indicated in Fig. 2.3

hanging walls of the faults, where the thickness of the sequence is maximum, the strike of the bedding deflects from the regional ~E-W to a WNW-ESE orientation. In the footwalls of the faults, the sequence shows local hiatuses and unconformities (e.g. Fig. 2.5).

At both ends of the fault array, the structure is more complex. At the rear of the array, in the eastern part of the area, the faults are folded and the internal structure of the sequence is chaotic (Fig. 2.3). Locally, parts of the sequence are south-younging (loc. A, Fig. 2.3). At the front of the fault array, in the western part of the area, the lower chert units of the BR-vsc show the same normal faulting as the rest of the complex. However, the upper chert units in that area form a complex stack of forward (westward) and backward (eastward) thrusted and rotated blocks (Figs 2.3 and 2.6). Eastward, these compressive structures seem to be linked to subordinate listric normal faults that affected the

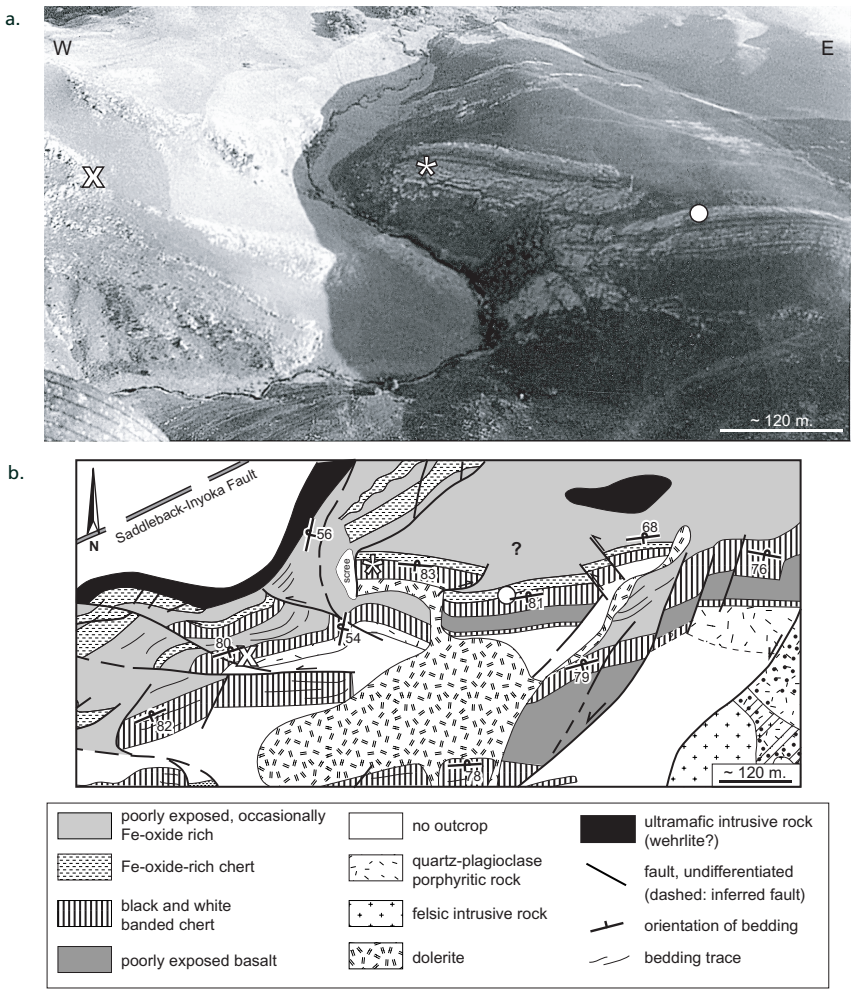

Figure 2.6: a. Oblique aerial photograph of thrust structures in the top of the BR-vsc in the western part of the area. b. Geological map of approximately the same area as shown in Fig. a. Symbols indicate corresponding locations in Figs a and b. Location indicated in Fig. 2.3.

uppermost part of the BR-vsc sedimentary top (notably units 3 and 4, Fig. 2.5).

At about 1.5-2 km below the top of the sedimentary sequence, a number of ~E-W striking shear zones occur in a dominantly mafic to ultramafic sequence (also mapped by King, unpubl. and Dann, unpubl., Fig. 2.3). In places, compressive features such as minor thrust faults with upper-block west displacement and S-shaped, 100 m-scale folds with near-vertical fold axes occur along and in the vicinity of the shear zones.

North of the BR-vsc

Reversals of younging direction from N to S are observed within the top of the BRC in the eastern part of the area and immediately north of the Buck Ridge in the entire area (Fig. 2.3; see also sections on Stratigraphy and Geochronology).

Stratigraphy

Fig. 2.3 shows an increased stratigraphic resolution of the upper Hooggenoeg Formation with respect to previous maps (for references, see introduction). The lower part of the BR-vsc consists predominantly of poorly exposed, massive and pillow basalts, and a minor amount of komatiites and thin, silicified sedimentary layers. The silicified sediments show well-preserved cross-bedding and grading. Stratigraphically upward, felsic layers are intercalated, which gradually become dominant over the basalts (Fig. 2.3). The felsic rocks are porphyritic and contain quartz and altered plagioclase phenocrysts in a cryptocrystalline groundmass. The phenocrysts are distributed homogeneously. Quartz phenocrysts are 0.5 – 3 mm large, and lath-shaped plagioclase phenocrysts are mostly ~1 mm, locally reaching up to 4 mm. The groundmass, which makes up ~65-80% of the rock, consists of microquartz and sericite. Rarely, the porphyritic rocks are flow banded or columnar jointed. A sample of such a flow-banded porphyritic rock from just below the BRC, in the footwall of one of the major normal faults (loc. LV01-23) was dated at 3451±5 Ma (U-Pb SHRIMP dating, Fig. 2.7a and Appendix A). This sample contains ~0.2-0.8 mm-sized euhedral quartz phenocrysts, rectangular, ~0.2-1.6 mm large plagioclase phenocrysts (completely altered to sericite) and <1% anhedral opaque material. The phenocrysts are homogeneously distributed in a groundmass of microquartz and sericite that constitutes for approximately 65% of the rock. Towards the top, volcaniclastic material is intercalated. In the eastern part of the area the volcaniclastic deposits include coarse conglomerates, while towards the west they generally consist of finer-grained deposits, ash and, rarely, accretionary lapilli layers. In the western part of the area, (pillow) basalts and sedimentary chert layers are intercalated in the top of the felsic volcanics.

Sedimentary sequence of the BR-vsc

The up to 400 metres-thick sedimentary top of the BR-vsc is divided into four lithofacies units: (1) a partly silicified volcaniclastic unit characterised by several tens to hundred metres-wide scour-and-fill structures, (2) a banded sedimentary chert, (3) an iron-oxide-rich sandstone-siltstone interval, which in places includes breccia and massive iron-oxide occurrences and, (4) a well-banded silicified sandstone. The latter three units, together with the pervasively silicified parts of unit 1, form the BRC. The contact between the volcaniclastic deposits of unit 1 and the underlying felsic lava flows is transitional (cf. Viljoen and Viljoen, 1969; Lowe and Fisher Worrell, 1999). Upward, the volcaniclastic deposits, and subsequently the chert, become dominant. In places, unit 1 is very thin or not present at all. In such places there is no intercalation of sedimentary chert beds between the felsic lava

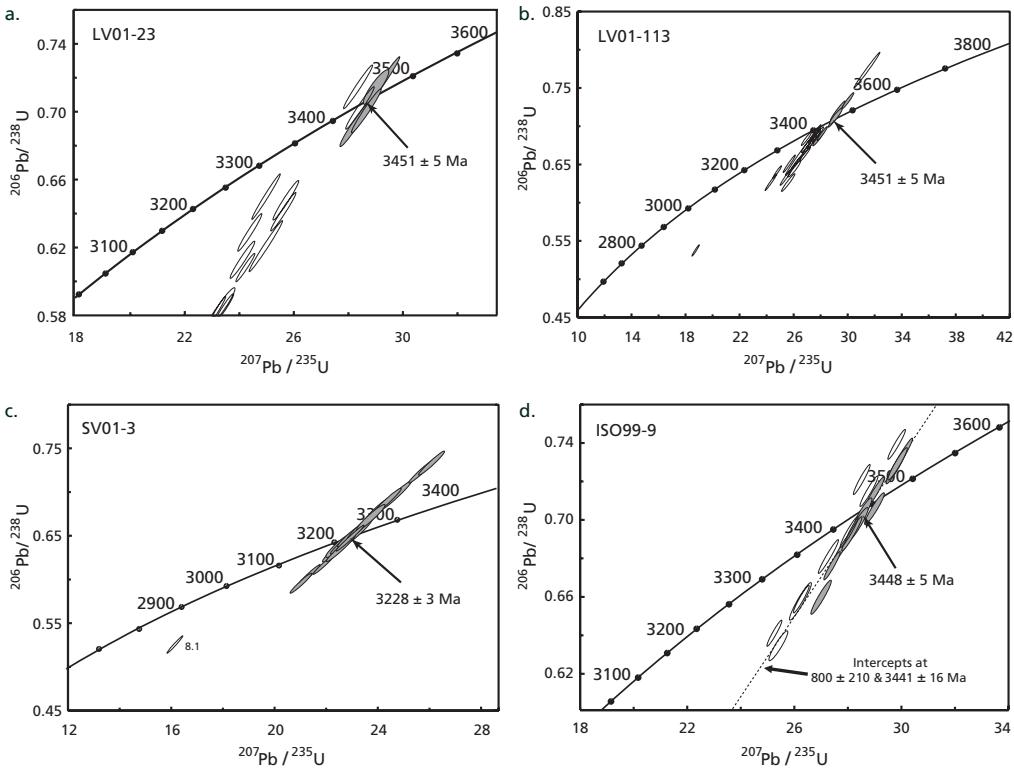

Figure 2.7: Concordia diagrams of U-Pb data for samples dated with the SHRIMP-RG of the Research School for Earth Sciences at the Australian National University in Canberra. Data in filled error ellipses were used to calculate the mean $^{207}Pb/^{206}Pb$ age. Data point error ellipses are 68.3% conf. Details on the analytical technique and the results for the individual samples are given in Appendix A.

flows, and the silicified crystal layers (Lowe and Fisher Worrell, 1999; Chapter 4 and 5), which are characteristic of this unit elsewhere, are absent. In these places, banded cherts of unit 2 directly overly quartz-plagioclase porphyritic lavas. The lower part of unit 2 hosts stalactite and stalagmite-bearing cavities. The upper part of the unit consists of very planar-banded chert. Unit 3 shows 20 m-cycles of planar (even) bedded iron-oxide-rich sandstone, with thin intervals with ripples and breccia towards the top of the cycles. The entire unit shows a lateral facies change from sandstone in the eastern part of the map area to distal, Fe-oxide-rich shale in the western part. Unit 4 contains low-angle trough cross-bedding and planar-laminated sets under low angles. For a more detailed description of the sedimentary environment see Chapter 4.

Intrusions

Several types and generations of igneous rock have intruded the BR-vsc. Most prominent are the 'main' felsic intrusive bodies (Fig. 2.3) that occur with a regular spacing in the lower part of the BR-vsc. The felsic bodies are asymmetric, with westward projecting sills. The bases of the felsic intrusions occur at approximately 1.5-2 km below the top of the BR-vsc. The cores of these 'main' felsic intrusions have an interlocking to semi-interlocking (up to 20% groundmass) texture. 1-2 mm large

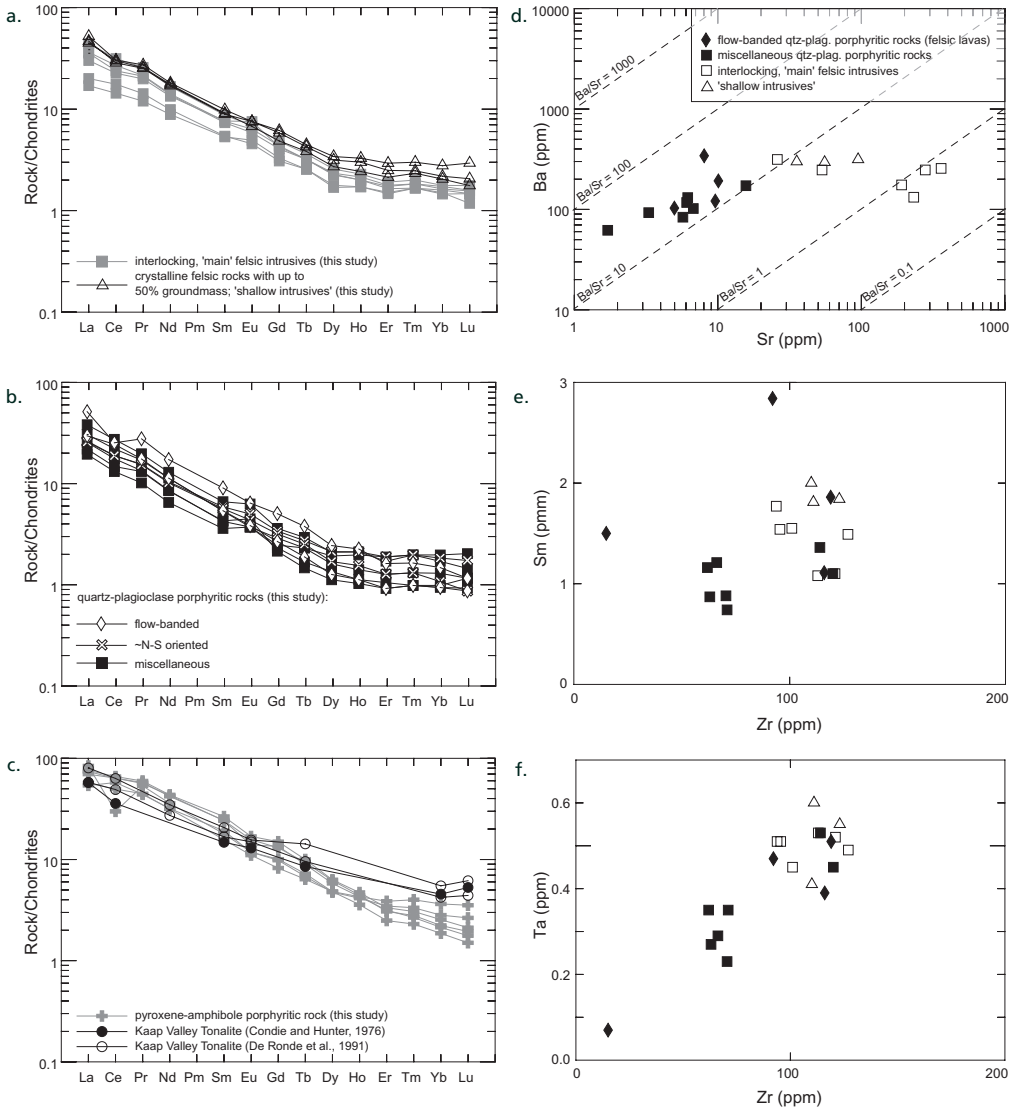

Figure 2.8: REE-diagrams for a. Interlocking and semi-interlocking, 'main' intrusives from the study area, b. Quartz-plagioclase porphyritic rocks from the study area, c. Pyroxene-amphibole intrusive rocks from the study area compared with data for the Kaap Valley Tonalite from literature. d. Concentration of Ba vs. Sr (in ppm). Note that the felsic lavas and quartz-plagioclase porphyritic rocks generally have higher ratios than the interlocking 'main' intrusives and the shallow intrusives, e. Sm against Zr (in ppm), and f. Ta against Zr (in ppm). Legend in Fig. d also applies to Figs e and f. Normalisation after Nakamura, 1974.

plagioclase crystals make up 65-75% of the rock, while quartz grains have an average size of 0.5 mm (max. 2.5 mm), and make up 15-25% of the total volume. Chlorite is present as a secondary phase. Towards the rims of the intrusions the percentage of groundmass increases. U-Pb SHRIMP dating of a sample from the core of one of the 'main' intrusions in the central part of the map area (loc. LV01-113) yielded 3451±5 Ma (Fig. 2.7b and Appendix A).

Crystalline felsic rocks with small amounts (up to 50% of the total rock volume) of groundmass in the lower part of the felsic sequence are interpreted as 'shallow intrusives'. They contain mainly plagioclase and quartz in a finely crystalline groundmass. Plagioclase is generally altered to sericite, but simple and multiple twinning have occasionally been preserved. The plagioclase grains are

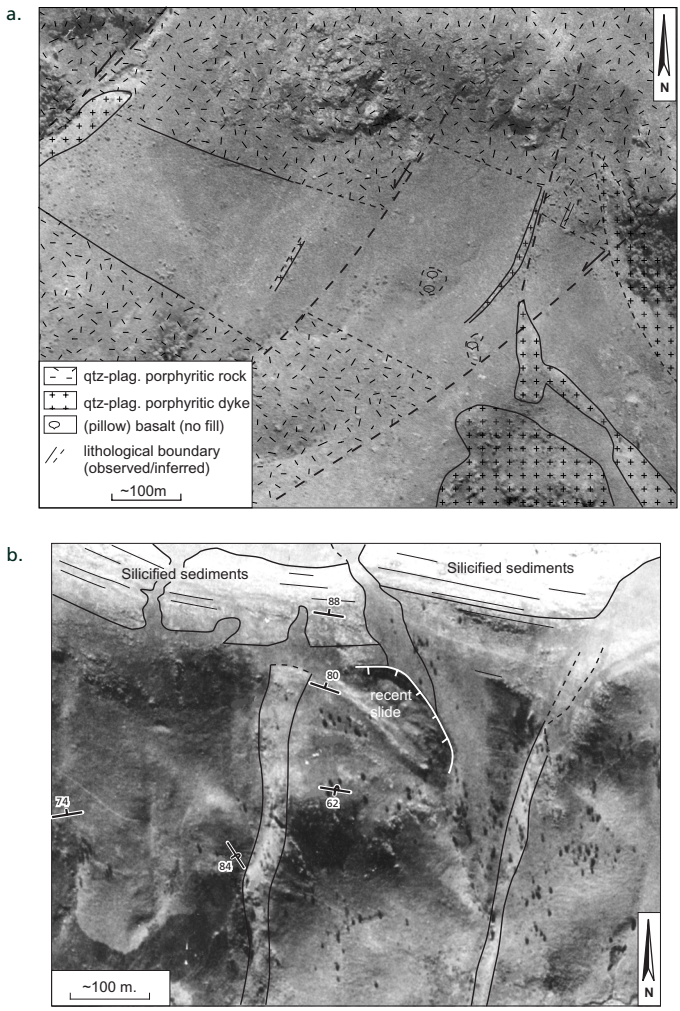

Figure 2.9: a. Quartz-plagioclase porphyritic dykes cutting a poorly exposed pillow basalt interval. b. Pale, approximately vertical structures in a poorly exposed felsic volcanic interval overlain by silicified sediments of the Buck Ridge Chert. Thin lines in the silicified sediments represent orientation of bedding. Locations are indicated in Fig. 2.3. Aerial photographs: Chief Directorate of Surveys and Mapping, South Africa.

rectangular and range in size from 0.5-3 mm. The REE patterns of the 'shallow intrusives' are similar to the interlocking to semi-interlocking 'main' felsic intrusives (Fig. 2.8a). The REE patterns broadly resemble those of the Stolzburg Pluton trondhjemites (cf. De Wit et al., 1987a).

Higher in the sequence, quartz-plagioclase porphyritic rocks without flow banding or columnar jointing, may have intruded as sills (but are difficult to distinguish from the extrusive porphyritic rocks, see discussion). There is no difference in the REE patterns of the porphyritic rocks with and without flow banding (Fig. 2.8b).

At several places in the study area, approximately bedding-perpendicular, light-weathered felsic outcrops stand out from the bimodal volcanic sequence, preferentially in the hanging walls of the normal faults. Fig. 2.9a shows such felsic outcrops, where they cut a poorly exposed pillow basalt interval. The felsic dykes consist of quartz-plagioclase porphyritic rocks. In areas where the light-weathered felsic outcrops occur in an otherwise felsic sequence (e.g. Fig. 2.9b), they are mineralogically and texturally almost similar to the surrounding rocks. In the field, the bright, vertical outcrops appear to have a glassier groundmass, however. It is unclear whether this is a primary feature of a felsic dyke, or whether the original composition of these rocks was the same as the host rock, and the change in colour and groundmass were due to local silicification. Geochemical analyses of rocks from an approximately N-S striking outcrop in the western part of the area, show that the bedding-parallel and bedding-perpendicular quartz-plagioclase porphyritic rocks have a similar REE pattern (Fig. 2.8b). The dykes (or silicified vertical structures) terminate in the highest bedding-parallel felsic units of the upper Hooggenoeg Formation (see also Chapter 4). Metres-wide black chert veins occur in the vicinity and have approximately the same (bedding-perpendicular) orientation. At depth, the felsic dykes or silicified vertical structures approach the interlocking to semi-interlocking 'main' felsic intrusions (Fig. 2.3). However, no direct connection was observed. The REE patterns of the porphyritic rocks are similar to those of the 'main' intrusives (Figs 2.8a and b). However, the two groups are not identical. The porphyritic rocks have distinctly higher Ba/Sr ratios (Fig. 2.8d). Given the potential mobility of these elements during rock diagenesis, this is not necessarily a primary feature. A similar difference between the porphyritic rocks and the main intrusives is indicated in Sm vs. Zr and Ta vs. Zr diagrams (Figs. 2.8e,f).

Mafic intrusions in the BR-vsc include silicified dolerite dykes in the top of the complex, which have approximately the same orientation as the quartz-plagioclase porphyritic dykes. Part of these dolerite dykes end in a basalt interval just below the BRC. Other, mostly less-weathered dolerite dykes cut through the entire BR-vsc.

The uppermost part of the BR-vsc has been intruded by (now altered) pyroxene-amphibole-bearing rocks (REE data in Fig. 2.8c). Porphyritic crystals include dark, thin, needle-shaped laths, more equidimensional laths, and altered, brown, hexagonal minerals. The thin needle-shaped laths have an average length of 0.6 mm, and are cryptocrystalline. The more equidimensional laths are larger (up to 2.2 mm), but less abundant. They are often twinned (i.e. presumably plagioclase). The 0.5-3 mm, euhedral to subhedral, brown-green, hexagonal minerals are cryptocrystalline. Presumably, the grains were originally pyroxenes or amphiboles. The grains float homogeneously in a fine-grained groundmass that constitutes 25-75% of the total rock volume. U-Pb zircon dating of these intrusions yielded an age of 3228±3 Ma (sample SV01-03, Fig. 2.8c and Appendix A).

The BR-vsc has also been intruded by several types of ultramafic rock. These include fresh, coarse-grained ultramafic rocks (including wehrlites, described by Dann, 2000), as well as very fine-grained and completely altered mafic rocks.

North of the BR-vsc

Road cuts and isolated outcrops immediately north of the Buck Ridge expose mafic intrusive rocks, basalts and shales. Quartz-plagioclase porphyritic rocks north of the latter, at loc. ISO99-9 (Fig. 2.3), strongly resemble the lava flows just below the BRC. They contain ~0.02-0.6 mm large, subhedral quartz phenocrysts and ~0.2-1.8 mm large, rectangular ghost minerals, that now completely consist of sericite. Despite the strong alteration, the outlines of these ghost minerals are still very rectangular (plagioclase was probably the precursor). The phenocrysts are surrounded by a cryptocrystalline groundmass, dominantly consisting of microquartz and sericite. U-Pb dating of this sample yielded an age of 3448±5 Ma (Fig. 2.7d and Appendix A for details and discussion on interpretation). Weathered volcaniclastic debris at the same location included silicified crystals, similar to those in the volcaniclastic unit (1) of the BR-vsc.

In the eastern part of the study area, BR-vsc deposits are locally directly juxtaposed with mafic lapilli attributed to the Kromberg Formation (loc. D, Figs 2.3 and 2.10a; cf. Ransom et al., 1999). In this area, several pronounced chert beds are exposed just north of the Buck Ridge (loc. E and north of it (not on map), Fig. 2.3).

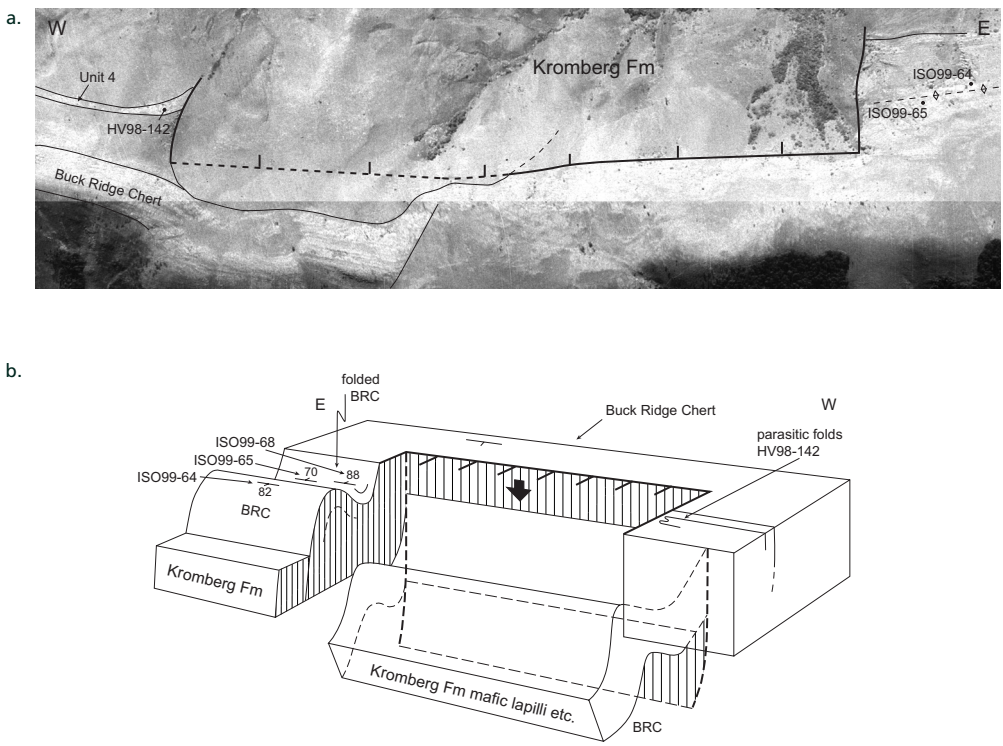

Figure 2.10: a. Aerial photograph (Chief Directorate of Surveys and Mapping, South Africa) of area D (Fig. 2.3) where, locally, the top of the BR-vsc is missing. b. Sketch model of how local folding and faulting of the upper part of the BR-vsc may have resulted in juxtaposition of BR-vsc sediments and Kromberg Formation mafic deposits in the area shown in Fig. a.

Interpretation and discussion

The dominantly mafic to ultramafic lower part of the BR-vsc is relatively poorly exposed, and consequently indications for the environment of deposition are sparse. The occasional occurrence of pillow basalts and chert with cross-bedding indicates subaqueous deposition for parts of the sequence. Upwards, the nature of the volcanism changes to bimodal. Flow banding and rare columnar jointing in the quartz-plagioclase porphyritic rocks suggest or shallow intrusive extrusive volcanism. The flow-banded felsic rocks are interpreted as lava flows. Many of the quartz-plagioclase porphyritic rocks are massive however, and it is difficult to distinguish whether they originated as extrusive or shallow intrusive rocks. In the top of the sequence, volcaniclastic layers and conglomerates indicate (local) erosion and transport of volcanic material. Rare (reworked) accretionary lapilli in the volcaniclastic deposits indicate that volcanism was occasionally explosive. The silicified, banded sedimentary deposits at the top of the BR-vsc indicate shallow water to subaerial conditions, followed by a slight deepening (for details on the depositional environment of the sediments, see Chapter 4).

Early, syndepositional deformation

Unravelling the earliest phase of deformation that affected the BR-vsc in the Barberton Greenstone Belt is essential for interpreting the dynamics of formation of this early basin. Syndepositional normal faulting, visible in the entire BR-vsc, indicates extension during its deposition. The location of the faults controlled the distribution of basalts and felsic volcanics. The distribution of the sedimentary facies was also influenced by the faults, for instance in the eastern part of the area, where coarse clastic deposits are concentrated along the down-thrown sides of the normal faults (Fig. 2.3). At depth, the traces of the normal faults are either poorly exposed or obscured by felsic intrusive bodies. However, from the shape and spacing of the intrusive bodies, the distribution of felsic and mafic volcanic rocks in the BR-vsc, and the preserved fragments of the fault traces, it is interpreted that the largest faults extended into the base of the BR-vsc (Fig. 2.3; dashed thick fault lines). Shear zones at the base of and just below the level of the felsic intrusions may have acted as the detachment level of such major normal faults. Vergence of the folds and the upper-block west displacement along minor thrust faults in the vicinity of the shear zones, are consistent with the west-block-down movement of the listric normal faults. The shear zones mark the southern limit of rotations and other complicated deformation. The progressive rotation of the volcanic sequence into a more NW-SE orientation in the hanging walls of the faults is interpreted to have resulted from rollover anticline development. In the eastern part of the area (in the rear of the fault array), progressive gravitational collapse led to folding of the fault planes, chaotisation of the stratigraphic sequence and oversteepening of the easternmost rollover anticlines. The latter resulted in local south-younging of the stratigraphic sequence. Hence, the local overturning of the stratigraphic succession in this area is interpreted to be a direct result of the gravitational collapse, and is therefore considered to have been contemporaneous with deposition of the felsic rocks in the upper Hooggenoeg Formation. Probably, the already complex structures at the rear of the fault array were further deformed as a result of space problems due to trondhjemite emplacement, or during formation of the Onverwacht Anticline.

Complicated structures in the western part of the area are interpreted to be due to thrusting and late gravitational collapse in the toe region of the normal fault array (e.g. Mandl and Crans, 1981), the latter lasting into post-BRC times.

The upper part of the sedimentary sequence in the western part of the area was affected by late-

stage superficial gravitational collapse (Fig. 2.5).

The 'main' felsic intrusives seem to have intruded along the major normal faults (Fig. 2.3). Dating shows that they were broadly contemporaneous with the extrusive felsic rocks in the top of the BR-vsc (Figs 2.7a and b). Their texture (high percentage of groundmass) shows that they solidified at shallow depth.

Apart from the sediments, extrusive volcanics and the 'main' felsic intrusions, the extension also created space, especially in the hanging walls, for the intrusion of quartz-plagioclase porphyritic rocks and dolerite dykes.

Timing of events

Thickness differences of rock units across the normal faults (Fig. 2.3) indicate that fault activity, and hence extension, were contemporaneous with deposition of the BR-vsc. The faults were most active during deposition of the main volume of felsic lavas and felsic volcaniclastics. During deposition of the upper sedimentary units of the BR-vsc, growth-fault activity diminished and felsic volcanism ceased.

The temporal relationship between the intrusive bodies and the lavas was established by U-Pb SHRIMP dating. One of the main felsic intrusions (LV01-113) and a lava flow (LV01-23) in the top of the BR-vsc are both 3451±5 Ma old (Figs 2.7a and b). Although the error on this age precludes unequivocal conclusions, it indicates that the extrusive felsic volcanics and the major felsic intrusions in the BR-vsc were broadly contemporaneous, and both have upper Hooggenoeg Formation ages. An age in the same range, 3452±3 Ma, was obtained previously for a dacitic tuff from the lowermost part of the felsic unit (sample SA351-2, Byerly et al., 1996, see Table 2.2). Previously, the same sample had been dated with Pb-Pb evaporation at 3445±3 Ma (Kröner et al., 1991, Table 2.2), i.e. a

	Sample number	*Age (Ma)*	*Latitude*	*Longitude*	*Reference*
A	LV01-113	3451±5	S 25°56.15′	E 30°53.37′	this study [1]
B	LV01-23	3451±5	S 25°56.11′	E 30°53.44′	this study [1]
C	SV01-3	3228±3	S 25°55.23′	E 30°53.02′	this study [1]
D	ISO99-9	3448±5	S 25°54.50′	E 30°53.57′	this study [1]
1	BSV 30/86	3445±8	composite sample		Armstrong et al., 1990 [1]
2	SA351-2	3445±3	S 25°56.7′	E 30°43.7′	Kröner et al., 1991 [2]
3	SA351-2	3452±3	S 25°56.7′	E 30°43.7′	Byerly et al., 1996 [1]
4	MW64	3416±5	S 25°55.5′	E 30°51.6′	Kröner et al., 1991 [2]
5	BA10&11	3438±6	composite sample		Kröner and Todt, 1988 [2]
6	Mudpools porphyry	3227±3			De Ronde et al., 1991 [3]
7	SA310-1	3258±3	S 25°54.4′	E 30°01.7′	Byerly et al., 1996 [1]
8	SA167	3298±3	S 25°53.3′	E 30°00.8′	Byerly et al., 1996 [2]
9	SA-57-1	3241±6			Kröner et al., 1991 [2]
10	L	3229+4/-3			Kamo and Davies, 1994 [3]

Table 2.2: Origin and age of zircon dating samples from the BR-vsc and the area immediately north of the BR-vsc on the northern limb of the Onverwacht Anticline in the southern Barberton Greenstone Belt. Letters refer to new dates presented in this study (locations indicated in Fig. 2.3), numbers refer to previously published dates. Dating method: [1]SHRIMP zircon U-Pb, [2]Pb-Pb evaporation, [3]conventional U-Pb isotope dilution. SHRIMP dating for this study was done at Australian National University in Canberra, Australia, details in Figs 2.7a-d, and Appendix A.

significantly younger age than with the U-Pb SHRIMP dating method. Also, an older dating of Armstrong et al. (1990) of a dacite to dacite-andesite composite sample from the main felsic unit, which yielded 3445±8 Ma, is within error of the two new dates (see Table 2.2). Hence, the intrusive and extrusive rocks of the felsic complex are approximately contemporaneous. If only the U-Pb zircon ages are considered, the maximum interval of deposition is ~10 Ma (ages in Table 2.2).

Only one age is available for the volcano-sedimentary sequence that overlies the felsic lavas and intrusives of the Hooggenoeg Formation. Kröner et al. (1991) dated a sample from the volcaniclastic top of the felsic volcanic zone or the base of the overlying silicified sedimentary sequence of the BR-vsc by Pb-Pb evaporation. Three zircons from a dacitic tuffaceous sandstone in this unit yielded an age of 3416±5 Ma, providing a maximum age for deposition of the tuffaceous sandstone. Considering the fact that this Pb-Pb age is probably slightly on the low side, as is suggested by the age of sample SA351-2 (Byerly et al., 1996 and Table 2.2), this still leaves a considerable time gap between the age deposition of the felsic volcanics and the overlying tuffaceous sandstone. Since the normal faults in the BR-vsc were active during deposition of the felsic lavas and felsic intrusions, as well as during deposition of the overlying sedimentary units of the BR-vsc, this implies a minimum duration for the extension of ca. ~35 Ma.

The pyroxene-amphibole porphyritic rock that intruded the BR-vsc is ~200 Ma younger than the complex itself. Its age of 3228 ± 3 Ma (Fig. 2.7c) suggests that the intrusion was related to the phase of igneous activity that also gave rise to the Kaap Valley Pluton, which was dated at 3227 ± 1 Ma (Kamo and Davis, 1994). Comparison of REE trends of the pyroxene-amphibole-bearing rocks (this study) and the Kaap Valley Tonalite (Condie and Hunter, 1976; Robb and Anhaeusser, 1983; De Ronde et al., 1991) shows that, nevertheless, the differentiation trend of the two rock types is slightly different (Fig. 2.8c). A detailed comparison between the two rock types is difficult, since the data sets for the Kaap Valley Tonalite and the pyroxene-amphibole-bearing rocks have been obtained by different techniques (neutron activation vs. ICP-MS), and some of the elements were not analysed for the Kaap Valley Tonalite.

Compression vs. extension

Observations of extensional deformation in the Barberton Greenstone Belt around ~3.4 Ga are not new. Extensional faulting in the uppermost part of the felsic volcanics and the lowermost part of the BRC was recognised previously (Viljoen and Viljoen, 1969; Lowe and Fisher Worrell, 1999), but this was explained as local faulting, perhaps related to cooling and subsidence of an underlying felsic intrusion (Lowe et al., 1999). For the area slightly northeast of the present study area, De Wit (1982) already introduced the concept of gravity tectonics based on observations in the upper Onverwacht and Fig Tree Groups. He described large-scale mass transport down an unstable paleoslope into deeper parts of the basin. The subhorizontal thrust or glide planes in that area were explained as either mass transportation during a later phase in a direction opposite to that of the gravitational mass transport, or contemporaneous nappe formation in the same direction, which caused gravitational instability in its front. However, in later articles about the deformation history of the southern Barberton Greenstone Belt the idea of gravitational deformation, either prior to a phase of thrusting or contemporaneous with thrusting, has not been considered anymore.

Gravitational deformation and the formation of extensional arrays of faults in one area often leads to compressive structures in the sole and in the toe region of the normal fault or fault array (e.g. Mandl and Crans, 1981). Therefore, observations of compressive structures in the study area by other

authors do not necessarily contradict the extension model proposed in this study. The observations near the base of the felsic complex of the upper Hooggenoeg Formation can be explained in this light. Lowe et al. (1985; 1999) and Lowe and Byerly (1999b) found a zone of shearing, intrusion and rotated mafic blocks in the upper part of the Hooggenoeg Formation, which they termed the Geluk disturbed zone. Since the lower contact of the zone, formed by the Geluk Fault, was not observed to cut the units overlying the felsic zone (or member H6; Lowe et al., 1999; Fig. 2.2), this deformation was considered to be pre-BRC (member K1 of Lowe et al., 1999; Fig. 2.2). The Geluk Fault of these authors coincides for the major part with the inferred detachment zone of the growth-fault model of this study. In the western part of the area the Geluk Fault coincides with the combined traces of growth faults and detachment faults in this study. The large, detached and rotated masses of basaltic and komatiitic volcanic rock from lower stratigraphic levels (Lowe et al., 1999; Lowe and Byerly, 1985, 1999), which were described to be surrounded by the felsic intrusive body of H6, are in the present model interpreted as *in situ* basalts alternating with bedding-parallel felsic porphyritic rocks, which systematically rotated along normal faults and were subsequently intruded by felsic magma.

De Ronde and De Wit (1994) regard the earliest phase of regional deformation (D1) to be compressional. This phase was timed at 3445-3416 Ma, based on the ages of felsic intrusives (ages listed in De Ronde and De Wit, 1994 and Table 2.3) that were interpreted to have been syntectonic. According to them, D1 deformation included the formation of recumbent nappes, downward facing sequences (De Wit, 1982; De Wit et al., 1987a) and the emplacement of ophiolite allochthons (De Wit et al., 1987b). New field and geochronological data have improved the relative and absolute timing of events during and just after deposition of the Hooggenoeg Formation. This leads to a different interpretation of previous observations; some observations previously thought to belong to different phases of deformation are now interpreted to be contemporaneous with deposition of the BR-vsc.

De Wit et al. (1987a) argued that the felsic intrusive rocks of the upper Hooggenoeg Formation were emplaced during thrusting at or near the boundary between the Onverwacht pillow lava-chert sequence and a cover of Fig Tree-like shales. According to them, the emplacement post-dated an early period of deformation, which included local overturning of Onverwacht stratigraphy. The upright folding of downward facing parts of the stratigraphic succession along parts of the lower contact of the felsic intrusion on the northern limb of the Onverwacht Anticline were explained as postdating or accompanying the felsic intrusion (De Wit et al., 1987a). It is equally likely however, that both folding and local overturning of stratigraphy were the direct effect of large-scale normal faulting (see above) during deposition of the felsic volcanic sequence in the top of the Hooggenoeg Formation. U-Pb SHRIMP dating has shown that the felsic extrusives near the top of the formation were approximately contemporaneous with emplacement of the felsic intrusions in the upper Hooggenoeg Formation. Hence, the local overturning of Onverwacht (Hooggenoeg) stratigraphy, folding, and the emplacement of felsic intrusions may have occurred during a single phase of deformation, rather than during two or three separate phases.

Comparison with other Archaean examples

The first recognised deformation structures in several greenstone belts of the Pilbara (Australia) are ~3.47-3.46 Ga. These include tilting of the Coonterunah Group (Buick et al., 1995; Green et al., 2000), and formation of arrays of syndepositional listric normal faults (Chapter 3; Zegers et al. 1996; Nijman et al., 1998a). The latter are comparable to and approximately contemporaneous with the

extensional structures in the upper Hooggenoeg Formation. Key structures are brittle extensional faults that crosscut the stratigraphic succession and at their sole merge into highly altered bedding-parallel ductile/brittle shear zones, usually located in ultramafic units. For more details on the Pilbara structures see Chapter 3.

The recognition of an early extensional phase of deformation in the Barberton Greenstone Belt makes the already very comparable tectonic histories of the Kaapvaal and Pilbara Cratons (Zegers et al., 1999) even more similar.

Post-BR-vsc compressive deformation: implications for stratigraphy

Field observations such as the possible folding of BR-vsc unit 4, reversals of younging direction both in the top and immediately north of the BR-vsc and complex and folding (e.g. loc. HV98-142, ISO99-64, Fig. 2.10) suggest the presence of larger NW-SE folds with approximately subhorizontal fold axes immediately north of the BR-vsc. The largest fold is the Granville Syncline (new name, Fig. 2.3). The interpretation of a relatively large-scale fold north of the BR-vsc is strengthened by the dating of sample ISO99-9 at 3448 ± 5 Ma, from the 'north limb' of the syncline. The similarity of ISO99-9 with sample LV01-23 suggests that it is also an extrusive volcanic rock, although the setting of this sample is not exactly known. Assuming that the 3416 ± 5 Ma (Kröner et al., 1991) gives a minimum age of deposition for the lower part of the BR-vsc sedimentary sequence, it follows that the stratigraphy does not continuously young upward in this part of the Barberton Greenstone Belt. It implies that the BR-vsc, or parts of it, may reappear in the area north of the Buck Ridge.

The folding immediately north of the Buck Ridge is interpreted to belong to the D2 phase of SW-NE directed regional compression, which was already known from the central part of the Barberton Greenstone Belt (Table 2.1), and dated at ~3228 Ma (De Ronde et al., 1991; Kamo and Davis, 1994; De Ronde and De Wit, 1994). Subsequent refolding during deformation phase D3 (<3226 Ma, De Ronde et al., 1991; De Ronde and De Wit, 1994; Kamo and Davis, 1994) resulted in the formation of the Onverwacht Anticline.

Our observations fit with the recognition of reversals of younging direction and fold closures north of the BRC by De Wit (1982). Furthermore, several workers have suggested that the uppermost ultramafic lavas of the Onverwacht Group and the overlying Fig Tree sedimentary rocks are repeated in a series of thrust and fold nappes (De Wit, 1982; De Wit et al., 1983; Lowe et al., 1985). However, the sparse available ages from the sequence immediately north of the BR-vsc (Table 2.2 and references therein) did not indicate major disruptions of stratigraphy in this area. De Ronde et al. (1991) dated the intrusive Mudpools Porphyry north of our study area at 3227 ± 3 Ma, and, further east, interpreted the Ironstone Porphyry as being of approximately the same age (ca. 3230 Ma). Other ages from the area were in the same range (nrs. 7-10, Table 2.2). These ages only indicated a minimum age for the sequence north of the BR-vsc, and could not give any information about the continuity of the stratigraphic sequence in this part of the greenstone belt.

The post-BR-vsc (D2) folding that resulted in the formation of the Granville Syncline is interpreted to have been indirectly responsible for the missing top of the BR-vsc at loc. D (Figs 2.3 and 2.10). The straight, bedding-perpendicular sides of the structure, visible on aerial photographs, suggest that the structure is fault-bound (Fig. 2.10a). It is interpreted that the structure is the result of dip-slip gravitational collapse of part of the southern limb of the Granville Syncline (Fig. 2.10b). This explains the local disappearance of the top of the BRC, and juxtaposition of Kromberg Formation mafic lapilli and lower sedimentary units of the BR-vsc at loc. D (Figs 2.3 and 2.10).

Previously, this structure was explained as a crater that had resulted from violent, hydromagmatic explosions, and was filled with mafic lapillistone and lapilli-tuff (Ransom et al., 1999).

Conclusions

Normal faulting influenced the deposition of the 3.45-3.41 Ga Buck Ridge volcano-sedimentary complex (BR-vsc). The BR-vsc is a bimodal volcanic complex, with felsic volcanism becoming increasingly dominant upward. The top of the complex is formed by a silicified volcaniclastic sequence. The BR-vsc was intruded by broadly contemporaneous, shallow felsic porphyritic rocks, which obscure the traces of the normal faults to a large extent. Extension also created space for the intrusion of approximately bedding-perpendicular felsic and mafic dykes, and black chert vein systems.

The growth-fault model accounts for previously unexplained structural observations, such as block rotations, in the top of the Hooggenoeg Formation.

Observations immediately north of the BR-vsc suggest the presence of a fold pattern in that area with approximately NW-SE fold axes. U-Pb dating of a felsic volcanic rock on the northern limb of one of the major inferred folds shows that they have approximately the same age as the felsic volcanic rocks in the BR-vsc.

Acknowledgements

I thank Prof. M.J. de Wit for suggesting the upper Hooggenoeg Formation as a study area, and Dr J.C. Dann for introducing us in the geology of the southern Barberton Greesntone Belt. MSc students O. Houtzager and K.L. Louzada contributed to this chapter with their theses on parts of the BR-vsc. The major part of the presented geochemical analyses were performed by K.L Louzada at the University of Cape Town, South Africa, as part of her MSc project. U-Pb SHRIMP dating was carried out by the author at the SHRIMP-RG of the Research School for Earth Sciences at Australian National University in Canberra (Australia), in cooperation with Dr. R.A. Armstrong. The Foundation Dr. Schürmannfonds partly supported the fieldwork with grants 1998/14, 1999/14, 2001/14 and 2002/10. U-Pb SHRIMP dating was financed with contributions from the Geodynamical Research Institute (GOI) and the Netherlands Organization for Scientific Research (NWO, grant R 75-394).

Chapter 3

Stratigraphic continuity and early deformation of the central part of the Coppin Gap Greenstone Belt, Pilbara, Western Australia

Abstract

This study focuses on the earliest phase of deformation and the stratigraphic continuity of the Warrawoona Group in the early Archaean Coppin Gap Greenstone Belt, Pilbara (Australia). The Warrawoona Group in this belt consists of ultramafic, mafic, intermediate and felsic rocks, with minor amounts of banded iron formation and silicified sediments. A major part of the rock succession is made up of intermediate to felsic volcanic rocks of the Duffer and Panorama Formations. The bulk of the Duffer Formation consists of massive quartz and plagioclase porphyritic rocks. The interbedding of these porphyries with agglomerates, banded iron formation and thin ash layers suggests that they have an extrusive origin. Field observations and geochemistry show that the nature of volcanism changed from dacitic to more andesitic from base to top within the Duffer Formation.

Nowhere in the study area do the rocks form a continuous stratigraphic sequence. Rather, the Warrawoona Group consists of slices of stratigraphy, bounded by deformation (mostly shear) zones. Despite the presence of such zones, new U-Pb zircon dating and geochemical analyses show that the chronostratigraphical succession in the Coppin Gap Greenstone Belt has not been fundamentally disturbed. The precision of the U-Pb SHRIMP ages is insufficient, however, to rule out small hiatuses or duplications of stratigraphy on the order of a few million years.

The Coppin Gap Greenstone Belt is cut by numerous west-block-down normal faults. They occur at the scale of the entire belt and, at a smaller scale, as arrays in several levels within the Warrawoona Group. Some of the normal fault arrays were syndepositional. Early gravitational collapse of a large part of the Duffer Formation in the study area also implies upper-block-west transport. Syndepositional extension of Warrawoona Group deposits occurred throughout the East Pilbara, and extension is therefore interpreted to have been the dominant tectonic regime at that time. In the Coppin Gap Greenstone Belt, the extension had a consistent, or regular, west-block-down orientation for a minimum period of 20 Ma.

Introduction

The major part of the rocks in the early Archaean Coppin Gap Greenstone Belt (Pilbara, Western Australia, Fig. 3.1) belongs to the Warrawoona Group. The Warrawoona Group was deposited roughly in the period between 3490 Ma (North Star Basalt; Beintema, 2003) and 3346 Ma (Euro Formation; Nelson, 2001, interpretation by Van Kranendonk et al., 2002). The major part of the succession in the Coppin Gap Greenstone Belt was deposited during the first half of this interval (i.e. > 3446 Ma, for dating see below). Deformation in other greenstone belts of the East Pilbara during that time interval includes local tilting of the Coonterunah Group (pre-3463 Ma, Buick et al., 1995; Green et al., 2000), and syndepositional normal faulting (ca. 3460 Ma, Coongan Greenstone Belt, Zegers et al., 1996; ~ 3490 Ma, North Pole Dome, Nijman et al., 1998a).

For the Coppin Gap Greenstone Belt, extensional deformation was proposed for the lower part of the Warrawoona Group (where the Coppin Gap Greenstone Belt bends into the N-S trending Marble Bar Greenstone Belt, Van Haaften and White, 1998; Beintema, 2003) and the upper part of the Warrawoona Group (Nijman et al., 1998b; Kloppenburg, 2003). The nature of the tectonic regime during deposition of the Duffer Formation (~3466 Ma, see Geochronology), which forms a major part of the Warrawoona Group in the Coppin Gap Greenstone Belt, is less clear.

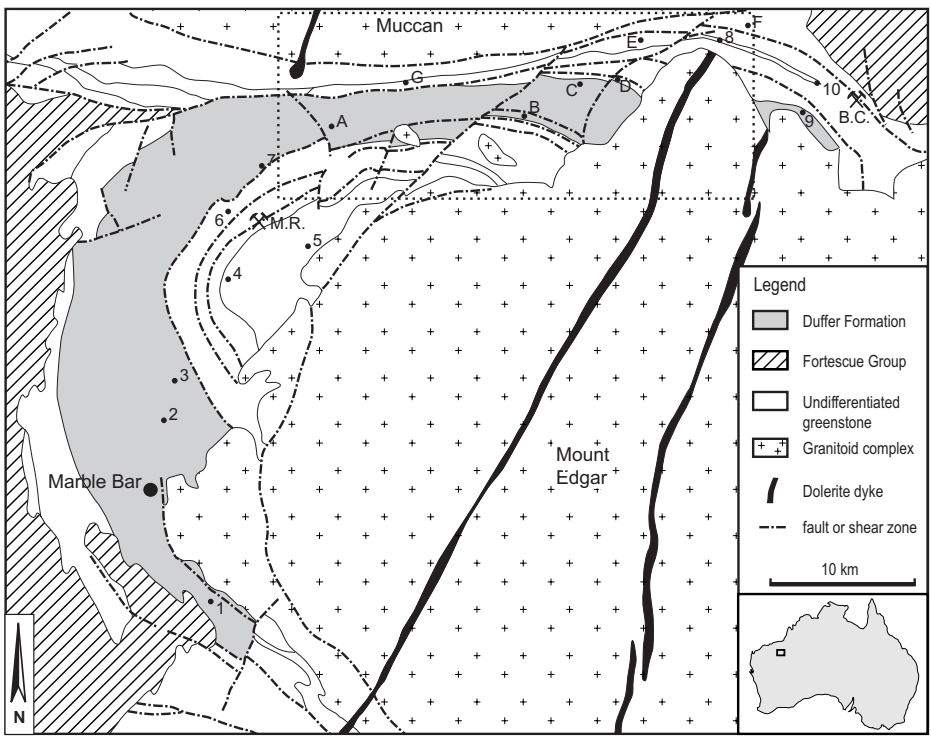

Figure 3.1: Schematic geological map of the N-S trending Marble Bar belt and the E-W trending Coppin Gap greenstone belt and surrounding granitoid complexes (modified after Nijman et al., 1998b; Van Haaften and White, 1998; Van Kranendonk et al., 2001b). Letters refer to new dates presented in this study, numbers refer to previously published dates of the Warrawoona Group in this area. Geochronology details and references in Table 3.1. M.R. = McPhee Reward mining area, B.C. = Bamboo Creek mining area. Outlines of Fig. 3.2 indicated with dashed rectangle.

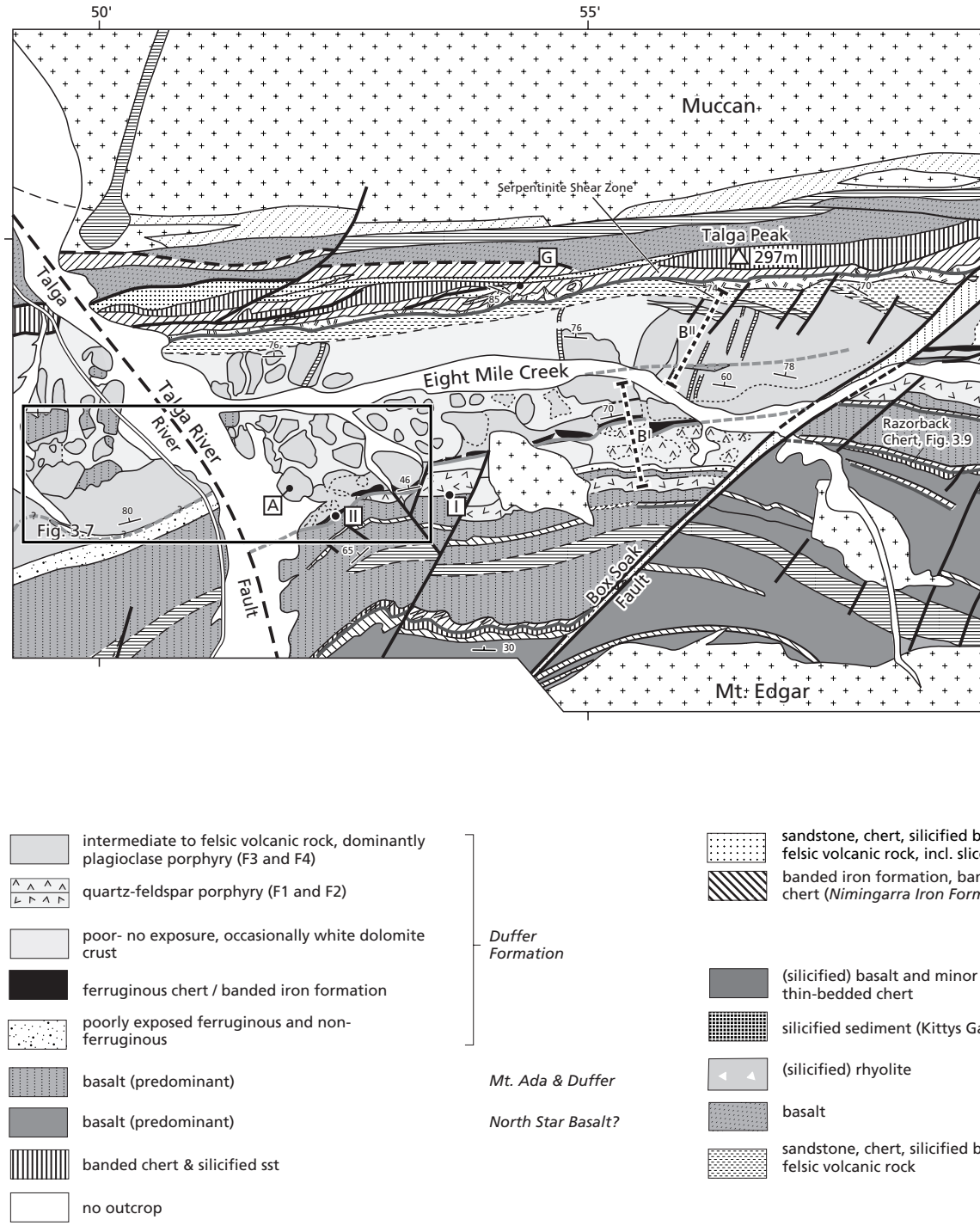

Figure 3.2: Geological map of the central part of the Coppin Gap Greenstone Belt (loc. indicated in Fig. 3.1).

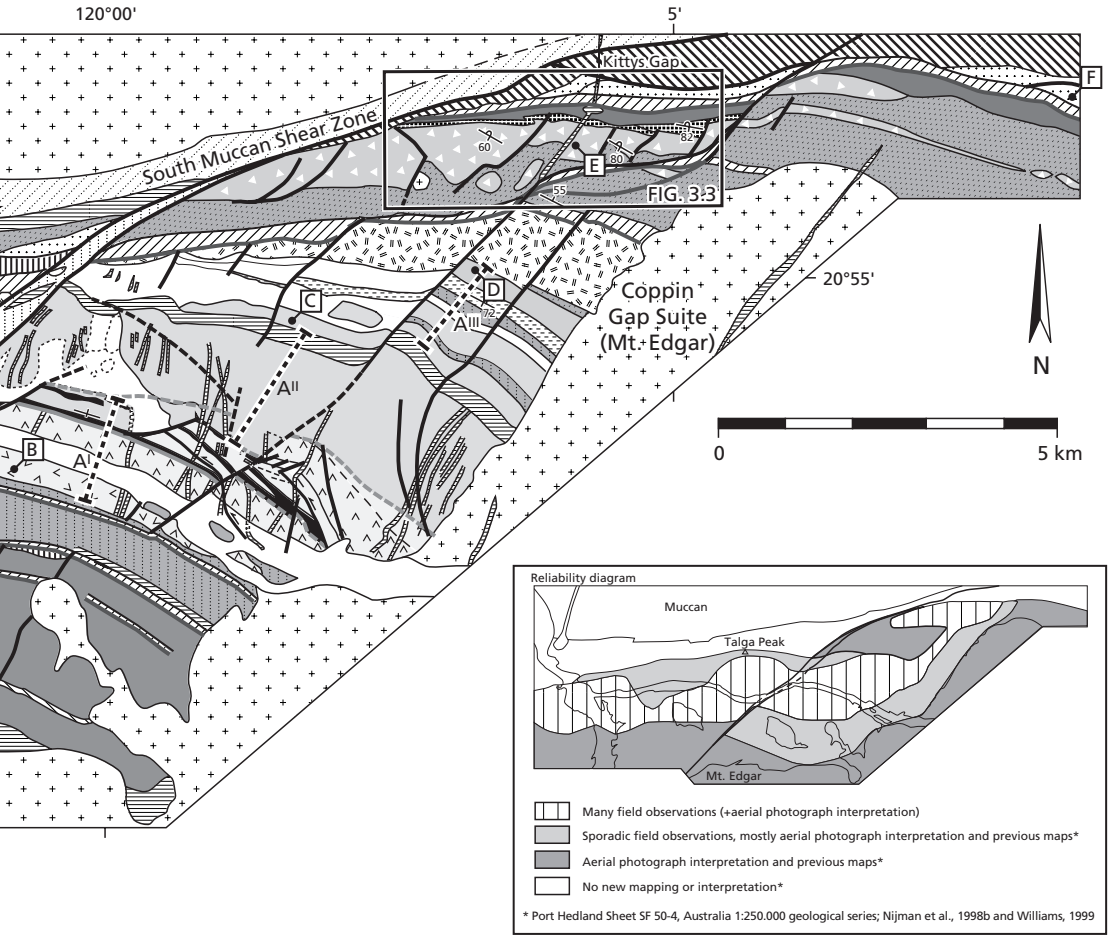

asalt and minor
es of *Wyman*
ded and ferruginous
ation)

Gorge Creek Group

ntercalated

Euro Formation

p Chert)

Panorama Formation

Apex Formation and undifferentiated along northern limb of the belt

asalt and minor

Towers Formation ?

granitoid complex

(meta) gabbro-pyroxenite / dolerite sill or dyke

serpentinised peridotite

fault

A U-Pb dating site

shear zone at granitoid margin

pre-3.3 Ga shear zone

fold / deformation zones and miscellaneous discontinuity zones (dashed) in the Duffer Fm

alteration zone often containing ultramafic rock; may be sheared

fault zone (Box Soak Fault)

To date, structural studies on the Coppin Gap Greenstone Belt and its westward extension towards the Marble Bar Greenstone Belt have mainly addressed the deformation and the stratigraphic continuity of the lowermost rocks in the belt, which belong to the Talga Talga Subgroup (Collins, 1989; Van Haaften and White, 1998; Van Kranendonk et al., 2001a; Beintema, 2003). Both these studies and the study of Nijman et al. (1998b) indicate that several structural discontinuities are present in the Coppin Gap Greenstone Belt. However, the degree of disruption of the original stratigraphic sequence of the belt is contentious. Nijman et al. (1998b) and Van Haaften and White (1998) suggest that major duplications of parts of the stratigraphy might have taken place. In contrast, Van Kranendonk et al. (2001a) and Beintema (2003) believe that there is little disruption and that the sequence is predominantly coherent. The latter three references refer only to the lower part of the stratigraphy of the Coppin Gap Greenstone Belt, where it bends into the Marble Bar Greenstone Belt.

Based on new field observations, U-Pb SHRIMP dating and geochemical studies, this study revisits the above-mentioned issues of 1) the tectonic regime during deposition of the Warrawoona Group and 2) the stratigraphic continuity of the Warrawoona Group deposits in the Coppin Gap Greenstone Belt. The observations are focussed on the Duffer and Panorama Formations, which contain some of the earliest preserved extrusive felsic volcanics in the East Pilbara.

General geology of the central Coppin Gap Greenstone Belt

The Coppin Gap Greenstone Belt (defined by Nijman et al., 1998b) is an east-west oriented greenstone belt, between the Mt Edgar and Muccan Granitoid Complexes (Fig. 3.1). It comprises a tightly folded synclinorium, with a well-preserved southern limb and a sheared northern limb. Along the southern limb the bedding is oriented roughly east-west, the dips are near-vertical and the younging direction is to the north. From south to north the southern limb provides a cross-section through part of the early Archaean crust.

The major part of the rocks along the southern limb of the syncline belong to the Warrawoona Group, which is, from base to top, subdivided into the North Star Basalt, McPhee, Mt. Ada, Duffer, Towers, Apex, Panorama, Euro Basalt and Wyman Formations (e.g. Van Kranendonk et al., 2002). The Warrawoona Group is overlain by Gorge Creek Group sediments. Regional metamorphism is low-grade, except adjacent to the granitoid complexes (cf. Williams, 1999).

The felsic rocks in the Coppin Gap Greenstone Belt occur dominantly in the Duffer and Panorama Formations. The Duffer Formation forms a major part of the Warrawoona Group in the Coppin Gap Greenstone Belt (Fig. 3.2). The Panorama Formation is exposed in the northeastern part of the Coppin Gap Greenstone Belt (south of Kittys Gap, Fig. 3.2), which was studied by Nijman et al. (1998b). They termed the rock-suite 'P-assemblage' because its correlation with the Panorama Formation was uncertain, due to the presence of important shear zones below and above the assemblage and elsewhere in the Warrawoona Group rock succession. Williams (1999) mapped the rocks in the Kittys Gap area as Panorama Formation, which is confirmed by a new U-Pb zircon date (see below).

The most prominent structural feature in the study area is a large NE-SW oriented west-block-down normal fault (Fig. 3.2), which divides the area into an eastern and a western part. This fault is termed the Box Soak Fault (BSF; after the abandoned Box Soak Well) in this chapter. Previously, it was referred to as the Talga Fault (Kloppenburg, 2003), but this may cause confusion with another inferred major fault along the Talga River (Fig. 3.2), which is called the Talga River Fault in this chapter.

East of the BSF, the stratigraphy in the study area is more complete than west of the fault. However,

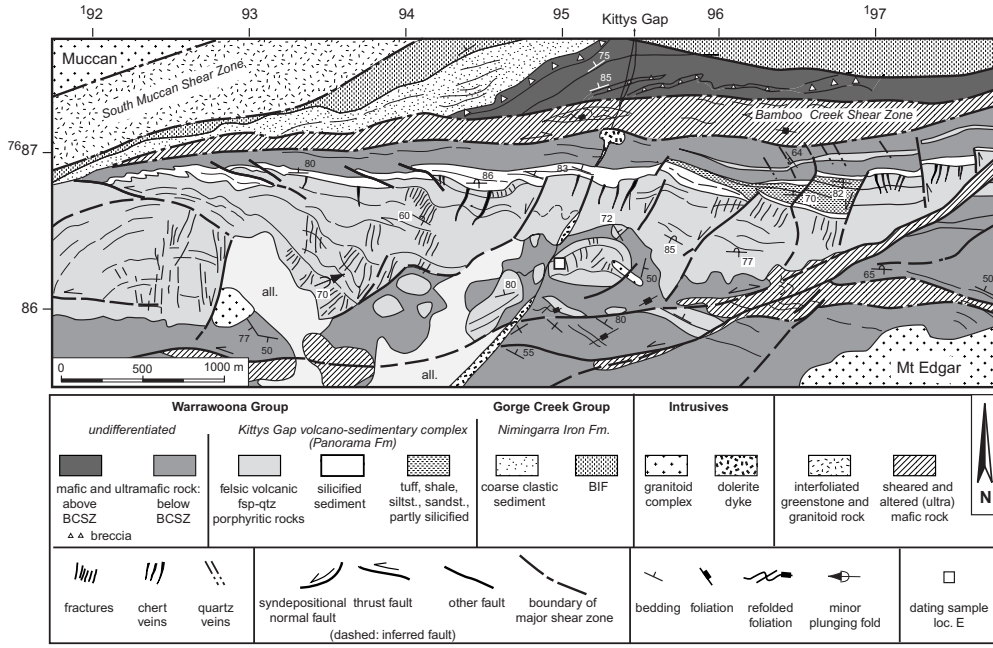

Fig. 3.3: Geological map of the normal-faulted Kittys Gap volcano-sedimentary complex (Panorama Formation) between mafic and ultramafic rocks of the Apex Formation (below) and the Euro Formation (above). The Euro Formation is cut by the Bamboo Creek Shear Zone (BCSZ). Hanging-wall blocks in the western part of the fault array have been rotated and deformed into rollover anticlines. Sediment wedges at the top of the complex in that area have been thrust over each other in westward direction. Eastward, the sediment wedges tend to onlap the previous ones. Location indicated in Fig. 3.2. Grid numbers refer to Australian Map Grid zone 51.

on both sides of the fault the rock sequence is interrupted by deformation zones (see below). These zones are bedding-parallel, or cut the rock succession at a low angle. Particularly along the eastern bank of the Talga River, the map view of the Duffer Formation differs from its general appearance. Here, well-preserved outcrops of Duffer Formation are surrounded by poorly to non-exposed areas (with occasional dolomite crusts). East of the BSF and in the western extension of the Coppin Gap Greenstone Belt outside the map area, the Duffer Formation is more uniformly exposed.

New data on the Coppin Gap Greenstone Belt

Most new field observations in the central part of the Coppin Gap Greenstone Belt (Fig. 3.2) concern the Duffer Formation and its contact with the underlying Mt. Ada Basalt. Also, the Panorama Formation in the Kittys Gap area (key area III of Nijman et al., 1998b) has been mapped in more detail (Fig. 3.3).

Stratigraphy

Duffer Formation

Since the Duffer Formation is cut by bedding-(sub)parallel deformation zones in the Coppin Gap Greenstone Belt (see Structure), it cannot be represented by one stratigraphic column. Therefore, the

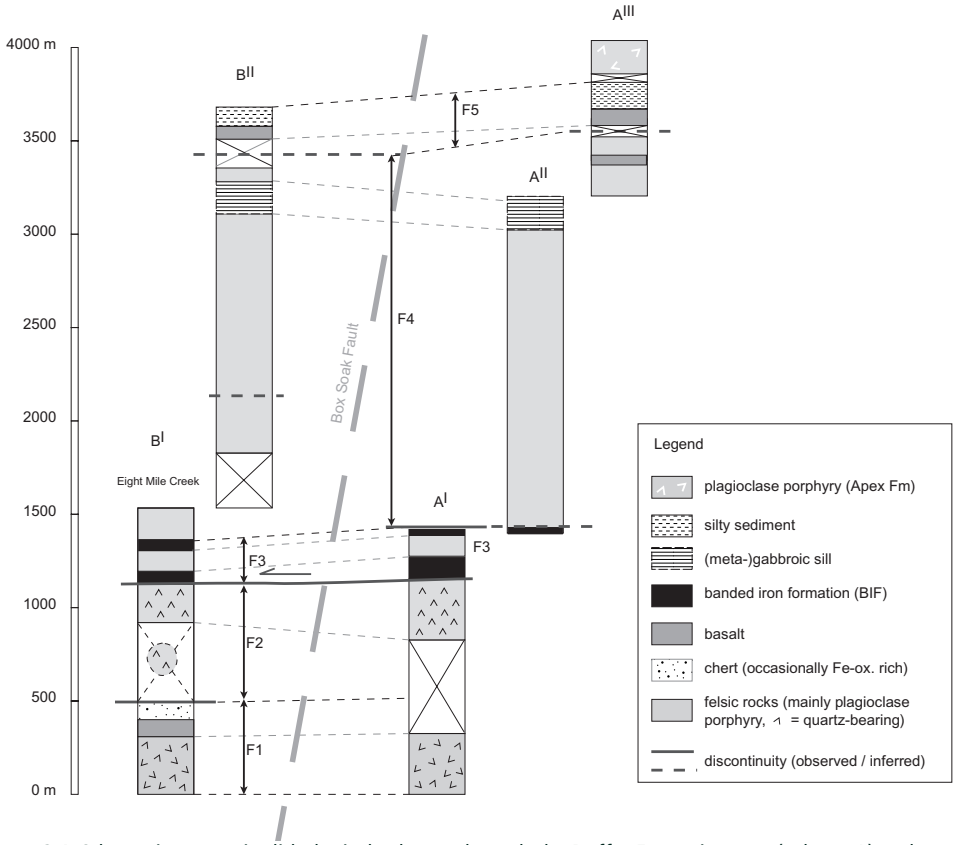

Figure 3.4: Schematic composite lithological columns through the Duffer Formation east (column A) and west (column B) of the Box Soak Fault. Locations of sections are indicated in Fig. 3.2. 'Fragments' of Duffer stratigraphy are number F1-F5.

formation will be described on the basis of two composite stratigraphic columns, on the east and west side of the BSF respectively (A and B, Figs 3.2 and 3.4). The fragments comprising the stratigraphy (F1-F5) are bounded by deformation zones and can be correlated across the BSF (Fig. 3.4).

Fragment 1 (F1). In both composite columns, the lowermost unit of the Duffer Formation is formed by an up to ~300 metre thick quartz-plagioclase porphyry[1] (Fig. 3.4). The quartz phenocrysts (average size 0.5 cm, occasionally up to 1 cm) and twinned plagioclase phenocrysts (average size 0.3 cm) are surrounded by an extremely fine-grained, dark, groundmass with a glassy field appearance. Most of the quartz-plagioclase porphyry is massive, and lacks stratification. Columnar jointing was observed about 1 km east of the BSF. The quartz-plagioclase porphyry shows up on satellite images as distinctly different from the other felsic volcanics in the Coppin Gap Greenstone Belt, probably because of its high quartz content. U-Pb SHRIMP analysis of this unit on the eastern side of the BSF has yielded a date of 3465±4 Ma (loc. B, Figs 3.1 and 3.2; details on dating in Fig. 3.5b, Tables 3.1 and Appendix B).

[1] In this thesis, the term porphyry is used for igneous rocks that are characterised by mm-sized phenocrysts hosted by abundant very fine-grained groundmass.

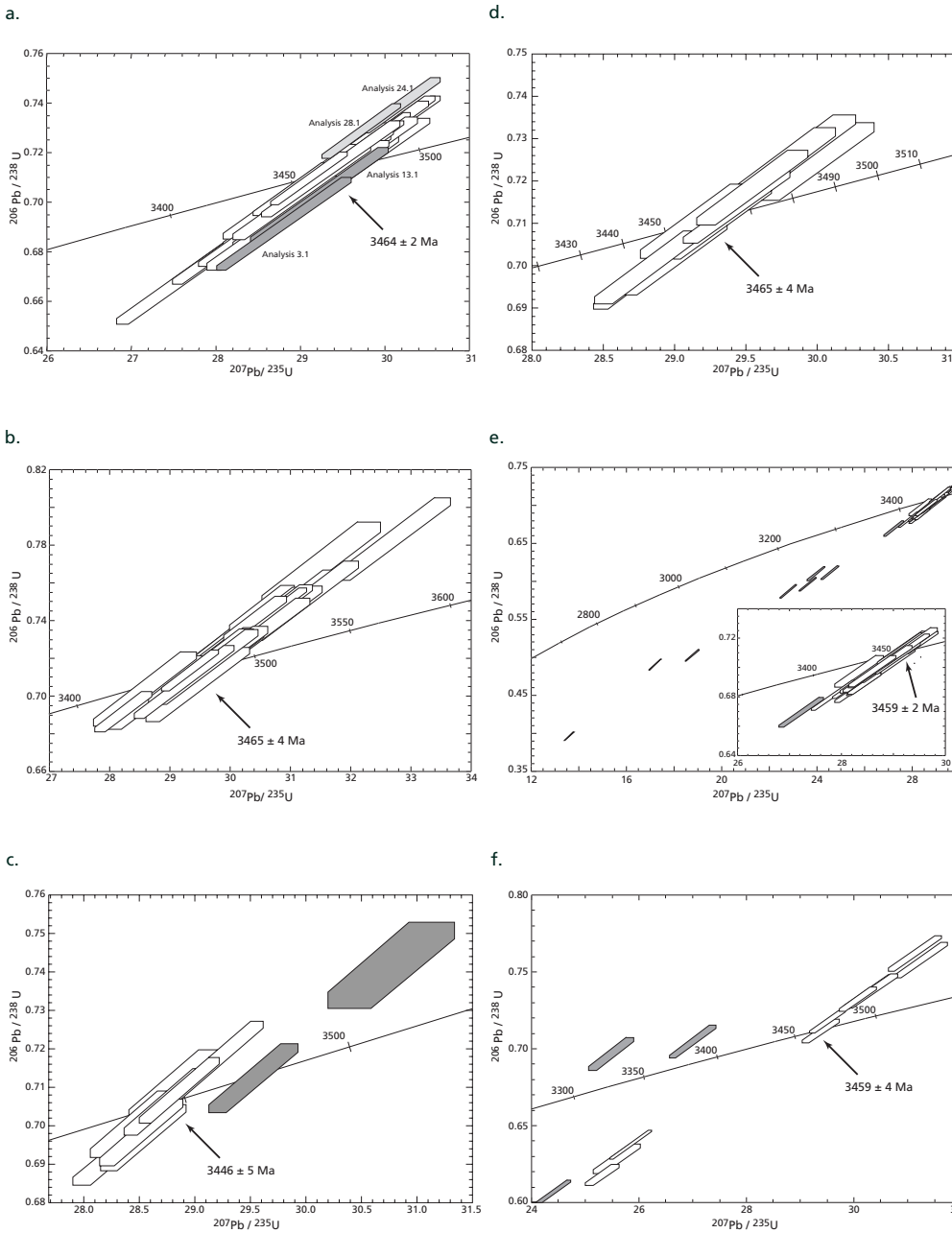

Figure 3.5a-f: Concordia diagrams of U-Pb SHRIMP dating results obtained at Curtin University of Technology in Perth (Australia), for samples A, B, C, D, E, and F respectively. For additional data see Appendix B. Locations of dated samples in Figs 3.1 and 3.2. Data in unfilled error ellipses were used to calculate the mean age. Data point error ellipses are 95% conf.

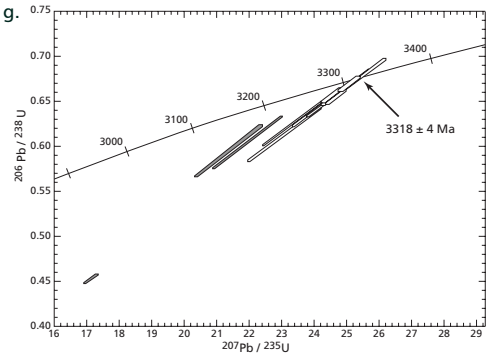

Figure 3.5g: Concordia diagram of U-Pb SHRIMP dating results obtained at Curtin University of Technology in Perth (Australia), for sample G. For additional data see Appendix B. Location of sample in Figs 3.1 and 3.2. Data in unfilled error ellipses were used to calculate the mean age. Data point error ellipses are 95% conf.

In column A, one outcrop of fine-grained mafic to ultramafic rock (containing 10 cm-sized enclaves with a larger grain size) is exposed immediately north of the quartz-plagioclase porphyry (~750 m east of column A, Fig. 3.2). The remainder of the interval north of the quartz-plagioclase porphyry is obscured by Eight Mile Creek. In column B (Fig. 3.4), the quartz-plagioclase porphyry is overlain by ~150 m of poorly exposed, fine-grained mafic rocks and dark-coloured chert (mostly present as debris). The succession ends with strongly foliated, very fine-grained, bright green rocks, which are in most places altered into carbonate, and occasionally incorporate quartz lenses (see Section Structure). In the same interval and to the north, scattered outcrops of quartz-plagioclase porphyry and banded iron formation (BIF) occur in an otherwise poorly exposed interval.

Fragment 2 (F2). A second fragment of stratigraphy on the eastern side of the BSF is formed by a ~200-300 m thick massive, silicified dacite with abundant plagioclase phenocrysts (size ~4 mm). Quartz phenocrysts are smaller (≤ 1 mm) and less abundant than plagioclase. The groundmass is grey-black and has a glassy field appearance. At one location east of the BSF the dacite is columnar jointed.

Loc.	*Sample number*	*Age (Ma)*	*AMG ref. / coordinates*		*Reference*
A	A (VM00-255)	3464±2	50KQB 981799		this study[1]
B	B (W95-28)	3465±4	50KRB 105813		this study[1]
C	C (W98-5)	3465±4	51KSS 913836		this study[1]
D	D (VM00-124)	3459±2	51KSS 935843		this study[1]
E	E (JW95-001)	3446±5	51KSS 950863		this study[1]
F	F (W94.22.3)	<3459±4	51KTS 025872		this study[1]
G	G (W95-36)	<3318±4	50KRB 022835		this study[1]
1		3465			Thorpe, 1999 written comm. (in Van Kranendonk et al., 2001b)
2	UWA-98076	3466±4	S 21°06'27''	E 119°45'28''	McNaughton et al., 1993[1]
3	GSWA 148509	3468±2	S 21°05'56''	E 119°46'30''	Nelson, 2000[1]
4	GSWA 148498	3477±2	S 21°03'11''	E 119°47'09''	Nelson, 2000[1]
5	96JW022	3490±15	7673414	795935	Beintema 2003[2]
6	GSWA 148500	3469±3	S 20°59'35''	E 119°49'19''	Nelson, 1999[1]
7	ANU89-332	3463±2	S 21°57'12''	E 119°50'59''	McNaughton et al., 1993[1]
8	GSWA 100511	3458±2	AMG 997866		Thorpe, 1991 written comm. (in Williams, 1999)[3]
9	GSWA 100512	3471±5	S 20°56'20''	E 120°10'09''	Thorpe et al. 1992[3]
10	GSWA 94770	3454±1	S 20°55'16''	E 120°11'01''	Thorpe et al. 1992b[3]
10*	GSWA 94770	3470±2	S 20°55'16''	E 120°11'01''	Thorpe et al. 1992b[3]

Table 3.1: Origin and age of dating samples from the Coppin Gap and Marble Bar Greenstone Belts. Sample locations are indicated in Figs 3.1 and 3.2. Dating method: [1]SHRIMP zircon U-Pb, [2]Ar-Ar, [3]Conventional zircon U-Pb. SHRIMP dating for this study was done at Curtin University of Technology in Perth, Australia, details in Figs 3.5a-g and Appendix B. 10*: Xenocrysts in sample 10.

Fragment 3 (F3). F3 is characterised by the intercalation of several layers of banded iron formation (BIF) in the felsic sequence. The base of F3 is formed by a BIF unit, which varies in thickness between 0 and 100 m, and has been folded along most of its exposure (see Structure). In places, small outcrops of plagioclase porphyritic rocks, sandstone or basalt (the latter westward, ~loc. I in Fig. 3.2) occur within the folded BIF unit. The lower BIF unit is overlain by ~200 m of felsic rocks, including agglomerate (cm to 30 cm-sized plagioclase porphyry and vesicular felsic clasts in a greenish groundmass) and plagioclase porphyry (2-3 mm phenocrysts in a light green groundmass with a glassy field appearance). North of the felsic unit, a poorly exposed interval has a similar characteristic dark appearance on aerial photographs as the lower BIF unit. In the field a broad zone of tens of metres thick is characterised by dark chert and BIF debris. Occasionally small outcrops of BIF are present, which generally have a strong bedding-parallel cleavage. The entire interval is termed BIF 2. Ca. 800 m east of column A, thin BIF layers are interbedded with plagioclase porphyritic rocks in an interval twice as thick as F3.

Fragment 4 (F4). F4 comprises the main volume of felsic rocks of the Duffer Formation. The rocks mainly consist of massive, dacitic to andesitic plagioclase porphyry, and generally lack stratification. In most rocks, plagioclase phenocrysts are abundant (15-40 %) and up to 2-5 mm in size. They are set in a very fine-grained, grey-green groundmass that often also contains small pyroxene phenocrysts (≤ 1 mm), and, in places, minor quartz (mostly in the lower part of the unit). Agglomerate occurs occasionally throughout the lower two-thirds of the main felsic unit. The components in the agglomerate include coarse plagioclase porphyry, fine-grained intermediate rock resembling the groundmass and flattened vesicular felsic rocks. They have average sizes of 2-5 cm. Rarely, up to tens of cm-thick, fine sand-sized, laminated tuff layers are intercalated in the plagioclase porphyry. In the upper half of F4, massive, vesicular, and occasionally pillowed basalts are interbedded with the plagioclase porphyries (e.g. Fig. 3.6a). In the central and eastern part of the area, the top of F4 is intruded by a (meta)gabbro-

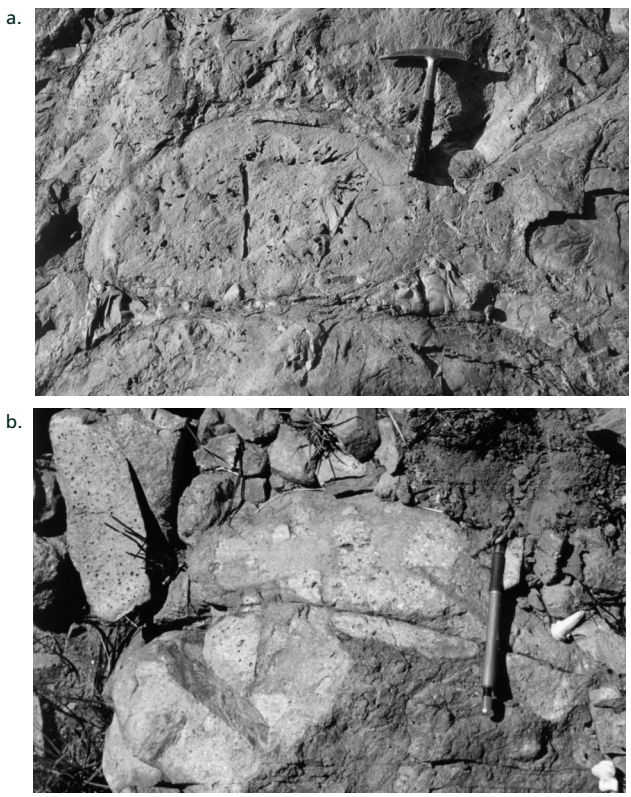

Figure 3.6: a. Vesicular pillow basalts near the top of the Duffer Formation. b. Pumice fragments in matrix at loc. VM00-67, in the Duffer Formation just east of the Talga River (Fig. 3.7).

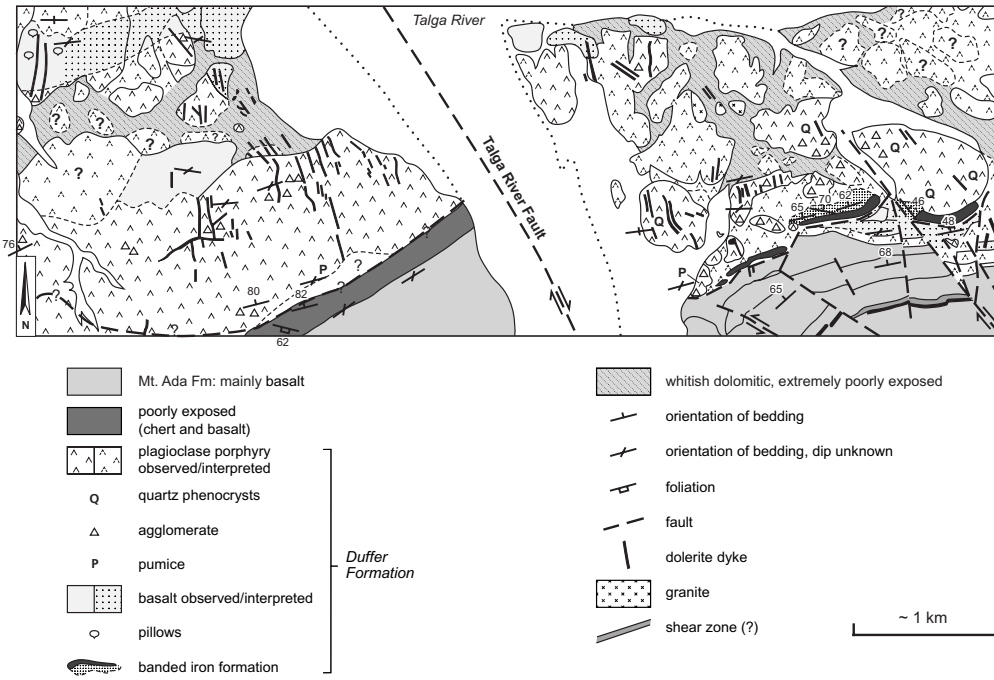

Figure 3.7: Detailed map of the lower part of the Duffer Formation in the western part of the study area, where it has a fragmented appearance. For location see Fig. 3.2.

pyroxenite sill (Fig. 3.2). U-Pb SHRIMP dating of the felsic rocks above this sill (loc. C, Fig. 3.2) yielded an age of 3465±4 Ma (Fig. 3.5c and Appendix B).

Fragment 5 (F5). F5 commences with a black-green, fine-grained, altered (chloritised and serpentinised) basalt. The basalt is poorly exposed, and generally has a massive appearance. Vesicles were observed in one location. The basalts are overlain by very poorly exposed, grey to reddish, silty to fine-sand sized sediments. The sediments are well bedded, and in places silicified. West of the BSF the basalts and silty sediments are truncated by a serpentinised peridotite sill, which is bounded by shear zones in the major part of the area (see Fig. 3.2 and Structure; the shear zone is hereafter called the 'Serpentinite Shear Zone').

Westward correlation. The lowermost felsic unit of the Duffer Formation west of the Talga River is ~860 m thick, and consists mainly of plagioclase porphyry (no quartz phenocrysts were observed) and agglomerate. Both in thickness and lithology, this unit resembles the main felsic unit in F4 in columns A and B. Near its base, the felsic unit contains pumice fragments (loc. in Fig. 3.7). Pumice fragments also occur in the Duffer Formation immediately east of the Talga River (Figs 3.6b and 3.7). Since pumice fragments have not been observed elsewhere in the study area, the pumice-bearing level is used to correlate the sections on either side of the Talga River. The quartz-porphyry and the BIF units that characterise columns A and B are absent west of the Talga River (see also Structure). Instead, the felsic to intermediate rocks of the Duffer Formation west of the Talga River are underlain by a poorly exposed interval that contains small outcrops of greenish-grey, silt-sized, finely laminated chertified sediments and scattered cherty debris.

Apex, Panorama and Euro Formation

The most complete succession of Warrawoona Group rocks is exposed close to the contact with the Coppin Gap Suite of the Mt Edgar Granitoid Complex (Fig. 3.2, segment AIII). The basalts and silty sediments (F5) are, after an unexposed interval, overlain by a dominantly plagioclase porphyritic unit (Fig. 3.2, assigned to the Apex Formation by Williams, 1999). Near the base of this unit, a finely laminated chert (~20-30 cm) is overlain by a ca. 3-4 m thick agglomeratic interval. Fragments in the agglomerate range from a few cm up to >10 cm, and are generally sub-rounded to rounded. The remainder of the unit consists of altered, light-grey andesite, which contains (altered) plagioclase, hornblende and pyroxene phenocrysts. The andesite (loc. D, Fig. 3.2) was dated at 3459±2 Ma (Fig. 3.5d and Appendix B). The interval is truncated on the northern side by a serpentinised peridotite sill.

North of the serpentinised peridotite sill, which is partly surrounded and affected by shear zones (see Structure), a slice of stratigraphy comprising mainly basalts and felsic volcanics has been preserved. The lowermost unit in this succession, a severely chloritised basalt (Apex Formation according to Williams, 1999) was not studied in detail during this study. It is overlain by a sequence of felsic volcanic and volcaniclastic deposits (Fig. 3.3), which mainly consists of altered and in places flow-banded quartz-feldspar porphyries (rhyolite to rhyodacite). Feldspar phenocrysts range in size from 1-5 mm and have mostly been altered to sericite. The unit contains minor amounts of agglomerate and pyroclastic rocks, the latter of which only occur in the top of the unit. U-Pb dating of a sample of felsic rocks from the base of the quartz-feldspar porphyry (loc. E, Fig. 3.2) yielded and age of 3446±2 Ma (Fig. 3.5e and Appendix B). The felsic rocks are overlain by silicified sediments that were deposited in shallow water (Chapter 4). Together, the felsic rocks and the silicified sediments of the Panorama Formation are called the Kittys Gap volcano-sedimentary complex (KG-vsc). The KG-vsc is overlain by serpentinised and carbonatised massive basalt (Euro Formation, Williams, 1999), which show occasionally hyaloclastic brecciation and columnar jointing. The Euro Formation is cut by the Bamboo Creek Shear Zone (BCSZ, Fig. 3.3; Nijman et al., 1998b; Williams, 1999; the westward extension of the BCSZ described by Zegers, 1996 and Zegers et al., 2002).

Deposits overlying the Bamboo Creek Shear Zone

The rocks overlying the Bamboo Creek Shear Zone and the Serpentinite Shear Zone (west of the BSF) have not been studied in detail. They comprise slices of Warrawoona Group and Gorge Creek Group, which are in turn unconformably overlain by younger Gorge Creek Group sediments (Nijman et al., 1998b; Williams, 1999). Two new U-Pb ages were obtained from these rocks to better constrain the timing of events in the Coppin Gap Greenstone Belt.

A silicified, banded sandstone ~6 km east of Kittys Gap (loc. F, Fig. 3.2) from a unit mapped as Gorge Creek Group (Williams, 1999) contains a population of detrital zircons of 3459±4 Ma (Fig. 3.5f and Appendix B). However, two other groups of analyses from this banded chert sample show significantly younger ages; 3280±13 Ma and 3352±4 Ma. Of these last two analyses, although discordant, the former age is interpreted as the maximum age of deposition of the banded cherts (highly discordant analyses were not taken into account, see appendix).

Westward, in the Talga Peak range, a zone of deformed and discontinuous rock units is exposed above the Serpentinite Shear Zone. A feldspar porphyry in this zone (loc. G, Fig. 3.2) was previously mapped as belonging to the 'P-assemblage' (Nijman et al., 1998b). Based on the U-Pb age of 3318±2 Ma (Fig. 3.5g and Appendix B) this unit is now placed in the Wyman Formation (cf. Nijman et al., 2001).

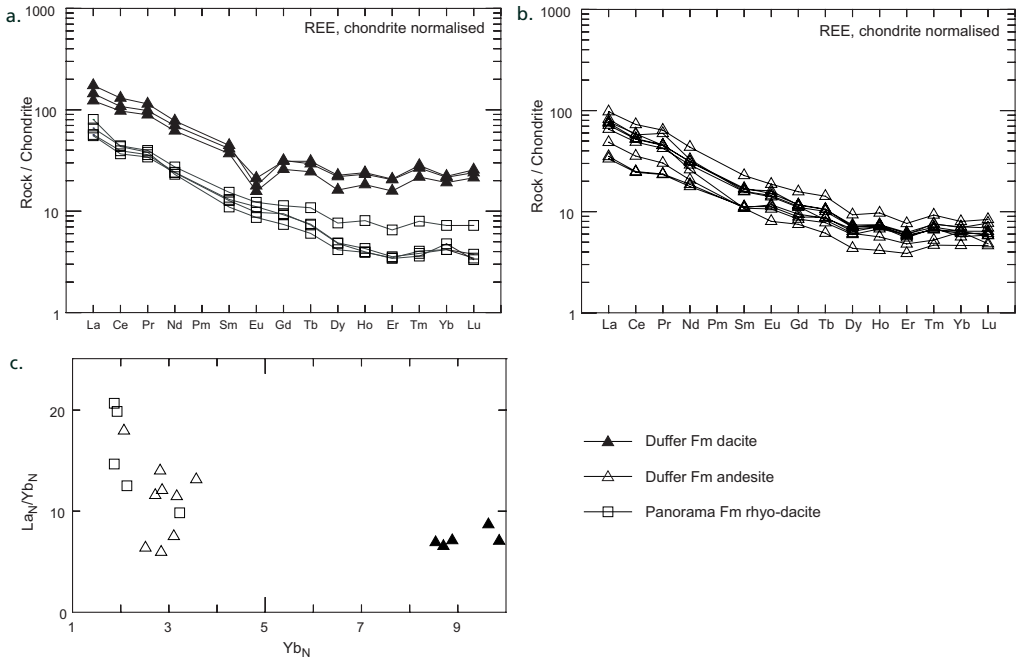

Figure 3.8: REE patterns for Duffer Formation dacites and Panorama Formation rhyodacite (a) and Duffer Formation andesite (b) samples. Concentrations are chondrite normalised (Nakamura, 1974). c. Chondrite normalised La/Yb ratio versus normalised Yb content. Note the difference between dacitic Duffer Formation and rhyodacitic Panorama Formation rocks.

Geochemistry

An extensive description and interpretation of the geochemistry of the Warrawoona Group in the Coppin Gap Greenstone Belt is beyond the scope of this thesis. However, a few Rare Earth Element (REE) diagrams (Fig. 3.8) are given to illustrate the difference between the felsic volcanic rocks of the Duffer and Panorama Formations. The REE patterns show that the Duffer dacites (from the lower part of the Duffer Formation) are characterised by a Eu-anomaly and a relatively flat trend in the heavy REE (Gd-Lu, Fig. 3.8a). Duffer andesites (from the middle and upper part of the main felsic Duffer unit in F4) have lower REE abundances, and do not have a negative Eu-anomaly, although the remainder of the REE patterns are similar to the dacites (Fig. 3.8b). The Panorama rhyodacites also have lower REE abundances than the Duffer dacites, and show no Eu-anomalies. Most samples have less flat heavy REE trends than the Duffer dacites (Fig. 3.8a). The latter have a much higher Yb content, and generally show lower (La/Yb)n ratios than Panorama rhyodacites (Fig. 3.8c).

Structure

Since the focus of this study is on the earliest deformation phases, the descriptions in this section will also be limited to early (i.e. pre-3.3 Ga) structures. The two major early structural features in the study area are normal faults, in places organised in arrays (with fault traces now oriented ~NNE-SSW), and bedding-parallel to low-angle deformation zones.

Normal faults

The Coppin Gap Greenstone Belt shows several arrays of west-block down normal faults, at different levels of the stratigraphy. Nijman et al. (1998b) described the syndepositional character of an array of normal faults in the Kittys Gap area, in the northeastern part of the study area, indicating that at least part of such normal faults formed early.

Kittys Gap volcano-sedimentary complex. The normal-faulted KG-vsc (see Stratigraphy and Fig. 3.3) is located between the BCSZ and a complex basal detachment zone at about 1 km below the top of the unit, into which the listric normal faults appear to merge (Fig. 3.3). The best evidence for the syndepositional character of the faults is the wedge-shaped character of the sedimentary sequence at the top of the KG-vsc; the thickness of the sediments increases eastward, in the hanging walls of the faults. The most obvious example of the westward increase in thickness is the siltstone-sandstone-shale wedge in the eastern part of the map area (Fig. 3.3). In this area, the sediment wedges onlap westward onto the previously deposited sediments. In the western part of the area, wedges of silicified sediments have been slightly thrust over each other in westward direction. Deposits in the hanging walls at the western end of the fault array show a progressive NW-SE deflection of the strike of bedding. Eastward, the faults extend to higher stratigraphic levels. At the base of the BR-vsc, 100 m-scale blocks of felsic volcanic rock and underlying pillow basalts have been rotated and displaced (cf. Nijman et al., 1998b).

Top Duffer Formation. In the central part of the study area, just south of Talga Peak, the top of the Duffer Formation is cut by an array of west-block-down normal faults. The strike of the gabbro-pyroxenite intrusion and the overlying poorly exposed basalts and silty sediments in this area have been rotated clockwise with respect to the general strike of the Duffer Formation (Fig. 3.2). The normal faults are best visible in the gabbro-pyroxenite intrusion, where the offset along a main fault immediately south of Talga Peak is 325 m. The offset of the serpentinised peridotite sill, slightly higher in the rock sequence, is less (~165 m). Because of the lack of clear reference levels in the felsic parts of the Duffer Formation, and the poor exposure of the basalts and silty sediments, no other reference horizons could be found to correlate the sequences across the faults.

The Razorback Chert. The oldest preserved chert unit of the Warrawoona Group east of the BSF, the Razorback Chert (*new name;* named after the Box Soak Razorback, the topographical ridge formed by the chert), is located approximately 1 km below the Duffer Formation, in a sequence of basalts. It consists of (grey-)black and white banded cherts, occasionally grading into grey-green massive chert, and has been affected by normal faults with west-block-down offsets. Smaller antithetic normal faults occur within the normal faulted blocks (e.g. Fig. 3.9). The chert has a maximum thickness of ~30 m near the eastern part of this outcrop. Westward, the thickness diminishes and the outcrop becomes poorer (Fig. 3.9). Within this fault array, there are smaller-scale deformations. In the eastern part of the outcrop intra-formational folds occur in the chert on a scale of tens of metres (with fold axes dipping ~70-80° N), while it is thrust-faulted in the western part (Fig. 3.9). Folds with fold axes in varying directions occur on a dm to metre-scale (Fig. 3.10).

Normal faults at greenstone belt scale. Normal faults also occur at the scale of the entire greenstone belt, the most prominent fault being the BSF. The offset on the lower part of the fault (~2600 m) is determined from the offset of the contact between the first felsic unit (base of F1) and the underlying basalt. Upward (northward), the offset of the gabbro sill along the fault is ~2200 m. The lack of reliable reference levels makes the offsets along the fault on non-intrusive units higher in the sequence difficult to assess. For a possible correlation of the basal part of the sequence, i.e. below the Duffer Formation, see Discussion.

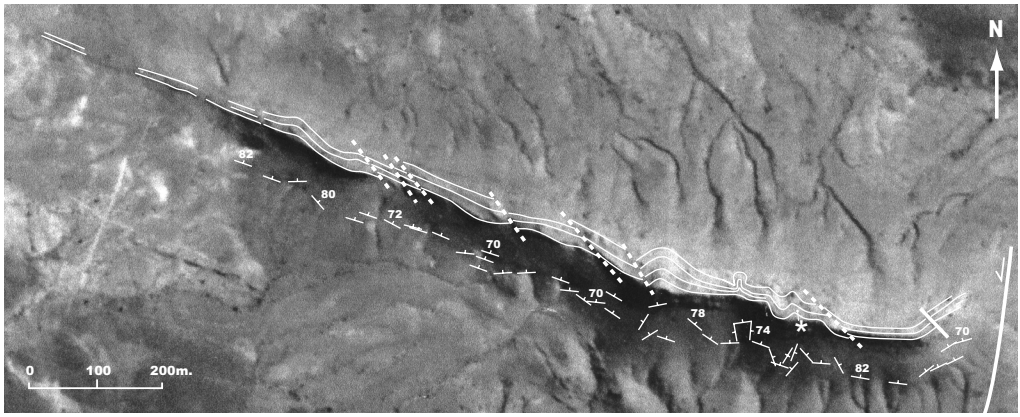

Figure 3.9: Western outcrop of the Razorback Chert, with folding (east) and antithetic normal faults, partly reactivated as thrust faults. Orientations of bedding are plotted below the outcrop. Eastern end of outcrop bends in northern direction, indicating west-block-down movement on normal fault. Approximate location of Fig. 3.10 indicated with an asterisk.

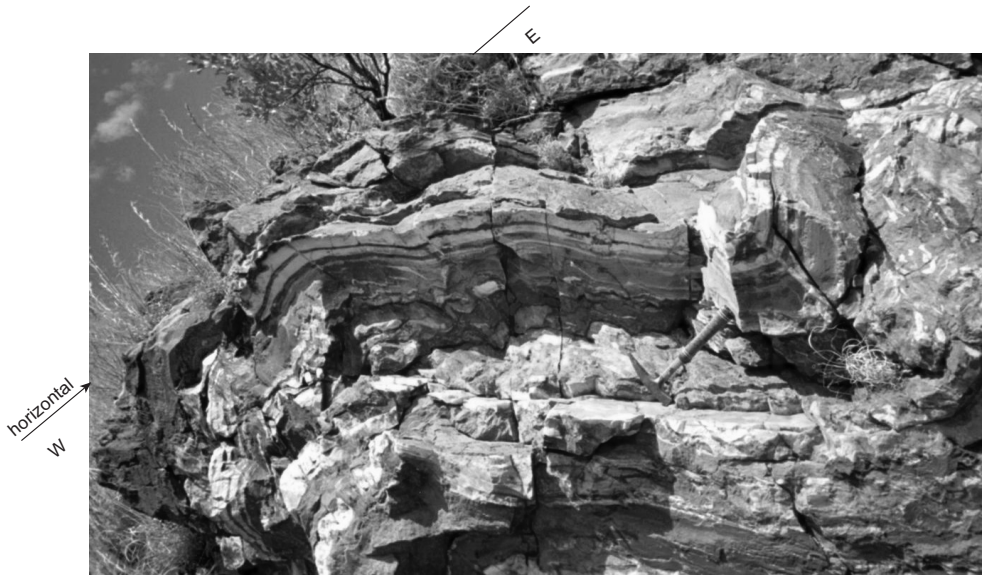

Figure 3.10: Intra-formational, metre-scale folding in the western chert ridge of the Razorback Chert. Approximate location indicated in Fig. 3.9.

Deformation zones

The study area contains a number of bedding-parallel to low-angle deformation zones. These deformation zones can broadly be divided into altered zones characterised by shear foliation, and deformation zones characterised by folding. Both types of deformation zones also show brittle deformation, and occasionally they are transitional. The style of deformation mainly depends on the

lithology. The deformation zones are cut by the 3314±13 Ma (Williams and Collins, 1990) Coppin Gap Suite of the Mt Edgar Granitoid Complex, and were therefore formed early in the history of the Coppin Gap Greenstone Belt.

Foliation zones. The Coppin Gap Greenstone Belt shows a number of approximately bedding-parallel zones that are characterised by intense chemical alteration of mafic and ultramafic rocks to, for example, dolomite, chlorite, talc and serpentinite (cf. Nijman et al., 1998b). On the map (Fig. 3.2) such zones have been marked as shear zones when a foliation was observed in the field, or was previously reported in literature. Other zones have a similar appearance on aerial photographs, but were not visited or were too poorly exposed to establish whether they indeed represent shear zones. They have been marked as alteration zones in Fig. 3.2.

East of the BSF, the basalts between the Razorback Chert and the quartz-plagioclase porphyry at the base of the Duffer Formation are deformed. The deformation is concentrated in a lower zone along the lower contact of the basalt with the Razorback Chert, and an upper zone ~100-200 m below the Duffer Formation. The anastomosing upper zone exhibits a well-developed foliation, orientated approximately E-W and dipping about 90°. The mafic rocks in which the shear zone is developed are preserved in relatively undeformed but strongly altered lenses. In the eastern part of the zone, the first foliation is folded on cm-scale and metre-scale as a result of a subsequent phase of deformation (Fig. 3.11a). Numerous quartz veins, ranging in size from 1 to 20 cm, intersect the shear zone. Occasionally, the veins are boudinaged or folded. To the west, the shear zone ends against the BSF.

At least one shear zone is inferred in the base of the Duffer Formation, between F1 and F2. Strong foliation was observed in the top of F1 at the location of column B. Laterally and upwards, the zone is extremely poorly exposed, and characterised by dolomitic crusts and debris. East of the BSF this interval is obscured by Eight Mile Creek (which indicates that this was a weak zone in the Duffer stratigraphy).

A second relatively well-exposed shear zone, the Serpentinite Shear Zone, occurs at the top of the Duffer Formation, closely associated with the serpentinised peridotite. Both the serpentinised peridotite and the shear zones obliquely truncate the top of the Duffer Formation, thereby cutting off the Duffer Formation stratigraphy to the west. The serpentinised peridotite is enclosed by the shear zone, and also shows some internal shearing. The lower part of the zone is poorly exposed and mainly marked by weathered crusts, but north of the serpentinised peridotite, where the shear zone is developed in basalt, it is locally well exposed (Fig. 3.11b).

Shear zones above this level, above and below the Kittys Gap volcano-sedimentary sequence, have been described by Nijman et al. (1998b).

Fold zones. The second type of deformation zones occurs in the lower part of the Duffer Formation, at the level of the BIF intervals. Roughly speaking the BIF intervals separate two parts of the rock sequence that are orientated slightly differently (Fig. 3.2, east of the BSF). This coincides with the level at which westwards an increasing part of the lower Duffer Formation stratigraphy is absent. At location I (Fig. 3.2, ~3 km west of composite column B), only F1 is observed, followed by approximately ~120m poor exposure (including BIF debris; dashed pattern in Fig. 3.2), before a BIF interval is exposed. Again 2 km to the west, along the east bank of the Talga River (loc. II, Fig. 3.2), a BIF interval is in direct contact with the Mt. Ada Basalt, and the entire lower part of the Duffer Formation is absent. West of the Talga River, the BIF intervals and all Duffer Formation units below it are absent (Fig. 3.2 and Stratigraphy).

In the entire study area, decimetre to metre-scale S-folds are observed in the lower BIF unit (Fig.

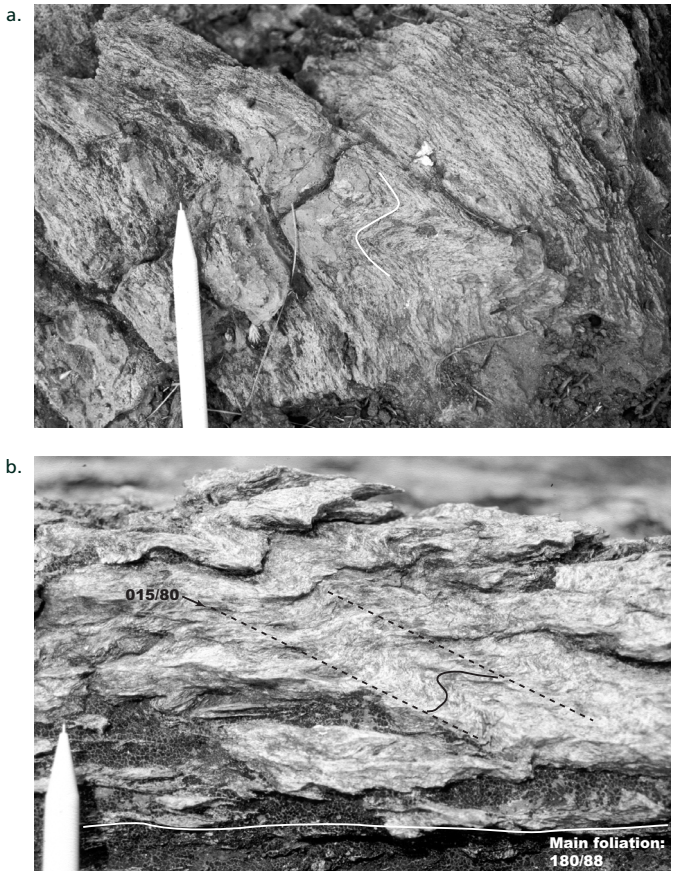

Figure 3.11: a. Cm-scale folding of the foliation in shear zone ~100-200 m below the Duffer Formation. b. Illustration of style of deformation in Serpentinite Shear Zone at the top of the Duffer Formation, south of Talga Peak.

3.12). Fold axes are dominantly subvertical, but vary and in places even become almost horizontal (Fig. 3.12a). At location SV01-70 (column B), the lower BIF unit is buckled and recumbently folded (Figs 3.12b and c). In places, the folded BIF slightly curves around fragmented outcrops of Duffer Formation felsic rocks (e.g. between loc. I and II, Fig. 3.2). Particularly westward, but locally also elsewhere in the area, the BIF unit is foliated.

In the eastern part of the study area, in the vicinity of the contact with the Coppin Gap Suite of the Mt Edgar granitoid complex, the strike of the BIF unit deflects from the general E-W into a more NW-SE orientation, and thrusting has complicated the succession. The deformed BIF is disconformably covered by felsic rocks of F4. Eastwards, more BIF layers become intercalated in the felsic sequence, and unit F3 increases in thickness.

East of the Talga River, the Duffer Formation overlying the BIF unit is exposed in isolated, well-preserved outcrops, surrounded by poorly to non-exposed areas (Fig. 3.7, cf. mega-breccia of Nijman et al., 1998b). West of the Talga River, the exposure is more uniform, and isolated outcrops are only

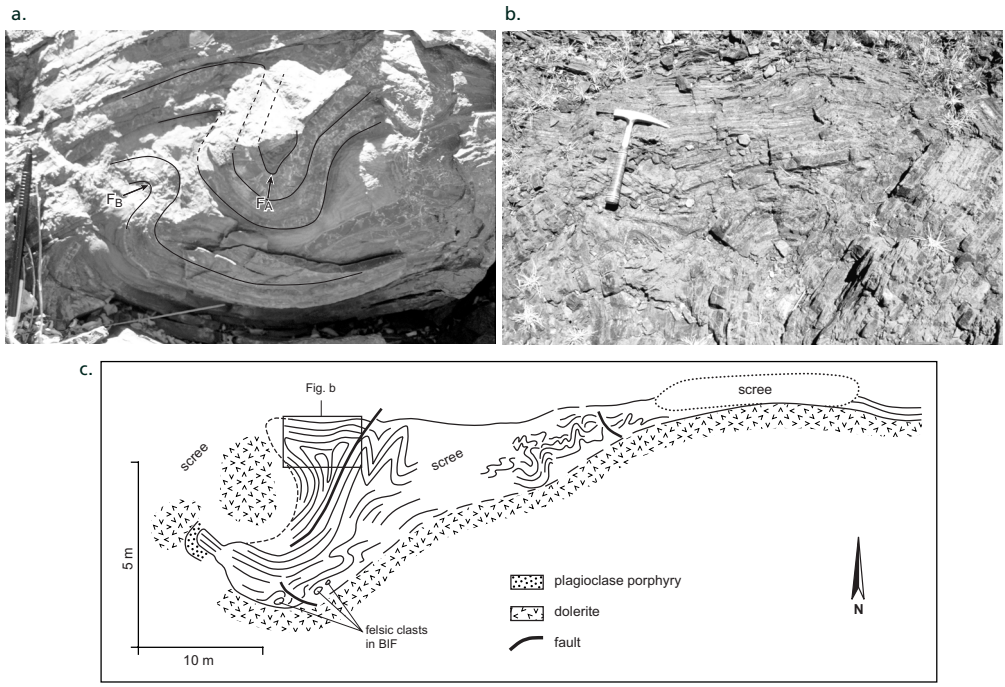

Figure 3.12: Examples of intra-formational folding of the lower BIF unit in the Duffer Formation. a. Folding in BIF unit north of loc. I (Fig. 3.2); fold axis F_A: 36/044; F_B: 44/036. b. Folding with near-vertical fold axes at location ST01-70 (just west of composite column B). c. Sketch of intensely folded lower BIF unit at location ST01-70. Location of Fig. b indicated with a rectangle.

observed in the upper half of the Duffer Formation (Figs 3.2 and 3.7). Lithologically the isolated outcrops are similar to the Duffer Formation at the same stratigraphic level where the outcrop is uniform and undisturbed. A quartz-bearing plagioclase porphyry in one of the lowermost isolated outcrops immediately east of the Talga River (loc. A, Fig. 3.2), was dated at 3464±2 Ma (Fig. 3.5a and Appendix B). The internal bedding of the outcrops, which could only rarely be distinguished (Fig. 3.5), is approximately E-W. The zones between the outcrops occasionally expose approximately N-S oriented dolerite dykes, white, altered dolomitic material and veins or 'crust'-like deposits of dolomite. Most of the area between the outcrops is covered with Quaternary alluvium.

Interpretation and Discussion

Interpretation of the Warrawoona Group rocks

Duffer Formation

Massive quartz and plagioclase porphyritic rocks make up the bulk of the Duffer Formation. Although it is difficult to distinguish whether such porphyries represent lavas or shallow intrusives, the interbedding of the porphyries with agglomerates and thin ash layers and the occasional occurrence of columnar jointing, suggest that they have an extrusive origin. This abundance of felsic to intermediate lavas indicates proximal, near-vent deposition. Nevertheless, no evidence for feeder

dykes or eruptive necks has been found in the study area (cf. DiMarco and Lowe, 1989b for other locations in the East Pilbara). The interbedding of ash layers and the incorporation of pumice indicate that volcanism was occasionally explosive. The generally well bedded to laminated ash layers suggest that deposition took place in a quiet, subaqueous environment. Field observations and geochemistry (Fig. 3.8) show that the nature of volcanism changed from dacitic to more andesitic from base to top within the Duffer Formation. The change to slightly more mafic volcanism is also indicated by the occasional intercalation of pillow basalts in the top of the Duffer Formation. These pillow basalts strengthen the interpretation of subaqueous deposition. The observed trend from dacitic to andesitic volcanism is different from that in the Marble Bar Greenstone Belt, where Hickman (1983) concluded from geochemistry that the Duffer Formation grades upward from andesite to dacite and rhyodacite. However, comparison of these trend is not straightforward, since they are highly dependent on whether the Panorama Formation is recognised as a separate felsic unit, and on the degree of tectonic disturbance of the rock succession.

The ages of the different felsic volcanic units indicate that the bulk of the Duffer Formation in the study area was deposited in less than 10 Ma, between 3469 and 3461 Ma (Fig. 3.13). The age of the felsic unit near the top of the Duffer Formation (3465±4 Ma; sample C, Fig. 3.2) is similar to the age of quartz-plagioclase porphyry unit F1 at the base of the Duffer Formation (3465±4 Ma, sample B, Fig. 3.2). This is comparable to dates of the Duffer Formation in the western extension of the greenstone belt, which define almost the same range between 3470 and 3461 Ma (Fig. 3.13, Table 3.1 and references therein).

Based on these new dates, the lowermost felsic unit west of the Coppin Gap Suite (loc. 9, Fig. 3.1) can be correlated with the Duffer Formation in the central Coppin Gap Greenstone Belt (Fig. 3.13, confirming the map correlation of Williams, 1999).

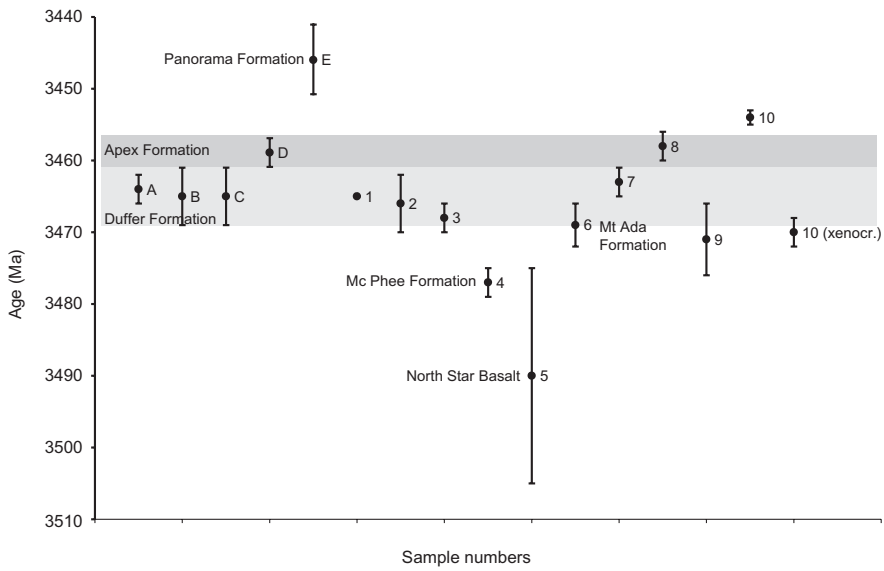

Figure 3.13: Plot of dates including error bars from Warrawoona Group in the Marble Bar and Coppin Gap Greenstone Belts. Letters refer to new dates presented in this study, numbers refer to previously published dates of the Warrawoona Group in this area. Shaded intervals are based on dates presented in this paper. For locations see Fig. 3.1, for details on geochronology and references, see Table 3.1.

A detailed stratigraphic and sedimentological study of felsic to intermediate successions in the adjacent Marble Bar Greenstone Belt and the Coongan and Kelly Greenstone Belts was carried out by DiMarco and Lowe (1989b). Compared to these sections, the section in the Coppin Gap Greenstone Belt contains a greater amount of lavas and agglomerates. The up to 2.8 km thick sequences of volcaniclastic breccia, conglomerate and turbiditic tuff that were reported from particularly the Coongan and Kelly Greenstone Belts, are absent in the study area. DiMarco and Lowe (1989b) assigned the major part of the felsic to intermediate succession in the Kelly Greenstone Belt to the Duffer Formation. Barley et al. (1998), however, showed that the age of the felsic rocks in the lower part of the Kelly Greenstone Belt is 3417±9 Ma, which is ca. 50 Ma younger than the Duffer Formation in the Coppin Gap and Marble Bar Greenstone Belts. Therefore, it is impossible to correlate the felsic to intermediate units between different greenstone belts as a single episode of volcanism under a single formation name (cf. Barley et al., 1998).

Towers Formation(?)

The poorly exposed basalts and the locally silicified, grey to reddish, silty to fine sand-sized sediments that were observed at several places at the top of the Duffer Formation, may represent the equivalent of the Towers Formation. The Towers Formation separates the Duffer Formation from the overlying Apex Basalt in the Marble Bar Greenstone Belt (Van Kranendonk et al., 2002). It consists of the thin, discontinuous Chinaman Pool Chert, a basalt unit (komatiites and pillows) and the Marble Bar Chert. Both chert units are characterised by blue-black, red and white chert (Van Kranendonk et al., 2001b; Oliver and Cawood, 2001). Williams (1999), who mapped part of the Coppin Gap Greenstone Belt east of the BSF, reported the Towers Formation to be absent in this area. However, based on their stratigraphic position and the crude resemblance in lithology with the succession in the Marble Bar Greenstone Belt, the basalts and coloured chert to siltstone interval in the study area may well be the equivalent of the Towers Formation in the Marble Bar Greenstone Belt. The sediments and basalts are poorly exposed and were not studied detailed enough to allow any conclusions about their depositional setting.

Apex Formation

The plagioclase porphyry between the 'Towers Formation' and the serpentinised peridotite (Fig. 3.13, sample D) is younger than the underlying felsic rocks of the Duffer Formation. Williams (1999) considered this unit to be part of the Apex Formation. However, the Apex Formation is a lithostratigraphic unit characterised by basalt (e.g. Hickman, 1983). Considering the andesitic character of the unit, and its geochemical similarity to the underlying andesites of the Duffer Formation, the unit may therefore be an intercalation of Duffer Formation in the Apex Basalt. Based on its age of 3459±2 Ma, which falls within the range of what is generally considered as Panorama Formation (ca. 3459-3428 Ma; Van Kranendonk et al., 2002 and references therein), the andesite could also be an intercalation of the Panorama Formation in the Apex Basalt. A slightly westward-located felsic unit of the same age (dating loc. 8 in Fig. 3.1) is, based on its quartz porphyritic character (Thorpe et al, 1992b), likely to be an intercalation of the Panorama Formation in the Apex Basalt. This quartz-porphyritic unit is not the lateral equivalent of the felsic Panorama Formation unit south of Kittys Gap however, since the latter is much younger (3446±5 Ma, sample E).

Panorama Formation

The interbedding of agglomerates, flow-banded porphyries and, near the top of the unit,

volcaniclastic layers, indicate that at least part of the massive Panorama Formation rhyolites and rhyodacites were extrusive. The overlying, now silicified, sediments were deposited in shallow water (see Chapter 3). The succession in the Coppin Gap Greenstone Belt seems comparable to the Panorama Formation at its type section (Panorama Ridge) in the North Pole Dome, where Hickman (1983) described the lower part of the formation as being composed of dacitic lava, tuff and agglomerate, and the upper part of the section as consisting predominantly of quartzite and chert. DiMarco and Lowe (1989b) regard the Panorama Formation in the North Pole Dome as a volcanically controlled fan-delta complex. They describe it as mainly consisting of shallow-water, volcaniclastic deltaic deposits that locally interfinger with volcaniclastic breccia and felsic lava.

Extension in the Coppin Gap Greenstone Belt

In the KG-vsc, thickness differences across the faults, the progressive tilting of the sequence and the presence of rollover anticlines indicate the syndepositional character of the normal faults that cut the complex (Fig. 3.3). The geometric relationships indicate a back (i.e. eastward)-stepping of the normal faults during deposition. During this process of back-stepping, compressive structures developed in the toe (west) of the fault-array while extension dominated at the rear (east). In the west, the sequences became progressively rotated and normal faults were folded. The normal faults end in a series of shear zones stratigraphically ~1 km below the top of the fault array (Fig. 3.3). Tensile faults occur at the rear of a fault array and broadly contemporaneous compressive features along the sole of the normal faults and in front of the fault array are characteristic of gravitational collapse (e.g. Mandl and Crans, 1981). Nijman et al. (1998b) observed inversion from tensile (sinistral) to compressive (dextral) displacement on this detachment zone. The rotation and displacement of large blocks at the base of the fault array (Fig. 3.3), and the broad, brittle deformation zone indicate that sliding at the detachment surface took place under relatively low overburden pressure, i.e. close to the paleo-surface. Dating of felsic rocks in the lower part of the KG-vsc (sample E, this study) constrains the time of deposition, and hence faulting in the KG-vsc at ~3446 Ma (i.e. Panorama Formation age).

Lower in the Warrawoona Group, there is also evidence for extensional faulting. The fault array in the top of the Duffer Formation has a similar orientations as the faults in the KG-vsc. Nijman et al. (1998b) described these normal faults as similar to those in the Kittys Gap area (see next section), thereby suggesting that the faults were syndepositional. This is indeed suggested by the strike rotation of the rocks in that area, and the differential offset of the gabbro intrusion and the (stratigraphically) slightly higher, serpentinised peridotite intrusion. However, due to the lack of reliable non-intrusive reference levels, syndepositional activity of these faults could neither be proven, nor be rejected.

The offset across the major fault in the Coppin Gap Greenstone Belt, the BSF, also seems to diminish between the base of the Duffer Formation and the serpentinised peridotite sill. However, the lack of reliable, non-intrusive reference levels, the presence of several (possible) subhorizontal deformation zones in the rock succession, and the possibility that oblique movements occurred along the fault, makes it difficult to assess whether these differential offsets along the BSF are really the result of syndepositional faulting. Further research is necessary to confirm the hypothesis that the BSF was (partly) syndepositional. The presence of large-scale, early structures in the Coppin Gap Greenstone Belt is also suggested by the absence of correlation between the rocks successions on both sides of the Coppin Gap suite of the Mt Edgar Granitoid Complex. Although the present-day distance between the sections of Warrawoona Group on both sides is only ~7.5 km, the rock successions (that can now be correlated based on the new U-Pb dates, see above) do not resemble each other (maps

by Nijman et al., 1998b; Williams, 1999). This suggests that a major normal fault or other structure occurred at the location of the Coppin Gap suite, prior to intrusion of the granitoid suite at ca. 3314±13 Ma (Williams and Collins, 1990). The exact timing and nature of these large-scale structures in the Coppin Gap Greenstone Belt require further research.

Low-angle discontinuities: surfaces of gravitational collapse? The folding of, and thickness differences in, the lower BIF unit of the Duffer Formation, as well as orientation differences of the sequences underlying and overlying the lower BIF unit indicate localised deformation along this unit. The dominance of S-folding throughout the unit points to a sinistral sense of movement (before rotation of the bedding into a vertical position: upper block to the west). Westward, i.e. in the direction of movement, the deformation zone cuts down into the underlying part of the Duffer Formation. These combined observations suggest gravitational deformation (or collapse) of a large part of the Duffer Formation. Gravitational deformation is also suggested by the variation in orientation of the fold axes in the lower BIF unit. The incorporation of felsic and mafic blocks in the folded outcrops, and the locally brittle character of the zone, indicate that the movement took place under a low overburden pressure. The decreasing 'consistency' of the Duffer Formation outcrop pattern east of the Talga River coincides with lowest level of BIF unit. This suggests that brittle fracturing of Duffer Formation was related to the gravitational collapse. Subsequently, the 'fracture' zones between the outcrops were used as pathways by fluids and magma, which resulted in veins, dykes and alteration of the host rocks.

A similar style of deformation, including recumbent northwest-facing folds, was described by Collins (1989) from the McPhee Reward area in the western extension of the greenstone belt (where it curves into the N-S oriented Marble Bar Greenstone Belt). The folds were interpreted as collapse structures resulting from doming of the (Mt Edgar) granitoid complex (Collins, 1989). However, the observations fit other causes of gravitational collapse equally well, and may represent gravitational collapse folds along similar detachment surfaces as described above from the central Coppin Gap Greenstone Belt.

Near the contact with the Coppin Gap suite of the Mt Edgar Granitoid Complex, a combination of extensional faulting and thrusting has complicated the lower Duffer Formation.

Extension of pre-Duffer Formation rocks. Lower in the Warrawoona Group, there is also evidence for extensional deformation. The lateral thickness differences away from the fault in the Razorback Chert (Fig. 3.9), suggest that the normal faults that cut this chert were active during its deposition (later reactivation may subsequently have caused a larger offset on the major faults). The normal-faulted Razorback Chert shows thrust faulting and internal compressive synsedimentary deformation in the frontal (i.e. western) chert bed (Fig. 3.9). The dm to m-scale internal folding of the frontal (i.e. western) chert bed suggests internal slip planes. Combined with the varying orientations of fold axes, this points to a synsedimentary origin of the folding. Small antithetic faults to the larger normal fault were (partly) reactivated as minor thrust faults during compression. The folds are interpreted as surficial collapse folds related to intra-formational slip, and the thrusts as subordinate compressional features in the toe-region of the normal faults. However, time control on the formation of the compressive structures in the Razorback Chert is less certain than in the Kittys Gap volcano-sedimentary complex.

The position of the Razorback Chert below the base of the Duffer Formation indicates that the extension took place prior to 3465±4 Ma (sample B; basal Duffer Formation quartz-plagioclase porphyry). Possibly, the Razorback Chert can be correlated westward across the BSF to a chert much

further south that shows pronounced drag along the BSF. Since dips of bedding are as low as 30° in the lower part of the sequence west of the BSF, the thickness difference of the rock succession between the Razorback Chert and the Duffer Formation east of the BSF and the only chert west of the BSF and the Duffer Formation, are not as large as they appear to be from the map view. The chert west of the BSF can be correlated to the McPhee Chert, part of the McPhee Formation, which was dated at 3469±3 Ma at the McPhee Reward Mine (loc. 6, Fig. 3.1).

Interpretation of the tectonic regime / persistence of normal faulting

The above observations are not the only indications for extensional deformation and normal faulting in the Coppin Gap Greenstone Belt. At the easternmost extremity of the Coppin Gap Greenstone Belt, where it curves into a NW-SE direction, an array of northwest-block-down normal faults affects a basalt unit and overlying silicified sediments (Nijman et al., 1998b; Zegers et al., 2002). Nijman et al. (1998b) mention the occurrence of a wedge of tuff and/or shale related to these faults, indicating their synsedimentary character (shale wedge also on Fig. 3.2 in Zegers et al., 2002). Deposition of these basalts and overlying silicified sediments, and therefore also the observed normal faulting, are constrained between 3454 Ma (dating 10 in Fig. 3.1) and 3415 Ma (Zegers et al., 2002, see previous paragraph).

Kloppenburg (2003) reported extension in the central part of the Coppin Gap Greenstone Belt during deposition of the Apex and/or Euro Basalts, based on observations on a swarm of dolerite dykes in the Duffer Formation. Dating from our study constrains the deposition of the Apex Basalt in this area between ca. 3459 and >3446 Ma (samples D and E). The Euro Basalt in the Kittys Gap area is underlain by the ~3446 Ma Panorama Formation (sample E), and truncated by the BCSZ (Nijman et al., 1998b). The Pb-Pb model age of galena from the BCSZ is 3415 Ma (Zegers et al., 2002; cf. Thorpe et al. 1992a), which provides a maximum age of deposition of the Euro Formation. Hence, the extension reported by Kloppenburg (2003) is here interpreted to have taken place between 3459 and 3415 Ma.

From the McPhee Reward area, faulting during deposition of the top of the North Star Basalt (Beintema, 2003) and/or the Warrawoona Group (Van Haaften and White, 1998) was reported. Both authors found subsequent east-west extension, and east-west compression that they interpreted to have occurred ~3450 Ma and ~3300 Ma, respectively.

The occurrence of growth faults and fault arrays at different stratigraphic levels, with a consistent E-W orientation, suggests that extension played a role over an extended period of time. From ca. deposition of the McPhee Formation at ~3469 Ma to the top of the Panorama Formation at ~3446 Ma, i.e. at least 20 Ma, there was either regular or continuous extension in the Coppin Gap Greenstone Belt. Possibly, the extensional deformation continued even into Euro Basalt-time (Kloppenburg, 2003 and Bamboo Creek area depending on the age of the basalts), i.e. from ~3469 to ~3415 Ma.

Extension during deposition of the Warrawoona Group was not a local phenomenon in the Coppin Gap Greenstone Belt, but occurred at several places in the East Pilbara (Coongan Greenstone Belt, Zegers et al., 1996; Kelly Greenstone Belt and Marble Bar area; Kloppenburg, 2003; North Pole Dome, Nijman et al., 1998a).

Stratigraphic continuity or not?

Both this and previous studies (see Introduction) recognise the presence of deformation zones in the Coppin Gap Greenstone Belt (and its westward extension into the Marble Bar Greenstone Belt). The

deformation zones were interpreted as early, originally horizontally oriented zones. Often, the shear zones had a multiphase history (e.g. Van Haaften and White, 1998; Nijman et al., 1998b; Zegers et al., 1996). The deformation along the shear zones may have influenced the stratigraphic thickness either in a negative (extensive) or a positive (compressive) sense. In the field, the amount of displacement is difficult to assess (see e.g. discussion in McPhee area in Van Haaften and White, 1998, 2001; Van Kranendonk et al., 2001a; Beintema, 2003). To establish whether the stratigraphic sequence in the Coppin Gap Greenstone Belt is continuous, absolute dating of sequences on either side of the shear zones is essential. The new dates (samples A-G, Fig. 3.1 and Table 3.1) have greatly increased the density of dates within this greenstone belt. Combined with existing dates from the Coppin Gap and the adjacent Marble Bar Greenstone Belt (Fig. 3.1 and Table 3.1, and references therein), the new dates confirm a general upward-younging of the stratigraphic sequence in the Coppin Gap Greenstone Belt; the andesitic unit (sample D, Fig. 3.2; assigned to the Apex Formation by Williams, 1999) is slightly younger than the felsic part of the underlying Duffer Formation, and the Kittys Gap felsic volcanic complex definitely belongs to the younger Panorama Formation (cf. interpretation of Williams, 1999). Hence, even with a higher density of dates, there is no indication for major duplications in the stratigraphy of the Coppin Gap Greenstone Belt, or for other significant disruptions of the stratigraphic sequence. The suggestion of Nijman et al. (1998b) that the felsic rocks of the P-assemblage could be a tectonic repetition of lower parts of Warrawoona stratigraphy is therefore rejected. This conclusion is confirmed by the geochemical data, which show that the felsic volcanic rocks of the Duffer and Panorama Formations are distinctly different.

Duplications of the stratigraphy on a smaller scale cannot be excluded, however. All dates from the main felsic unit of the Duffer Formation are within error of each other. Therefore, it is impossible to draw conclusions about the ages of the different levels of the main felsic unit relative to each other. It is known, for example from Alpine-type collisional orogens, that tectonic juxtaposition through shortening may involve successions formed in only a few million years, i.e. smaller than the resolution of the dates (best resolution so far is $\pm$ 2 Ma, Table 3.1) in the Coppin Gap Greenstone Belt. Unless the precision in greenstone belts of the East Pilbara is increased, tectonic superposition on a scale of a few million years cannot be excluded.

In addition, it is impossible to define how much of the Warrawoona Group stratigraphic sequence has been lost as a result of the deformation. As can be seen, for example along the east bank of the Talga River, where the lower part of the Duffer Formation is absent (unit F1 to BIF1), gravitational collapse has caused a local hiatus in the sequence.

Conclusions

The Warrawoona Group in the Coppin Gap Greenstone Belt (Pilbara, Australia) consists of deformation zone-bounded slices of ultramafic, mafic, intermediate and felsic rocks, with minor amounts of banded iron formation and silicified sediments. New U-Pb zircon dates and geochemical analyses, show that the chronostratigraphical succession in the Coppin Gap Greenstone Belt has not fundamentally been disturbed. Precision of the U-Pb SHRIMP dates is insufficient, however, to rule out small hiatuses or duplications of stratigraphy on the order of a few million years.

West-block-down normal faults occur in the Coppin Gap Greenstone Belt at the scale of the entire greenstone belt, and, at a smaller scale, as arrays in several levels of the greenstone belt stratigraphy. At least part of these normal fault arrays was syndepositional. Early, gravitational collapse of a large

part of the Duffer Formation in this greenstone belt also implies upper-block-west transport. Extension in the Warrawoona Group was not a local phenomenon, but occurred throughout the East Pilbara, indicating that extension was probably the regional tectonic regime at that time. This extensional regime lasted for a minimum period of 20 Ma. In the Coppin Gap Greenstone Belt, the orientation of normal faulting remained constant during that time.

Acknowledgements

MSc students I.M.A. Vos, J.P.M. van der Meer, K.L. Louzada, T. Benedictus and S.H.J.M. van den Boorn took part in the fieldwork. J.P.M. van der Meer analysed the geochemistry samples discussed in this chapter as part of an undergraduate project at Utrecht University. U-Pb SHRIMP dating of samples A, C, D, F was carried out by the author at Curtin University of Technology in Perth (Australia) in cooperation with Dr. D.R. Nelson. Dating samples B, E and G were analysed at Curtin University by Dr. J.R. Wijbrans of the Free University of Amsterdam, also in cooperation with Dr. D.R. Nelson. The Foundation Dr. Schürmannfonds supported part of the fieldwork with grants 2000/14, 2001/14 and 2002/10. U-Pb SHRIMP dating was financed with contributions from the Geodynamical Research Institute (GOI) and the Netherlands Organization for Scientific Research (NWO, grant R 75-394).

Chapter 4

Early Archaean sediments of the Buck Ridge volcano-sedimentary complex (South Africa) and the Kittys Gap volcano-sedimentary complex (Australia)

Abstract

The sediments at the top of two early Archaean volcano-sedimentary complexes have been studied by a combination of mapping and detailed sedimentary logging. The Buck Ridge volcano-sedimentary complex (Barberton Greenstone Belt, South Africa) and the Kittys Gap volcano-sedimentary complex (Coppin Gap Greenstone Belt, East Pilbara, Australia) have a similar geological setting, and are of similar age (~3.45 Ga). Deposition of the sediments in both complexes was influenced by normal faulting. Both sedimentary sequences experienced thorough, early diagenetic silicification, which has in many places led to an excellent preservation of the sedimentary structures, while in other places it has resulted in the complication and loss of sedimentary textures and structures. In both sequences, high-energy breccias are juxtaposed with the 'normal' sandy to silty sediments. Despite the similarities in geological setting and timing of the two complexes, there are small differences in the sedimentary sequences. The sediments of the Buck Ridge volcano-sedimentary complex form a regressive-transgressive sequence, which was deposited close to base level and experienced occasional emersion. The sediments of the Kittys Gap volcano-sedimentary complex have mostly been reworked and were deposited predominantly subaqueously, close to base level. Deposition of the sediments of the Kittys Gap volcano-sedimentary complex was possibly influenced by tidal activity.

Introduction

The oldest significant volumes of arkosic and quartz arenitic clastic deposits on Earth are ~3.3-3.0 Ga old and include the Fig Tree and Moodies Groups in the Barberton Greenstone Belt (South Africa), and the Mosquito Creek Basin deposits (Gorge Creek Group) in the Pilbara, Australia (e.g. Eriksson, 1980a,b , 1981, 1982; Lamb and Paris, 1988; Nocita and Lowe, 1990; Krapez, 1993; Eriksson et al., 1994; Heubeck and Lowe, 1994, 1999; Lowe and Nocita, 1999; Toulkeridis et al., 1999). There are several studies on sedimentary deposits older than 3.3 Ga. In the Barberton Greenstone Belt those deposits include the Middle Marker, Buck Ridge and Msauli Cherts of the Onverwacht Group (e.g.

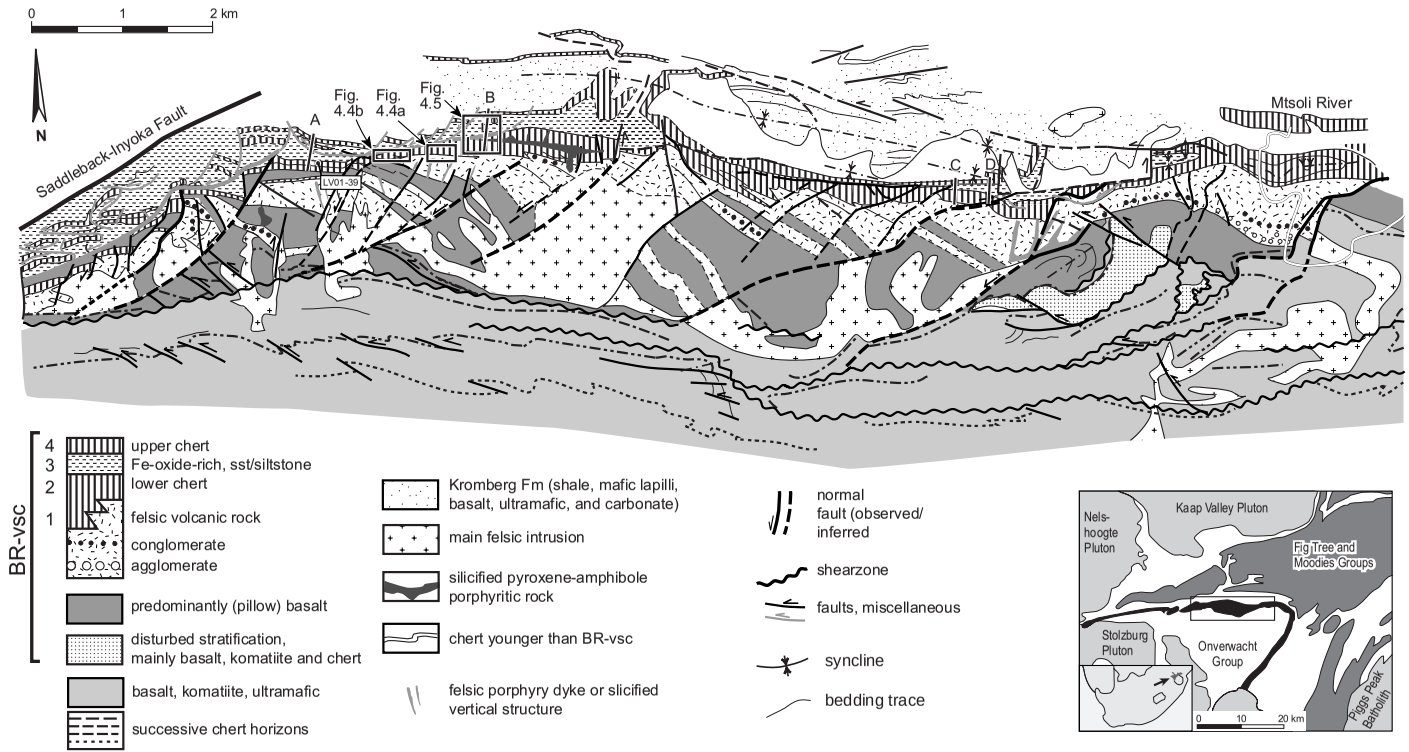

Figure 4.1: Simplified geological map of the Buck Ridge volcano-sedimentary complex and its substrate, both part of the upper Hooggenoeg Formation (map after Chapter 2; for location in southern Barberton greenstone belt see inset). The entire sequence has been rotated into a vertical orientation, younging direction is to the north. A-D refer to log locations; A = West, B = Central, C = East, D = E-east BR-vsc log. The locations of Figs 4.4a and b and Fig. 4.5 are indicated with rectangles. Legend applies to main figure, not to inset.

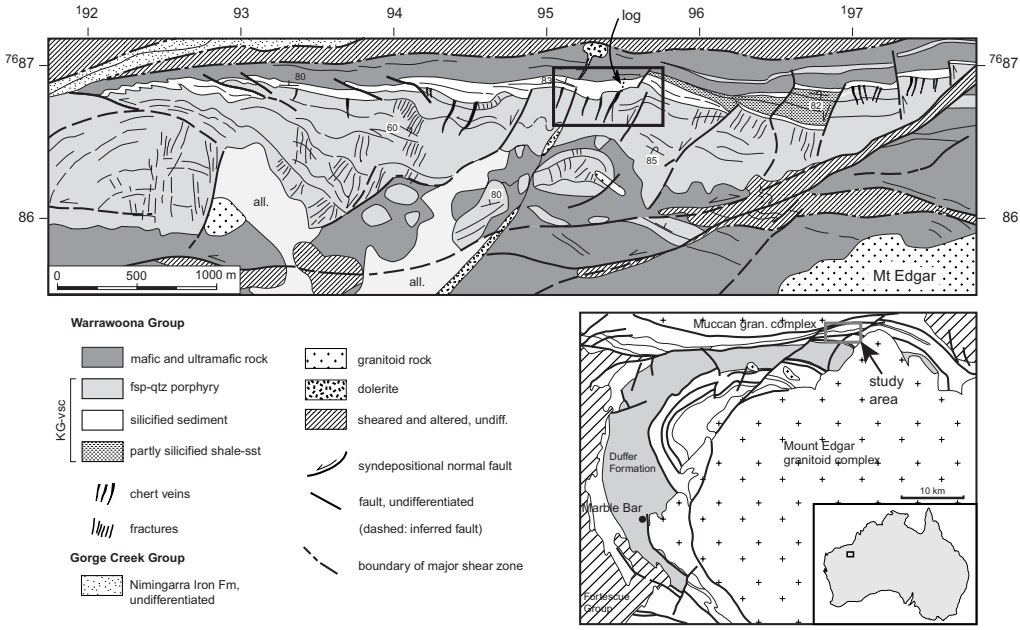

Figure 4.2: Simplified geological map of the Kittys Gap volcano-sedimentary complex (KG-vsc, Panorama Formation) and surrounding rocks. Main study area indicated with a rectangle, location of Fig. 4.2 within the Coppin Gap Greenstone Belt indicated in inset. Legend applies to main figure, not to inset.

Lowe and Knauth, 1977; Lanier and Lowe, 1982; Lowe, 1982, 1999a, 1999b; Heinrichs, 1984; Paris, 1990; Lowe and Fisher Worrell, 1999; Ransom et al., 1999; Walsh and Lowe, 1999), and in the Pilbara they include the silicified sediments of the Warrawoona Group (e.g. Barley et al., 1979; Dunlop and Buick, 1981; Barley, 1993; Lowe, 1983; Buick and Barnes, 1984; DiMarco and Lowe, 1989a,b; Buick and Dunlop, 1990; Nijman et al., 1998a). Controversies exist regarding the interpretation of sedimentary units, especially about those that have been thoroughly silicified. Interpretations range from deep-sea environments to shallow water, sometimes for the same units (e.g. for the North Pole chert-barite unit in the Pilbara, see discussion). Therefore, more detailed sedimentological studies are necessary.

Relatively little is known about the geometry, i.e. shape and size, of >3.3 Ga sedimentary basins. The geometry of sedimentary basins provides insight into the setting in which they were formed, which may in turn give information about the tectonic regime or crustal development in the early Archaean.

This chapter focuses on some of the oldest and relatively little metamorphosed sedimentary deposits preserved on Earth; early Archaean sediments of the ~3.45-3.41 Ga old Buck Ridge volcano-sedimentary complex (BR-vsc) in the Onverwacht Group, Barberton Greenstone Belt (South Africa, Fig. 4.1, see also Chapter 2) and the ~3.45 Ga Kittys Gap volcano-sedimentary complex (KG-vsc) in the Warrawoona Group, Coppin Gap Greenstone Belt (Pilbara, Western Australia, Fig. 4.2, see also Chapter 3). These two complexes were selected because they are well exposed and of overlapping age. Deposition of the sedimentary part of these complexes occurred in a similar geological setting, at the top of a dominantly felsic volcanic complex. In both areas, the felsic volcanics and sediments were deposited during large-scale normal fault activity. The main difference

between the two complexes is their size. Sediments of the BR-vsc are up to 400 metres thick, and exposed for at least 15 km along strike. Interpretation of several sections through the sedimentary sequence gives a 2-D image of the sequence with its lateral variations. Sediments of the KG-vsc are on average only 35-40 metres thick and exposed for ~5 km along strike. The preservation of sedimentary textures and structures in the Kittys Gap Chert (KGC; the silicified sediments at the top of the KG-vsc) is variable. In the central part of the area silicification has led to an excellent preservation of the sedimentary textures and structures. Sedimentary structures are also well preserved in the less silicified sandstone-siltstone-shale wedge (see below and Fig. 4.2). In other places, texture and structures have completely or almost completely been lost due to thorough, glassy silicification. In the BR-vsc, different stratigraphic levels show differences in degree of silicification.

Lowe and Fisher Worrell (1999) described the lowermost part of the Buck Ridge (or Reef) Chert (BRC; the silicified sediments at the top of the BR-vsc), which includes a silicified 'evaporite' sequence, in detail. The sedimentology of the BRC was also described briefly in more general papers about the cherts of the Onverwacht Group (e.g. Lowe and Knauth, 1977; Lowe, 1999a; Walsh and Lowe, 1999).

The sediments of the KGC in the Coppin Gap Greenstone Belt were mentioned by Nijman et al. (1998b), but were not studied in detail.

Sediments may provide information about the depositional environment, relative water depth (in case of subaqueous deposition), and composition of the hinterland. In this chapter, attention is furthermore paid to the geometry of the sedimentary deposits, and the relation of this geometry to the general geological framework. Together with structural and geochemical data, this sedimentological study aims at contributing to the reconstruction and understanding of early Archaean basins.

Sedimentological studies of the early Archaean are difficult because of the lack of organisms as paleo-environment indicators, and the possibility that conditions on the early Earth were different from those of today. In the study areas, thorough, multi-phase silicification has greatly influenced the appearance of the sedimentary sections. This syndepositional to early diagenetic process, which is hardly known from the modern Earth, complicates the interpretation of the sedimentary sequences, and is therefore addressed in this chapter as well.

Geological framework

The sediments that were studied in the Barberton Greenstone Belt form part of the BR-vsc in the top of the Hooggenoeg Formation (Fig. 4.1). The BR-vsc is a mixed mafic-felsic volcanic complex, with an upward increasing amount of felsic volcanic rocks and silicified sedimentary layers. The thickest sedimentary sequence occurs at the top of the BR-vsc (Fig. 4.1 and Chapter 2). The term BRC is applied from the level where the sedimentary sequence has been thoroughly silicified, a transition that is clearly visible on aerial photographs.

The rocks overlying the BRC are mainly mafic to ultramafic intrusives and extrusives, siltstones and shales. Generally, they are poorly exposed in the study area. This chapter focuses on the sedimentary sequence at the top of the BR-vsc, i.e. the volcaniclastic top of the felsic volcanics and the sedimentary BRC. The BR-vsc felsic lavas and intrusives have been dated at 3451±5 Ma (Chapter 2), while the volcaniclastic rocks were assigned a maximum age of 3416±5 Ma by Kröner et al. (1991). The top of the felsic volcanics and the lower part of the BRC were deposited during the activity of an array of large-scale normal faults (Fig. 4.1 and Chapter 2), which led to thickness dif-

ferences in the sequence across the faults. The study area (Fig. 4.1) is located on the northern limb of the Onverwacht Anticline. The BRC is mostly regarded to be absent on the southern limb of the Onverwacht Anticline (Viljoen and Viljoen, 1969 and others), although Lowe et al. (1985) and Lowe and Byerly (1999b) consider 'three chert layers inter-bedded with thicker volcanic units' on the southern limb of the anticline to represent the BRC. The volcanic units include massive and pillow basalts, mafic pyroclastic layers, komatiitic flows and intrusive units.

The KG-vsc (Fig. 4.2 and Chapter 3) in the Coppin Gap Greenstone Belt of the Pilbara is part of the Panorama Formation (Williams, 1999 and Chapter 3). The silicified sediments of the KGC form the top of the KG-vsc. The felsic volcanics underlying this chert have been dated at 3446±2 Ma (Chapter 3). Like those of the BR-vsc, the felsic volcanics and sediments of the KG-vsc were deposited during normal fault activity (Nijman et al., 1998b; Chapter 3). The KG-vsc is overlain by the Euro Basalt, which shows hyaloclastic brecciation and columnar jointing.

Results

Buck Ridge Chert and underlying volcaniclastic deposits

Fig. 4.1 gives an overview of the aerial extent and distribution of the sedimentary sequence at the top of the BR-vsc, including the locations of the sedimentary logs. We divide the sedimentary sequence into four lithofacies units (Fig. 4.3) based on the central part of the map area, where units are well exposed.

General geometry

The thickness of the sedimentary sequence is related to distance with respect to the normal faults (Chapter 2) in the BR-vsc; the thickest deposits occur in the hanging walls. The greatest variation in thickness across the normal faults occurs in the lower part of the sedimentary sequence (Fig. 4.1).

The base of unit 1 is difficult to establish in the major part of the area, since the contact with the underlying felsic volcanic lavas is transitional and interdigitating. The unit is thickest in the hanging walls of normal faults in the central and eastern part of the area (the normal faults are therefore interpreted as syndepositional; see Chapter 2). Westward, the thickness of the volcaniclastic deposits decreases to ~250 m and several, up to 100s of metres wide, laterally discontinuous chert layers occur intercalated with the volcanic rocks (e.g. log A, Fig. 4.1). Hundreds of metre-scale scour structures (see Facies description) are best preserved in the central part of the map area (Fig. 4.4). They occur mainly near the hinges of the rollover anticlines (Chapter 2) and in the hanging walls of the normal faults. In the footwalls, erosion has formed local unconformities (see also Chapter 2).

Unit 2 is thoroughly silicified and is therefore assigned to the BRC. The unit is well exposed and up to 180 metres thick (Figs 4.1 and 4.3). Its thickness varies across the normal faults in the BR-vsc (Fig. 4.1). Towards the west unit 2 becomes thinner (~70 m), and splits into two chert units (2a and 2b, log A, Fig. 4.3) separated by a poorly exposed interval.

The overlying unit 3, and locally also the top of unit 2 (e.g. in Fig. 4.5), is poorly exposed. The nature and the exact location of the contact between units 2 and 3 are therefore difficult to establish in the major part of the area. The contact is generally taken above the uppermost, well-banded chert outcrop.

Unit 3 is poorly exposed in the major part of the area. Thickness differences across the normal faults also occur in this unit. In the westernmost part of the area, unit 3 seems to increase in thickness

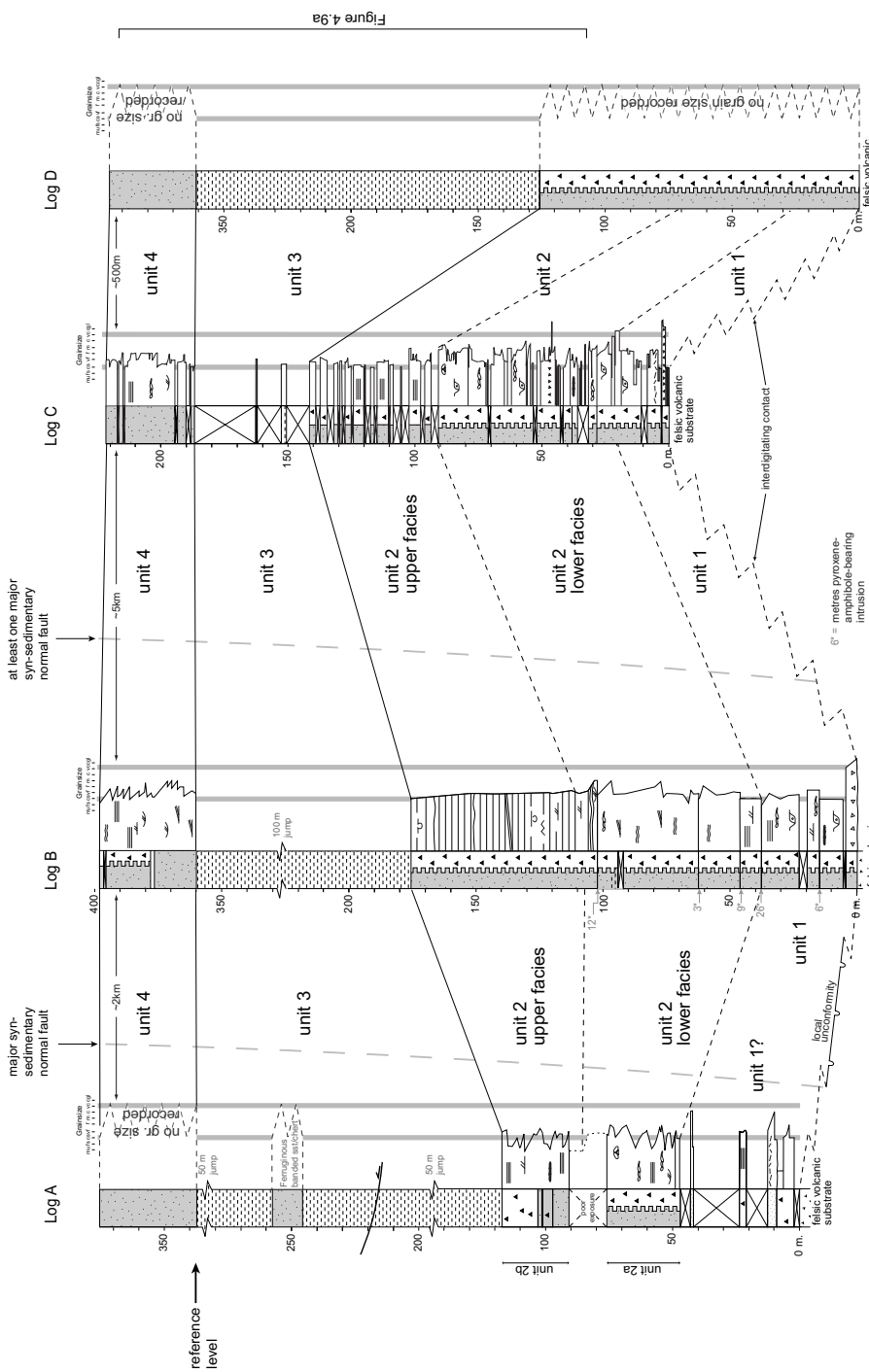

Figure 4.3: Correlation of simplified logs of sedimentary sequences of the Buck Ridge volcano-sedimentary complex. The base of unit 4 is taken as a reference level. Log locations are indicated in Fig. 4.1, detailed parts of the logs are given in Fig. 4.7 (lower part of unit 2, log C), Fig. 4.8 (upper part of unit 2, log B), Fig. 4.9 (unit 3, log D) and Fig. 4.10 (unit 4, log B). Correlation of the sections is (partly) based on aerial photographs. Legend on next page.

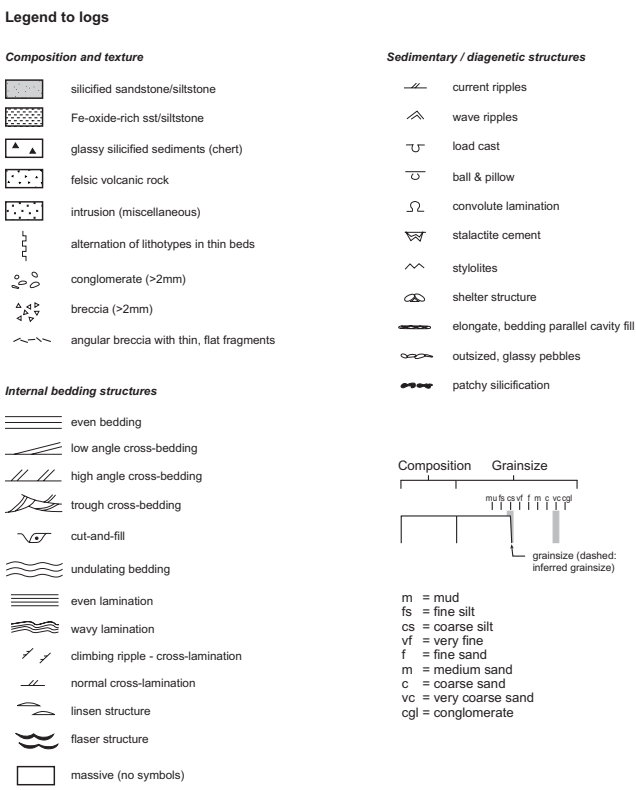

(Fig. 4.1 and 3). However, exact thicknesses of unit 3 in logs A and B are difficult to measure due to (post-depositional) faulting (Chapter 2). In the central part of the area (near the location of log B, Fig. 4.1), the exposure is limited to occasional massive iron-oxide occurrences and a few isolated slabs of banded chert that have been rotated with respect to the overall strike of the BRC. The slabs are metres thick and up to tens of metres wide (Fig. 4.5). They are composed of planar-bedded chert, which strongly resembles the upper part of unit 2, and some of the slabs have been folded on decametre-scale (see also Chapter 2).

Unit 4 is best exposed in the central part of the map area (log B, Figs 4.1 and 4.3). To the east the outcrop is discontinuous (Fig. 4.1). The base of unit 4 is taken where the first outcrops of banded chert occur above the poorly exposed and less silicified interval of unit 3. The thickness of unit 4 is ~40m, and does not vary significantly along strike. Unit 4 has been offset by normal faults, which seem to have been active only after deposition (during later gravitational collapse, see Chapter 2).

Facies description

Unit 1. Unit 1 is characterised by scour structures of several tens to hundred metres-wide and metres-deep, which are visible on aerial photographs and detailed (grid) maps of the area. Fig. 4.4a shows an aerial photograph of a ca. 250m-wide scour that cuts into felsic volcanic rocks in the central part of the area, and Fig. 4.4b shows a field sketch of scour structures ~350 m further west. The scour structures have been filled with volcaniclastic deposits, banded chert and, occasionally, felsic lavas.

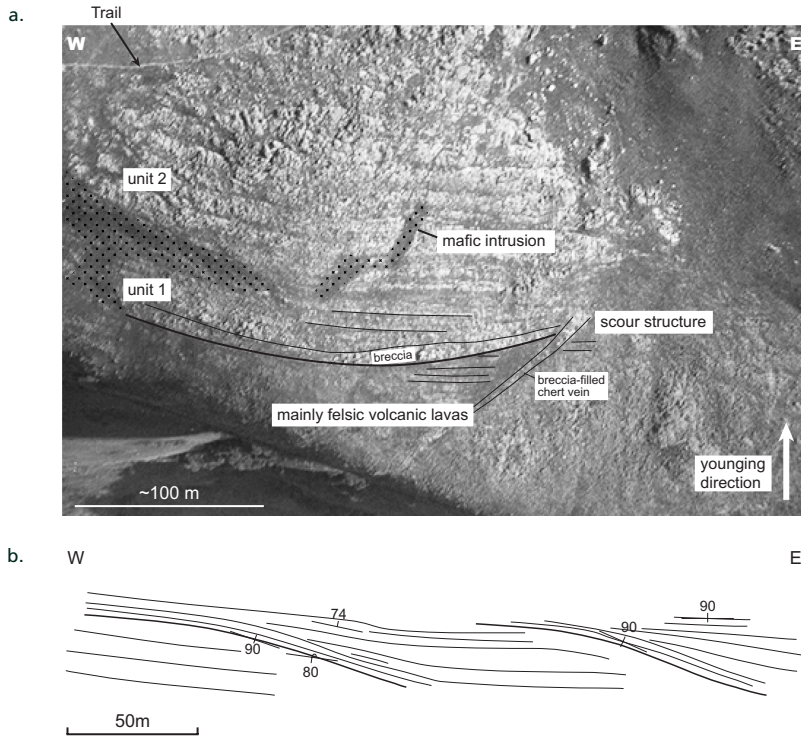

Figure 4.4: Near-vertical dipping scour structures in unit 1 of the BR-vsc. Locations indicated in Fig. 4.1. a. Aerial photograph of scour structure in felsic volcanic rocks. Unit 1 consists of breccia layers, silicified crystals and banded chert (not distinguishable on photo). b. Field sketch of scour structures approximately 350m west of the structure in Fig. 4.6a. The scours are in eastward direction filled with banded chert.

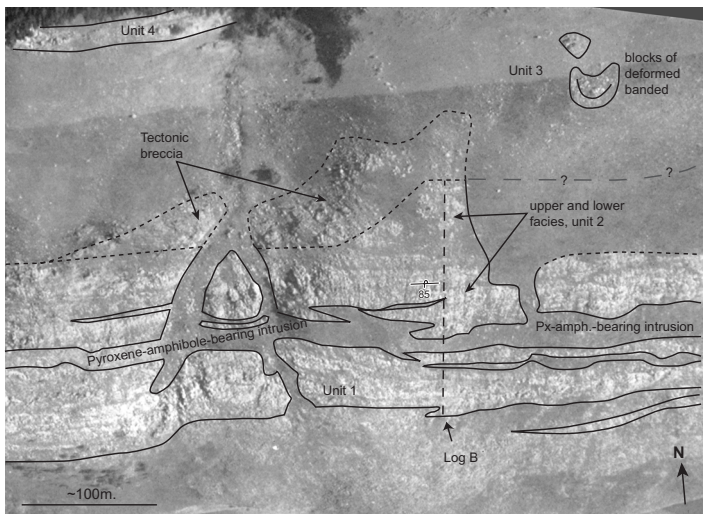

Figure 4.5: Oblique aerial photograph of the top of the BR-vsc, with the division in four units based on lithofacies. The position of log B is indicated. Also shown are the large, isolated slabs of banded chert in unit 3, and the locally poorly exposed top of unit 2. Orientation of bedding near log location: 190/85, hill slope dips ~25-35° north.

The scour structures in Fig. 4.4b have, in eastward direction, progressively been filled with banded cherts that onlap the scoured surfaces. The scour in Fig. 4.4a is filled with volcanics, silicified crystal layers and a breccia layer, all of which occur throughout unit 1.

The layers with silicified crystals and crystal palisades in unit 1 (the crystals have been described before by De Vries, 1999; Lowe and Fisher Worrell, 1999) occur in close association with black chert veins and grew in or just above finely laminated sediments. In places, the sedimentary layers curve slightly upward against the silicified crystals (Fig. 4.6a). Lowe and Fisher Worrell (1999) traced the stratigraphic level with the crystals approximately 15 km along strike along the western limb of the Onverwacht anticline. The individual crystal layers, however, are discontinuous. In the western part of the area (log location A and further west), both scour structures and crystal layers are absent.

The breccia layers that are occasionally incorporated in the fill of the scours are 0.5-2 m thick, and consist of 0.5-20 cm large black and white banded chert, felsic volcanic and (<1%) fuchsitic fragments. At one location, a 1.2 by 1m large block with laminated chert layers and silicified crystals is incorporated in the breccia layer. At the same stratigraphic level as the crystal layers, thin

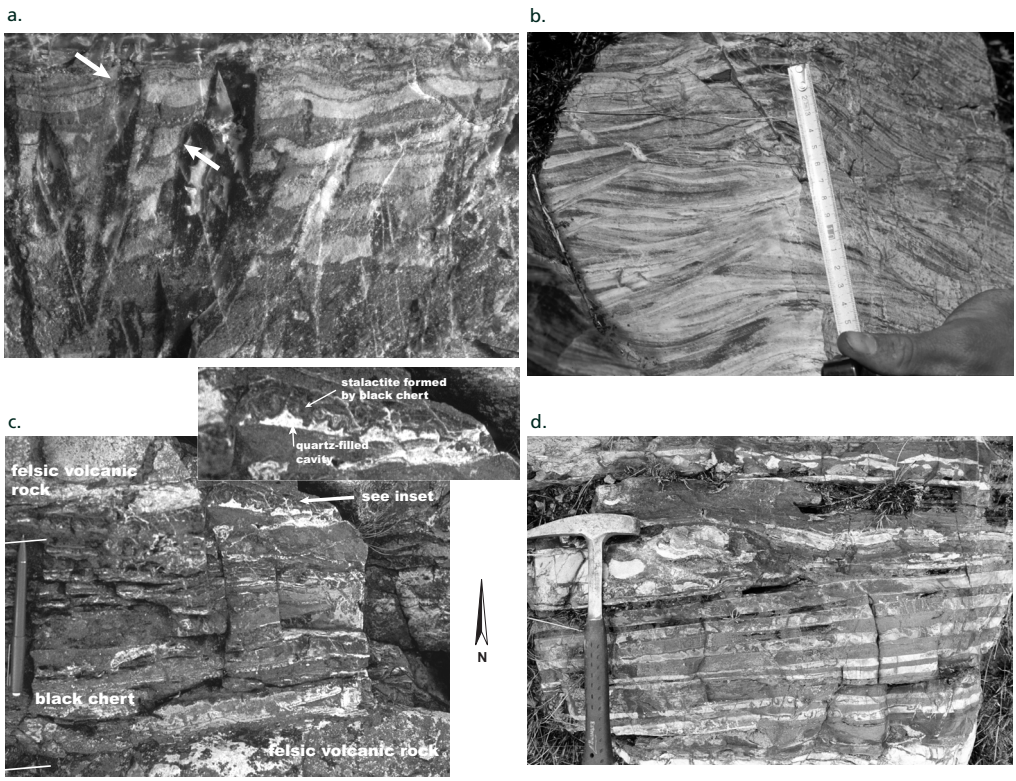

Figure 4.6. a. Silicified crystals in layered sediments, BR-vsc unit 1. In places, the bedding slightly curves up against the black, silicified crystals (e.g. at locations of white arrows). Approximate width of photo: 12 cm. b. Climbing ripples in a chert layer intercalated between felsic lavas and felsic volcaniclastic layers of BR-vsc unit 1. c. Black chert layer between two yellow weathered felsic volcanic layers of the BR-vsc, showing bedding-parallel floored cavities (see inset) filled with dark chert stalactites, and coarse quartz. d. Low-angle cut-and-fill structure in banded chert-sandstone in unit 2 of the BR-vsc.

sedimentary chert layers are intercalated in the volcano-sedimentary sequence. Sedimentary structures in these chert layers include abundant cm-scale ripples, climbing ripples (Fig. 4.6b) and layers with reworked accretionary lapilli. In the eastern part of the area, some of these chert layers are lens-shaped, a few metres wide, and include mm-scale laminated intervals. Cavities in the laminated cherts have been filled with chert and quartz. Some cavities in this interval show geopetal structures, with stalactitic-quartz or chert at the top, and sediments and/or coarse quartz at the bottom (Fig. 4.6c).

Part of the sediments of unit 1 was also described and interpreted in detail by Lowe and Fisher Worrell (1999, their lithofacies 1-7).

Volcaniclastic sediments in the eastern part of the area, where the Mtsoli River cuts the upper part of the BR-vsc, are coarse and include agglomerate (cf. De Wit, 1983) and polymictic pebble-cobble conglomerate (Fig. 4.1).

Unit 2. Unit 2 is well banded and thoroughly silicified. Its thickness and appearance vary considerably along strike (Figs 4.1 and 4.3). Nevertheless, the unit can broadly be divided into two intervals, which are recognisable along most of the exposure of the BR-vsc. Sections have been made at three different locations (logs A, B and C, indicated on Fig. 4.1).

The lower facies is characterised by a rhythmic pattern of deposition. This is best visible at log location C (Fig. 4.7). The rhythmic pattern is formed by a stack of four to five well-exposed chert sequences. The individual sequences are 8-15 metres thick, generally show a fining upward trend (occasionally preceded by a slight coarsening up trend), and are capped by a thin, poorly exposed

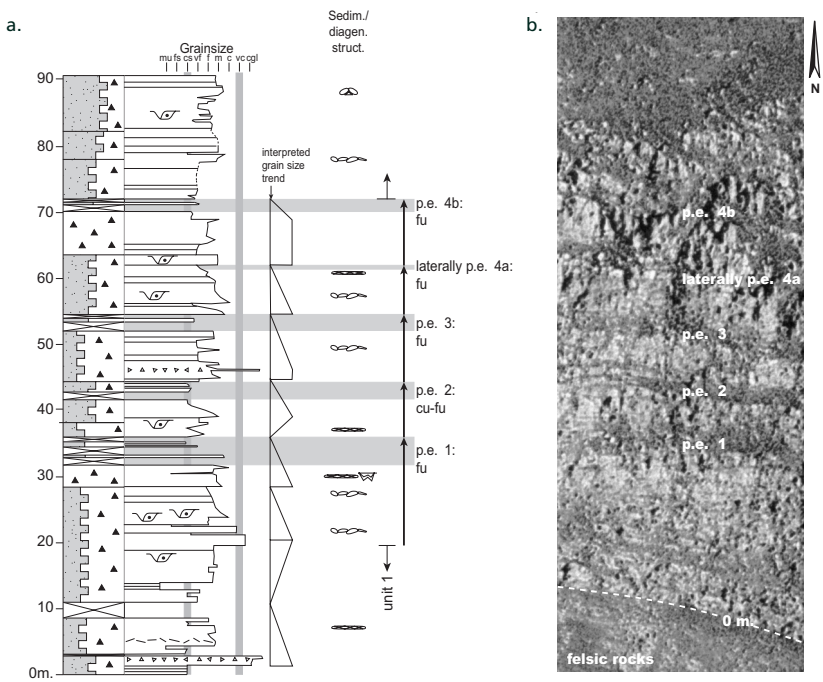

Figure 4.7: a. Simplified sedimentary log of the lower part of BR-vsc unit 2 in the eastern part of the map area (log C). Location indicated on Fig. 4.1. Legend in Fig. 4.3. b. Aerial photograph of the same section for comparison.

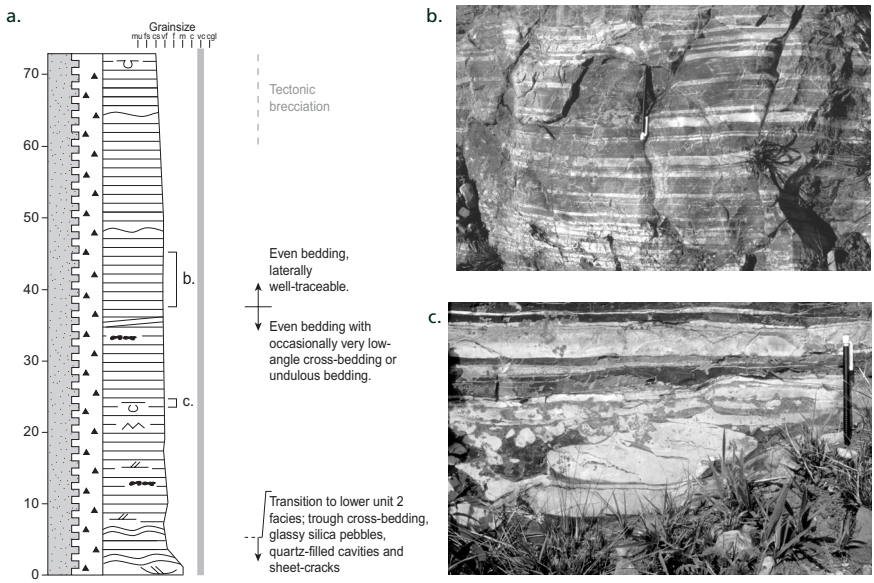

Figure 4.8: Simplified sedimentary log of the upper part of BR-vsc unit 2 in the central part of the area (log B). Location indicated in Fig. 4.1, for legend see Fig. 4.3. b. Illustration of cm-scale even bedding, characteristic for the major part of this unit. c. Illustration of ball-and-pillow-like loading structures.

interval (Fig. 4.7a). The well-exposed parts of the sequences are mostly glassy silicified. They show abundant metre-scale, trough-laminated cut-and-fill structures, soft-sediment deformation structures and quartz-filled sheet cracks. The cut-and-fill structures occur particularly near the bases of the sequences, in the lower part of the unit. Often, glassy, silicified (sometimes floating) pebbles occur at the base of such cut-and-fill structures (Fig. 4.6d). They are overlain by 3-10 cm thick layers of generally planar-bedded sandstone and chert. Pebbles also occur isolated, intercalated in coarse-sandy sediments, sometimes in stacks with coarse quartz crystals between them (see also Chapter 5). Occasionally, the unit includes finely banded iron-oxide-rich sandstone and chert alternations (e.g. log B in Fig. 4.3). In the central part of the map area, the lower part of unit 2 has been intruded by a pyroxene-amphibole-rich porphyry (Fig. 4.5).

The upper facies of unit 2 is characterised by planar bedding and a very fine sandy to silty grain size. It is well exposed in the central area (log B, Fig. 4.1; detail in Fig. 4.8), where it consists of extremely even-bedded black and white banded chert (Fig. 4.8b). It contains structures that resemble ball-and-pillow load structures (Fig. 4.8c).

In the western part of the area, unit 2 consists of two cherts (2a and 2b) separated by a poorly exposed interval (Fig. 3).

Unit 3. Unit 3 is iron-oxide-rich, and much less silicified than the underlying and overlying units. The grain size decreases from dominantly sand in the east (e.g. Fig. 4.9) to dominantly silt (and shale) in the west of the area. The type section through unit 3 was taken at 'log' location D (Fig. 4.1; detail in Fig. 4.9). Here, unit 3 consists of cm-scale banded sandstone-siltstone alternating with chert. At regular intervals of ~20m, the sequence contains a coarse breccia layer (Figs 4.9b and c). Breccia clasts

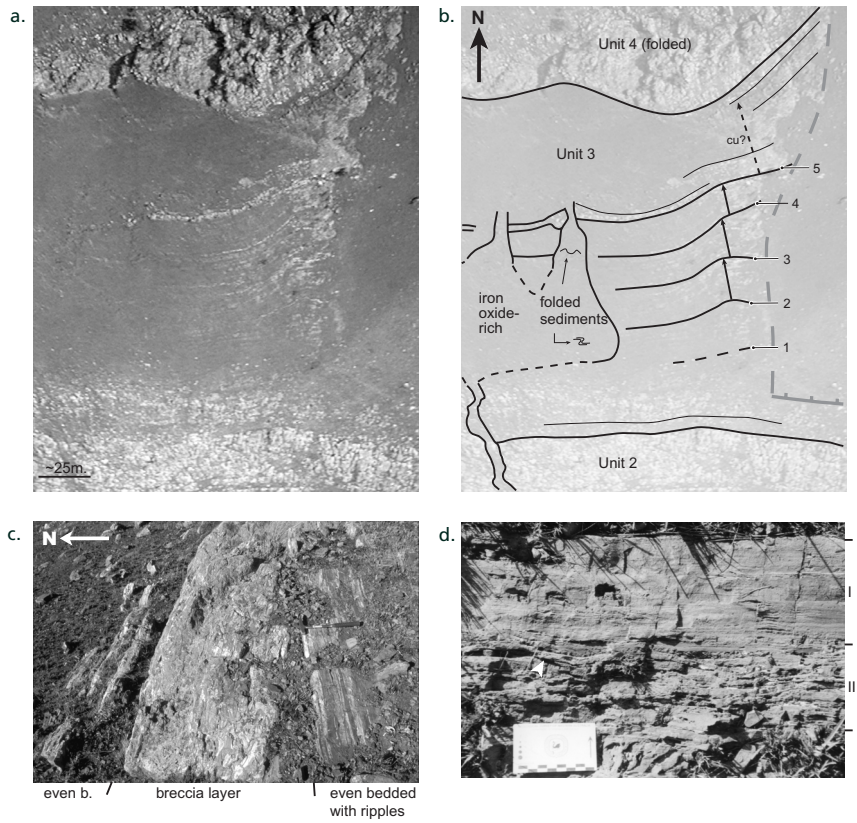

Figure 4.9: Unit 3 of the BR-vsc in the eastern part of the map area ('log D', location indicated in Fig. 4.1). a. Oblique aerial photograph of the section (left) and b. line drawing of same area (right). Breccia layers are numbered from old to young. Average distance between the breccia layers is ~20 metres, approximate thickness of unit 3 is 135 metres. Note that unit 4 is intensely folded at this location and therefore has a different appearance than elsewhere in the area (see Chapter 2) c. Detail of breccia layer 5 and underlying and overlying even bedded sediments. Hammer for scale on lower even bedded interval. d. Detail of even laminated layer (I) with (possible wave-)ripples (II) just below breccia layer 4.

are generally thin and platy, with angular to rounded edges. In the upper 20m-intervals, the breccia layers are more silicified, and are underlain by even-bedded and cm-scale (possibly wave-)rippled sandstone (Fig. 4.9d). Eastward, the layers end against a fault (see Chapter 2). Westward, the sequence grades into a poorly exposed interval. The interval (Fig. 4.9) is iron-oxide-rich, and locally contains dm-scale folded iron-oxide-rich sandstone and chert alternations. Upwards, the iron-oxide-rich interval splits into two several metres-wide vertical structures, which cut or end at breccia layer 5 (Figs 4.9a and b). The breccia thickens westward towards the iron-oxide-rich structure. Immediately east of the contact between the iron-oxide-rich structure the breccia layer is fragmented.

Unit 4. The type section of unit 4 is taken in the central part of the area (log B, Fig. 4.1; details in Fig. 4.10). The base of unit 4 is sandy and shows 1-2 metre-thick sets of planar beds at low angles with respect to each other (Fig. 4.10). The sandstone is generally very well sorted, well rounded and almost exclusively consists of quartz. Upward, the unit is more silicified, and shows abundant 2-3

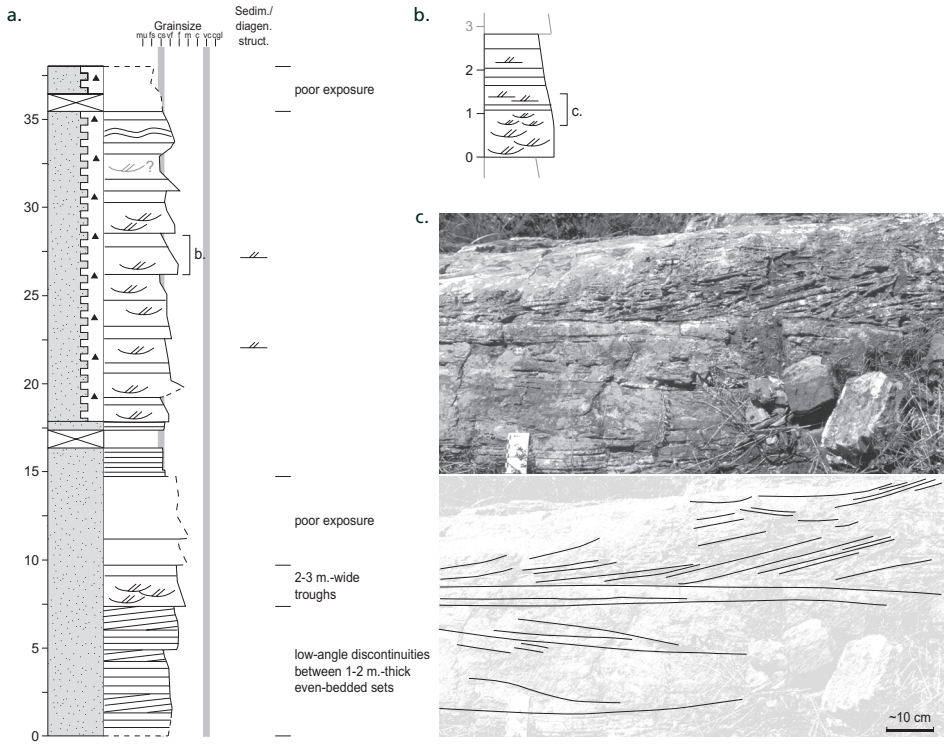

Figure 4.10: Simplified sedimentary log through BR-vsc unit 4 in the central part of the area (log B). Location indicated in Figs 4.1 and 4.5.

metre-wide, low-angle troughs. The fill of the troughs is illustrated in Fig. 4.10b; a base of large-scale troughs, overlain by small trough structures and high-angle cross-bedding. The trough beds are overlain by decimetre-scale undulous bedding, which flattens towards the top and are subsequently incised by overlying troughs. Imbricate stacking of flat chert pebbles is occasionally observed in the high-angle cross-bedded interval.

Kittys Gap Chert

General geometry

Fig. 4.2 gives an overview of the thickness and distribution of the silicified sedimentary sequence (KGC) at the top of the KG-vsc. In the major part of the area, an upper and a lower chert unit can be distinguished, which are separated by a poorly exposed interval (Fig. 4.11a).

The lower chert unit is characterised by one or more *en echelon* stacked, tens of metres-wide plano-convex, lens-shaped chert beds (e.g. Fig. 4.11b). At the log location (indicated in Fig. 4.2), the lower unit mainly consists of two of such chert 'lenses' (Fig. 4.11a and schematic diagram in Fig. 4.12), separated by a 40 m thick poorly exposed, probably intrusive interval (see below).

The upper chert unit is laterally well traceable, and its thickness varies mainly across the normal faults (Fig. 4.2) that cut it. This is particularly well visible approximately 750m west of the log

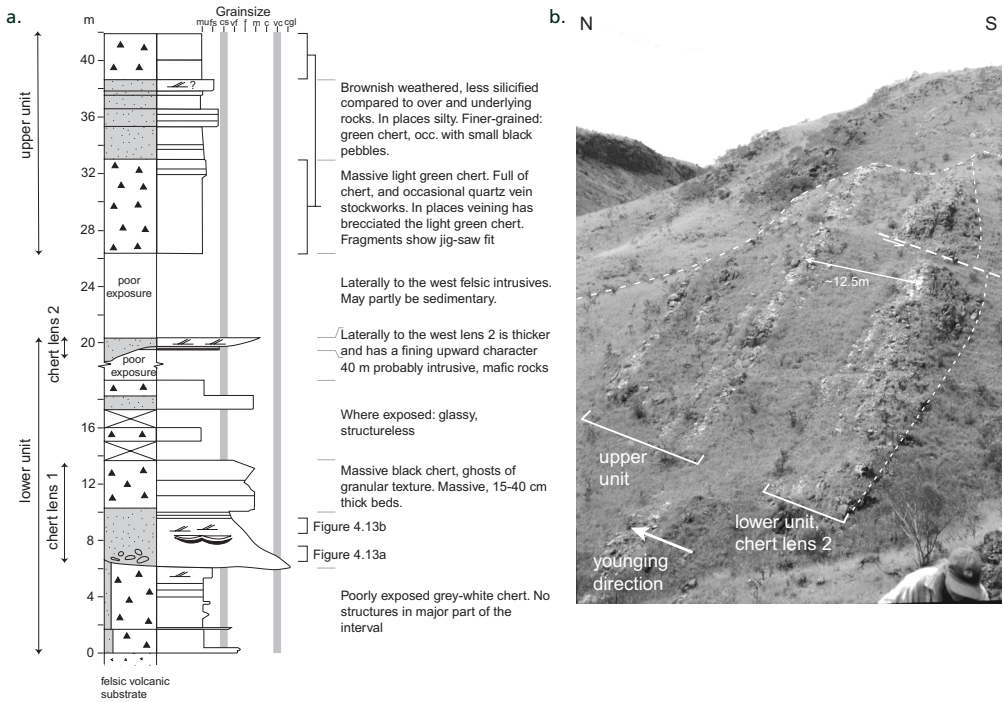

Figure 4.11: a. Sedimentary log of the Kittys Gap Chert, Coppin Gap greenstone belt, Pilbara. b. Overview photo of the upper part of the sedimentary sequence at Kittys Gap. Note the plano-convex shape of the chert in the lower unit. Log (Fig. a) was taken just behind the crest of the hill, where chert lens 2 is much thinner.

location, where the thickness of the upper unit rapidly increases towards a normal fault in the east (Figs 4.2 and 4.12), resulting in a wedge-shaped geometry of the unit (cf. Nijman et al., 1998b).

Intrusions. The geometry of the KGC has partly been modified by intrusions. Weathered rocks in the poorly exposed interval between chert lenses 1 and 2 of the lower unit show small (0.1-0.2 mm) ghost structures of a mineral now consisting of sericite and quartz. The homogeneous distribution of minerals and the interlocking texture suggests that the rocks are of intrusive origin. Partly molten and quenched silica-rich xenocrysts, which are not in equilibrium with the surrounding minerals, indicate that the host rock was probably relatively mafic in composition.

West of the log location, quartz-phenocryst-rich intrusive rocks are present between the upper and the lower unit (Fig. 4.2). At the log location, the interval between the upper and the lower chert units contains weathered, yellow, very fine to fine-grained rocks that are 'bedded' at 10-20 cm-scale. Due to the strong weathering, it remains unclear, also after thin section analysis, whether these rocks are of sedimentary or igneous origin.

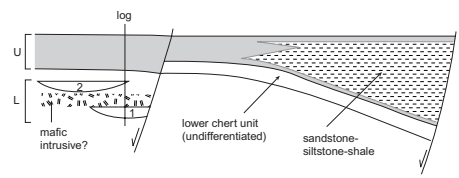

Figure 4.12: Schematic drawing (not to scale) of the geometry of the different units and lenses of silicified sediments at the top of the KG-vsc. L= lower unit, U = upper unit, 1 = chert lens 1, 2 = chert lens 2.

a.

b.

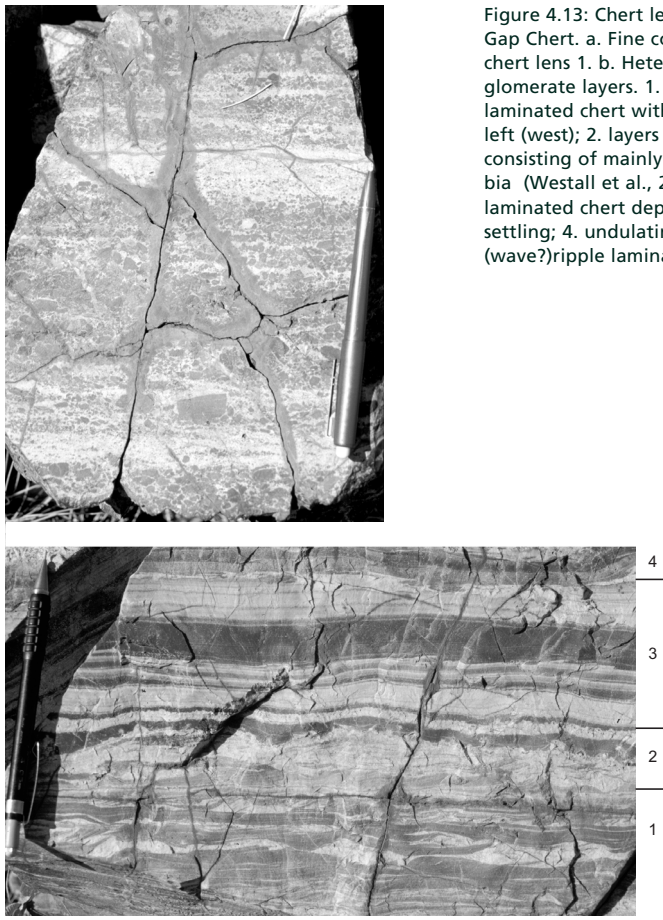

Figure 4.13: Chert lens 1 in the lower unit of the Kittys Gap Chert. a. Fine conglomerate layers at the base of chert lens 1. b. Heterolithic chert overlying the conglomerate layers. 1. small-scale heterolithic ripple-laminated chert with paleocurrent dominantly to the left (west); 2. layers with pumice clasts and biofilms consisting of mainly filamentous and coccoidal microbia (Westall et al., 2004); 3. even to low-angle laminated chert deposited mainly through suspension settling; 4. undulating stratification transitional into (wave?)ripple lamination.

Facies description

Lower unit. The chert lenses 1 and 2 both consist of fining-upward, silicified, black and white sediments, with well-preserved original grain sizes and sedimentary structures, such as cm-scale ripples and flaser-linsen bedding. Chert lens 1 (Fig. 4.11) has its maximum thickness at the log location, where several 1-7 cm thick layers of conglomerate overly poorly exposed layered silty sediments (Fig. 4.13a). The black pebbles have a pale-coloured, fine-grained to medium-grained sandy matrix. The pebbles are well rounded, slightly elongate, with a long axis of up to ca. 1.5 cm. The ungraded, sometimes poorly sorted, to fining-upward conglomerate layers are incorporated in larger, 1-5 metre-scale fining-upward sequences. The layers are laterally discontinuous; within 1.5 m the conglomerates laterally grade into very coarse-grained sandstone beds of 0.5 cm thick. The conglomerate layers are overlain by layers with ripples, flaser-linsen structures and undulating lamination (Fig. 4.13b). Since in the immediately underlying sediments dark sediments are coarser-grained than pale, beige sediments, gradational colour differences from dark to light in very fine-grained millimetre-scale laminated sets overlying the ripple structures, may indicate normal grading.

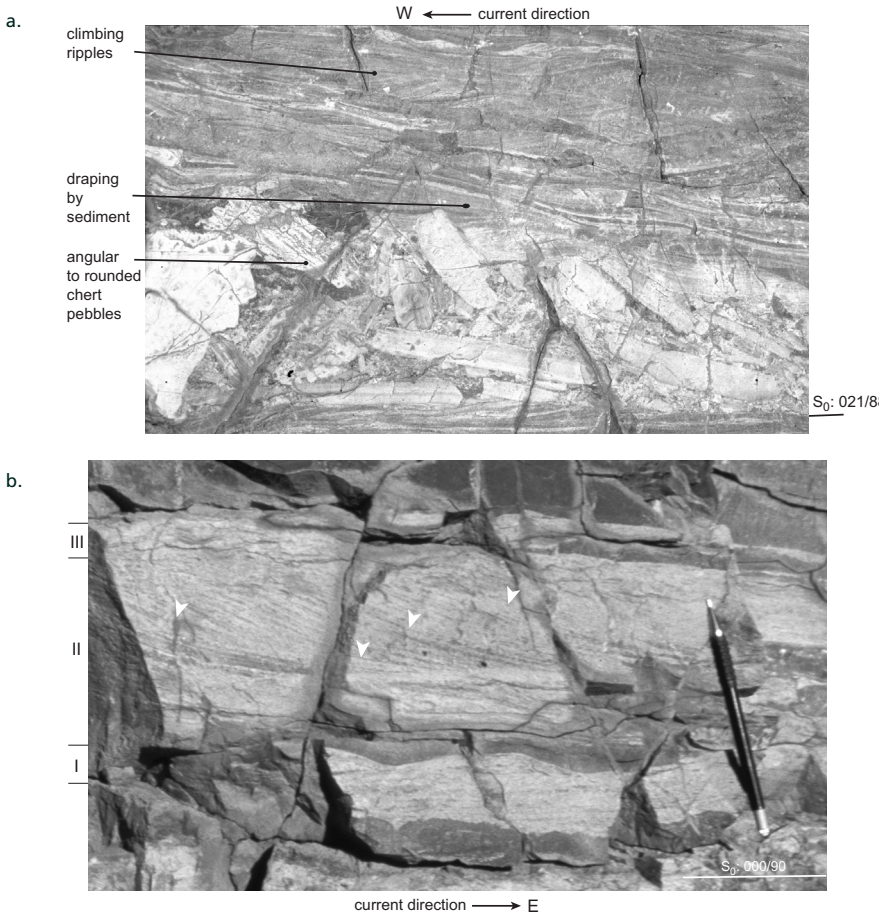

Figure 4.14: Lower unit of the Kittys Gap Chert (lens 1). a. Conglomerate/breccia of banded chert pebbles, with elongated pebbles occasionally in near-vertical orientation. The conglomerate/breccia is draped by very fine-grained sediments, overlain by climbing ripples. Width of photo approximately 25 cm. b. Dm-scale ripples with tangential foresets and repeated reactivation surfaces (indicated with arrows, interval II). Top sets of small ripples (III). Interval II is underlain by climbing ripples (I).

The fining upward interval has a glassy, black chert top, which locally shows relics of a medium-grained precursor texture (at ca. 10-13.5 m in log).

Occasionally, a few floating pebbles are incorporated in the base of the lower chert unit away from the log location, but mostly it consists of coarse to very coarse-grained sand. 20 m west of the log location, the sedimentary sequence contains elongated, angular to sub-rounded banded chert pebbles, which are occasionally oriented vertically. The laterally discontinuous pebble layer is underlain by, and draped with, fine-grained sediments. Above the pebbles, the fine-grained sediments show climbing ripples (Fig. 4.14a). Climbing ripples are observed at several places in the basal part of the lower unit. Approximately 35m west of the log location, ~5-7 cm-scale ripples with tangential foresets show repeated reactivation surfaces (Fig. 4.14b).

a.

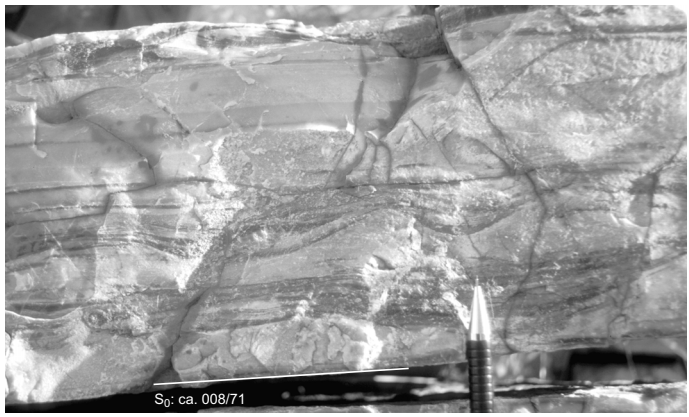

b.

Figure 4.15: a. Wave ripples with a crest spacing of ca. 6 cm in chert lens 2 (lower unit of the KGC). b. Breccia of angular, laminated black chert fragments in a pale-coloured, sand-sized matrix (upper unit of the KGC).

Reliable measurements of the current direction are sparse, and insufficient to plot. There are indications that the current direction was bimodal. Imbrication of pebbles in the basal conglomerates suggests an ENE current (directions 056°, 103°). Ripple foresets in lens 1 also suggest a dominantly eastward current (e.g. Fig. 4.14b), but westward directions are also present (e.g. in the climbing ripples of Fig. 4.14a).

Chert lens 2 has its maximum thickness ~50m west of the log location (Fig. 4.2). The base of the lens is locally conglomeratic, and it has a fining upward character (not visible at the log location). Upward, it contains abundant small-scale sedimentary structures such as current and wave ripples (Fig. 4.15a). Spacing between the crests of the wave ripples is about 11 cm. As in chert lens 1, the nature of the sediments is in places heterolithic. Paleocurrent directions were dominantly to the west (to south-west), but opposing current directions were also observed (dip-directions of foresets after correction for tilt of sequence: 090°; 270°).

Upper unit. At the log location the upper unit consists of glassy silicified, cryptocrystalline, pale green chert without any sedimentary structures (Fig. 4.11). Occasionally, pitch-black outsized, mm to cm-sized grains (or diagenetic colourations; owing to the cryptocrystalline textures of the rock, it is unclear whether or not the black material once formed a distinct grain) are present in some of the

extremely fine-grained chert layers. There are no indications for a coarser-grained texture in the pale green chert prior to silicification. The unit is intensely veined, with translucent veins in the lower part, and black chert vein networks in the upper part of the unit. 200 m west of this location, the upper unit contains coarse breccia layers. The breccia fragments are rounded to angular, black, banded chert of up to 15 cm large in a pale green chert matrix (Fig. 4.15b). The lower breccia layers are matrix-supported. Upwards, the percentage of matrix decreases. The breccia layers are overlain by approximately 2 m wide, 80 cm high low-angle trough fills. The fills are composed of very fine-grained, finely laminated sediments, in which cm-scale ripples become abundant upwards. Along strike, the colour of the upper unit varies between pale green and glassy black. The latter is usually observed in places where the original, often granular, texture is almost completely obscured due to the thorough silicification (except on some weathered surfaces).

Approximately 750 m east of the log location, eastward thickening, poorly silicified sandstone, siltstones/tuffs, and shales become intercalated in the upper chert unit (wedge-shaped geometry, see above and Fig. 4.2). Occasionally more silicified beds are intercalated. The less silicified shales and tuffs are kaolinitic to illitic in composition (H. Kisch pers. comm., 2002). The deposits are dominated by even bedding and lamination. Occasionally, the sandier beds show climbing ripples and small-scale convolution and loading structures. Tight dm-scale folding was locally observed in the shales. The uppermost layers of the shale wedge are silicified and show well-developed cm-scale current ripples.

Also in the upper unit, paleocurrent measurements are sparse. At the log location, indications for the paleocurrent direction were absent. 200m west, ripple foresets indicate current directions dominantly to the E-SE (dip-directions of foresets after correction for tilt of sequence: 088°; 116°; 152°). In the sandstone-siltstone-shale sequence 750m east of the log location, paleocurrent directions both to the E and W(-SW) were found.

Silicification

The sediments of both the BRC and the KGC have been affected by silicification. The degree or intensity of silicification is here taken as the degree to which the original texture can be distinguished in the rock. Poorer preservation of the original texture, and hence a usually more glassy appearance, are interpreted as a higher degree of silicification. Intensities of silicification range from the only slightly silicified BRC unit 3, through the partly silicified sandstone, siltstone and shale wedge in the KGC, to the thoroughly silicified BRC units 2 and 4, and most of the KGC. Also within the thoroughly silicified units, there is a wide range in silicification intensity, from dense cherts with perfectly preserved sedimentary fabrics to massive, glassy, often black cherts lacking any original fabric. These stages also occur side by side; in the same outcrop, a silicification front may completely obscure the original texture in one place, while the texture is silicified but preserved elsewhere (see below).

Other observations on the style and intensity of silicification include:

1. Heterogeneous silicification (i.e. not everywhere the same intensity of silicification) occurs in layered sandstone-chert sequences such as shown in Figs 4.16a and b. In this example, he white layers are more intensely silicified, and mostly show no texture preservation. Contacts with the less silicified, grey, sandy layers are either straight (e.g. along some original layer-boundaries) or irregular (usually when the contact occurs inside a sedimentary layer). Pebbles or fragments of silicified sandstone containing such irregular silica fronts and heterogeneous silicification are incorporated in breccias in the same sedimentary sequence (Fig. 4.16c). The matrix of these breccias is also silicified.

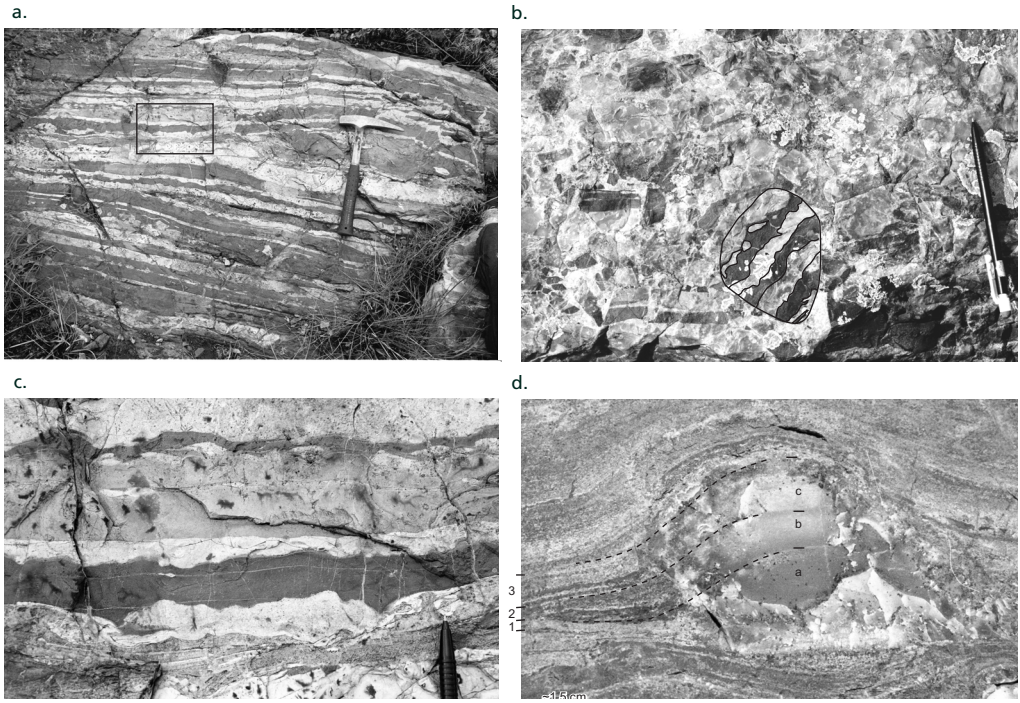

Figure 4.16: a. Bedded, grey sandy chert, showing layer parallel silicification by white chert and low-angle discontinuities in orientation of bedding. b. Detail of area indicated with a rectangle in Fig. 4.16a. c. Breccia in unit 1 of the BR-vsc, including components banded chert-sandstone that show irregular layer parallel silicification (outlined). d. Silica concretion in rhythmically laminated, sandy chert. Uncompacted laminated sets (a, b and c) within the concretion, and corresponding compacted laminated sets (1, 2 and 3). Unit 2, BR-vsc.

2. Angular and thin fragments of chert are incorporated in less-silicified parts of the sedimentary sequence.

3. At several places in the BR-vsc, large, isolated pebble-like silicified objects occur in much finer-grained, less silicified sediments. The objects resemble outsized pebbles, but close inspection shows that lamination of the surrounding sediments passes through the silicified objects (Fig. 4.16d). Hence, they are silica concretions rather than outsized pebbles. The laminations in the surrounding sediments drape the concretion (Fig. 4.16d).

4. Soft-sediment deformation-like structures occur in numerous places in glassy silicified parts of the sequence, especially in the lower part of BR-vsc unit 2.

5. Already silicified sequences (including angular breccias as described above) have been cut by later silica veins or were affected in a later stage, by new silicification fronts (Fig. 4.17a).

6. Veins through silicified sequences show multiple phases of silica deposition in one vein (Fig. 4.17b)

7. Up to ~10cm-large concentric structures of several mm-scale rings or bands occur on bedding planes in both iron-oxide-barren and iron-oxide-rich sediments of the BR-vsc.

a.

b.

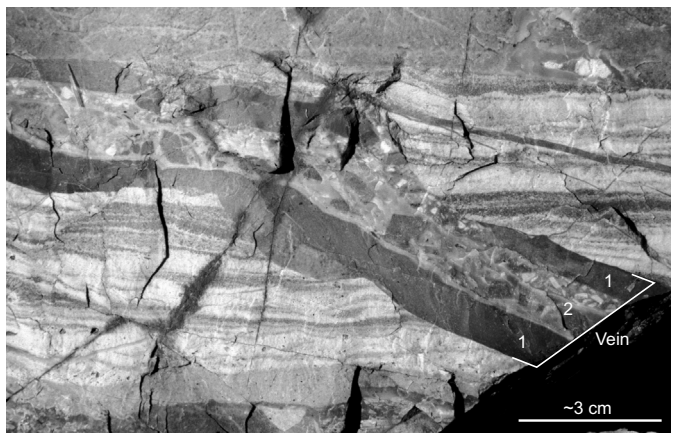

Figure 4.17: a. Silicification fronts (fuzzy, pale grey) affecting dark grey and white cherts in the lower KGC unit. Contacts between silica front and dark grey and white chert indicated with arrows. b. Multiple phases of veining and brecciation of the silicified sediments in the lower unit of the KGC. Black chert along outside of vein (1) is interpreted to have formed first, followed by pale grey chert hosting predominantly black chert fragments (2).

Interpretation and discussion

BR-vsc facies interpretation

Type sections

The sediments in unit 1 generally represent high-energy conditions, particularly the hundred-metre-scale scour structures (see also next section). Unit 1 contains evidence for primary volcanic (pyroclastic) deposition as well as for reworked volcanic (epiclastic) deposits. Primary deposits include lava flows, accretionary lapilli beds and, possibly, surge deposits. The accretionary lapilli implicate 'moist', explosive volcanism (cf. Fisher and Schmincke, 1984; Cas and Wright, 1987). Cross-bedding in (reworked) accretionary lapilli-bearing layers indicate that deposition of unit 1, at least partly, took place in water. Climbing ripple structures may have formed on land, as a result of pyroclastic surges (e.g. Cas and Wright, 1987). Alternatively, they may have formed in water from reworked volcaniclastic material. The climbing ripples point to pulses of high sediment supply. The stalactites in cavity fills in unit 1 indicate that these cavities were at least intermittently air filled. Hence, unit 1 experienced occasional emersion (cf. Lowe and Fisher Worrell, 1999), probably u nder vadose conditions.

Silicified crystals and crystal palisades in unit 1 were used by Lowe and Fisher Worrell (1999) to characterise the paleo-seawater composition. They interpreted the crystals in the BR-vsc to be evaporites that had precipitated from an ocean or coastal water body. Lowe and Fisher Worrell (1999) considered it unlikely that the crystals precipitated from a water body nourished by hydrothermal discharge, because they were 'unable to locate any tufas, spring mounds, or other deposits that are common around hydrothermal discharge sites'. However, we find abundant indications for hydrothermal activity in the vicinity of the crystal occurrences, such as black chert vein stock works, hydrothermal breccias, iron enrichment, and possible sinter deposits (see Chapter 5). Therefore, it seems equally likely that the source of the fluid from which these crystals precipitated was hydrothermal in origin. The input of hydrothermal fluids into surface waters may have led to the formation of a stratified water body, from which the crystals could precipitate. Alternatively, the crystals may have precipitated from hydrothermal fluids in the subsurface, before the fluids reached the Earth's surface. This could explain why, in places, crystals appear to originate from tiny veins in finely laminated sediments (see Chapter 5). The slight upward curvature of the sedimentary layers against some of the silicified crystals (Fig. 4.6a) may have resulted from water-escape prior to crystal growth, or from the force of crystallisation (e.g. Maliva and Siever, 1988) of the growing crystals on the surrounding sediments. Lowe and Fisher Worrell (1999) attributed the curvature to compaction effects adjacent to the crystals. They regarded the disruption too small to have resulted from sediment displacement due to diagenetic crystal growth within sediments.

The lower facies of unit 2 is characterised by a rhythmic pattern of deposition on a scale of 8-15 m. Although 100m-scale scour structures are absent, the abundance of metre-scale cut-and-fill structures, notably in the lower part of the unit, indicates that energy conditions remained relatively high. Within the individual sequences of 8-15m, energy conditions decreased, indicated by a slight trend from cut-and-fill structures near the bases of the sequences to even bedding near the tops. Also within the entire lower facies of unit 2, cut-and-fill structures become less abundant upward at the expense of more even bedding, indicating a gradual decrease in energy level. The badly sorted, repeated (stacks of) outsized pebbles in the coarse-grained sediments indicate that sedimentation was rapid.

Stalactite and stalagmite-filled cavities, particularly in the eastern part of the area, indicate that these cavities were air-filled, at least during the initial stages of quartz precipitation. Hence, like unit 1, the lower part of unit 2 experienced shallow water to occasionally subaerial conditions. The absence of stalactites and stalagmites in the fills of most cavities in the central and western exposures of unit 2 indicates that they were water-filled when the chert and/or quartz fills were precipitated. The observations suggest that in the eastern part the lower facies of unit 2 was occasionally subaerial, while the central and western parts were subaqueous. More research is necessary to confirm this suggestion.

The planar-bedded, fine-grained sediments in the upper part of unit 2 (Fig. 4.8b) mark a transition to much quieter conditions of deposition. Structures in this unit are mainly limited to loading (e.g. Fig. 4.8c), which suggest water-rich sediments and density contrasts between the white and black chert (or their precursors), the white chert being denser.

In the eastern part of the area ('log' D), unit 3 is characterised by rhythmicity on a scale similar to that in the lower part of unit 2. Although the general energy conditions during deposition of unit 3 were also low (unit 3 is dominated by cm-scale even bedding), the structures indicate more variation in energy level than those in the upper part of unit 2. Increased energy levels in the tops of the 20m-sequences are expressed by even-laminated and cm-scale rippled sandstone (Fig. 4.9c). The coarse breccias at the top of the sequences indicate sudden, aberrantly high-energy conditions compared to

the surrounding sediments. The thin, flat components of the breccia suggest that they were of local origin. The thickening of one of the layers towards a vertical, Fe-oxide-rich structure against which it suddenly ends, suggests a relationship between the breccias and the iron-oxide occurrence. Possibly, the breccias were related to hydrothermal (surface) processes, since there are abundant indications for hydrothermal activity in the BR-vsc (Chapter 5). Brecciation due to hydrothermal eruption is a mechanism to juxtapose the aberrantly high-energy breccias with sediments deposited during quieter environmental conditions. A different process that may cause such juxtaposition is, for instance, slumping. However, the breccia layers show no internal consistency or folding, and possible source areas for slumps were not found. It is unclear why the breccia layers form the top of the ca. 20 m sequences.

Both the ripple intervals and the breccia layers become more pronounced in the upper sequences, indicating an upward increase in energy level in unit 3.

Unit 4 shows a further increase in energetic conditions. The laterally well traceable, even bedding that characterises the top of unit 2 and the major part of unit 3 are absent in this unit. Instead, the abundant occurrence of low-angle discontinuities between even-bedded sets, troughs and foresets indicate high-energy conditions. The well-sorted, unimodal quartz composition of the less-silicified basal part of the sequence indicates transport or movement of the grains.

In summary, unit 1 is composed of volcanic and volcaniclastic material, deposited under high-energy conditions and during pulses of high sediment supply. Notably on the higher parts of the fault blocks, this phase was accompanied by local erosion. A high-energy environment and high supply of sediment also characterise the lower part of unit 2. However, sediment in this unit seems to be mostly reworked, i.e. the primary volcanic influx seems less. Both unit 1 and the lower part of unit 2 were deposited in shallow water, and experienced occasionally subaerial conditions. This reflects a regression with respect to the underlying pillow basalts in the upper part of the Hooggenoeg Formation (Chapter 2). The upper part of unit 2 was deposited in a low-energy, sheltered environment, probably under lagoonal or lacustrine conditions. During deposition of unit 3, the energy conditions gradually increased in a rhythmic manner. The successive tops of the sequences, interpreted as increasingly littoral conditions, indicate a gradual transgression, which continued during deposition of unit 4. Relative sea-level rise may already have started during deposition of the upper part of unit 2. The 20m rhythmic pattern of deposition that characterises units 2 and 3, could be related to higher order sea-level fluctuations. Deposits of unit 4 resemble those of modern-day littoral environments. The low-angle discontinuous even-bedded sets, composed almost exclusively of well-sorted quartz, may be compared to beach deposits. The overlying low angle troughs, filled by cross-bedded sets and undulating layers of sandstone that flatten towards the top, could be interpreted as shoreface deposits in such a model.

Facies distribution within the structural framework

The distribution of the sediments at the top of the BR-vsc is related to the normal fault pattern. The thickness differences of the lower units across the faults indicate that the faults were active at the time of deposition of the sediments. Growth faulting ceased during deposition of the higher sedimentary units.

The tens of metres wide scour structures in unit 1 are a local erosive phenomenon and do not mark a regional unconformity. Local unconformities did form in the footwalls of the normal faults, while deposition in adjacent, subsiding areas continued (cf. Lowe and Fisher Worrell, 1999, De Vries, 1999). The scours may have resulted for instance from mass-transport off the higher parts of the fault

blocks, or by pyroclastic surges that affected the fault blocks. The eastward oriented foresets in the scour structure of Fig. 4.4b indicate eastward-directed sediment transport. This may be the reflection of volcanic activity in the western part of the area, or of the local gradient due to tilting of the fault blocks.

In general, the sediments of the BR-vsc consist mainly of locally derived volcanic and volcaniclastic material. The volcanic deposits were either primary, sometimes water-reworked soon after deposition, or products of local erosion caused by tilting and slight uplifts of blocks due to normal fault activity. The locally present thin, breccia layer in BR-vsc unit 1 contains fragments of banded cherts, silicified crystals and felsic components of the same composition as the unit in which they were deposited. Sparse, small, fuchsitic chert fragments in the breccia probably represent altered basalt detritus from underlying stratigraphic levels. Apart from that, there is no evidence for erosion of the underlying pile of mafic and ultramafic material rocks. Also, there is no evidence for supply from granite or gneiss terrains in the hinterland. This lack of evidence for regional erosion of older units indicates that there was probably no significant subaerial relief in the deposition area around 3.4 Ga ago.

Both the block motion (west-block down normal faulting) and the general fining of the sediments from east to west, notably in the felsic volcaniclastic deposits and the third sedimentary unit, indicates that the basin margin was to the east, while the deeper parts of the basin were in the west. Westward-directed foresets in unit 4 are in agreement with this.

KG-vsc facies interpretation

Type section

The lens-like geometry of the chert bodies in the lower unit of the KGC, with conglomerates at the base and a generally fining upward trend in grain size, suggests that these cherts represent (*en echelon*) stacked channel deposits. Within the individual chert lenses, the energy decreases from a high-energy environment marked by conglomerates at the base to medium, fluctuating energy level marked by rippled sandy sediments to a low-energy environment in the top, expressed by mm-scale rhythmic sets of even-laminae. Climbing ripples overlying the conglomerates (Fig. 4.14a) and elongate chert pebbles incorporated in the sediments in a vertical position indicate that sediment supply and energy-level were high. Heterolithic sediments indicate rapid fluctuations in energy level, and the availability of different types of sediment. Ripple foresets and imbrication of pebbles suggest varying (bimodal) current directions throughout the lower unit. Repeated reactivation surfaces (Fig. 4.14b) indicate alternating periods of ripple migration and periods of (partial) erosion of the ripples by opposite currents. The basal pebbles, as well as most of the overlying deposits represent reworked volcanic and clastic material. Exception is a erosion surface capped by pumice fragments (Westall et al., 2004), which occurs in a heterolithic interval of chert lens 1 (Fig. 4.13b) and, possibly, some of the even-laminated fine-grained layers, which may be primary ash fall deposits.

In most places, the environment of deposition of the upper KGC unit is similar to that of the lower unit. The upper unit also contains abundant small-scale ripple structures, including climbing ripples indicating pulses of high sediment supply and ripples indicating variable current direction. However, the upper unit does not show the strong lens-shaped geometries or fining upward trend that are characteristic of the lower unit. Furthermore, it includes, for example at the log location, finer-grained, massive deposits, probably reflecting lower-energy conditions.

The thicker, poorly silicified sandstone, siltstone and shale interval towards the east also represents a lower-energy, and probably more distal, facies. Despite the low-energy environment, occasional

climbing ripple structures indicate pulses of high sediment supply. Small-scale convolutions indicate that the sediments were water-rich. These deposits may represent distal turbidites.

Exceptionally coarse and angular breccias that occur in the upper unit west of the log location indicate abrupt changes in the otherwise rather stable energy conditions. The angularity of many of these fragments and the lack of an erosional base indicate that they are not likely to be channel fills. Despite syndepositional fault activity, the breccias do not seem to be geometrically related to the fault locations. Considering the vicinity of black chert vein systems in the underlying volcaniclastic deposits and lavas (see also Chapter 5), these breccias may have resulted from explosive hydrothermal activity.

The varying current directions and the wave ripples in both the upper and lower unit of the KGC may be the result of tidal action, or currents due to winds from varying directions. However, the combination of heterolithic deposits (indicating rapid fluctuations in energy level), rhythmic lamination in the lowest-energy deposits, ripples with repeated reactivation surfaces that indicate a bimodal current direction, and wave ripples suggest that tidal action may indeed have influenced the deposition of the KGC.

In such an interpretation, the lens-shaped, fining upward sequences of the lower KGC may be compared to modern-day (stacked) tidal channels and tidal flats. The massive, medium-grained interval capping the fining-upward sequence of chert lens 1 at the log location (Fig. 4.11) may represent the reworked channel-fill top, analogous to channel-fill deposits in modern estuarine environments.

Facies distribution within the structural framework

The influence of syndepositional faulting on the KG-vsc sediments is most evident from the wedge-shaped siltstone-sandstone-shale interval in the top of the upper chert unit. Grain-size trends or sedimentary facies changes directly related to tectonic activity during deposition of the KGC (e.g. coarse deposits along fault scars) were not found.

The sediments of the KG-vsc seem to consist mainly of locally derived volcanic detritus and chert. The products of volcanism and hydrothermal activity were either incorporated in the sedimentary sequence directly, or reworked soon after deposition and immediately re-deposited. There is no evidence for the erosion of rocks below the KG-vsc, or of older granitoid complexes. This lack of evidence for erosion indicates that there was no significant subaerial relief in the Kittys Gap area at the time of deposition of the KGC.

Post-sedimentary, diagenetic effects on the BR-vsc and KG-vsc sediments

Silicification has strongly influenced the original sedimentary fabric of the BR-vsc and KG-vsc sediments, thereby complicating the interpretation of their environments of deposition.

Apart from the complete loss of fabric in the most thoroughly silicified parts of the sequences, heterogeneous silicification of the sedimentary sequence has resulted in many complications of the sedimentary structures. In originally layered sediments, heterogeneous silicification has obscured original contacts between layers in places where the silica-rich fluids could freely percolate into adjacent layers, while the original contacts have been accentuated in other places, probably due to permeability differences between the layers. Within layers, irregular silica fronts have been formed independently of the original sedimentary bedding or structures. The implication of this is that observations and interpretations of sedimentary structures, notably of cross-bedding and crosscutting relationships between different 'layers' in chertified sediments, can only be made with extreme care. To exclude confusion between original sedimentary features and artefacts due to silicification,

observations on sedimentary structures should preferable be based only on layers or laminae within a layer with a uniform degree of silicification.

Part of the soft-sediment deformation structures (e.g. loading, ball and pillow structures) in BR-vsc unit 2 may have been caused by heterogeneous silicification, due to density differences between the silicified sediments and the original or less silicified sediments. Triggers for convolution of the sediments could be movement on the growth faults, pressure build-up and release in hydrothermal systems, earthquakes, storms, etc.

Concentric, circular structures in both iron-oxide-rich and iron-oxide-barren sediments of BR-vsc are also interpreted as the result of discontinuous Fe- and Si-precipitation (concentric bands due to discontinuous precipitation are known as Liesegang bands, e.g. Varghese and George, 2004 and references therein). The concentric circles resemble structures that were described previously from the overlying Fig Tree group (De Wit et al., 1982; De Ronde et al., 1994). The latter were interpreted as mudpool structures. In the study area there is no evidence that these concentric structures are the result of hydrothermal activity at the surface. The structures in the BR-vsc are interpreted as a later, diagenetic effect, and therefore do not give any information about the environment of deposition of the sediments in which they occur.

Timing of the silicification

Pebbles or fragments of banded chert containing silica fronts and irregularly silicified sediments are incorporated into breccias in the same sedimentary sequence, indicating that this type of heterogeneous silicification must have occurred during deposition of the sequence, prior to the incorporation of the fragment in the breccia (Fig. 4.16c). Similarly, angular and thin fragments of (now silicified) sediment preserved in the sequence indicate that already silicified layers were broken up and the fragments re-deposited in the immediate vicinity. This also suggests that silicification was contemporaneous with deposition of the sediments.

Differential compaction within and outside the concretion in Fig. 4.16d led to the draping of sediments over the concretion, and indicates the early diagenetic formation of the concretion.

Pebbles or fragments consisting of a heterogeneously silicified banded sediment, including silica fronts (Fig. 4.16c) are incorporated in breccias in the sedimentary sequence. The matrix of these breccias is now silicified as well. Likewise, the host rock to silica concretions (Fig. 4.16d) is now silicified, both examples indicating that silicification was a multiphase process.

Origin of the silica

Tracing of the origin of the silica responsible for the thorough silicification of the BR-vsc and KG-vsc sediments is beyond the scope of this study. However, there are indications that the silicification of the BR-vsc and KG-vsc sediments was, at least in part, related to hydrothermal systems that were active in those areas during and immediately after deposition of the sediments (Chapters 5 and 6). In addition to a magmatic silica source, a large part of the silica may have originated from seawater supersaturated with respect to Si, which was circulated through the sedimentary pile by the hydrothermal systems. It has been suggested that the Si content in Archaean seawater was much higher than today, since the silicious organisms that buffer the silica concentrations in the oceans today, did not exist yet (e.g. Holland, 1972; De Ronde et al., 1997b).

Discussion and Conclusions; preserved early Archaean sedimentary deposits of ~3.5-3.4 Ga

The geological settings of the BR-vsc (Barberton, South Africa) and KG-vsc (Pilbara, Australia) are very comparable. The geometry of the sedimentary sequences at the top of these complexes, and, locally, the facies distribution within the sequences, were influenced by syndepositional normal faulting. The sedimentary sequences were deposited in shallow water close to base level, and are mainly composed of locally derived volcanic and volcaniclastic detritus. The sediments were affected by silicification during and immediately after deposition, which led to excellent preservation of sedimentary textures and structures in some places, and complicated the interpretation of the environment of deposition in other places. Silicification was a contemporaneous and early diagenetic, multiphase process, which occurred heterogeneously throughout the sedimentary pile. Despite these similarities, the sedimentary facies of both complexes also show differences. The lower BR-vsc sediments contain both primary and reworked volcanic and volcaniclastic deposits, and occasionally experienced emersion. They show a regressive trend with respect to the underlying pillow basalts. These sediments are overlain by a sequence deposited under low-energy, possibly lagoonal conditions, which is in turn capped by littoral deposits. The upper part of the BR-vsc sedimentary sequence is interpreted to have been deposited during a transgression. The KGC consists almost exclusively of reworked sediments that were mostly deposited subaqueously. The channel-flat geometry, fining upward sequences, heterolithic sediments, varying current directions and the reactivation surfaces that indicate a bimodal current direction, suggest that the KGC sediments may have been deposited under tidal influence.

The main difference between the two sedimentary sequences seems to be that the energetic conditions during deposition of the KGC were on average slightly higher than those during deposition of the middle and upper parts of the BR-vsc sedimentary sequence. Compared to modern-day sedimentary environments, this could reflect, for instance, the presence or absence of a barrier with open marine conditions, resulting in lagoonal conditions (BR-vsc) and (possible) tidal influence (KG-vsc), respectively.

The BR-vsc and KG-vsc sedimentary sequences are comparable to the sediments at the top of the ~3.49 Ga old North Pole volcano-sedimentary complex (NP-vsc) on the eastern flank of the North Pole Dome (East Pilbara, Australia; Nijman et al., 1998a). The geological setting of the NP-vsc is broadly comparable to those of the BR-vsc and KG-vsc. The most important difference is the absence of felsic volcanic or felsic igneous rocks in the NP-vsc; the NP-vsc sediments were deposited on a basaltic substrate. The distribution of the sedimentary facies was strongly controlled by syndepositional normal faults, which resulted for example in the clustering of stacked channel fills in the hanging walls of the faults (Nijman et al., 1998a). Sedimentary structures indicate that the now silicified sediments were dominantly deposited in an inter-tidal environment. The approximate maximum depth of the North Pole Chert basin floor facies was estimated at about 50-70 m, based on the total thickness of infill of accommodation space.

Acknowledgements

Fieldwork for this research was supported by the Stichting Dr. Schürmannfonds, grants 1998/14-2001/14 and 2002/10. MSc students O. Houtzager, I.M.A. Vos and K.L. Louzada took part in the fieldwork.

Chapter 5

Faults, veins and breccias: early Archaean hydrothermal systems in the Barberton and Pilbara Greenstone Belts

Abstract

This chapter provides detailed field relationships between faults, veins and breccias in felsic volcanic deposits and overlying sediments from both the Barberton Greenstone Belt (South Africa) and the Coppin Gap Greenstone Belt of the East Pilbara (Australia). It aims at giving insight into the general geologic setting of early Archaean hydrothermal systems, and providing information about their geometry, and the locations of vent-systems at the surface.

The Buck Ridge volcano-sedimentary complex in the Barberton Greenstone Belt (South Africa) and the Kittys Gap volcano-sedimentary complex in the Coppin Gap Greenstone Belt (Australia) are of approximately the same age (~3.4 Ga). The geology of these two areas is similar; both areas comprise a dominantly felsic volcanic complex capped by a silicified sedimentary sequence, deposited during the activity of normal faults. In the top of the volcanic sequences, just below the sediments, metre-wide black chert veins occur in both complexes. They are interpreted to be remnants of early Archaean hydrothermal systems. The vein systems tend to occur preferentially in the hanging walls of the normal faults. The hydrothermal systems were active during or shortly after deposition of the sediments and caused early and multi-phase silicification, veining and brecciation of the sediments. The BR-vsc and KG-vsc hydrothermal systems are interpreted to have vented in shallow water, near base level. They were not formed in a deep-sea environment or a mid-ocean ridge setting, as was suggested for some other early-mid Archaean hydrothermal systems.

Introduction

The study of early Archaean hydrothermal systems contributes to the understanding of the environmental conditions that once existed near the Earth's surface. Hydrothermal systems connect processes operating at the surface to those in the subsurface, and are generally linked with processes at deeper crustal levels. Another important aspect, particularly in the early Archaean, is the possible relationship between hydrothermal activity at the surface and the development of early life on Earth. Hydrothermal systems are also considered primary targets in the search for life on other bodies in the solar system (Farmer, 2000). Consequently, studies on and the search for life on planets like Mars may

greatly benefit from studies on early Archaean hydrothermal systems.

The occurrence of hydrothermal systems in the early Archaean has already been mentioned by various authors. So far, studies on hydrothermal activity mostly focussed on alteration and mineralisation. Barley (1984) used the alternation of strongly altered pillow basalt flows and relatively unaltered flows in the Warrawoona Group (Pilbara, Western Australia) as evidence that this alteration resulted from interaction with a circulating hydrothermal fluid. Both Barley (1984) and Buick and Barnes (1984) stated that chertification of the Warrawoona Group sediments may have been caused by the circulation of hydrothermal fluids. Based on geochemical analyses, Sugitani (1992) and Minami et al. (1995) confirmed that cherts from various locations in the Pilbara are of hydrothermal origin. Mid Archaean hydrothermal systems were reported by Vearncombe et al. (1995; 1998; Pilbara, Western Australia) and De Wit et al. (1982) and De Ronde et al. (1994; Barberton, South Africa). Vearncombe et al. (1995, 1998) described ~3.26 Ga old volcanogenic massive sulphide deposits related to hydrothermal systems in the Strelley Greenstone Belt (also referred to as Soanesville Belt, Hickman, 1983; Van Kranendonk, 1998). The identification of the major hydrothermal centres in this area was mainly based on mineralisation and the degree of alteration. De Ronde et al. (1994) described ~3.2 Ga old ironstone pods from the southern part of the Barberton Greenstone Belt, which were interpreted as hydrothermal discharge zones on the seafloor (an interpretation recently disputed by Lowe and Byerly, 2003).

Limited information is available, however, on the recognition in the field of early Archaean hydrothermal systems. Their geometry, timing and surface locations are not well known.

Nijman et al. (1998a) described a hydrothermal system from the Panorama Greenstone Belt (nomenclature by Van Kranendonk, 1998) in the Pilbara, where black chert veins ascend from a basaltic substratum towards the overlying ~3.49 Ga North Pole chert-barite unit (model lead age recalculated by Thorpe et al., 1992a from data of Richards et al., 1981). The chert-barite unit was placed stratigraphically in the Dresser Formation by Van Kranendonk (2000). The Dresser Formation, formed by silicified sedimentary cherts interbedded with pillow basalt, was interpreted to have been deposited during normal fault activity (Nijman et al., 1998a). The veins, which are up to 10 metres wide, are geometrically related to the fault pattern, and are syndepositional with the chert-barite unit.

The present study extends the work by Nijman et al. (1998a) to two other early Archaean greenstone belts. It provides detailed field relationships between vein systems, host rock, and overlying sediments from both the Barberton Greenstone Belt (South Africa) and the Coppin Gap Greenstone Belt of the East Pilbara (Australia). Together with the Panorama belt example, it improves the insight into the general geologic setting in which early Archaean hydrothermal systems occurred, and provides information about their geometry and the locations where they vented at the surface.

General geology of the study areas

The ~3.45-3.42 Ga Buck Ridge volcano-sedimentary complex (BR-vsc) in the Barberton Greenstone Belt (South Africa, Chapter 2) and the ~3.45 Ga Kittys Gap volcano-sedimentary complex (KG-vsc) in the Coppin Gap Greenstone Belt (Australia, Chapter 3) show similar stratigraphy and large-scale geometry. The BR-vsc forms the uppermost part of the Hooggenoeg Formation (study area indicated in Fig. 5.1). It consists of an alternation of basalts with shallow felsic intrusives and rhyolitic to dacitic lavas, capped by a sedimentary sequence (Chapter 2). The sedimentary sequence is divided into four units: (1) a partly silicified volcaniclastic unit characterised by several

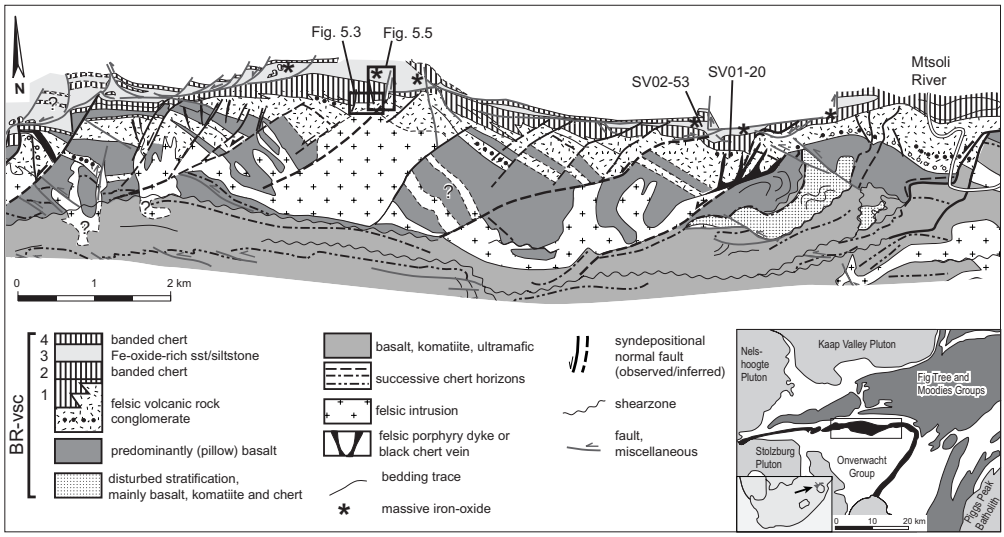

Figure 5.1: Simplified geological map of part of the BR-vsc (after Chapter 2; for location in southern Barberton Greenstone Belt, South Africa, see inset). Legend applies to main figure, not to inset.

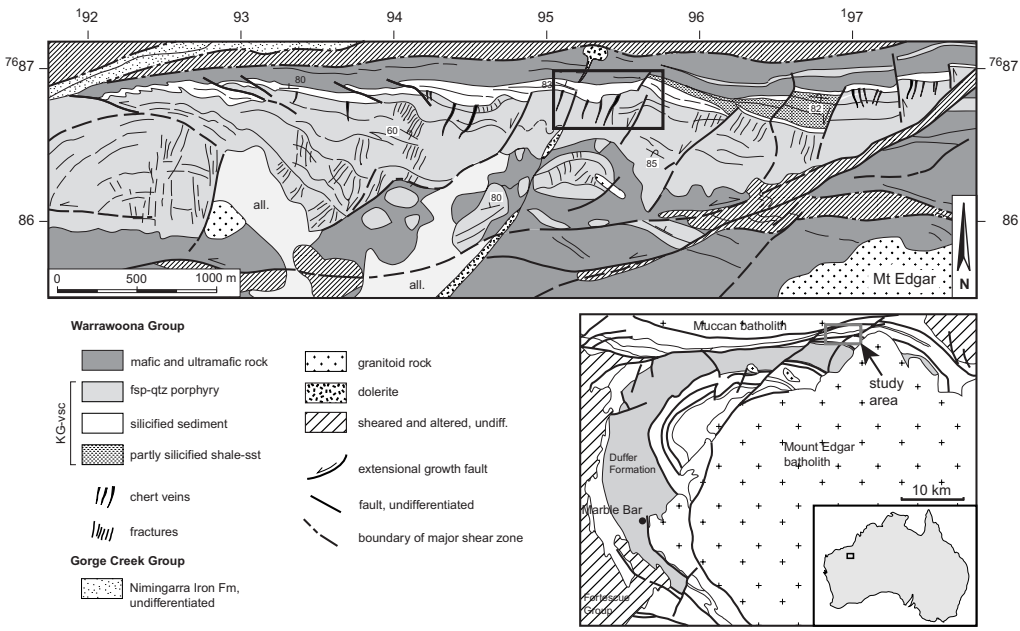

Figure 5.2: Geological map of the Kittys Gap volcano-sedimentary complex (KG-vsc) and surrounding rocks. Location in Coppin Gap - Marble Bar Greenstone Belt indicated in inset. Black chert veins occur in the top of the quartz-feldspar porphyry. Fractures with a similar orientation occur at several levels in the quartz-feldspar porphyry. Main study area indicated with a rectangle. Legend applies to main figure, not to inset.

tens to hundred metre-wide scour-structures, (2) a banded sedimentary chert, (3) an iron-oxide-rich sandstone-siltstone interval, which in places includes breccia and massive iron-oxide occurrences and, (4) a well-banded silicified sandstone (Chapter 4). The latter three units are usually considered to form the Buck Ridge Chert (BRC). Occasionally, the first unit is glassy silicified and is also regarded as BRC (Chapter 4). The KG-vsc, in the upper Warrawoona Group of the Coppin Gap Greenstone Belt (study area indicated in Fig. 5.2) has a similar stratigraphy. A felsic volcanic complex, consisting mainly of rhyolitic porphyritic rock, is overlain by a chertified sedimentary sequence, the Kittys Gap Chert (KGC, Chapter 3). The KGC consists of a relatively coarse-grained lower interval with abundant sedimentary structures and an upper interval that occasionally shows sedimentary structures, but consists mostly of massive, extremely fine-grained (cryptocrystalline) chert (Chapter 4). Both the BR-vsc and the KG-vsc are cut by large-scale normal faults (Figs 5.1 and 5.2). On the basis of field observations, these faults appear to have been active during deposition of the BR-vsc and KG-vsc (Chapters 2 and 3). Small felsic intrusive bodies with an approximately similar U-Pb-age as the felsic lavas (3451± 5 Ma, Chapter 2), intruded the BR-vsc preferentially along the normal fault planes. The intrusions are interpreted to have occurred at a depth of ~1.5 km below the Earth's surface at that period (Chapter 2).

Within these two areas with well-known geological settings and sedimentology, key localities were selected for detailed mapping and small-scale observations related to hydrothermal activity.

Results

The Buck Ridge and Kittys Gap volcano-sedimentary complexes (Figs. 5.1 and 5.2) are cut by approximately bedding-perpendicular fractures and veins. In the KG-vsc, fractures are present at several levels of the quartz-feldspar porphyritic unit (Fig. 5.2). In the upper 200m of this unit, metre-wide black chert veins occur. Both the veins and the fractures tend to concentrate in the hanging walls of the normal faults. In the BR-vsc fractures occur only occasionally. In addition to metre-wide black chert veins, the top of this volcanic complex comprises felsic and mafic to ultramafic dykes in the same orientation as chert veins (see Chapter 2). The felsic porphyritic dykes reach high up into the felsic sequence. The black chert veins occur in the upper 100-125m of the felsic sequence, and can be traced up to the silicified sediment interval (Fig. 5.1). The fractures, veins and dykes occur preferentially in the hanging walls of the faults.

The focus in this chapter is on the chert vein systems in the upper part of the volcano-sedimentary complexes in both areas.

Chert veins in the felsic lavas and volcaniclastic sequence

Black chert veins occur in the upper 125-200 metres of the felsic volcanic units of the BR-vsc and KG-vsc (Figs 5.1 and 5.2). At depth they consist of fine networks of mm-scale veinlets, which gradually merge stratigraphically upwards to form large, up to two metre-wide, black chert veins. Occasionally, black chert and vein-parallel, minor quartz in the veins show a crack-and-seal structure.

In the KG-vsc, centimetre-large fragments of felsic host rock are incorporated into the veins. Close to the overlying sedimentary cherts, the fragments in the veins include banded sediments. The fragments range from slightly silicified, with total preservation of texture, similar to the surrounding felsic volcanic host rock, to pervasively glassy-black silicified, making the fragments almost indistinguishable from the black chert veins.

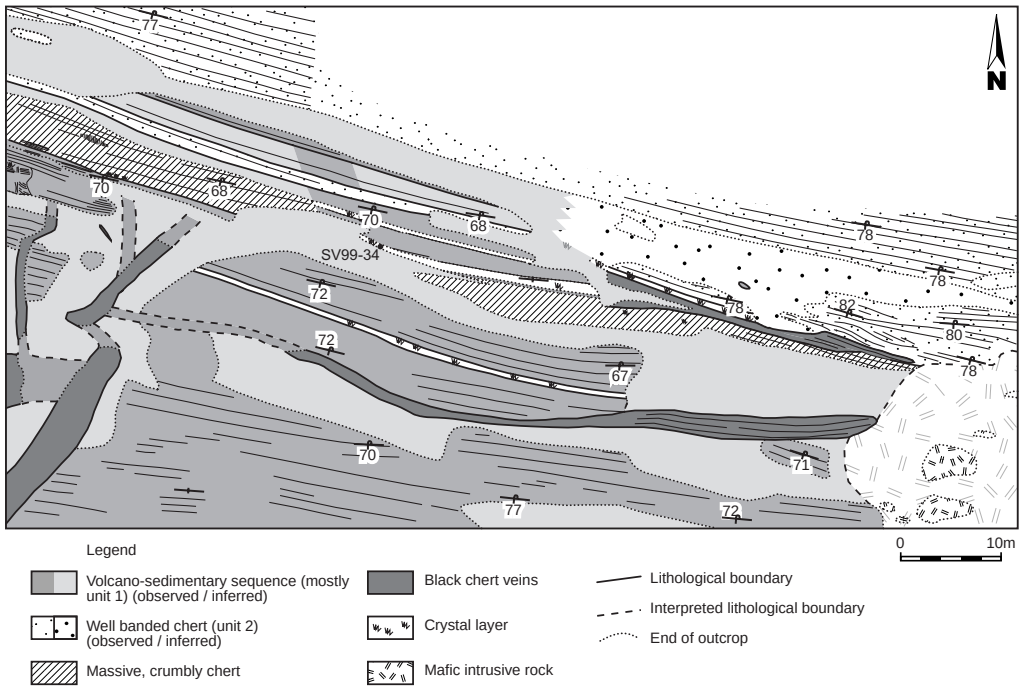

Figure 5.3: Detailed map of black chert veins ascending trough felsic host rock, but not crosscutting the overlying silicified sediments (BR-vsc, Barberton Greenstone Belt, South Africa). Location indicated in Fig. 5.1.

In the BR-vsc, a chert vein shows bedding-parallel offshoots just below the main sedimentary unit (Fig. 5.3). This is expressed by bedding-parallel veins and intensely silicified host rock layers.

Although at the macroscopic scale the veins appear to consist of pure, textureless chert, in thin section a precursor texture is visible in most samples. Samples from the North Pole Dome in the Pilbara, where Nijman et al. (1998a) described veins in a similar setting, also show ghost-textures in what macroscopically seems to be a pure, textureless chert.

Chert veins and breccias in the silicified sediments

The metre-wide black chert veins that occur in the felsic lavas and volcaniclastic sequence (see previous section) cannot be traced into the overlying sedimentary sequences that form the top of the BR-vsc and KG-vsc. Although the sedimentary sequences are intensely silicified (see Chapter 4), they generally lack chert veins of more than a centimetre in width. However, they do show brecciation and intense mm to cm-scale veining. Based on field observations, these breccias and veins are divided into five types. The first two types occur in the sediments immediately above or within tens of metres of the metre-wide black chert veins in the underlying felsic volcanic unit. The latter three types occur in the silicified sediments apparently unrelated to the locations of the metres-wide black chert veins.

The first type of breccia is characterised by *in situ* derived breccia fragments that have been rotated and displaced with respect to each other (i.e. there is no 'jigsaw' fit between the fragments, and fragments from different layers have been mixed), and are hosted by a translucent chert matrix (Fig.

5.4a). This type of brecciation occurs for instance ten metres west of the termination of one of the main chert veins at Kittys Gap, where the original sedimentary layering has completely been destroyed over an area of about 5 metres wide. Locally, the sedimentary fabric has completely been lost due to pervasive silicification (see also Chapter 3). Further away from the vein, the sediments are brecciated but the individual fragments still show a 'jigsaw' fit, or the sediments are still in tact but are cut by abundant mm-scale veins.

A second type of breccia that is spatially related to the vein systems is characterised by fragments of different sizes (cm up to metres) in an extremely iron-oxide-rich matrix. The most prominent example of this is found in the BR-vsc, immediately above the major black chert vein system that is partly shown in Fig. 5.3. At this location, a hundred-metre-scale funnel-shaped breccia (Fig. 5.5) cuts through BR-vsc unit 2 and ends in unit 3. The matrix-supported breccia consists of fragments of banded chert and felsic volcanic rocks, in an extremely iron-oxide-rich matrix. This breccia type was only observed in the BR-vsc.

The third type of veins and breccias are metre-scale breccias, breccia-filled veins and intensely veined parts of the host rock. The breccias and veins are almost perpendicular to bedding. Some of

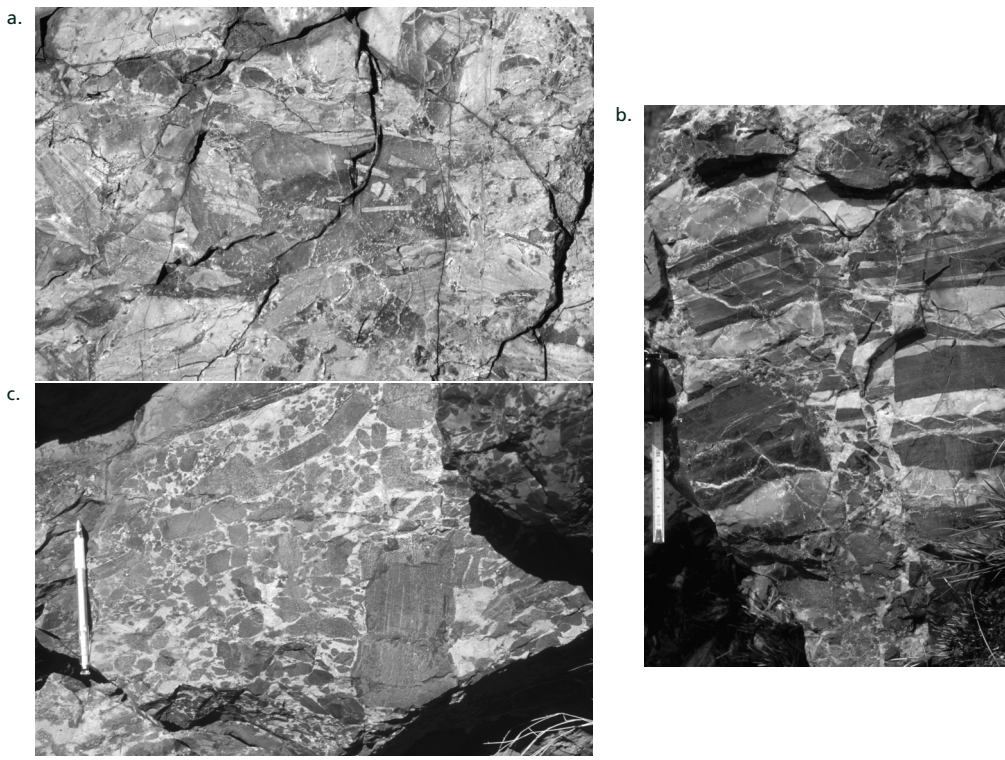

Figure 5.4: Different types of breccia in the KG-vsc and BR-vsc. a. completely mixed breccia fragments in matrix of translucent chert, occurring close to a major vein termination in the KG-vsc. b. bedding-perpendicular hydraulic breccia, angular fragments almost in-situ, BR-vsc. c. Unsorted sedimentary breccia in the upper unit of the KGC.

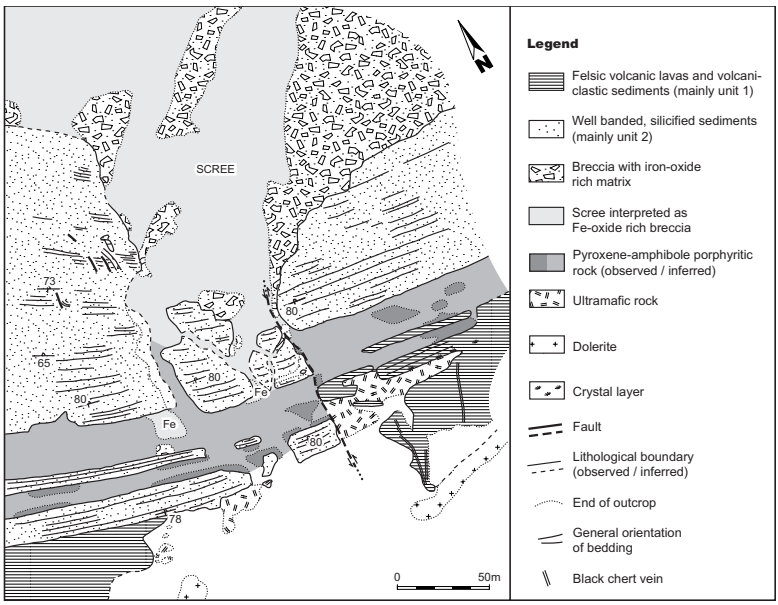

Figure 5.5: Detailed map of funnel-shaped breccia in the BR-vsc. Location indicated in Fig. 5.1.

the veins and breccia bodies widen upwards. Breccia fragments are mostly angular and usually show only slight displacements with respect to each other (Fig. 5.4b). The vein fills and breccia cement consist of coarse quartz or chert. This type of veining and brecciation occurs mainly in the first and second unit of the BR-vsc and was not observed in the KG-vsc.

The fourth type of breccia shows a range of sub-angular to well-rounded fragments in a chert matrix. In places, the fragments are so well rounded that they are more like a conglomerate. These breccias may sometimes be discordant, but are mostly parallel to bedding. The bedding-parallel bodies are usually restricted to layers of a few tens of centimetres thick and sometimes grade along strike into a banded chert sequence. They mainly consist of platy, but rounded slabs of chert in a glassy chert matrix. This type of breccia is not abundant; it was rarely observed in the BR-vsc. Previously, breccias of this type were described and illustrated by Stanistreet and Hughes (1984), who termed them pseudoconglomerates, and by Paris et al. (1985).

The fifth type of breccia includes coarse, unsorted breccia layers with completely silicified banded chert cobbles in a matrix of light-green chert in the upper unit of the KGC (Fig. 5.4c). Contrary to the previous four types, this breccia type has a sedimentary matrix. The breccia layers are part of the normal stratigraphic sequence, but the breccia fragments are aberrantly coarse compared to the otherwise silty to medium sand-sized sediments. Occasionally, the surrounding sand-sized beds show centimetre-scale rippled sediments, wavy beds of very fine-grained, finely-laminated sediments and trough cross-bedding. Similar layers of relatively coarse breccia in otherwise sand-sized sediments are present in the third sedimentary unit of the BR-vsc (loc. SV02-53, Fig. 5.1). However, the fragments in these layers are more rounded, thin and elongated. They resemble type 4 breccias, but lack a glassy chert matrix. They occur at more or less regular intervals of about 20 metres, capping sequences of iron-oxide-rich banded chert and sandstone (see for details Chapter 3).

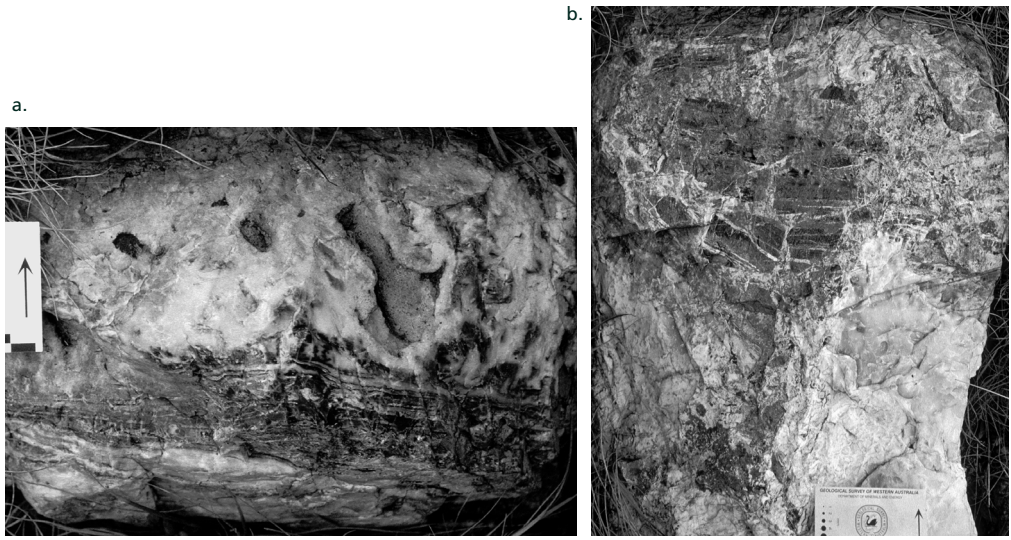

Figure 5.6: a. Finely laminated black chert and agate-like cavity fills in a thin chert layer intercalated in the felsic volcanic sequence in the eastern part of the BR-vsc. For location see Fig. 5.1. b. Brecciation of finely laminated chert layer in the vicinity of SV02-20.

Precipitation from fluids: sinters, polyphase cavity fills and mineralisation

Apart from veins and breccias, there are a number of other observations indicating fluid activity and mineral precipitation from the fluids in the top of the volcanic unit and the overlying sedimentary sequence.

At loc. SV01-20 (Fig. 5.1), at the top of the felsic volcanic complex of the BR-vsc, pure white chert lenses and laterally inconsistent, locally finely laminated chert layers of a few tens of centimetres thick and a few metres wide occur intercalated between the felsic lava flows, brecciated volcanic rocks and volcaniclastic beds (Fig. 5.6). In the top, the chert layers contain chert-filled and quartz-filled (paleo-)cavities. Some of the cavities seem to be floored, with sediments preserved at the bottom. However, the latter is difficult to prove, due to pervasive silicification. The layer-parallel chert outcrops are underlain by felsic volcanic rocks that are cut by mm to cm-scale black chert and quartz veins. They are not directly associated with metre-wide black chert veins such as found elsewhere in the felsic volcanic succession (see previous section). The felsic volcanic rocks also contain agate-like cavity fills, with chert at the rims and coarser quartz in the centres. In places, the cavity fills occur associated with brecciation of the felsic volcanic sequence.

Quartz and chert have also been precipitated in the space between stacked, rounded chert pebbles

Type	*Description*
1	large, individual prismatic crystals as much as 20 cm long that increase in diameter upward
2	small, isolated microscopic crystals having the same shapes as type 1 crystals
3	small, tapering-upward prismatic crystals as much as 5 cm long
4	small acicular crystallites forming halous around type 1 crystals
5	tightly packed, subvertical crystal aggregates within which individual crystal shapes cannot be distinguished

Table 5.1: Summary of principal crystal types distinguished by Lowe and Fisher Worrell, 1999.

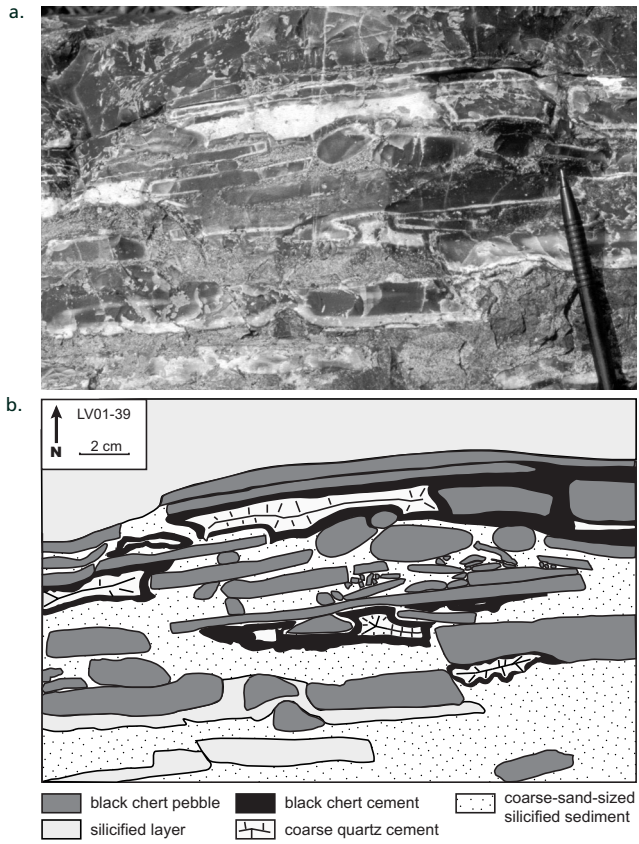

Figure 5.7: Picture (a.) and interpretation (b.) of stacked pebbles showing cavity with sediment at the base and black chert and coarse quartz filling the remaining space. Location indicated in Fig. 4.1.

and thin chert slabs that occur in otherwise medium to coarse-grained sediments in the lower part of BR-vsc unit 2 (Fig. 5.7). In places, a sediment layer occurs in the lower part of these cavities, while the upper part is filled by chert and quartz cement (Fig. 5.7). Quartz is also present below elongated, thin pebbles and as long thin, bedding-parallel cavity-fills, sometimes in the form of stalactites and stalagmites (Fig. 5.8)

In BR-vsc unit 1 (Fig. 5.1) completely silicified crystals occur. The pseudomorphed crystals were described in detail by Lowe and Fisher Worrell (1999), who distinguished five different types (summarised in Table 5.1). Our observations concern the relationships of the crystals with the bedding and the vein systems. The crystals mostly occur in bedding-parallel layers or as isolated crystals incorporated in sedimentary layers. At loc. SV99-34 (Fig. 5.3), crystals comparable to type 3 of Lowe and Fisher Worrell (1999; Table 5.1) nucleated on discrete layers (~1-3 cm apart) within the sediment. Occasionally, the sedimentary layers hosting the crystals bend concavely upward against them.

Fig. 5.9 shows a cluster of crystals (cf. type of Lowe and Fisher Worrell, 1999; Table 5.1) that nucleated immediately above bedding-perpendicular chert veinlets. These veinlets traverse the underlying finely laminated and occasionally rippled chert layers that are intercalated in the volcanic sequence.

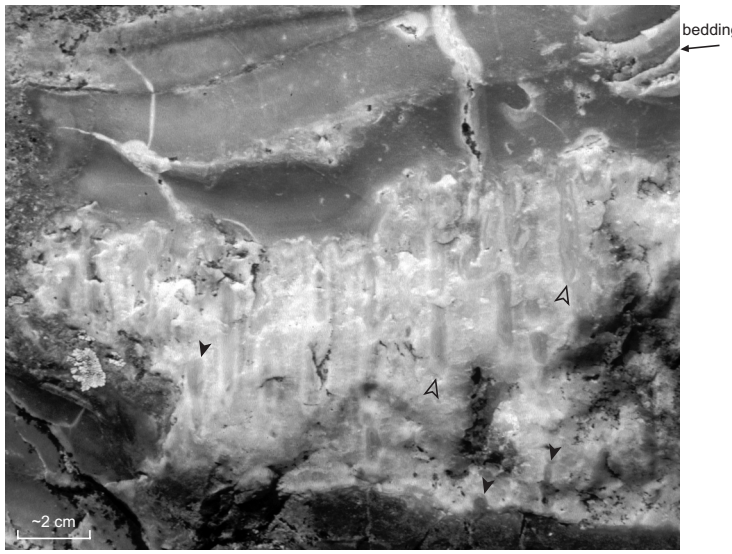

Figure 5.8: Part of a bedding-parallel cavity filled with quartz stalactites (open arrows) and stalagmites (solid arrows), indicating that the cavitiy was air-filled during the early stages of fill. Orientation of bedding: 181/85; younging to the north (i.e. towards the top of the picture).

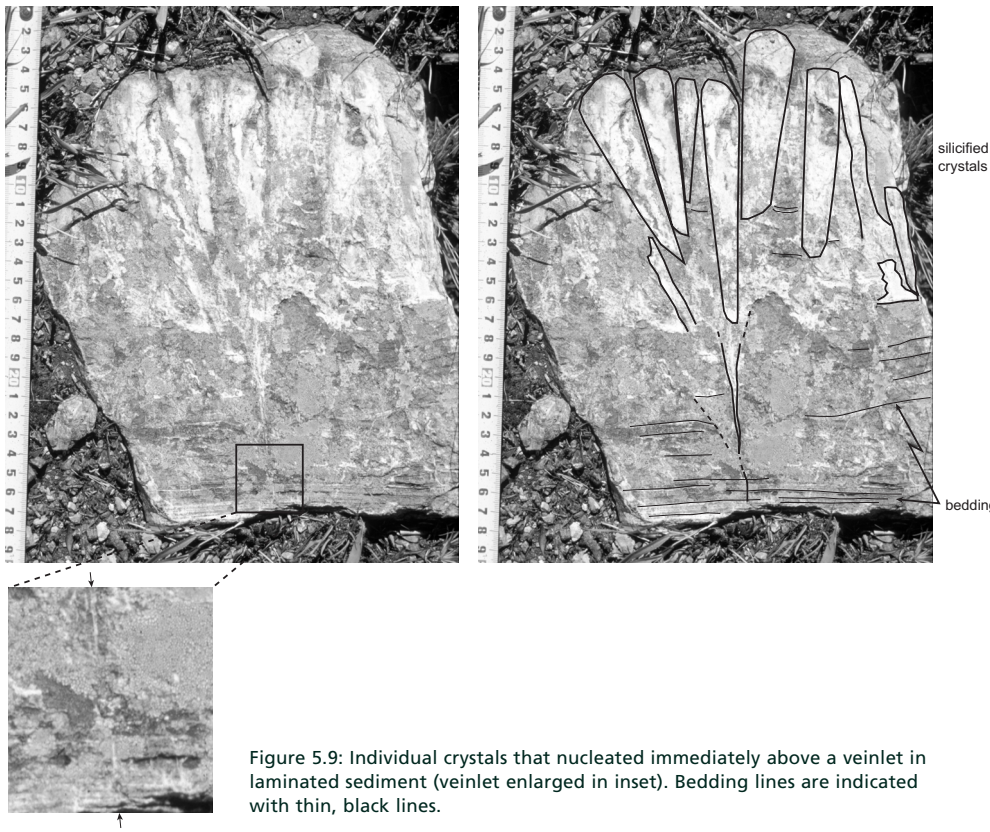

Figure 5.9: Individual crystals that nucleated immediately above a veinlet in laminated sediment (veinlet enlarged in inset). Bedding lines are indicated with thin, black lines.

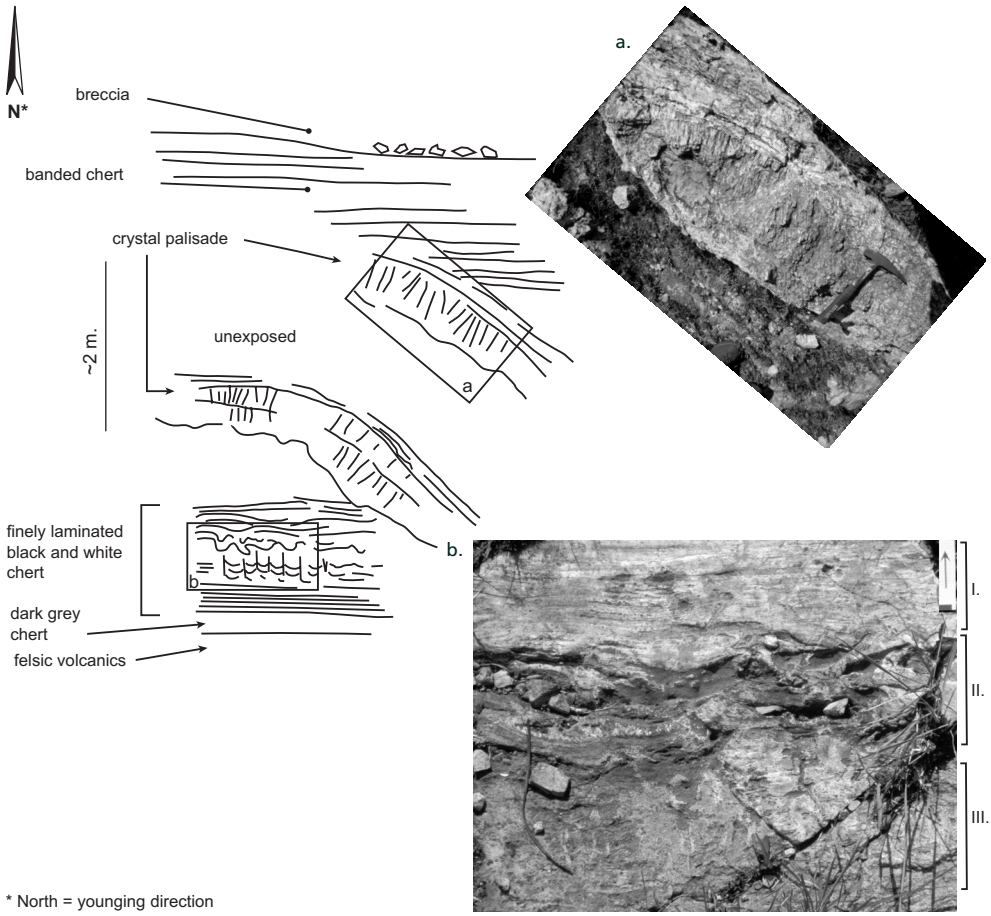

Figure 5.10: Sketch of layer with palisade crystals cross-cutting finely laminated chert layers with base surge and water escape structures (loc. SV01-20). Insets: a. palisade crystals oriented almost perpendicular to the fracture direction. b. finely, even-laminated chert (I) showing convolute lamination (II) and water-escape structures (III).

In the same unit, crystals occur in palisades, such as shown in Fig. 5.10. Here, crystal palisades (cf. crystal type 5 Lowe and Fisher Worrell, 1999; Table 5.1) occur oblique to finely laminated and rippled black and white chert. The laminated chert shows small water escape structures, convolutions and thin veins (Fig. 5.10b). Crystals forming the palisade appear to have grown from the sides of a fracture inward (Fig. 5.10a).

Iron enrichment is most characteristic of the third unit (Fig. 5.1) of the BR-vsc. It occurs as an iron-oxide-rich sandstone-siltstone-chert alternation, or as massive crusts of iron-oxide (also described as ironstone pods; De Wit et al., 1982, see discussion). Thinner iron-oxide-rich sandstone-siltstone layers, alternating with chert, occur in the second unit (Fig. 5.1) of the BR-vsc. Apart from that, fault-bound iron-oxide occurs in the second unit of the BR-vsc. In the KG-vsc, iron-oxide enrichment is rare. It is limited to parts of the less silicified sandstone-siltstone-shale wedge close to the normal faults (Fig. 5.2).

Erratum

On p. 96 some of the breccia types have been mislabelled. The correct text (2nd and 3rd paragraph) with the correct breccia-type numbers is:

Breccia types **1**-4 are interpreted as hydraulic breccias caused by the hydrothermal fluids. These breccias have a non-sedimentary matrix. Indications for a tectonic origin, such as gauge or grinding, are absent. The angularity of the fragments of types **1** and 3 also indicates a hydrothermal origin (Hulen and Nielson, 1988). The rounded shapes of type **4** breccia fragments indicate a different type of hydrothermal breccia. Stanistreet and Hughes (1984) termed these deposits pseudoconglomerates, and attributed the rounding of the fragments to in situ abrasion by hydrothermal fluids. This process is also known from younger hydrothermal systems (e.g. Hulen and Nielson, 1988; breccias that have undergone fluidisation), and indicates an energetic hydrothermal regime. Breccia types **1,** 3 **and 4** are post-depositional.

Possible surface expressions of hydrothermal activity are found in the immediate vicinity of the main vein systems. The finely laminated cherts and agate-like cavity fills incorporated in the top of the volcanic sequence of the BR-vsc (loc. SV01-20, Fig. 5.6) may have precipitated from hydrothermal fluids when they cooled upon reaching the surface (i.e. sinter deposits). Other possible surface expressions of the hydrothermal systems are the breccia layers found in the silicified sediments in the second unit of the KGC (breccia type **5**, Fig. 5.4**c**).

Interpretation and discussion: hydrothermal systems

The observations listed above are interpreted in terms of hydrothermal systems that were active around 3.4 Ga ago. Fig. 5.11 summarises the different observations schematically.

In both the BR-vsc and the KG-vsc, ascending black chert vein systems were found in the top of the felsic volcanic sequence. The ascending character is suggested by the upward increasing width of the veins, and, in the KG-vsc, by the brecciating effect of the veins on the overlying sedimentary chert. The veins in the BR-vsc and KG-vsc are interpreted to represent the subsurface plumbing system of ancient hydrothermal systems.

Breccia types 2-4 are interpreted as hydraulic breccias caused by the hydrothermal fluids. These breccias have a non-sedimentary matrix. Indications for a tectonic origin, such as gauge or grinding, are absent. The angularity of the fragments of types 3 and 4 also indicates a hydrothermal origin (Hulen and Nielson, 1988). The rounded shapes of type 2 breccia fragments indicate a different type of hydrothermal breccia. Stanistreet and Hughes (1984) termed these deposits pseudoconglomerates, and attributed the rounding of the fragments to in situ abrasion by hydrothermal fluids. This process is also known from younger hydrothermal systems (e.g. Hulen and Nielson, 1988; breccias that have undergone fluidisation), and indicates an energetic hydrothermal regime. Breccia types 2-3 are post-depositional.

Possible surface expressions of hydrothermal activity are found in the immediate vicinity of the main vein systems. The finely laminated cherts and agate-like cavity fills incorporated in the top of the volcanic sequence of the BR-vsc (loc. SV01-20, Fig. 5.6) may have precipitated from hydrothermal fluids when they cooled upon reaching the surface (i.e. sinter deposits). Other possible surface expressions of the hydrothermal systems are the breccia layers found in the silicified sediments in the second unit of the KGC (breccia type 1, Fig. 5.4a). The coarse, unsorted breccia layers are of

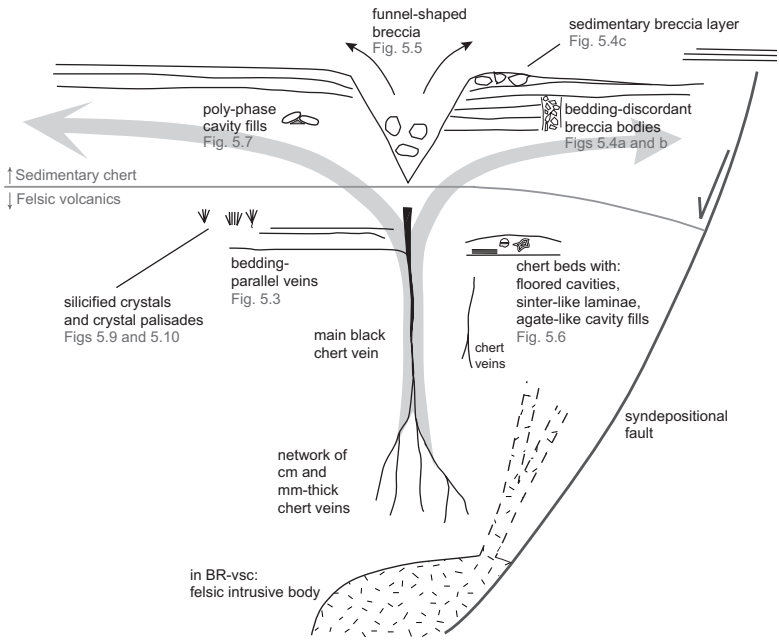

Figure 5.11: Summary diagram of observations related to hydrothermal systems in the KG-vsc and the BR-vsc (not to scale). Grey arrows indicate interpreted direction of fluid movement.

sedimentary origin, but indicate energetic conditions that sharply contrast with those of the surrounding sediments (see also Chapter 4). This may be due to pulses of hydrothermal activity, which resulted in violent breaking of recently deposited and already silicified sediments. The fragments were re-deposited in breccia layers. Other mechanisms to get such unusually coarse breccias, such as channel fills or storm events, are unlikely here (Chapter 4). The breccia layers in the third unit of the BR-vsc may be of similar origin. The decreasing thickness of the upper breccia layer away from crosscutting iron-oxide-rich vertical structures suggests that they are related. The iron-oxide-rich structures may have been the conduits for hydrothermal fluids (see also section on Circulation of fluids), and the breccia layers may represent the associated hydrothermal eruption breccias. Why the breccia layers in BR-vsc unit 3 occur exactly at the top of ~20 m-scale sedimentary cycles (Chapter 4) remains an interesting question that requires further research. It may suggest a relationship between sea-level fluctuation and hydrothermal activity.

The large, iron-cemented breccia body that occurs above a major vein system in the BR-vsc (Fig. 5.5) may also be an expression of explosive hydrothermal activity at the surface. This is suggested by the funnel shape of the breccia body and its location directly above the vein system. However, no definite constraints could be placed on the time of formation of this breccia.

Timing of the hydrothermal activity

The major part of the felsic volcanic rocks and sediments of the BR-vsc and KG-vsc were deposited during the activity of large-scale normal faults (Chapters 2 and 3). The most convincing evidence for this are the thickness differences of the volcanic and sedimentary rock units across these faults (Fig. 5.1 and 2). The hydrothermal surface deposits within the top of the felsic volcanic rocks and the sedimentary sequence indicate that the hydrothermal systems in the BR-vsc became active during the final stages of felsic volcanism, and remained active throughout deposition of the overlying sediments. In the KG-vsc no evidence for hydrothermal activity at the surface was found in the volcanic sequence. Therefore, it is likely that the systems in the KG-vsc became active slightly later, during deposition of the (covering) sediments. The abundant presence of (post-sedimentary) breccias and veins caused by hydraulic fracturing, indicate that hydrothermal activity, at least in the BR-vsc, continued after deposition of the sedimentary units.

The location of the fractures and vein systems is related to the faults; they are concentrated in the hanging walls of the major normal faults (Chapters 2 and 3). A close relationship between normal faulting and hydrothermal activity is not uncommon (e.g. Phillips, 1972). In addition to the normal faults themselves forming pathways for hydrothermal fluids, extension in the hanging wall creates additional possibilities for the fluids to migrate upwards. In case of the BR-vsc and KG-vsc, some of these fractures were used as a pathway by silica-rich fluids. Other fractures remained unused, or were, in case of the BR-vsc, used later by felsic porphyritic and mafic to ultramafic intrusions.

These relationships between faulting, deposition and hydrothermal activity are important, because they show that the described hydrothermal systems are definitely early Archaean. That timing of the hydrothermal activity in early to mid Archaean rocks is not unequivocal is shown by the discussion about the timing of formation of ironstone pods in the southern Barberton Greenstone Belt. The interpretation of these ironstone pods as hydrothermal discharge zones on the ~3.2 Ga seafloor (De Wit et al., 1982; De Ronde et al., 1994) has recently been disputed by Lowe and Byerly (2003), who argue that the ironstone pods are in fact Quaternary subaerial spring deposits (but see comment by De Ronde et al., 2004).

Venting depth of the hydrothermal systems

From the interpretation that the hydrothermal systems were active during deposition of the BR-vsc and KG-vsc sediments, it follows that the venting depth of the systems can be deduced from the sediments. A sedimentological study of both sequences (Chapter 4) has shown that generally, the sediments were deposited in shallow water, around base level. The lower part of the BR-vsc shows indications of occasional emersion, while the KG-vsc sediments were deposited mostly subaqueously and were possibly influenced by tidal activity (Chapter 4). The hydrothermal systems of BR-vsc and KG-vsc are therefore interpreted to have vented in shallow water, around base level.

Circulating fluids

The most obvious effect of fluid circulation is the extremely high silica content of the BR-vsc and KG-vsc sediments. Since silicification took place from very early stage during deposition on (Chapter 4) and since the main vein systems are filled with chert, a large part of the silica was probably introduced by the hydrothermal systems. Oversaturation with respect to quartz or amorphous silica is also the case in many modern-day hydrothermal systems (e.g. Spooner and Fyfe, 1973). The silica may have been derived from carbonatisation processes in the underlying mafic to ultramafic rock pile, analogous to what has been described from the overlying upper Kromberg Formation (Hanor and Duchacv, 1990). However, the extreme amount of silicification observed in early Archaean rocks is unknown from younger deposits. In addition to the supply of silica from below by hydrothermal systems, seawater may have been supersaturated with respect to silica in the (early) Archaean, since the organisms buffering the silica concentrations in the oceans today, did not exist yet (e.g. Holland, 1972; De Ronde et al., 1997b). This seawater may have mixed with magmatic hydrothermal fluids, and have circulated through the sedimentary pile.

Several other observations in the BR-vsc may be related to hydrothermal activity, such as the silicified crystals at the top of the volcanic sequence. Our observation that a number of the crystals nucleated in, or immediately above tiny chert veins, suggests that these crystals may have precipitated from the fluids in these veins. The crystals may either have grown in the subsurface or at the surface, directly in or from veins. They may also have precipitated from a hydrothermally-nourished brine. The occurrence of crystal palisades discordant to bedding, with crystals radiating from both sides inwards, suggests that this type of crystal formed post-sedimentarily.

Based on measurements of interfacial angles, Lowe and Fisher Worrell (1999) interpreted type 1 crystals as Nahcolite ($NaHCO_3$). Their remark that this mineral was found in the Roman hot water plumbing systems strengthens the suggestion that the BR-vsc crystals could have grown in the plumbing system of a hydrothermal vent. However, Lowe and Fisher Worrell (1999) interpreted the crystals (all types) in the BR-vsc to be evaporites that had precipitated from an ocean or coastal water body. They considered the nourishing of such a water body by hydrothermal fluids unlikely, because they were 'unable to locate any tufas, spring mounds, or other deposits that are common around hydrothermal discharge sites'. Considering the many indications for hydrothermal systems presented in this chapter, it seems equally likely that the source of the fluid from which these crystals precipitated was hydrothermal.

The quartz-filled cavities and bedding-parallel (paleo-)cavities also indicate the circulation of fluids through the sedimentary pile. The bedding-parallel cavities may have formed analogous to sheet cracks described from carbonate environments. Those cracks are interpreted to have formed due to shrinkage of the carbonate sediments due to drying out or dewatering in an aqueous environment (Fisher, 1964; Wilson, 1975). Sheet cracks in carbonate environments are also interpreted to form as

a result of differences in crystallisation force (e.g. Bathurst, 1971). The 'sheet cracks' in the sedimentary sequence of the BR-vsc are interpreted to have formed in a similar way, as a result of crystallisation force during the silicification process. Stalactites and stalagmites in some of the cavities indicate that these cavities were air-filled, at least during the initial stages of cavity fill. Others have been filled with concentric layers of chert and quartz, indicating that these cavities were water-filled.

The fluids that circulated through the BR-vsc hydrothermal system were characterised by analysing fluid inclusions (Chapter 6). The study was performed on inclusions trapped in the matrix of hydrothermal breccias, veins and quartz cavity fills below pebbles. The measured salinities (ca. 0.7-19.6% NaCl equivalent) are much higher than both the modern-day seawater salinity and the ~3.2 Ga seawater salinity interpreted by De Ronde et al. (1994). Both the salinity and the presence of CO_2 in some of the inclusions point to a hydrothermal origin of the fluids. Pressures under which the inclusions formed indicate that the fluids from which the quartz precipitated were highly pressurised.

Part of the iron-oxide in the BR-vsc may have been introduced by hydrothermal fluids, in particular the layer-bound iron-oxide in sandstone-siltstone and chert alternations, and the iron-oxide associated with breccia pipes. These iron-oxide occurrences are unrelated to the present-day surface, and are therefore not associated with Quaternary processes as has been suggested for iron-oxide occurrences elsewhere in the southern Barberton Greenstone Belt (Lowe and Byerly, 2003). Neither is the iron-oxide primarily related to the original permeability of the sediments, as would be expected if iron was post-depositional; the iron-oxide occurs throughout BR-vsc unit 3, which changes in lithology from sandstone in the east to shale in the west. Hence, these iron-oxide occurrences are interpreted to be of early Archaean origin, and were most likely related to the hydrothermal systems. Enrichment in iron-oxide is also known from modern-day hydrothermal systems, such as e.g. the Reykjanes system (Spooner and Fyfe, 1973).

The massive occurrences of iron-oxide in BR-vsc unit 3 may be compared to the ironstone pods in overlying deposits in the Barberton Greenstone Belt, which were interpreted as hydrothermal discharge zones on the ~3.2 Ga seafloor (De Wit et al., 1982; De Ronde et al., 1994). However, interpretation of the massive iron-oxide occurrences in the BR-vsc needs to be circumspect, since the control on their time of formation is limited. It is equally likely that they were related to later mafic to ultramafic igneous intrusions that cut through the BR-vsc sediments. Some of the massive iron-oxide could even have accumulated in (relatively) recent times, as has been suggested for iron-oxide occurrences elsewhere in the southern Barberton Greenstone Belt (Lowe and Byerly, 2003).

Comparison with other early Archaean hydrothermal systems

The two above described cases are comparable with the hydrothermal systems interpreted from the ~3.49 Ga Dresser Formation (nomenclature by Van Kranendonk, 2000) and underlying basalts along the eastern side of the North Pole Dome (Pilbara, Western Australia; Nijman et al., 1998a, Isozaki et al., 1999, Kitajima et al., 2001b). The large-scale geometry of the area is similar to that of the two study areas; the rocks were affected by an approximately ten kilometres wide array of normal faults (Nijman et al., 1998a, Van Kranendonk, 2000). Metres-wide black chert veins radiate from the fault planes, through a basaltic volcanic sequence, up into the overlying sediments. Like in the BR-vsc and KG-vsc, faulting and hydrothermal activity were contemporaneous with deposition (Nijman et al., 1998a, Isozaki et al., 1999, Van Kranendonk, 2000). The main differences are that in the North Pole area the veins originate in a basalt substrate instead of in felsic volcanic rocks, and that barite veins are present in addition to black chert veins.

As in the BR-vsc, crystal growth occurred in the Dresser Formation sediments. These crystals, now consisting of barite, are interpreted either as a replacement product after gypsum (Buick and Dunlop, 1990 and references therein), or as primary barite crystals resulting from hydrothermal activity (Nijman et al., 1998a; Runnegar, 2001).

The venting depth of the North Pole area hydrothermal systems is subject of debate. Nijman et al. (1998a) interpreted the systems to have vented at a maximum depth of ~50 metres. This depth was calculated from the maximum thickness of the basin fill, and the generally shallow-water environment in which the chert-barite unit sediments were deposited. The latter conclusion was also reached from sedimentological studies by Dunlop et al. (1978), Barley et al. (1979), and Dunlop and Buick (1981). In strong contrast with the interpretation of a shallow venting depth is the view of the Japanese workers in the North Pole area. Kitajima et al. (2001a; 2001b) studied fluid inclusions in the North Pole hydrothermal system, and stated that the hydrothermal fluids were vented at a mid-ocean ridge, at a depth of 1600 metres. The depth interpretation was based on abstracts by Maruyama et al. (1991) and Isozaki et al. (1998). Maruyama et al. (1991) suggested a mid-ocean ridge setting for the chert-barite unit, because of 'the stratigraphically controlled occurrence of barite ore' and because 'the concentric or onion-like structure of the barite deposits are well-known from the modern deep sea-floor'. Isozaki et al. (1998) interpret a mid-ocean ridge setting because of 'the absence of coarse-grained terrigenous clastics' and the 'extensional tectonic regime' in the North Pole area. However, this interpretation of deep-water, mid-ocean ridge depth is mainly based on analogies with modern barite occurrences and non-unique characteristics such as the absence of coarse-grained clastics and an extensional tectonic regime. The evidence for shallow-water deposition of the sediments (Dunlop et al., 1978; Barley et al., 1979; Dunlop and Buick, 1981 and Nijman et al., 1998) is considered to be stronger, and therefore a shallow venting depth of the North Pole hydrothermal systems is considered more likely.

Apart from the already mentioned similarities with the hydrothermal system in the Dresser Formation near the North Pole Dome (Nijman et al., 1998a), there are also similarities between the systems described in this chapter and slightly younger (mid Archaean) hydrothermal systems in the Strelley Greenstone Belt (Pilbara; Vearncombe et al., 1995, 1998, 1999; Brauhart et al., 1998). The most significant similarities include a close spatial relationship of the hydrothermal systems with felsic volcanic rocks and a spatial link between the products of hydrothermal activity (in case of the Strelley Greenstone Belt massive sulphide deposits) and syn-volcanic normal faults (Vearncombe et al., 1998). The main differences between the hydrothermal systems described in this chapter and the systems in the Strelley Greenstone Belt are the occurrence of significant mineralisation in the form of massive sulphide deposits and the deep marine environment of the Strelley Greenstone Belt deposits. The deep-water environment was interpreted from the fact that, in the Strelley deposits, (i) there is no evidence for explosive eruption, (ii) there are only minor, local fault-derived volcaniclastic sediments, and (iii) there is a close association with substantial sulphide accumulation (Vearncombe et al., 1995). In the KG-vsc and BR-vsc there is also little evidence for explosive volcanic eruption close to the study areas. Moreover, the sediments consist almost exclusively of local volcaniclastic detritus. However, no sulphide deposits are found in these two areas and, from the sedimentary sequence, it is clear that deposition took place in shallow water. Thus, whereas the Strelley Greenstone Belt deposits may be interpreted as hydrothermal vents in a mid-ocean ridge, black-smoker type setting, sedimentological analysis shows that this is not a suitable explanation for the BR-vsc and KG-vsc hydrothermal systems.

Implication for the study of early life on Earth and other planets

The study of early Archaean hydrothermal systems is important for studies of early life on Earth, because life on Earth is generally thought to have developed in the vicinity of warm hydrothermal vents. The Dresser Formation was one of the first localities where stromatoloids were discovered in early Archaean rocks (Dunlop et al., 1978). Nijman et al. (1998a) showed that the hydrothermal activity was contemporaneous with the stromatoloid-hosting sediments. De Wit et al. (1982) and Westall et al. (2001) suggested a connection between early life and hydrothermal activity in the Barberton Greenstone Belt.

However, there are no studies that show that life was not present or decreased in abundance away from hydrothermal vents in the early Archaean. Neither are there any studies in early Archaean areas of known hydrothermal activity, that show whether there was a relationship between the vent locations and the type and abundance of life. De Ronde and Ebbesen (1996), addressing the same problem, found no difference in the organic content of samples near to sea-floor hydrothermal vents and away from them at ~ 3.2 Ga. It remains unclear whether life in the period ~3.5-3.4 Ga was restricted to the sites of hydrothermal activity, or whether it already occurred in various different environments. With studies like the present one, which constrain the timing of the hydrothermal activity and the venting locations at the surface, systematic studies of the distribution and abundance of life in the period ~3.5-3.4 Ga become possible.

If a relationship between hydrothermal vents and early life could be established, the larger-scale part of this study may provide a tool for the search for life on other planets (e.g. Farmer, 1996; Westall, 2004). It shows how a selection can be made of the sites with the highest potential of finding remains of life. By looking at the broad scale of tens of kilometres first, i.e. recognition of faults and vein systems on aerial photographs or satellite images, followed by stepwise focussing on small key areas near the termination of the veins, and distinct horizons within those key areas, the best places to sample can be selected.

Conclusions

Remnants of early Archaean hydrothermal systems, which operated at or near the Earth's surface, were found in the Buck Ridge volcano-sedimentary complex, Barberton Greenstone Belt (South Africa) and the Kittys Gap volcano-sedimentary complex, Coppin Gap Greenstone Belt (Australia). The systems are of approximately the same age (~3.4 Ga) and occur in similar geological settings: a dominantly felsic volcanic complex capped by a sedimentary sequence, which were deposited during the activity of normal faults. The vein systems are geometrically related to normal faults; they occur preferentially in the hanging walls. The hydrothermal systems were active during and/or immediately after deposition of the sediments, as demonstrated by synsedimentary, early diagenetic, multi-phase silicification, veining and brecciation of the sediments. The hydrothermal systems in the BR-vsc and KG-vsc show many similarities, both in geological setting and venting environment, with the approximately contemporaneous hydrothermal system in the North Pole area (Pilbara, Australia), and the slightly younger hydrothermal systems described from the Strelley Greenstone Belt (Pilbara, Australia) and the Fig Tree Group (Barberton, South Africa; for references see discussion). However, the BR-vsc and KG-vsc hydrothermal systems vented in shallow water, and do not represent a deep-water or mid-ocean ridge setting, as was suggested for the latter two systems.

This study provides a framework for systematic studies on the distribution and abundance of life around ~3.4 Ga ago.

Acknowledgements

The Foundation Dr. Schürmannfonds supported part of the fieldwork with grants 1998/14, 1999/14, 2000/14, 2001/14 and 2002/10.

Chapter 6

Early Archaean hydrothermal fluids; a study of inclusions from the ~3.4 Ga Buck Ridge Chert, Barberton Greenstone Belt, South Africa

Abstract

The top of the early Archaean (~3.4 Ga) Buck Ridge volcano-sedimentary complex in the Barberton Greenstone Belt (South Africa) was affected by hydrothermal alteration during or immediately after its deposition. In banded, silicified sandy sediments this alteration is marked, amongst others, by quartz-cemented hydrothermal breccias, layer-bound stockworks of cm-size quartz veins and quartz-filled cavities below stacked pebbles. Quartz grains in these hydrothermal deposits contain numerous fluid inclusions filled with either two-phase aqueous or mixed H_2O-CO_2 fluid. The aqueous inclusions are divided into three different groups, based on their microthermometric characteristics; type H_A (12.6-19.6 wt % NaCl equivalent, Th 116-200°C), type M_A (7.7-12.1 wt % NaCl equivalent, Th 96-152°C) and type L_A (0.7-7.0 wt % NaCl equivalent, Th 141-216°C). Optical and microthermometric characteristics of the mixed H_2O-CO_2 fluid (CO_2 volume = 40 to 60% of the total inclusion volume, Th CO_2 (liquid) between 5 and 20°C) indicate that it was homogeneous at the time of trapping, and that some minor changes occurred after trapping. The best estimate of the X_{CO2} of the initial fluid is 0.3, for a total molar volume of 31 cm^3/mol.

Type H_A and mixed H_2O-CO_2 (type C) fluids show evidence for immiscibility at the time of trapping. Minimum trapping temperature is given by total homogenisation of both fluids: about 150°C for the brine, but at least 255°C for the mixed H_2O-CO_2 fluid. From phase relations in the H_2O-CO_2 system a pressure of 2.2 kb is expected at total homogenisation. The pressure estimate given by the brine at the same temperature is similar, suggesting that vein opening coincided with the unmixing of a previously homogeneous fluid. This homogeneous fluid, with a moderate salinity and low CO_2 content, separated into a more salty brine and a low-salinity aqueous, CO_2-bearing fluid (salting-out effect). The fluid pressure at the time of vein opening was at least 2 kb, significantly more than regional tectonic conditions would suggest. Hence, the hydrothermal veins were formed by hydraulic fracturing caused by overpressured fluids.

Type M_A fluid probably resulted from the mixing of the high-salinity fluid with a low-salinity fluid at decreasing temperature. Type L_A may have been formed from a second unmixing of the type C fluid.

Introduction

The top of the early Archaean (~3.4 Ga) Buck Ridge volcano-sedimentary complex (BR-vsc, Fig. 6.1) in the Barberton Greenstone Belt (South Africa) was affected by hydrothermal activity during and shortly after deposition (Chapter 5). The BR-vsc forms the top of the Hooggenoeg Formation and has a well-known geological setting (Fig. 6.1; Chapter 2, and references therein). Hydraulic breccia bodies and quartz-filled cavities in the sediments in the top of the BR-vsc were related to, or formed as a result of hydrothermal activity (Chapter 5). Fluid inclusions in these deposits may provide information about the temperature and composition of the fluids that once circulated through the BR-vsc hydrothermal system.

So far, the majority of fluid-inclusion studies involving Archaean rocks have been done on hydrothermal ore deposits (mostly gold). Fluid-inclusion data on other Archaean magmatic and metamorphic fluids are limited (for an overview see de Ronde et al., 1997b). Studies on fluid inclusions in early to mid Archaean rocks are scarce, especially those related to fluids at or near the Earth's surface.

In this chapter, for the first time the results of fluid-inclusion studies from cavities and breccias in *sedimentary* rocks from the early Archaean BR-vsc in the Barberton Greenstone Belt are presented.

Location and description of investigated samples

Geological setting

The Barberton Greenstone Belt (South Africa) contains some of the best-preserved early Archaean sedimentary rocks on Earth. The Onverwacht Group, the oldest group in the belt, comprises predominantly mafic and ultramafic rocks, with minor intercalations of chertified sediments (e.g. De Wit and Ashwal, 1997; Lowe and Byerly, 1999b). The top of the Onverwacht Group is formed by the ~3.45-3.16 Ga Buck Ridge volcano-sedimentary complex (BR-vsc, Fig. 6.1, see also Chapter 2), which consists of an alternation of basalts with felsic lavas and porphyries, and a capping silicified sedimentary sequence. These rocks only experienced very low-grade metamorphism. The sedimentary sequence is divided into four units: (1) a partly silicified volcaniclastic unit characterised by several tens to hundred metre-wide scour structures, (2) a banded sedimentary chert, (3) an iron-oxide-rich sandstone-siltstone interval, which in places includes breccia and massive iron-oxide occurrences and, (4) a well-banded silicified sandstone (Chapter 4). The latter three units form the Buck Ridge Chert (BRC). Occasionally, the first unit is very silicified and is also regarded as part of the BRC. Deposition of the BR-vsc took place during activity of large-scale normal faults (Chapter 2). The sediments were subject to heavy alteration and became silicified during and/or soon after deposition. For details on the sedimentary and diagenetic environment of the BRC, see Chapter 4.

Contemporaneous with faulting and BR-vsc deposition, a hydrothermal system was active, the field evidence for which is given in Chapter 5. Preserved remnants of this system include metre-wide black chert veins that cut through the felsic volcanic rocks, and numerous types of veins and breccias in the overlying silicified sediments.

Investigated samples

Four samples from BR-vsc unit 2 were selected for the fluid-inclusion study; three from the central part of the study area (SV99-L1-19, SV01-23 and SV01-24b) and one from the same unit further to the east (SV01-L3-29, for locations see Fig. 6.1).

Inclusions in samples SV99-L1-19 and SV01-23 are hosted by quartz veins. Sample SV99-L1-19

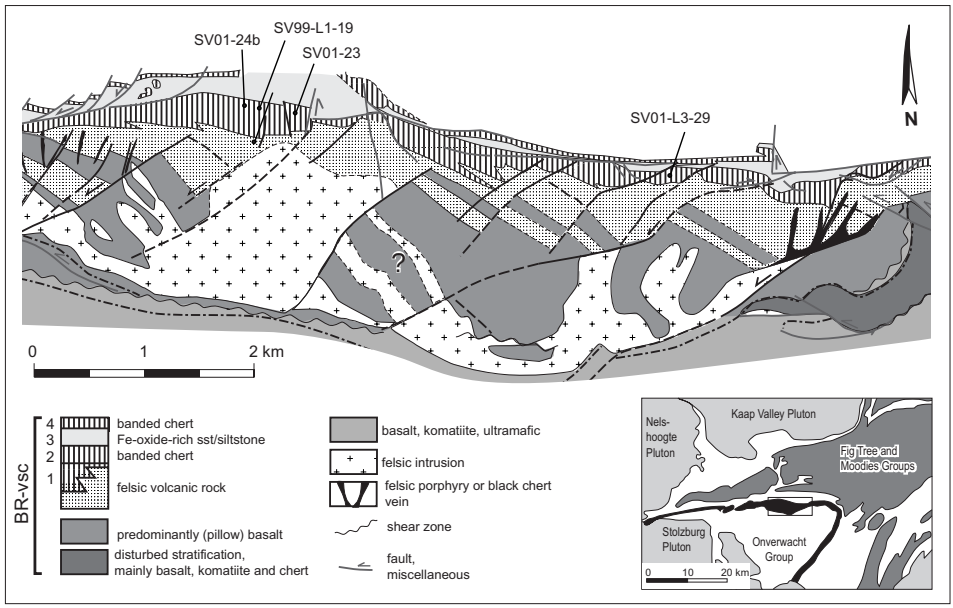

Figure 6.1: Geological map of part of the Buck Ridge volcano-sedimentary complex, simplified after Chapter 2 (for location in southern Barberton Greenstone Belt see inset). All four samples are from unit 2 of the silicified sedimentary sequence at the top of the BR-vsc. Sample locations are indicated in the figure. Legend applies to main figure only, not to inset.

shows both bedding-parallel and bedding-perpendicular quartz and chert cutting through a multi-coloured banded chert (Fig. 6.2a). Bedding-parallel layers of quartz crystals were formed first, and subsequently coated by multiple layers of precipitated quartz and chert. Primary inclusions hosted by the bedding-parallel quartz are therefore expected to represent the earliest fluids in the system. In sample SV01-23, a quartz vein cuts step-wise through grey, banded, sandy sediments. It forms part of a layer-bound stockwork of veins that were cut by small-scale faults. Time control on the growth of quartz in this sample is limited.

Inclusions in sample SV01-24b are hosted by quartz that forms the cement to a breccia in BR-vsc

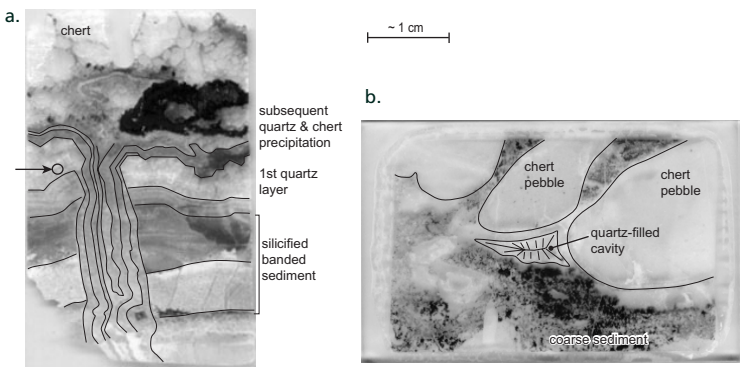

Figure 6.2: Photos of fluid-inclusion samples. a. Sample SV99-L1-19; analysed inclusions are from a grain within the circle. b. Sample SV01-L3-19; analysed fluid inclusions are from quartz-filled cavity below chert pebbles.

unit 2. The breccia body is discordant with bedding and is associated with intense (local) veining of BRC unit 2. The breccia was generated *in situ*; fragments of host rock rotated and moved slightly with respect to each other (type 3 in Chapter 5). The breccia is interpreted to have formed as a result of hydraulic fracturing and fluid flow just below the surface.

The fourth sample (SV01-L3-29) was taken about 4 km along strike to the east. The studied inclusions are hosted by quartz that fills a cavity below two chert pebbles (Fig. 6.2b). The pebbles were stacked during deposition, leaving voids through which early diagenetic fluids could circulate and in which quartz could precipitate (Chapter 5).

Method

A doubly polished, 100 μm thick section was made of each of the four samples. From each section, up to five quartz grains were selected and their fluid inclusions precisely drawn. For microthermometric measurements, an Olympus BH-2 microscope with a Linkam THM600 freezing/heating stage connected to a Linkam CS196 cooling system and a TP91 heating system were used. The stage was calibrated against the melting point of CO_2 in H_2O/CO_2 inclusions in quartz from Binn, Switzerland (Tm=-56.6ºC). Melting temperatures were recorded at 1 ºC/min, homogenisation temperatures at 1-5 ºC/min. All measurements were repeated at least once.

Results

Visual characteristics of the inclusions

Quartz-hosted fluid inclusions from the BR-vsc are generally very small. The average size of the analysed inclusions is 7-8 μm, but overall average inclusion size is much smaller. Based on visual observation, two groups of inclusions were identified. The first group of inclusions is two-phase, liquid-rich aqueous at room temperature, and shows a relatively constant liquid-to-vapour ratio (Fig. 6.3a). The average vapour content of this group of inclusions, based on comparison charts by Roedder (1984) and Mercolli (1979), is <<10 volume %. Inclusions of the second group are also two-phase at room temperature, but are characterised by a relatively large bubble of a different phase (P_{II}, Fig. 6.3b). An additional bubble (i.e. a third phase, P_{III}) occurs either at room temperature or slightly below that (above 5°C, see below). There is no indication of significant post-trapping changes of type C inclusions. Rarely, inclusions of this group include a birefringent solid phase (P_{IV}), presumably calcite.

The surface of the second phase relative to the total surface of the inclusion (S_{II}/S_{total}) at room

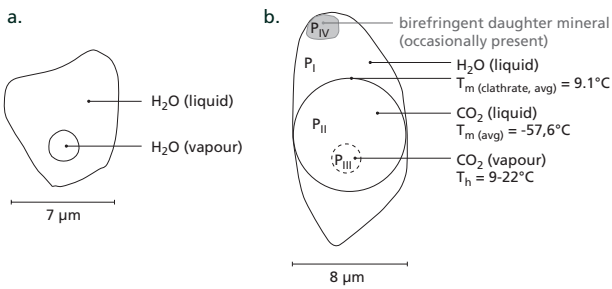

Figure 6.3: a. Schematic drawing of a typical aqueous inclusion. For a summary of microthermometric data see Table 6.1 and Fig. 6.6. b. Schematic drawing of a typical type C inclusion, with a summary of microthermometric data.

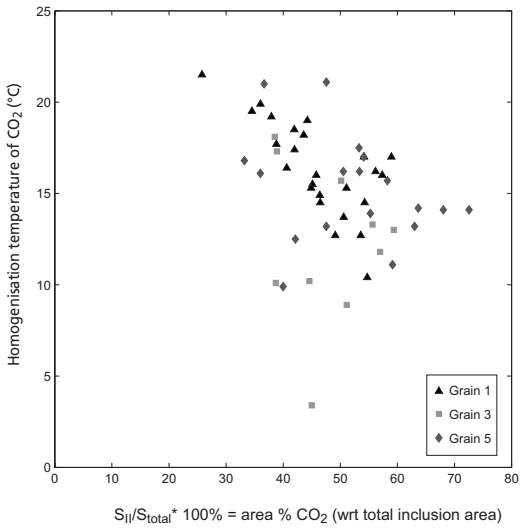

Figure 6.4: Area occupied by CO_2 bubble (S_{II}) with respect to total inclusion area (S_{total}) for type C inclusions in sample SV01-23. The distribution shows that the area % CO_2 (and hence also the volume %) is fairly homogeneous, and there are no indications for major post-trapping changes.

temperature was calculated using the program Image Tool and digital images of the individual inclusions. The ratio (S_{II}/S_{total}) was found to be relatively constant, roughly between 0.40 and 0.60 (average ratio 0.48; Fig. 6.4). Based on the rather flat shape of the inclusions, the volume ratio V_{CO2}/V_{Total} is taken to be equal to the surface ratio (this is probably a slight overestimate of the true volume ratio; cf. Roedder, 1984).

Spatial distribution of the inclusions

The hypothesis that the analysed inclusions are primary, and therefore contain the oldest fluids, is supported by a number of arguments based on the distribution of the inclusions within the quartz grains: (a.) Each of the grains has its own inclusion population, which differs somewhat from grain to grain. (b.) The analysed inclusions are generally irregularly distributed (clustered) across the grain. (c.) Some grains show a number of inclusions that are distinctly aligned along the growth zones of the quartz (e.g. Fig. 6.5, SV01-23 grain 2). In sample SV01-24b, the growth zones are

Figure 6.5: Inclusions in sample SV01-23, grain 2. Part of the inclusions is distinctly aligned along the growth zones of the quartz crystal that hosts them.

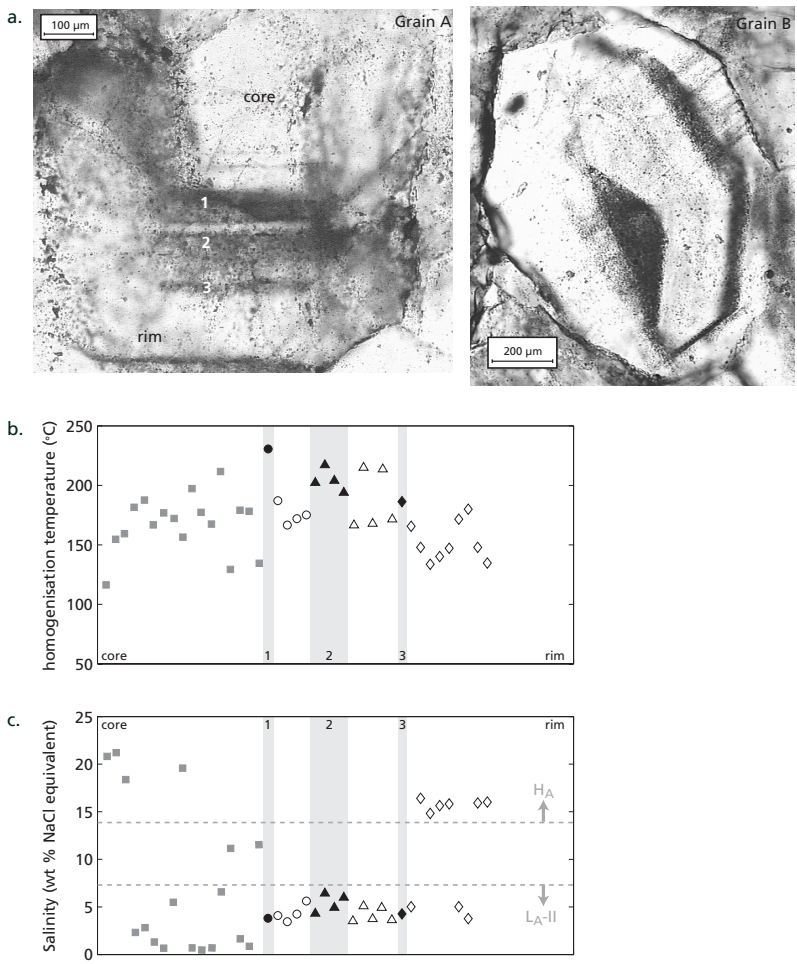

Figure 6.6: Sample SV01-24b. a. Microphotographs of grains A and B, showing growth zones in quartz. b. Relationship between growth zoning and homogenisation temperature in grain A. c. Relationship between growth zoning and salinity in grain A. Numbered dark growth zones in Fig. a correspond to numbered bands in Figs b and c.

characterised by slight colour differences within the quartz grains (Fig. 6.6a). The shape and amount of inclusions do not seem to be related to the growth zones. The micro-thermometric characteristics (see below) of the inclusions are occasionally, and only slightly, related to the growth zones.

In addition to the large clustered inclusions, smaller inclusions occur aligned along intra-grain trails perpendicular to the growth zones. The bimodal distribution of the inclusion sizes could indicate that post-trapping transposition took place. However, inclusions along the intra-grain trails have the same micro-thermometric characteristics (see below) as the rest of the inclusions. Hence, they are pseudo-secondary inclusions, which were formed during growth of the host crystal (cf. Roedder, 1984).

A strong bimodal size distribution among the aqueous inclusions is observed in sample SV01-23,

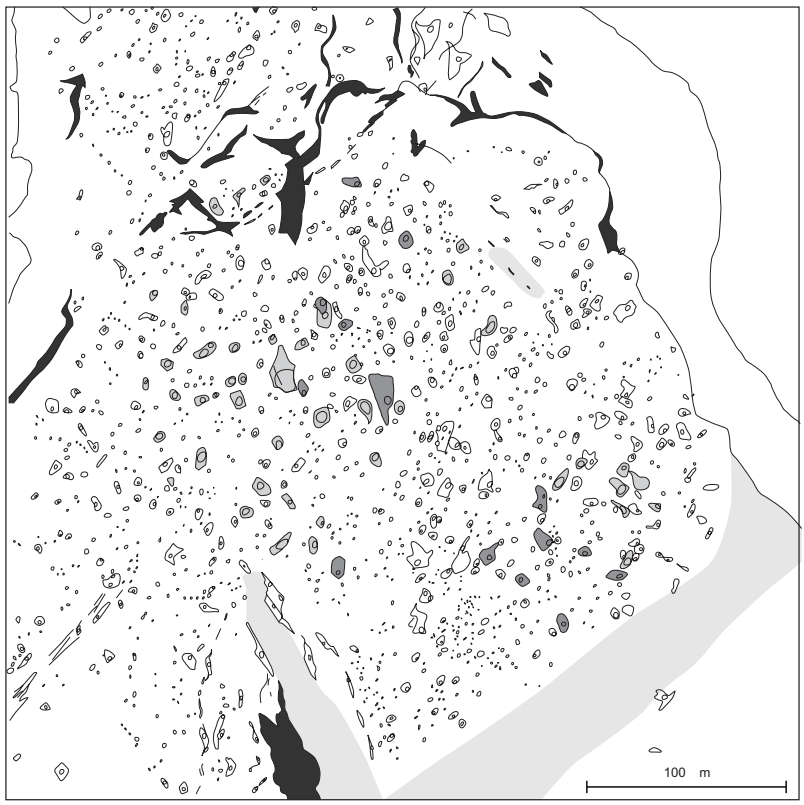

Figure 6.7: Inclusions in sample SV01-23, grain 1. High-salinity aqueous inclusions (type H_A) are dominant in this grain. Low-salinity mixed H_2O-CO_2 inclusions (type C) occur as discrete domains within the group of high-salinity aqueous inclusions. Measured type H_A inclusions are dark-grey shaded, type C inclusions are pale-grey shaded.

grain 1 (Fig. 6.7). The smaller inclusions in this grain may represent transposed inclusions, which resulted from post-trapping changes. Since the smaller inclusions have roughly the same liquid/vapour-ratio as the larger inclusions, measurements on the larger inclusions are thought to be representative of the entire inclusion population. In the same grain, locally strongly elongated inclusions are present (e.g. in the lower left corner, Fig. 6.7), which also indicate post-trapping modification of the inclusion population. However, in the bulk of the grain the inclusions are spherical to elliptical.

Hence, although there is evidence for post-trapping changes, these changes appear to have remained minor. This interpretation is strengthened by the microthermometric data (next section).

Microthermometric data

Based on microthermometric measurements, the two-phase, liquid-rich aqueous inclusions of the first group were subdivided into three types; high-salinity (type H_A), intermediate-salinity (type M_A), low-salinity (type L_A) inclusions. The microthermometric results for the three groups of aqueous inclusions are summarised in Table 6.1 and Fig. 6.8a. The three-phase inclusions were not subdivided. A summary of the microthermometric characteristics of this group of inclusions (type C) is given in Fig. 6.3b.

Type	*Tm range (°C)*	*Tm average (°C)*	*NaCl range (%)*	*NaCl average (%)*	*Th* range (°C)*	*Th* average (°C)*
H_A	-18.8 to -8.4	-12,2	21.5 to 12.2	16,0	115.7 to 199.8	153,9
M_A	-8.3 to -4.1	-6,7	12.1 to 6.6	10,1	96 to 160	130
L_A-II**	-4.4 to -2.2	-3,2	7.0 to 3.7	5,3	97.8 to 116.5	106,1
L_A-I	-4.2 to -1.4	-2,9	6.7 to 2.4	4,7	140.9 to 216.1	182,2

** Always liquid homogenisation*

***All L_A -II inclusions disappear when only the most reliable data are plotted.*

Table 6.1: Summary of microthermometric data for the four groups of aqueous inclusions. Tm = final melting temperature, Th = homogenisation temperature, NaCl = % NaCl equivalent

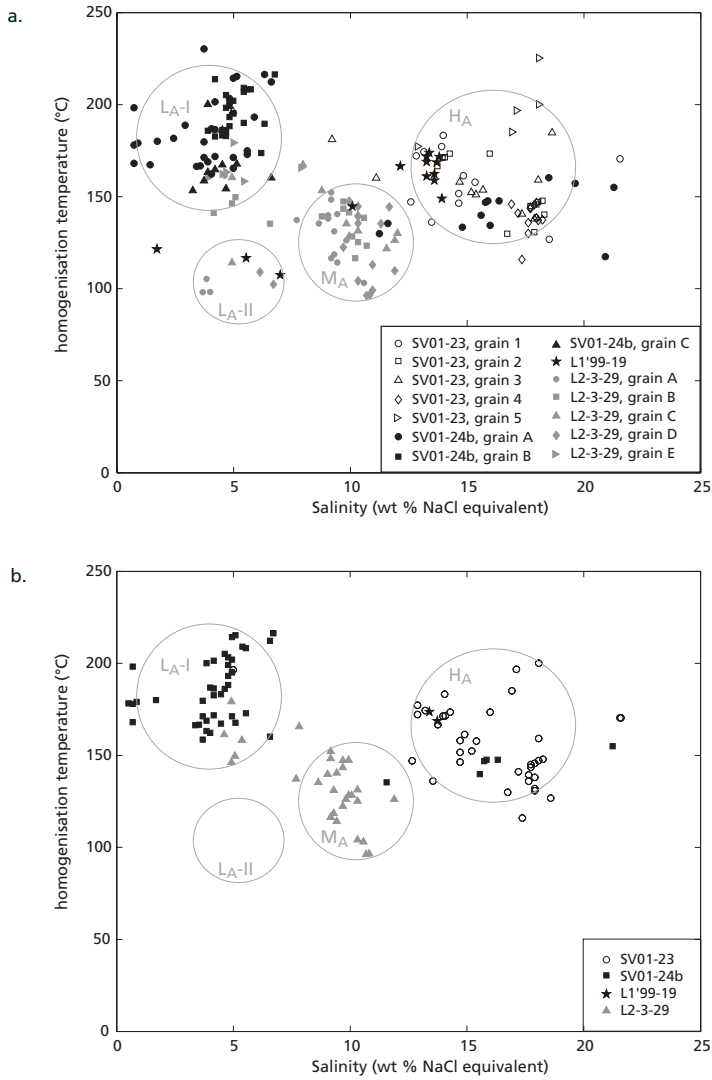

Figure 6.8: Plot of homogenisation temperature against salinity for analysed two-phase aqueous inclusions from the Buck Ridge Chert. CO_2-bearing inclusions are not shown in this figure. a. All measured aqueous inclusions. b. Most reliable data only; reliability based on inclusionshape and accuracy and reproducibility of the analyses.

Aqueous inclusions

Type H_A (high salinity)

The final melting temperatures of type H_A inclusions range from –16.2 to –8.8°C, which corresponds to salinities of 19.6-12.6 wt % NaCl equivalent (salinities calculated from the freezing point depression using the table given by Bodnar and Vityk, 1994). The homogenisation temperatures (to liquid) are in the range of 116-200°C.

Type M_A (intermediate salinity)

The final melting temperature of type M_A inclusions is clearly higher than that of type H_A inclusions, and ranges between –8.3 and –4.9°C. This corresponds to salinities between 12.1 and 7.7 wt % NaCl equivalent. Homogenisation temperatures are slightly lower than those of type H_A inclusions, between 96 and 152°C.

Type L_A (low salinity)

Type L_A inclusions have relatively high final melting temperatures (-4.4 to –0.4°C) and corresponding low salinities, between 7.0 and 0.7 wt % NaCl equivalent. Most analyses combine to form a group with relatively high homogenisation temperatures, between 141 and 216°C (type L_A-I). Nine analyses show significantly lower homogenisation temperatures, ranging between 98 and 117°C, suggesting the existence of a second type of low-salinity inclusion (type L_A-II). However, when only the most reliable microthermometric data are plotted (Fig. 6.8b), the inclusions with the relatively low homogenisation temperatures disappear.

CO_2-bearing inclusions

Type C

The average melting temperature of phase II (P_{II}) in type C inclusions is around –57.6°C, about one degree below the melting temperature of the standard (CO_2 inclusions in quartz from Binn, Switzerland). This indicates the presence of almost pure CO_2 in type C inclusions. No final melting temperatures for H_2O could be obtained. However, melting was observed in several inclusions between 8.3 and 10°C, indicating the presence of clathrate (hydrated CO_2). CO_2 homogenisation temperatures (to liquid) vary between 9 and 22°C, with a peak around 17°C (Fig. 6.9). Total homogenisation temperatures could not be measured, as inclusions started to decrepitate around 225°C, prior to homogenisation.

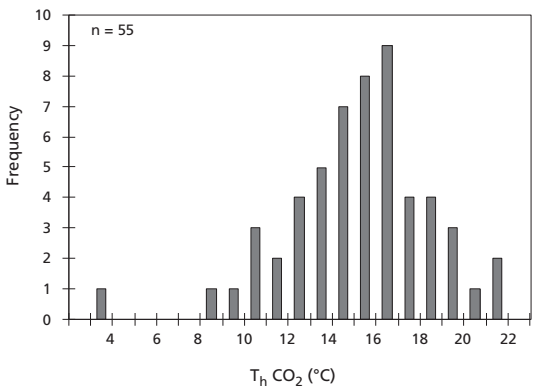

Fig. 6.9: Frequency histogram of homogenisation temperatures for type C inclusions (Th CO_2) in sample SV01-23.

The CO_2 molar volume (X_{CO2}) was determined from the diagram in Diamond (2001), using the ratio V_{CO2}/V_{total} and $T_{h\ CO2}$ for type C inclusions. This yielded X_{CO2} values of 0.21-0.37 and a V_{tot} of 26-31 cm^3mol^{-1}. The expected total homogenisation temperature (from the same diagram) is 263-273°C.

Interpretation

Spatial distribution of the aqueous inclusions

The summary diagram of all Th and salinity data for the aqueous inclusions (Fig. 6.8a) shows a relatively clear trend from H_A to M_A to L_A-II. From H_A to L_A-II, the salinity decreases from about 20 to 5 wt % NaCl equivalent, while the homogenisation temperature decreases from 190 to 100°C. The relatively high temperature (equal to or higher than H_A), low-salinity fluid L_A-I is apparently relatively independent of this trend. The same relationships remain visible when only the most reliable measurements are taken into account (Fig. 6.8b); groups H_A, M_A and L_A-I are well defined. Only type L_A-II disappears in this plot, and therefore its significance is questionable.

The spatial distribution of the different inclusion types in the quartz grains does not show a clear relationship between the different aqueous groups. However, the groups are not intimately mixed. The grains show domains, sometimes of inclusion size, in which one type is dominant or exclusive, such as L1'99-19, where type H_A inclusions are dominant in the central part of the grain (Fig. 6.10). The inclusions in this grain display a very slight trend from L_A-II to M_A through to H_A groups from the margin to the core of the grain (for this trend see also discussion of T_h vs. salinity diagram below). For SV01-24b, grain A (Fig. 6.6a), two well defined H_A and L_A-I groups were trapped at the same homogenisation temperature (Fig. 6.6b). L_A-I type inclusions occur throughout the sample, whereas

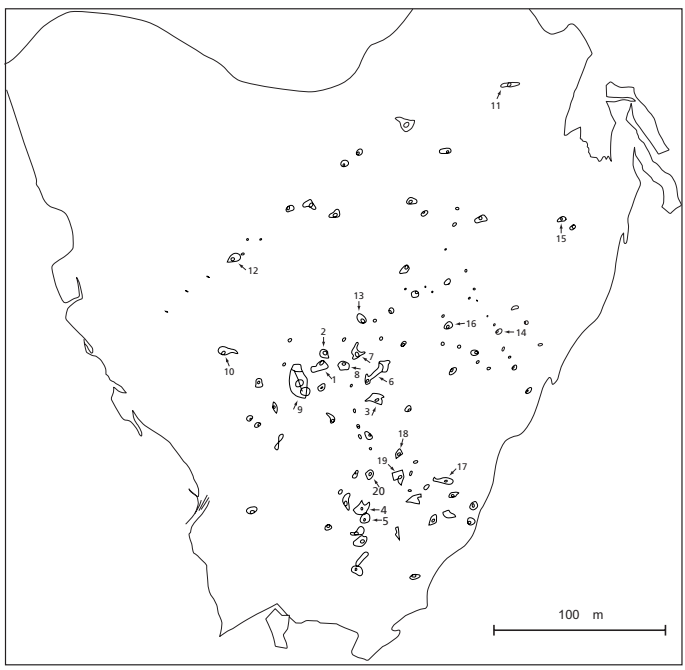

Figure 6.10: Inclusions in sample L1'99-19. Within this quartz grain, there seems to be a very slight trend from type H_A to type M_A through to type $L_{A\text{-}II}$ inclusion groups from the core to the margin of the grain. Inclusions 4 and 5 are type $L_{A\text{-}II}$, inclusion 20 is type M_A and the other numbered inclusions are type H_A. Un-numbered inclusions were not analysed.

H_A type inclusions are restricted to the core and the outer margin of the grain (Fig. 6.6c). Generally however, no relation was found between inclusion characteristics and growth zoning.

Immiscibility between high-salinity aqueous (type H_A) and CO_2-bearing (type C) inclusions

Low-salinity mixed H_2O-CO_2 inclusions (type C) and high-salinity aqueous inclusions (type H_A) occur together in grain 1 of sample SV01-23 (Fig. 6.7).

The relatively constant V_{CO2}/V_{total} ratio of the type C inclusions (Fig. 6.4), and the monopeak histogram of the $T_{h\ CO2}$ (Fig. 6.9), indicate that the fluid was an homogeneous mixture of H_2O and CO_2 at the time of trapping. Type C inclusions occur as discrete domains within the grain. In these domains type C inclusions dominate, surrounded by more homogeneous type H_A inclusions, indicating immiscibility of the two fluids. The sporadic solid found in type C inclusions is a further indication for immiscibility. In those inclusions, mechanically trapped type C and H_A fluids reacted to form calcite.

PT conditions of fluid trapping

The interpretation of the PT conditions is based on data from inclusion types H_A and C, because they represent the most obvious immiscible fluids. For an homogeneous fluid (i.e. with constant composition and density), the homogenisation temperature fixes a lower limit of fluid trapping. This also holds for type H_A and type C fluids. For the latter, the total homogenisation (mixed H_2O-CO_2) must be considered. Owing to decrepitation of the inclusions at ~215°C, the total homogenisation temperature could not be measured directly and had to be estimated from the phase diagram of the H_2O-CO_2 system (Diamond, 2001). For an average V_{CO2}/V_{tot} ratio of 0.5, the average molar volume (X_{CO2}) of type C inclusions is 0.3 (see results), which corresponds to a total homogenisation temperature of about 270°C. The pressure of the fluid system under these conditions is poorly constrained, as the critical curve runs then almost parallel to the pressure axis (Fig. 6.11). However, internal pressure at decrepitation for this type of inclusion is at least 1-1.5 kb (Naumov and Malinin, 1968). The minimum trapping pressure for type C inclusions should therefore at least be in the order of 2 kb.

Since types H_A and C were contemporaneous (immiscible) fluids, the pressure for type C inclusions can be taken to evaluate the 'pressure correction' (Roedder, 1984) relevant to type H_A inclusions. This requires first the selection of a representative isochore, which can be made from the Th histogram of type H_A inclusions (Fig. 6.12). Th data for the most reliable type H_A inclusions show a relatively large variation range, but have two rather well defined peaks at 150°C and 170°C, respectively. For a two-phase (liquid/vapour) system, post-trapping changes will mainly result in overestimating

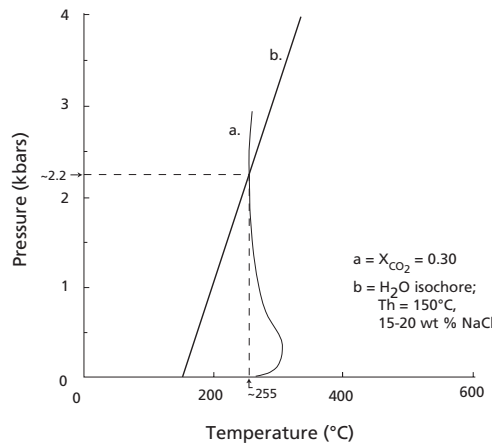

Figure 6.11: Sketch of PT conditions. H_2O isochore (a.) taken from Bodnar and Vityk (1994), critical curve of the H_2O-CO_2 system (b.) from Touret (1977).

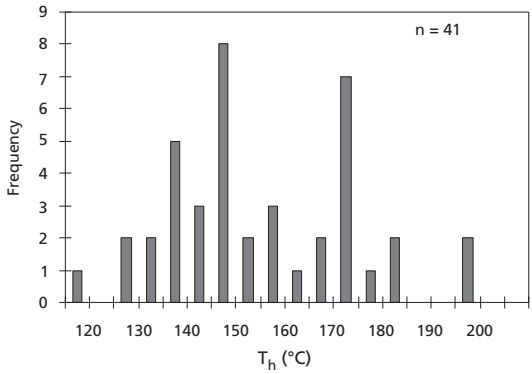

Figure 6.12: Frequency histogram of homogenisation temperature (Th) for the most reliable high-salinity aqueous (type H_A) inclusions.

the original volume of the water bubble, leading to increased homogenisation temperatures (e.g. Touret, 1977). Therefore, T_h = 150°C was selected from the T_h histogram (Fig. 6.12) as a first approximation of the most representative homogenisation temperature of type H_A inclusions. The resulting isochore (from Bodnar and Vityk, 1994), for an average salinity of 15-20% is plotted in Fig. 6.11. At a pressure of 2 kb, the isochore is very close to the critical curve of the H_2O-CO_2 system for X_{CO2}=0.3; intersection of the two curves occurs at a pressure of 2.2 kb (Fig. 6.11).

This result strongly suggests that the high-salinity aqueous (type H_A) and the CO_2-bearing (type C) fluids originated from unmixing of a previously homogeneous H_2O-CO_2-NaCl fluid. The estimated pressure of ~2 kb seems in contradication with the regional geological context. However, a pressure on the order of 1-2 kb may be explained by overpressured fluids, causing hydraulic fracturing (Touret, pers. comm., 2004). Such a hypothesis fits well with the occurrence of veins and quartz hosted breccias in the area, which were interpreted to have resulted from hydraulic fracturing (Chapter 5). The hot fluids intruded and broke up the rock succession, leading to a sudden pressure drop in the opened fractures, which resulted in fluid unmixing.

This first unmixing may have been followed by a second unmixing of the mixed H_2O-CO_2 fluid (see below).

Fluid origin

Field relationships indicate that the quartz hosting the fluid inclusions originated from hydrothermal systems that were active contemporaneous with or immediately after deposition of the Buck Ridge volcano-sedimentary complex. Both microthermometric and visual characteristics of the inclusions point to a primary origin of the inclusions, with only minor post-trapping changes. Therefore, the fluid inclusions are interpreted to have been unaffected by regional metamorphism of the area.

The salinities of type H_A and M_A inclusions are too low to represent dissolution of evaporites, but they are significantly higher than both the modern-day seawater salinity and the ~3.2 Ga seawater salinity interpreted by De Ronde et al. (1994). This could either be due to magmatic influence, or due to a highly saline seawater component in the fluid. The presence of CO_2 suggests that there is at least some magmatic component in the hydrothermal fluid. Further analysis of the fluids is necessary to determine whether part of the fluids are indeed of seawater origin (cf. De Ronde et al., 1997a). The trapping temperature of the inclusions is in the range of modern-day hydrothermal fluids. A

fluid-inclusion study of the active Los Azufres geothermal system (related to Los Azufres caldera, Mexico) yielded homogenisation temperatures of ~200-330°C (Cathelineau et al., 1989), and venting temperatures in mid-ocean ridge systems are ~180-400°C (e.g. Spooner & Fyfe, 1973; Seyfried et al., 1999).

The trend from H_A to M_A to L_A-II in Fig. 6.6a may represent mixing of a high-salinity fluid with a low-salinity fluid at decreasing temperature. The relatively high T_h, low-salinity fluid (L_A-I) behaves in an apparently independent manner compared to this trend. One explanation is that L_A-I originated from a second unmixing of the C fluid (partly suggested by Fig. 6.10). Pure CO_2 either escaped to a more superficial level, or was trapped in carbonates outside of the domain where L_A-I inclusions were formed. Further analysis is necessary to confirm or reject the hypothesis of a second unmixing.

Comparison with other Archaean hydrothermal systems

Fluid-inclusion studies on roughly similar-aged hydrothermal systems were previously carried out in the low-grade metamorphic Barberton Greenstone Belt (South Africa) and the North Pole area in the Pilbara (Australia), and in the medium to high-grade metamorphic Isua Greenstone Belt (Greenland).

De Ronde et al. (1994, 1997a) studied fluid inclusions from mid Archaean ironstone pods in the Barberton Greenstone Belt, which were interpreted as hydrothermal discharge zones of the seafloor. From fluid-inclusion data they interpreted that ~3.2 Ga vent fluids had chemical and isotopic signatures similar to those of modern vents. The seawater salinity and chemistry in the Mid Archaean were also rather similar to those of today, except for the halide ratios and higher concentrations of Ca, Sr and NH_4.

Kitajima et al. (2001a, b) studied inclusions in barite and quartz veins below the ~3.49 Ga old North Pole chert-barite unit (Pilbara). They found a hydrothermal fluid that they interpreted to have boiled or phase-separated at about 150°C and 1000 m below the seafloor. They concluded that, because of mixing of this fluid with cold seawater during its ascent below the seafloor, the vent fluids were relatively cold (<150°C). However, Kitajima et al. (2001a, b) interpreted the chert-barite unit and the contemporaneous vein systems as having developed in a mid-ocean ridge setting, whereas there is a general agreement that the North Pole chert-barite unit was deposited in shallow water (Dunlop et al., 1978; Barley et al., 1979; Dunlop and Buick, 1981; Nijman et al., 1998a, see Chapter 5).

Appel et al. (2001) reported the oldest known example of a seafloor hydrothermal system based on evidence from fluid inclusions. They studied inclusions from quartz vesicles in >3.75 Ga old altered pillow basalts in the Isua Greenstone Belt. Touret (2003) elaborated this inclusion study. The inclusions contain remnants of two independent fluid/mineral systems; pure methane and highly saline aqueous fluids (~25 wt % NaCl equivalent). The latter bear a strong resemblance to modern seafloor hydrothermal fluids and were interpreted to be responsible for the alteration of the pillow fragments. The interpretation of these inclusions as being original, i.e. >3.75 Ga old, is controversial however, since the entire surrounding rock sequence at that location has experienced medium to high-grade amphibolite facies metamorphism. Rosing and Frei (2004) for instance, state that there are no pristine early Archaean rocks and that all available sample material from the area has been ubjected to high-grade metamorphic recrystallisation.

Apart from the slightly higher salinities of the fluids in the Isua Greenstone Belt, the aqueous inclusions described by Appel et al. (2001) and Touret (2003) are very similar to the inclusions in the

BR-vsc. The difference in the gaseous component in the hydrothermal systems of the Isua Greenstone Belt (CH_4) and the Barberton Greenstone Belt (CO_2) may can be explained by a deeper-sea origin for the Isua Greenstone Belt hydrothermal system compared to the shallow water system described in this article, since mid-ocean ridge vent-fluids are characterised by significant amounts of CH_4 (e.g. Von Damm, 1995; Seyfried et al., 1999). This strengthens the conclusion of Chapter 5 that the BR-vsc hydrothermal system did not occur in a deep-water, mid-ocean ridge type setting.

Conclusions

Hydrothermally deposited quartz in the Buck Ridge volcano-sedimentary complex (Barberton Greenstone Belt, South Africa) contains relatively simple two-phase aqueous and mixed H_2O-CO_2 inclusions. The fluids are interpreted to be primarily of magmatic hydrothermal origin. High-salinity aqueous inclusions and low-salinity mixed H_2O-CO_2 inclusions show unmixing. The hydrothermal fluids had a minimum temperature of ~250°C and were highly pressurised (~2.2 kb). Unmixing of the fluids was probably associated with the opening of the hydrothermal veins. The observed low-salinity fluids probably resulted from mixing with lower temperature fluids (to produce medium-salinity and low-salinity inclusions), and/or from a second unmixing (to produce low-salinity, high-temperature fluids).

Acknowledgements

I thank Dr C.E.J. de Ronde for initially advising me on the practical aspects of fluid inclusion studies during my visit to the Institute of Geological and Nuclear Sciences (New Zealand) in 2000. I am grateful for the help of E.A. Campos Sepúlveda and B. Fu during microthermometric measurements in the lab at the Free University of Amsterdam. Technical support at the Free University was kindly provided by W.J. Lustenhouwer. Fieldwork for this study was supported by the Foundation Dr. Schürmannfonds, grants 1999/14 and 2001/14. J.L.R. Touret will be co-author of the article that will result from this chapter.

Chapter 7

Synthesis: ~3.5-3.4 Ga sedimentary basins and hydrothermal systems

Introduction

The previous chapters have addressed different aspects of the ~3.5-3.4 Ga old basins in the Pilbara and Barberton Greenstone Belts, from the geological framework, the sedimentology and hydrothermal systems, to the micrometer-scale of the fluid inclusions. Combined, a number of these aspects provide information about, for instance, the scale, shape and setting of ~3.5-3.4 Ga basins, which may in turn contribute to the understanding of the tectonic regime and crustal development in the early Archaean.

Basin fills younger than ~3.3 Ga are broadly comparable to those in modern settings (Chapter 4), and can thus be interpreted analogous to modern sedimentary settings. Sedimentary sequences older than ~3.3 Ga generally lack significant volumes of arkosic and quartz-arenitic deposits that are characteristic of many younger sedimentary deposits. This is either the result of poor preservation, or it is due to the fact that major uplifts of crustal material had not yet taken place when these basins formed, so that no granites and gneisses were available for erosion. Early Archaean basins and basin fills may also have been different from later ones because of differences in crustal strength and/or global tectonic regime. There is debate on the question whether plate tectonics already operated in the Archaean, and if so, whether it was comparable to modern plate tectonics (e.g. De Wit, 1998; Hamilton, 1998; Van Kranendonk, 2004 and references therein).

So far, most studies of early Archaean (> 3.3 Ga) sediments have focussed on the depositional environments and on the possible preservation of remnants of early life in those deposits (e.g. Dunlop and Buick, 1981; Buick and Dunlop, 1990; Barley, 1993; Lowe and Knauth, 1977; Lanier and Lowe, 1982; Walsh, 1985, 1992; Paris, 1990, see also Chapter 4). Here, the mechanism of formation, the size and the shape of preserved ~3.5-3.4 Ga old basins is addressed based on data and conclusions on the Barberton and Pilbara Greenstone Belts in the previous chapters.

3.5-3.4 Ga old preserved basins in South Africa and Australia, and related hydrothermal systems

The upper Hooggenoeg Formation in the Barberton Greenstone Belt, South Africa, and the Coppin Gap Greenstone Belt in the Pilbara, Australia, both experienced syndepositional extensional deformation in the period ~3.5-3.4 Ga. Extension occurred for at least 20 Ma (Coppin Gap Greenstone Belt, Pilbara) to 35 Ma (Barberton). In the East Pilbara, extension was not a local phenomenon, but occurred in various contemporaneous greenstone belts (e.g. Coongan Greenstone Belt, Zegers et al. 1996; North Pole Dome, Nijman et al., 1998a). During this extensional phase, normal-fault-controlled, dominantly felsic volcanic complexes, capped by (now silicified) sediments, were deposited on a mafic to ultramafic substrate. The Buck Ridge volcano-sedimentary complex

(BR-vsc, in the upper Hooggenoeg Formation) and the Kittys Gap volcano-sedimentary complex (KG-vsc, in the Coppin Gap Greenstone Belt) are roughly contemporaneous; felsic volcanics in both complexes have been dated at 3.45 Ga. The sediments at the top of the BR-vsc and the KG-vsc indicate deposition in shallow water, close to base level, and occasional emersion, which followed a period of subaqueous deposition (expressed by pillow basalts). The observed faulting controlled basin formation in the early Archaean. The deposition close to base level and the occasional emersion imply that the BR-vsc and KG-vsc were located along basin margins. For the Duffer Formation in the Coppin Gap Greenstone Belt, less is known about the exact depth of deposition, but the general structural setting was similar. The sediments in the BR-vsc and KG-vsc mainly consist of locally derived, primary and reworked volcanic and volcaniclastic material. There is no evidence for erosion of granites and gneisses, and hardly any evidence for the breakdown of older greenstone belt lithologies, or for long-distance transport of detrital material.

Hydrothermal systems venting in shallow water occurred in the vicinity of the syndepositional normal faults in both study areas. They affected the sediments during deposition and early diagenesis.

Many aspects of the KG-vsc and BR-vsc are similar or comparable to those of the ~3490 Ma North Pole volcano-sedimentary complex (NP-vsc). In that area, shallow-water sediments (e.g. Dunlop, 1978; Barley et al., 1979; Nijman et al., 1998a) and hydrothermal systems (Nijman et al., 1998a; Kitajima et al., 2001b) occurred in an extensional, growth-fault-controlled setting (Nijman et al., 1998a).

Vertical crustal movement and deposition

The near base-level environment inferred for deposits at the top of the BR-vsc and KG-vsc points to a regressive trend with respect to the underlying, regionally dispersed, subaqueous pillow basalts. The regression coincided with maximum activity of the normal faults that affected the complexes. In the BR-vsc, the regression was followed by a transgression during the final stages of normal fault activity. A regressive-transgressive trend is contrary to what would be expected from an area that experiences syndepositional normal faulting. Regression may either be caused by uplift, by increased supply, or by eustatic sealevel fall, or a combination of these factors. Since the regressive and subsequent transgressive trends are related to the normal fault activity, it is unlikely that they were caused by eustatic sea-level changes. Increased volcanic and/or sedimentary supply may have caused the regressive trend (up to overfilling), during normal fault activity. However, a decrease in sediment supply alone cannot account for a transgression in the final stages of normal faulting.

Uplift may have caused regressive conditions, while it contemporaneously caused normal faulting and the creation of accommodation space. During the main phase of activity of the faults, felsic volcanism produced enough material to fill this accommodation space. Faulting also created restricted source areas in the vicinity, which supplied sufficient volcaniclastic sediments to compensate for subsidence in the late stages of volcanic activity. The latter phase was accompanied by hydrothermal activity, which caused the formation of chert veins, and brecciation and pervasive silicification of the sediments. For some time, the total balance of uplift, collapse, and sediment and lava input apparently stabilised the sediment-water interface of these basins at about sea level. If isolated from large bodies of open water, the basin would have experienced lagoonal or caldera-lake-like conditions, such as in the BR-vsc. If the basin was connected to larger masses of open water, deposition in the basin may have been influenced by tidal action, as suggested for the KG-vsc (this study) and the NP-vsc (Nijman et al., 1998a).

In the BR-vsc, fault activity waned during deposition of the uppermost sedimentary unit, which occurred under littoral conditions. By that time, the uplift and the resulting collapse and extension had terminated, and the original subaqueous position had been re-established. Subaqueous conditions are also indicated by the occurrence of pillow basalts well above the BR-vsc.

Regional tectonic regime

Most greenstone sequences and fault arrays preserved in the East Pilbara dip almost vertically and are tightly folded between mostly younger granitoid bodies. Reconstruction of the original orientation of the fault arrays requires back-rotation of the sequences into a horizontal position, thereby correcting for folding and doming. Kloppenburg (2003) rotated extensional structures in the Marble Bar and Coppin Gap Greenstone Belts back by assuming they were part of a cylindrical fold. She thus interpreted the syn-Warrawoona Group dyke swarms in the Kelly, Marble Bar and Coppin Gap greenstone belts (Kloppenburg, 2003) as the result of a regional, linear field of NE-SW extension. This method is not applicable to the eastern parts of the Coppin Gap Greenstone Belt and to other normal-faulted areas in the East Pilbara. Owing to the semi-circular outcrop patterns of the greenstone sequences around the granitoid complexes, a reconstruction primarily based on rotation around axes parallel to the outlines of these complexes, as made by Nijman and De Vries (2004), is preferred for the entire East Pilbara. Their Fig. 4 contains a reconstruction of the original vergence of extensional faults and associated folds throughout the East Pilbara. It shows that the normal-fault arrays and associated compressional folds in the Coppin Gap Greenstone Belt were originally oriented approximately E-W, and hence that they are incompatible with a NE-SW field of extension. Moreover, the combined near-surface extensional structures in the East Pilbara, i.e. the normal fault arrays and associated compressional folds, do not fit any linear field of extension (Nijman and De Vries, 2004). This does not preclude linear extension at deeper levels in the crust.

Collins (1989) suggested that the initial stages of doming of a large granite batholith in the Pilbara created a gradient sufficiently steep to initiate gravitational collapse. He used this to explain gravitational folding in the McPhee Formation (Chapter 3). The reconstruction of the original orientations of the extensional structures from throughout the East Pilbara by Nijman and De Vries (2004) shows that, except in the McPhee area, these orientations do not fit with the present-day locations of the granitoid complexes. Therefore, the extensional structures cannot be explained as a result of doming of these complexes.

Hence, it seems that the ~3.5-3.4 Ga syndepositional extensional structures in the East Pilbara were not caused by a regional, linear field of extension and were unrelated to doming of the granitoid complexes.

Basin size

Assuming that the BR-vsc and KG-vsc were indeed located on basin margins, the size of those basins can be estimated. In the Barberton Greenstone Belt, the BR-vsc has been affected by a fault array with a minimum width of 15 km. Within these 15 km, the capping sediments of the BR-vsc change from marginal facies to a slightly more shaly basin slope facies. For an approximately symmetric basin, this implies a minimum diameter of 30 km (omitting the presence of a basin floor).

Nijman and De Vries (2004) suggested a diameter of about 140 km for ~3.5-3.4 Ga basins in the East Pilbara, based on a tentative reconstruction of a traverse correlating the Coppin Gap Greenstone Belt with the North Pole Dome (their Fig. 5).

Possible analogues for the early Archaean basins

Several analogues can be considered for the preserved early Archaean, 30-140 km-scale normal-fault-controlled basins, unrelated to a linear tectonic regime, with dominantly volcanic fills, and affected by hydrothermal systems with vents around base level.

Calderas

The abundance of volcanic deposits, hydrothermal activity and the occurrence of normal faults in the BR-vsc, KG-vsc and NP-vsc, make volcanism-related structures such as calderas (i.e. roughly circular normal faulted structures caused by the collapse of volcanoes) potential analogues. The occurrence of large quantities of Si and Ba in the BR-vsc, KG-vsc (this study) and e.g. the NP-vsc (Nijman et al., 1998b), suggest that areas with hydrothermal fields and associated smokers in the Atlantic Ocean near the mid-ocean ridge may also serve as analogues. An example of the latter is the Lucky Strike hydrothermal field, where hydrothermal fluids have highly silicified the host rocks, and have introduced barite and pyrite (Fouquet, pers.comm., 2004). However, these hydrothermal systems are associated with mafic volcanism, calderas are absent, and they vent at a depth of 1600-1700m (e.g. Langmuir et al., 1997; Humphris et al., 2002), which is much deeper than the observed Archaean examples. Calderas and smokers that produce Ba are also known from back-arc spreading areas, such as e.g. the Lau-Havre zone, north of New Zealand (e.g. Stoffers et al., 1999). The submarine calderas in the Lau-Havre zone also have a considerably greater depth than the Archaean examples presented here; they occur at depths of >1000m, and have diameters of ~3 km (Wright and Gamble, 1999). The associated Kermadec ridge shows similarly sized calderas that are subaerial, such as the Denhem and Raoul Calderas (Worthington et al., 1999).

Most calderas on Earth are much smaller than the ~30 km diameter inferred for the BR-vsc structure. Only the largest resurgent calderas (i.e. calderas injected by new magma) reach that size. Examples are the ~65 x 35 km Yellowstone Caldera (Wyoming, USA; Smith and Braile, 1984), the ~ 17 x 32 Long Valley Caldera (California, USA; Bailey, 1976) and the Cerro Galan Caldera (Argentina; Francis, 1993), with a diameter of ~35 km. The largest caldera known on Earth is the approximately 100x30 km Toba Caldera (Sumatra, Indonesia; Chesner and Rose, 1991). There are no resurgent calderas on Earth of ~140 km, the size proposed for an early Archaean basin in the Pilbara by Nijman and De Vries (2004). The duration of the extension in both the BR-vsc and the Pilbara (35-20 Ma) is much longer than expected if the extension were due to the local collapse of a magma chamber or a resurgent caldera. Most important, however, is the lack of large volumes of pyroclastic rocks in both areas, which would be expected from a caldera setting. Both the BR-vsc in the Barberton Greenstone Belt and the Duffer Formation and the KG-vsc in the Coppin Gap Greenstone Belt only show minor indications for explosive volcanic activity.

Impact structures

Other structures that bear resemblance to the observed structures are impact craters, which are also characterised by a circular pattern of normal faults. In both the Barberton Greenstone Belt and the East Pilbara, there are indications that impacts occurred around ~3.5-3.4 Ga. Four 3,470 to 3,243 Ma old spherule-bearing beds in the Barberton Greenstone Belt have been described by Byerly et al. (2002), and spherule beds of a similar age in the Pilbara were described by Glikson (2001) and by Byerly et al. (2002). Ir and Cr measurements indicate that the material in the beds is indeed extraterrestrial in origin. The spherule beds are interpreted to have formed by meteorite impacts, 20-

50 km wide (Byerly et al., 2002). The two older spherule layers in the Barberton Greenstone Belt (3470 and 3260 Ma) consist of clastic sediments with a 5-50% admixture of spherules of different composition. The authors explain the high-energy character of these spherule-bearing beds in a generally low-energy environment as the result of tsunamis below wave base.

Based on theoretical estimates, Glikson (2001) calculated that impacts occurred more frequently in the early Archaean than today, and that impact-sizes were on average larger.

The diameter of impact structures can easily reach ~30 km, i.e. the diameter calculated for the BR-vsc if it were a circular basin (see above). Examples of impact structures of this size-range include Mistastin Lake (Canada) with a diameter of 28 km (Pilkington and Grieve, 1992), Clearwater Lakes (Canada) with diameters of 22 and 32 km (French, 1998), Gosses Bluff (Australia) with a diameter of 24 km (Prinz, 1996) and Azuara (Spain) with a diameter of 30 km (Pilkington and Grieve, 1992). Impact structures with diameters of 140 km and more, which would compare to the calculated basin size of Nijman and De Vries (2004), are also known on Earth. The largest impact structures include the Chixulub Crater (Mexico) with a diameter of >180 km, the Sudbury Crater (Canada) with a diameter of >200 km and the Vredefort impact structure, which is thought to have had an original diameter of 200-300 km (French, 1998).

Despite the comparable size of impact structures and the notion that impacts did occur in the early Archaean, no traces of a potential impact have been found in the study areas. Pseudotachylite breccias, crater-fill breccias, shatter cones, etc. that are characteristic of impacts (French, 1998) were not observed in the BR-vsc or the Coppin Gap Greenstone belt. The vertical sequence from felsic lava and coarse volcaniclastic sediments to low-energy sediments and occasional emersion features, records a well-organised system of decreasing volcanic activity and related sedimentation, rather than a catastrophic impact. The high-energy scour-and-fill and cross-bedded structures observed in the lower BR-vsc sedimentary units (Chapter 4) also fit better in a model of volcanic extrusion and volcaniclastic sedimentation than in a model with impact-related tsunamis.

Neither volcanic nor impact structures on the modern-day Earth are really comparable to the early Archaean basins preserved in the Barberton and East Pilbara Greenstone Belts. The ~3.5-3.4 Ga basins bear most resemblance to volcanic structures, although no match of any of the present-day volcanic settings is clearly preserved. Possibly, the geodynamic regime in the early Earth and/or the early Archaean crust differed in such a way that a different type of volcanism-related basin formed.

Possible analogues on Mars and Venus

If the mechanism of plate tectonics did not yet operate in the early Archaean (see Introduction), deformation processes and structures on the Earth's surface may have been similar to deformation processes and structures on the present-day surfaces of the terrestrial planets Mars en Venus, which lack plate tectonics. Therefore, structures on these planets are also worth considering as analogues for early Archaean structures such as observed in the BR-vsc and the Coppin Gap Greenstone Belt.

Venus. The crust of Venus shows a variety of extensional structures, such as coronae and chasmata (Solomon et al., 1992; Phillips and Hansen, 1994). The corona structures are, both in size and shape, comparable to the early Archaean basins (Nijman and De Vries, 2001). They have been described as being volcano-tectonic in origin, and are generally distinguished by a quasi-circular pattern of concentric extensional faults and fractures, with a diameter of 100-2600 km (Solomon et al., 1992). The interiors of the coronae stand higher than the surrounding mesolands (the intermediate

topographic level of Venus). Volcanic flows from the faults and fractures cover large portions of the interior and periphery of the coronae. The coronae are interpreted to be related either to the ascent of mantle diapirs that resulted in uplift of the lithosphere and the development of a topographic dome, followed by relaxation of the uplift and concentric faulting as the flattened diapir cools (Watters and Janes, 1995, and references therein), or to small-scale mantle upwellings impinging on the base of the lithosphere that initially led to doming of the lithosphere, followed by subsidence and 'delamination' (or sinking) of the lower lithosphere (Smrekar and Stofan, 1997, 1999).

The scale of the corona structures and the possible relationship of the structures with long-lasting (crustal) processes fit with the observations in the BR-vsc and in the Coppin Gap Greenstone Belt.

Mars. Mars also shows structures that have similarities with the early Archaean volcano-sedimentary complexes in the Barberton and East Pilbara Greenstone Belts. Farmer (2000) describes chaos terranes, or collapse features that show associations with potential magmatic heat sources. Although active surface hydrological systems appear to have largely disappeared on Mars after ~3.5 Ga, the global groundwater system could still be present on Mars today, and may be reflected by large outflow channels that originate within the chaos terranes (Farmer, 2000).

Due to the lack of more detailed data on the structures on Venus and Mars, the comparison with the early Archaean structures remains superficial. Nevertheless, particularly the corona structures on Venus are likely analogues for the observed early Archaean structures.

Conclusions

The BR-vsc (Barberton, South Africa) and KG-vsc (Pilbara, Australia) are interpreted as growth fault-controlled basin margins that were associated with dominantly felsic volcanism and hydrothermal activity. The extensional structures in the Pilbara were not related to granitoid doming or to a regional, linear extensional stress field. The minimum size of the basins was on the order of ~30 km, but they may have been much larger, depending on the size of the basin floor. Neither volcanic structures nor impact structures on the present-day Earth are really comparable to the preserved early Archaean basins of ~3.5-3.4 Ga. The suggested basin size and fill, and the hydrothermal activity seem to be most comparable to a combination of back-arc type calderas and resurgent calderas. Possibly, the geodynamic regime in the early Earth and/or the early Archaean crust differed in such a way that a different type of volcanism-related basins formed in the early Archaean. Mars and Venus show what kind of basins may form in the absence of plate tectonics. Particularly the corona structures on Venus show a number of similarities with the early Archaean basins in the Barberton and East Pilbara Greenstone Belts.

Acknowledgements

Parts of the discussion and conclusions from this chapter have been published as:
Nijman, W. and De Vries, S.T., 2004. Early Archaean crustal collapse structures and sedimentary basin dynamics. In: Eriksson, P.G. et al. (Eds.), The Precambrian Earth: Tempos and Events. Developments in Precambrian Geology. Elsevier, p. 139-155.

Appendices

Appendix A - Geochronology data Chapter 2

Analytical technique

Zircons were separated from 8 to 9 kg rock samples at the mineral separation laboratory of the Free University in Amsterdam. The samples were crushed and ground with a rock splitter, jaw crusher and disk mill to a size of < 500 μm. The samples were then sieved to obtain a fraction smaller than 250 μm. Light particles smaller than 32 μm were removed. Zircons were separated from the remaining fraction using standard heavy liquid and magnetic separation techniques. At ANU, the handpicked zircons, together with the zircon standards SL13 and FC1, were mounted in epoxy resin and polished. Spots for analyses were selected using transmitted and reflected light microscopy images, as well as SEM cathodoluminescence images of the mounted zircons. The analyses were carried out at the SHRIMP-RG of the Research School for Earth Sciences at the Australian National University in Canberra. The SHRIMP data were collected and reduced in a manner similar to that described by Compston et al. (1992) and Williams and Claeson (1987). U/Pb ratios in the unknown samples were normalised to a $^{206}Pb/^{238}U$ value of 0.1859, equivalent to and age of 1099.1 Ma (Paces and Miller, 1993) for zircon standard FC1. U and Th concentrations were determined relative to those measured in the SL13 standard (Claoué-Long et al., 1995). Corrections for common lead were made using the measured $^{204}Pb/^{206}Pb$ ratios and the appropriate common Pb compositions (Cumming and Richards, 1975). Uncertainties in the SHRIMP results (tables and plots) are reported at the 1 sigma level, whilst final ages are reported as weighted means with 95% confidence limits. Statistical analyses and age calculations were done using the software Isoplot/Ex version 2.00 (Ludwig, 1999).

Results

LV01-23

The zircons from this flow-banded, quartz-plagioclase bearing porphyritic rock are pink, generally 110-130 μm long, and mostly stubby. They are magmatic, with well-developed compositional zoning. 28 Spots were analysed on 25 grains from this sample (Table A1). Most of the analyses show disturbance due to recent as well as older Pb-loss and are discordant. Only five analyses are concordant within error. The age based on these five analyses has a large error and a very large MSWD. Rejecting the youngest one (20.1), assuming it has suffered Pb-loss like most other zircons in this sample, significantly improves the error and MSWD. The four remaining analyses (1.1, 7.1, 15.1 and 16.2) combine to define a weighted mean $^{207}Pb/^{206}Pb$ age of 3451 ± 5 Ma (MSWD = 0.71; probability = 0.55).

LV01-113

The zircons from this plagioclase and quartz-bearing intrusive rock are pink, 70-190 μm in length, subhedral to euhedral, with magmatic compositional zoning preserved. Many zircons are fractured. 29 analyses were made on 22 different zircons (Table A2). Analysis 1.1 is excluded from the diagrams and calculations because analytical problems occurred during measurement. The overall trend of the data indicates non-recent Pb-loss. Duplicate measurements on several zircons show that this is a real trend and not an artefact resulting from analytical problems. Hence, the resulting $^{207}Pb/^{206}Pb$ ages must be regarded as minimum ages, and determination of an absolute age by calculating a regression line is statistically impossible. Six analyses together (1.2, 11.2, 15.1-17.1 and 20.1) define a mean $^{207}Pb/^{206}Pb$ age of 3451 ± 5 Ma (MSWD = 1.2; probability = 0.30).

SV01-03

Zircons from this altered, pyroxene-amphibole-bearing intrusive rock are pink, very clear (translucent) and show little fracturing. Most of the crystals are highly elongated, generally 110-180 μm in length, euhedral and compositionally zoned. The sample contains many fragments of zircons. Twenty grains were analysed with one single spot per grain (Table A3). Apart from one discordant analysis (8.1, Fig. 2.7c), all data plot in one group, which gives a weighted mean $^{207}Pb/^{206}Pb$ age of 3228 ± 3 Ma (MSWD = 0.71; probability = 0.80).

ISO99-9

The zircons from this quartz-plagioclase-bearing porphyritic rock are generally small (70-135 μm), stubby, pink and vary in shape from anhedral to euhedral. The cathodoluminescence images of these zircons show that they are zoned. 25 Grains were analysed with one spot per grain (Table A4). Most of the data are discordant, and they are clearly scattered. Because there are no systematic differences in shape, size or other optical properties of the zircons, there is no reason to assume that the scatter in the data is due to different populations of zircons.

No single date can be calculated, but combining the oldest group of data from zircons, which appear to be homogeneous (eleven analyses; 1, 2, 5, 6, 8-10, 12, 17, 22 and 24), results in a mean $^{207}Pb/^{206}Pb$ age of 3448 ± 5 Ma. This is the best estimate of the age of crystallisation of the rock.

The scatter in the data may be the consequence of Pb-loss soon after crystallisation, causing a Pb-loss discordia parallel to the concordia curve, overprinted by recent Pb-loss. In this case, the calculated weighted mean $^{207}Pb/^{206}Pb$ age should be regarded as a minimum age for the sample. A second possibility for the spread in the data is that the zircons contain inherited cores and younger rims. The younger ages tend to be from analyses closer to the rim of the zircons, while the older ones are mostly from closer to the centre. Although there are no obvious cores visible on the cathodoluminescence images of the zircons, the inherited grains or cores may look the same and have similar chemistry to the magmatic rims if they come from the same magmatic system. The relatively narrow spread in the data indicates that the inheritance would have been from a source (or sources) not much older than the host rock. If this is indeed a real core/rim relationship, the calculated weighted mean $^{207}Pb/^{206}Pb$ age represents a maximum age for the sample. An alternative option for the fact that the younger ages tend to be near the rims of the zircons is that the Pb-loss is through diffusion, with the margins more affected than the interiors, giving the former younger apparent ages. However, the apparent core-rim relationship observed in the zircons from sample ISO99-9 could just be fortuitous, the data are not sufficient to really prove such a trend, and therefore it is impossible to confirm or reject the last two options. In any case, neither of the above options, if they were true, would shift the age of sample ISO99-9 to younger than ~3441 Ma, so the interpretation of this sample in the text (section Post BR-vsc compressive deformation) would not significantly change.

Grain.spot	U (ppm)	Th (ppm)	Th/U	Pb* (ppm)	f_{206} (%)	Radiogenic Ratios						Ages (in Ma)				
						$^{206}Pb^*/^{238}U$	± (%)	$^{207}Pb^*/^{235}U$	± (%)	$^{207}Pb^*/^{206}Pb^*$	± (%)	$^{206}Pb/^{238}U$	±	$^{207}Pb/^{206}Pb$	±	Disc. (%)
1.1	155	83	0.55	95.1	0.00	0.7146	0.94	29.05	1.1	0.2948	0.48	3,476	±25	3,443.4	± 7.4	-1
2.1	321	218	0.70	156	0.03	0.5652	0.84	21.77	0.87	0.27938	0.21	2,888	±20	3,359.5	± 3.3	14
3.1	231	202	0.90	116	0.05	0.5852	0.87	23.54	0.91	0.29171	0.25	2,970	±21	3,426.8	± 3.8	13
4.1	255	167	0.68	133	0.04	0.6083	0.91	24.27	0.94	0.28942	0.22	3,063	±22	3,414.5	± 3.5	10
5.1	342	182	0.55	151	0.04	0.5135	1.4	19.54	1.4	0.27592	0.21	2,672	±31	3,340.0	± 3.3	20
6.1	250	160	0.66	117	0.13	0.5434	0.89	21.08	0.94	0.28137	0.29	2,798	±20	3,370.6	± 4.5	17
7.1	235	133	0.59	145	–	0.7184	1.3	29.32	1.3	0.29601	0.23	3,490	±35	3,449.5	± 3.6	-1
8.1	563	426	0.78	119	0.33	0.2454	1.5	8.94	1.5	0.26410	0.26	1,415	±19	3,271.3	± 4.1	57
9.1	282	170	0.62	98.8	0.15	0.4075	1.3	15.99	1.4	0.2845	0.45	2,204	±25	3,388.0	± 7.0	35
10.1	194	130	0.69	103	0.05	0.6209	1.6	25.02	1.6	0.29230	0.26	3,114	±39	3,429.9	± 4.0	9
11.1	266	195	0.75	144	0.07	0.6290	1.2	24.44	1.2	0.28178	0.27	3,146	±29	3,372.8	± 4.3	7
11.2	260	155	0.62	102	0.04	0.4552	1.2	17.62	1.3	0.2808	0.50	2,418	±24	3,367.3	± 7.7	28
12.1	281	258	0.95	157	0.01	0.6501	1.4	25.03	1.4	0.27923	0.22	3,229	±35	3,358.7	± 3.4	4
12.2	261	169	0.67	138	0.08	0.6129	1.2	24.17	1.2	0.28603	0.29	3,082	±29	3,396.2	± 4.6	9
13.1	218	131	0.62	120	0.06	0.6412	1.2	25.66	1.2	0.29028	0.25	3,194	±30	3,419.1	± 3.8	7
14.1	336	219	0.68	129	0.10	0.4463	1.2	16.93	1.5	0.2752	1.0	2,379	±23	3,336	±16	29
15.1	140	70	0.52	83.1	0.04	0.6924	1.2	28.27	1.3	0.29610	0.32	3,392	±32	3,450.0	± 4.9	2
16.1	222	138	0.64	136	0.01	0.7148	1.2	28.39	1.2	0.28802	0.24	3,477	±32	3,407.0	± 3.7	-2
16.2	137	69	0.52	82.5	0.02	0.7006	1.2	28.69	1.3	0.29707	0.28	3,423	±32	3,455.0	± 4.3	1
17.1	176	91	0.54	88.7	0.05	0.5859	1.2	23.44	1.3	0.2902	0.43	2,973	±29	3,418.9	± 6.7	13
18.1	215	131	0.63	120	0.03	0.6479	1.2	25.75	1.2	0.28823	0.28	3,220	±30	3,408.1	± 4.4	6
19.1	280	199	0.74	115	0.12	0.4787	1.2	18.61	1.3	0.28201	0.30	2,522	±26	3,374.1	± 4.7	25
20.1	195	117	0.62	118	0.02	0.7023	1.2	28.46	1.2	0.29393	0.25	3,430	±31	3,438.5	± 3.9	0
21.1	245	155	0.66	122	0.05	0.5804	1.2	23.13	1.3	0.28898	0.22	2,950	±29	3,412.2	± 3.5	14
22.1	1098	731	0.69	162	0.34	0.1712	1.2	5.231	1.5	0.2217	0.88	1,018	±11	2,993	±14	66
23.1	1186	624	0.54	184	0.44	0.1796	1.2	5.313	1.4	0.2146	0.66	1,065	±12	2,941	±11	64
24.1	555	348	0.65	171	0.11	0.3587	1.5	13.57	1.6	0.27443	0.33	1,976	±26	3,331.5	± 5.1	41
25.1	231	144	0.64	111	0.06	0.5586	1.3	21.50	1.4	0.27910	0.24	2,861	±31	3,357.9	± 3.7	15

Table A1: Summary of SHRIMP U-Th-Pb data for sample LV01-23, flow-banded lava. Errors listed are 1σ, f_{206} (%) denotes the percentage of ^{206}Pb that is common Pb. Error in Standard calibration was 0.27% (not included in above errors but required when comparing data from different mounts). Common Pb corrected using measured ^{204}Pb.

Grain.spot	U (ppm)	Th (ppm)	Th/U	Pb* (ppm)	f_{206} (%)	Radiogenic Ratios						Ages (in Ma)				
						$^{206}Pb^*/^{238}U$	± (%)	$^{207}Pb^*/^{235}U$	± (%)	$^{207}Pb^*/^{206}Pb^*$	± (%)	$^{206}Pb/^{238}U$	±	$^{207}Pb/^{206}Pb$	±	Disc. (%)
1.2	127	71	0.58	78.8	0.03	0.7202	1.2	29.32	1.2	0.29525	0.28	3,497	±31	3,445.5	± 4.4	-1
2.1	798	613	0.79	235	0.64	0.3407	1.2	10.26	1.3	0.21834	0.25	1,890	±20	2,968.5	± 4.0	36
3.1	253	172	0.71	150	0.05	0.6900	1.1	27.60	1.1	0.29014	0.22	3,383	±29	3,418.4	± 3.4	1
3.2	243	157	0.67	131	0.10	0.6262	1.1	24.35	1.2	0.28208	0.21	3,135	±28	3,374.5	± 3.3	7
4.1	204	152	0.77	114	0.05	0.6510	0.96	26.22	0.99	0.29214	0.23	3,232	±24	3,429.1	± 3.6	6
5.1	205	139	0.70	122	0.08	0.6894	0.93	27.85	0.97	0.29302	0.26	3,380	±24	3,433.7	± 4.1	2
6.1	576	382	0.68	266	0.22	0.5368	0.90	18.79	0.93	0.25386	0.21	2,770	±20	3,209.0	± 3.2	14
7.1	332	164	0.51	195	0.06	0.6833	0.85	26.99	0.88	0.28649	0.25	3,357	±22	3,398.7	± 3.9	1
7.2	977	490	0.52	287	0.63	0.3392	1.2	9.37	1.4	0.2002	0.71	1,883	±19	2,828	±12	33
8.1	229	150	0.67	131	0.04	0.6634	0.94	26.89	0.97	0.29404	0.24	3,280	±24	3,439.1	± 3.7	5
9.1	396	276	0.72	147	0.39	0.4308	0.87	14.31	0.99	0.2410	0.48	2,309	±17	3,126.5	± 7.6	26
10.1	249	167	0.69	148	0.03	0.6894	0.87	27.65	0.90	0.29083	0.23	3,380	±23	3,422.1	± 3.5	1
11.1	155	96	0.64	97.7	0.04	0.7333	0.93	30.07	0.97	0.29741	0.28	3,546	±25	3,456.8	± 4.3	-3
11.2	193	145	0.77	108	0.09	0.6506	1.2	25.73	1.2	0.28676	0.23	3,231	±29	3,400.1	± 3.6	5
12.1	331	214	0.67	182	0.14	0.6399	0.84	24.83	0.87	0.28147	0.22	3,189	±21	3,371.1	± 3.5	5
13.1	206	90	0.45	118	0.07	0.663	2.8	26.54	2.8	0.29043	0.33	3,278	±71	3,419.9	± 5.2	4
14.1	192	104	0.56	111	0.05	0.6747	0.90	27.00	0.94	0.29025	0.26	3,324	±23	3,418.9	± 4.1	3
14.2	194	105	0.56	112	0.11	0.6752	1.3	27.21	1.3	0.29228	0.29	3,326	±33	3,429.8	± 4.5	3
15.1	154	78	0.52	90.3	0.04	0.6839	0.94	27.86	0.98	0.29551	0.29	3,359	±25	3,446.8	± 4.5	3
16.1	134	75	0.58	82.2	0.03	0.7129	0.95	29.16	1.0	0.2967	0.40	3,469	±26	3,453.0	± 6.3	0
17.1	150	81	0.56	91.0	–	0.7084	0.91	29.03	0.94	0.29722	0.25	3,453	±24	3,455.8	± 3.9	0
17.2	100	63	0.64	54.0	0.00	0.6259	1.2	25.64	1.2	0.29711	0.31	3,133	±30	3,455.2	± 4.8	9
18.1	134	113	0.87	74.2	0.20	0.6442	1.1	26.09	1.2	0.2938	0.41	3,206	±28	3,437.7	± 6.3	7
19.1	503	323	0.66	189	0.40	0.4360	0.85	16.57	0.90	0.27561	0.29	2,333	±17	3,338.3	± 4.5	30
20.1	197	118	0.62	117	0.04	0.6902	0.88	28.17	0.91	0.29597	0.23	3,383	±23	3,449.2	± 3.6	2
20.2	210	131	0.64	70.8	0.23	0.3913	1.3	15.42	1.3	0.28579	0.33	2,129	±23	3,394.8	± 5.2	37
21.1	233	129	0.57	137	0.05	0.6826	1.2	27.56	1.2	0.29277	0.22	3,354	±30	3,432.4	± 3.4	2
22.1	211	150	0.73	115	0.07	0.6336	1.2	25.52	1.2	0.29209	0.27	3,164	±29	3,428.8	± 4.1	8

Table A2: Summary of SHRIMP U-Th-Pb data for sample LV01-113, (semi-)interlocking felsic intrusive. Errors listed are 1σ, f_{206} (%) denotes the percentage of ^{206}Pb that is common Pb. Error in Standard calibration was 0.27% (not included in above errors but required when comparing data from different mounts). Common Pb corrected using measured ^{204}Pb.

Grain.spot	U (ppm)	Th (ppm)	Th/U	Pb* (ppm)	f_{206} (%)	Radiogenic Ratios						Ages (in Ma)				
						$^{206}Pb^*/^{238}U$	± (%)	$^{207}Pb^*/^{235}U$	± (%)	$^{207}Pb^*/^{206}Pb^*$	± (%)	$^{206}Pb/^{238}U$	±	$^{207}Pb/^{206}Pb$	±	Disc. (%)
1.1	205	373	1.88	113	0.03	0.6413	1.3	22.64	1.3	0.25609	0.33	3,194	±32	3,222.8	±5.2	1
2.1	48	30	0.66	26.4	0.18	0.6394	1.5	22.55	1.6	0.2558	0.59	3,187	±37	3,220.7	±9.2	1
3.1	118	135	1.18	67.0	0.00	0.6594	1.3	23.31	1.3	0.25642	0.36	3,265	±32	3,224.8	±5.6	-1
4.1	171	208	1.25	96.3	0.03	0.6542	1.2	23.17	1.2	0.25685	0.29	3,245	±30	3,227.5	±4.5	-1
5.1	181	237	1.35	95.8	0.05	0.6170	1.2	21.94	1.2	0.25790	0.27	3,098	±30	3,233.9	±4.3	4
6.1	136	133	1.01	69.4	0.01	0.5955	1.3	21.04	1.3	0.25627	0.34	3,012	±30	3,224.0	±5.3	7
7.1	100	9	0.09	60.0	0.05	0.696	1.6	24.70	1.6	0.25757	0.37	3,404	±42	3,231.9	±5.9	-5
8.1	361	89	0.25	163	0.05	0.5255	1.3	16.17	1.3	0.22320	0.23	2,722	±28	3,003.9	±3.8	9
9.1	57	23	0.42	33.1	0.00	0.6710	1.5	23.75	1.5	0.2567	0.49	3,310	±38	3,226.3	±7.7	-3
10.1	137	163	1.24	86.1	0.04	0.7331	1.2	26.09	1.3	0.25813	0.32	3,545	±33	3,235.3	±5.0	-10
11.1	198	231	1.21	103	0.06	0.6048	1.3	21.35	1.4	0.25599	0.29	3,049	±32	3,222.2	±4.7	5
12.1	109	9	0.09	60.6	0.00	0.6496	1.3	22.92	1.3	0.2559	0.41	3,227	±32	3,221.8	±6.4	0
13.1	124	112	0.93	67.9	0.03	0.635	1.6	22.46	1.7	0.2563	0.49	3,171	±40	3,224.4	±7.8	2
14.1	152	206	1.40	87.5	0.06	0.6714	1.2	23.80	1.2	0.25715	0.30	3,311	±31	3,229.4	±4.7	-3
15.1	167	238	1.47	104	0.02	0.7243	1.3	25.73	1.3	0.25764	0.29	3,512	±34	3,232.3	±4.6	-9
16.1	111	111	1.03	65.1	0.05	0.6805	1.3	24.01	1.3	0.2559	0.39	3,346	±33	3,221.3	±6.2	-4
17.1	111	42	0.39	60.6	0.00	0.636	1.6	22.59	1.7	0.2577	0.39	3,172	±40	3,232.6	±6.2	2
18.1	229	247	1.11	127	0.04	0.6474	1.5	22.95	1.5	0.25709	0.29	3,218	±39	3,228.9	±4.5	0
19.1	141	189	1.38	83.7	0.02	0.6890	1.4	24.37	1.5	0.25656	0.35	3,379	±38	3,225.7	±5.6	-5
20.1	67	45	0.70	37.8	0.00	0.653	1.7	23.20	1.7	0.2576	0.52	3,241	±42	3,231.8	±8.2	0

Table A3: Summary of SHRIMP U-Th-Pb data for sample SV01-03, pyroxene-amphibole porphyry. Errors listed are 1σ, f_{206} (%) denotes the percentage of ^{206}Pb that is common Pb. Error in Standard calibration was 0.27% (not included in above errors but required when comparing data from different mounts). Common Pb corrected using measured ^{204}Pb.

Grain.spot	U (ppm)	Th (ppm)	Th/U	Pb* (ppm)	f_{206} (%)	Radiogenic Ratios						Ages (in Ma)				
						$^{206}Pb^*/^{238}U$	± (%)	$^{207}Pb^*/^{235}U$	± (%)	$^{207}Pb^*/^{206}Pb^*$	± (%)	$^{206}Pb/^{238}U$	±	$^{207}Pb/^{206}Pb$	±	Disc. (%)
1.1	166	107	0.67	104	0.00	0.7270	0.77	29.77	0.81	0.29700	0.25	3,522	±21	3,454.7	± 3.8	-2
2.1	194	141	0.75	122	0.03	0.7307	1.1	29.92	1.1	0.29696	0.24	3,536	±29	3,454.4	± 3.7	-2
3.1	287	175	0.63	158	0.07	0.6405	0.70	25.25	0.74	0.28592	0.22	3,191	±18	3,395.5	± 3.4	6
4.1	184	113	0.64	110	0.00	0.6933	0.77	28.04	0.81	0.29336	0.25	3,395	±20	3,435.5	± 3.9	1
5.1	92	49	0.55	54.9	0.09	0.6966	0.89	28.31	0.96	0.2948	0.34	3,408	±24	3,443.0	± 5.3	1
6.1	185	128	0.72	116	0.02	0.7289	0.76	29.83	0.81	0.29684	0.25	3,529	±21	3,453.8	± 3.9	-2
7.1	238	165	0.72	139	0.01	0.6805	0.85	27.26	0.88	0.29049	0.23	3,346	±22	3,420.2	± 3.5	2
8.1	188	135	0.74	115	0.03	0.7135	0.79	28.97	0.83	0.29447	0.25	3,472	±21	3,441.4	± 3.9	-1
9.1	162	95	0.60	91.7	0.03	0.6593	0.89	26.99	0.94	0.29687	0.30	3,265	±23	3,454.0	± 4.7	5
10.1	241	137	0.59	143	0.03	0.6924	0.86	28.15	0.89	0.29482	0.24	3,392	±23	3,443.2	± 3.8	1
11.1	224	151	0.70	127	0.03	0.6583	0.72	26.26	0.76	0.28936	0.23	3,260	±18	3,414.2	± 3.5	5
12.1	155	86	0.57	94.0	0.00	0.7055	0.77	28.99	0.82	0.29796	0.27	3,442	±21	3,459.7	± 4.1	1
13.1	238	191	0.83	148	0.00	0.7207	0.71	28.51	0.74	0.28688	0.21	3,499	±19	3,400.8	± 3.3	-3
14.1	194	130	0.69	88.9	0.05	0.5321	0.79	20.92	0.84	0.28511	0.28	2,750	±18	3,391.1	± 4.3	19
15.1	506	286	0.58	173	0.16	0.3968	0.66	12.314	0.74	0.22508	0.32	2,154	±12	3,017.4	± 5.2	29
16.1	200	158	0.82	123	0.00	0.7146	0.74	28.77	0.77	0.29201	0.23	3,476	±20	3,428.4	± 3.6	-1
17.1	214	168	0.81	124	0.04	0.6758	0.72	27.40	0.75	0.29411	0.23	3,328	±19	3,439.5	± 3.5	3
18.1	313	292	0.96	130	0.16	0.4816	0.87	17.96	0.90	0.27040	0.23	2,534	±18	3,308.3	± 3.7	23
19.1	256	206	0.83	140	0.08	0.6340	0.81	25.40	0.88	0.29053	0.34	3,165	±20	3,420.4	± 5.3	7
20.1	249	199	0.83	141	0.02	0.6571	0.98	26.22	1.0	0.28941	0.34	3,256	±25	3,414.4	± 5.2	5
21.1	252	175	0.72	160	0.00	0.7390	0.70	29.82	0.73	0.29265	0.20	3,567	±19	3,431.8	± 3.1	-4
22.1	185	143	0.80	112	0.02	0.7032	0.74	28.54	0.81	0.29435	0.32	3,433	±20	3,440.7	± 5.0	0
23.1	154	82	0.55	79.7	3.46	0.5692	1.0	21.75	1.7	0.2773	1.3	2,904	±22	3,347	±21	13
24.1	300	230	0.79	177	0.01	0.6854	0.74	27.80	0.77	0.29419	0.22	3,365	±19	3,439.9	± 3.4	2
25.1	251	282	1.16	92.9	0.15	0.4298	1.3	17.08	1.3	0.2882	0.35	2,305	±24	3,407.7	± 5.5	32

Table A4: Summary of SHRIMP U-Th-Pb data for sample ISO99-9, felsic porphyritic rock. Errors listed are 1σ, f_{206} (%) denotes the percentage of ^{206}Pb that is common Pb. Error in Standard calibration was 0.27% (not included in above errors but required when comparing data from different mounts). Common Pb corrected using measured ^{204}Pb.

Appendix B - Geochronology data Chapter 3

Analytical technique

Zircons were separated from 8 to 9 kg rock samples at the mineral separation laboratory of the Free University in Amsterdam. The samples were crushed and ground with a rock splitter, jaw crusher and disk mill to a size of < 500 μm. The samples were then sieved to obtain a fraction smaller than 250 μm. Light particles smaller than 32 μm were removed. Zircons were separated from the remaining fraction using standard heavy liquid and magnetic separation techniques. The handpicked zircons, together with zircon standard CZ3 (Pidgeon et al., 1994), were mounted in epoxy resin and polished. Spots for analyses were selected using transmitted and reflected light microscopy images, as well as SEM cathodoluminescence images of the mounted zircons. Analyses were performed on the SHRIMP II at Curtin University of Technology in Perth, Australia. Operating procedures for U, Th and Pb isotopic measurements on zircon are based on those described by Compston et al. (1984) and Williams et al. (1984). The data acquisition and processing were done as described in detail by Nelson (1997; 1999).

Results

Sample A

Sample A contains abundant zircons of > 90 μm. The zircons are light pink and very translucent. They are short, columnar and extremely euhedral shaped. The population is very homogeneous and contains only rarely more elongate, whitish-coloured zircons. Cathodoluminescence images show well developed, but on the images very faint, magmatic compositional zoning in about 75% of the zircons. The other zircons show no internal structure.

30 analyses were made, all on different zircons (Table B1). 26 analyses together define a mean $^{207}Pb/^{206}Pb$ age of 3464 ± 2 Ma (95% confidence level; chi-square 1.2). Four analyses were excluded from the age calculation because statistically they do not belong to the main group. Analyses 3.1 and 13.1 are slightly older, and may represent xenocrysts. Analyses 24.1 and 28.1 are slightly younger and reversely discordant. The age of 3464 ± 2 Ma is interpreted as the age of crystallisation of the quartz-plagioclase porphyry.

Sample B

Zircons of sample B are very much like the zircons of sample A. The translucent zircons are between 100 and 200 μm, and form a very heterogeneous population. The zircons are short and stubby, and very euhedral. Cathodoluminescence images reveal a well-developed but faintly visible magmatic zoning. A number of zircons are fractured, but these were avoided during analysis.

10 analyses were made, all on different zircons (Table B2). Together, these analyses define a mean $^{207}Pb/^{206}Pb$ age of 3465 ± 4 Ma (95% confidence level; chi-square 0.61). This age is interpreted as the age of crystallisation of the quartz-plagioclase porphyry.

Sample C

Sample C contains abundant zircons of > 90 μm. The zircons are translucent, and pink to reddish-coloured. There are two different shapes of zircons; elongate ones with a long c-axis, and more round ones, with a c-axis that is only slightly longer than the short axis of the zircons. On cathodoluminescence images, most zircons display a clear magmatic zoning. Some zircon grains have a distinct core. 30 analyses were made, all on different zircons (Table B3). Together, these analyses define a mean $^{207}Pb/^{206}Pb$ age of 3465 ± 4 Ma (95% confidence level; chi-square 1.23). This age is interpreted as the age of crystallisation of the plagioclase porphyry.

Sample D

Sample D contains only a few zircons of >90μm, most zircons are between 60-90 μm in size. Most zircons are colourless to purple, and are not very translucent. The outlines of the zircons are rough and the surfaces are pockmarked. Euhedral zircons are rare. Internally, many zircons are fractured and have small inclusions. Magmatic zoning is well visible on cathodoluminescence images.

30 analyses were made on 27 different zircons (Table B4). 26 analyses together define a mean $^{207}Pb/^{206}Pb$ age of 3459 ± 2 Ma (95% confidence level; chi-square 1.42). 8 highly discordant analyses were excluded from the age calculation. The age of 3459 ± 2 Ma is interpreted as the age of crystallisation of the plagioclase porphyry.

Sample E

The total zircon population of sample E looks rather inhomogeneous. Apart from nicely euhedral zircons, there are also subhedral ones, and many fragments. Part of the euhedral zircons displays clear magmatic zoning. Most zircons or fragments of zircons are between 100 and 200 μm. Both strongly elongated as well as more rounded zircons are present. Most zircons are transparent, some are fractured or have a pockmarked surface.

10 analyses were made, all on different zircons (Table B5). 8 analyses together define a mean $^{207}Pb/^{206}Pb$ age of 3446 ± 2 Ma (95% confidence level; chi-square 0.44). Two analyses fall statistically outside the main group. They are older, and give a combined age of 3473 ± 2 Ma. They most probably represent xenocrysts. 3446 ± 2 Ma is interpreted as the age of crystallisation of the rhyolite.

Sample F

The zircon population in sample F is extremely heterogeneous. There is a wide range of colours. The fraction of >90 μm contains translucent as well as milky-white, non-translucent zircons. Zircons in the 60-90 μm fraction are frequently stained with a rust-colour. The shape of the zircons ranges from very elongate to short and stubby, and the crystals are euhedral to anhedral. Fragments of zircons are abundant. The most transparent zircons were used for analysis. The cathodoluminescence images of the zircons show the same heterogeneity. Some zircons are magmatically zoned, while others show no internal structure at all.

25 analyses were made on 17 different zircons (Table B6). 10 analyses together define a mean $^{207}Pb/^{206}Pb$ age of 3459 ± 4 Ma (95% confidence level; chi-square 1.12). Two other groups of analyses show significantly younger ages. Four analyses combine together to an age of 3280±13 Ma (95% confidence level; chi-square 0.82). Two other analyses give a combined age of 3352±4 Ma (± 1 sigma error). However, apart from two slightly reversely discordant analyses, all analyses making up the latter two groups are highly discordant, as are the remaining 7 analyses. The abundance of zircons with an age of 3459 ± 4 Ma is an indication of the age of the main source area for this sediment. The sediment is therefore definitely younger than 3459 ± 4 Ma. Probably, it is younger than 3352±4 Ma, and maybe even younger than 3280±13 Ma. However, the exact maximum age is difficult to establish, because the analyses combining to the latter two dates are highly discordant.

Sample G

Sample G displays a very homogeneous zircon population. The zircons are nicely translucent, and range in size from 100-200 μm. They are slightly elongate, and are very euhedral. Cathodoluminescence

imaging shows that the zircons are magmatically zoned. Many zircons show a core.

12 analyses were made, all on different zircons (Table B7). 9 analyses together define a mean $^{207}Pb/^{206}Pb$ age of 3318 ± 2 Ma (95% confidence level; chi-square 1.28). Three analyses fall statistically outside the main group. Two of those are slightly discordant, and have probably suffered some lead loss early in history. The age of 3318 ± 2 Ma is interpreted as the age of crystallisation of the felsic porphyry.

Grain .spot	U (ppm)	Th (ppm)	Pb (ppm)	f206%	$^{207}Pb/^{206}Pb$	±1σ	$^{208}Pb/^{206}Pb$	±1σ	$^{206}Pb/^{238}U$	±1σ	$^{207}Pb/^{235}U$	±1σ	% concordance	$^{207}Pb/^{206}Pb$ Age	±1σ
255-1.1	236	180	215	0.076	0.30027	0.00121	0.20435	0.00142	0.7007	0.0191	29.010	0.812	99	3472	6
255-2.1	150	107	137	0.042	0.30066	0.00134	0.19251	0.00159	0.7076	0.0193	29.332	0.826	99	3474	7
255-3.1	263	259	246	0.087	0.30225	0.00098	0.26454	0.00126	0.6912	0.0187	28.805	0.795	97	3482	5
255-4.1	229	177	212	0.072	0.29851	0.00104	0.20625	0.00118	0.7134	0.0193	29.361	0.814	100	3462	5
255-5.1	223	170	198	0.022	0.29908	0.00102	0.20633	0.00120	0.6856	0.0185	28.270	0.782	97	3465	5
255-6.1	247	195	222	0.057	0.29930	0.00103	0.21040	0.00121	0.6928	0.0187	28.589	0.792	98	3467	5
255-7.1	125	83	111	0.180	0.30114	0.00150	0.17451	0.00185	0.6916	0.0189	28.715	0.815	97	3476	8
255-8.1	166	111	150	0.229	0.30034	0.00129	0.17674	0.00155	0.7058	0.0192	29.226	0.821	99	3472	7
255-9.1	162	113	139	0.193	0.29923	0.00132	0.18397	0.00158	0.6690	0.0182	27.603	0.775	95	3466	7
255-10.1	311	313	295	0.010	0.29882	0.00090	0.27113	0.00112	0.7010	0.0189	28.880	0.795	99	3464	5
255-11.1	233	185	218	0.120	0.30147	0.00109	0.21196	0.00133	0.7146	0.0194	29.702	0.826	100	3478	6
255-12.1	204	148	184	0.126	0.30062	0.00116	0.18957	0.00137	0.7004	0.0190	29.031	0.809	99	3473	6
255-13.1	240	190	220	0.042	0.30157	0.00107	0.21286	0.00122	0.7029	0.0191	29.227	0.812	99	3478	5
255-14.1	207	159	190	0.064	0.29905	0.00111	0.20326	0.00125	0.7103	0.0193	29.287	0.815	100	3465	6
255-15.1	267	225	248	0.052	0.29965	0.00101	0.22116	0.00120	0.7082	0.0192	29.260	0.810	100	3468	5
255-16.1	197	144	182	0.064	0.29990	0.00120	0.19492	0.00133	0.7148	0.0195	29.556	0.828	100	3470	6
255-17.1	193	152	177	0.059	0.29753	0.00118	0.20876	0.00140	0.7043	0.0191	28.893	0.807	99	3457	6
255-18.1	215	171	198	0.222	0.29896	0.00122	0.20769	0.00154	0.7040	0.0191	29.017	0.812	99	3465	6
255-19.1	285	295	275	0.133	0.29746	0.00077	0.27519	0.00104	0.7096	0.0106	29.101	0.452	100	3457	4
255-20.1	169	123	159	0.024	0.29848	0.00098	0.19445	0.00109	0.7317	0.0111	30.115	0.480	102	3462	5
255-21.1	148	89	136	-0.022	0.29855	0.00104	0.15866	0.00106	0.7296	0.0111	30.032	0.482	102	3463	5
255-22.1	243	201	230	0.040	0.29897	0.00080	0.21922	0.00092	0.7219	0.0109	29.758	0.465	101	3465	4
255-23.1	299	245	283	0.035	0.29843	0.00074	0.21719	0.00083	0.7252	0.0109	29.839	0.463	102	3462	4
255-24.1	180	111	167	0.106	0.29613	0.00095	0.15926	0.00101	0.7390	0.0112	30.176	0.480	103	3450	5
255-25.1	180	116	167	0.076	0.29904	0.00095	0.17308	0.00099	0.7318	0.0111	30.174	0.479	102	3465	5
255-26.1	263	224	248	0.054	0.29898	0.00077	0.22415	0.00089	0.7170	0.0108	29.559	0.460	101	3465	4
255-27.1	207	172	191	0.094	0.29854	0.00087	0.21599	0.00102	0.7042	0.0106	28.986	0.455	99	3463	5
255-28.1	206	145	192	0.035	0.29575	0.00084	0.18693	0.00088	0.7288	0.0110	29.718	0.467	102	3448	4
255-29.1	288	289	280	0.035	0.29744	0.00072	0.26671	0.00090	0.7212	0.0108	29.577	0.458	101	3457	4
255-30.1	301	255	279	0.028	0.29712	0.00076	0.22929	0.00091	0.7052	0.0106	28.891	0.449	100	3455	4

Table B1: Ion microprobe analytical results for sample A (original number VM00-255)

Grain .spot	U (ppm)	Th (ppm)	Pb (ppm)	ƒ206%	$^{207}Pb/^{206}Pb$	±1σ	$^{208}Pb/^{206}Pb$	±1σ	$^{206}Pb/^{238}U$	±1σ	$^{207}Pb/^{235}U$	±1σ	% concordance	$^{207}Pb/^{206}Pb$ Age	±1σ
9528-1	280	227	256	0.056	0.29919	0.00083	0.21620	0.00094	0.6978	0.0083	28.788	0.362	98	3466	4
9528-2	278	261	260	0.107	0.29990	0.00085	0.24382	0.00105	0.7013	0.0084	28.998	0.366	99	3470	4
9528-3	136	76	123	0.149	0.30040	0.00121	0.14449	0.00130	0.7241	0.0091	29.990	0.410	101	3472	6
9528-4	130	81	119	0.178	0.29843	0.00122	0.16231	0.00141	0.7257	0.0092	29.861	0.411	102	3462	6
9528-5	246	195	228	0.095	0.29944	0.00085	0.21008	0.00098	0.7098	0.0085	29.306	0.372	100	3467	4
9528-6	143	102	133	0.188	0.29822	0.00114	0.18743	0.00136	0.7230	0.0090	29.729	0.400	101	3461	6
9528-7	177	134	162	0.224	0.29755	0.00102	0.19529	0.00127	0.7101	0.0087	29.135	0.382	100	3458	5
9528-8	201	136	180	0.152	0.29878	0.00101	0.18142	0.00117	0.6993	0.0085	28.808	0.375	99	3464	5
9528-9	267	241	254	0.158	0.29924	0.00084	0.23747	0.00107	0.7134	0.0086	29.433	0.373	100	3466	4
9528-10	172	130	160	0.152	0.29840	0.00108	0.19902	0.00128	0.7180	0.0089	29.541	0.393	101	3462	6

Table B2: Ion microprobe analytical results for sample B (original number W95-28)

Grain .spot	U (ppm)	Th (ppm)	Pb (ppm)	f206%	$^{207}Pb/^{206}Pb$	±1σ	$^{208}Pb/^{206}Pb$	±1σ	$^{206}Pb/^{238}U$	±1σ	$^{207}Pb/^{235}U$	±1σ	% concordance	$^{207}Pb/^{206}Pb$ Age	±1σ
w98-1.1	67	51	67	0.295	0.29672	0.00281	0.19386	0.00422	0.7703	0.0220	31.513	0.983	107	3453	15
w98-2.1	107	115	108	0.112	0.29878	0.00168	0.28345	0.00241	0.7373	0.0203	30.375	0.875	103	3464	9
w98-3.1	100	105	101	0.126	0.30117	0.00169	0.27816	0.00234	0.7380	0.0204	30.645	0.885	102	3476	9
w98-4.1	59	48	58	0.154	0.30064	0.00225	0.21244	0.00310	0.7456	0.0210	30.908	0.928	103	3474	12
w98-5.1	94	100	94	0.036	0.30163	0.00180	0.28476	0.00237	0.7317	0.0203	30.431	0.887	102	3479	9
w98-6.1	83	88	85	-0.014	0.30161	0.00192	0.29047	0.00260	0.7505	0.0209	31.212	0.916	104	3479	10
w98-7.1	103	106	110	0.008	0.30275	0.00194	0.28101	0.00239	0.7832	0.0219	32.695	0.961	107	3484	10
w98-8.1	74	58	68	-0.044	0.30264	0.00187	0.21179	0.00244	0.7061	0.0196	29.463	0.859	99	3484	10
w98-9.1	41	35	39	0.336	0.30036	0.00272	0.23612	0.00404	0.7157	0.0205	29.639	0.921	100	3472	14
w98-10.1	68	62	66	0.092	0.29934	0.00192	0.24042	0.00260	0.7293	0.0203	30.103	0.884	102	3467	10
w98-11.1	85	80	82	0.108	0.30014	0.00174	0.25777	0.00240	0.7153	0.0198	29.603	0.857	100	3471	9
w98-12.1	120	127	116	0.154	0.29968	0.00144	0.28507	0.00197	0.7075	0.0194	29.234	0.829	99	3469	7
w98-13.1	72	67	70	0.272	0.30089	0.00193	0.25072	0.00274	0.7171	0.0199	29.749	0.872	100	3475	10
w98-14.1	60	44	55	0.382	0.29458	0.00214	0.19080	0.00291	0.7038	0.0197	28.585	0.853	100	3442	11
w98-15.1	61	50	57	0.019	0.29918	0.00190	0.21500	0.00214	0.7156	0.0200	29.519	0.869	100	3466	10
w98-16.1	69	57	64	0.315	0.29773	0.00199	0.21765	0.00285	0.7018	0.0195	28.808	0.847	99	3458	10
w98-17.1	145	138	138	0.037	0.29812	0.00103	0.25008	0.00127	0.7136	0.0109	29.332	0.470	100	3460	5
w98-18.1	59	43	56	0.115	0.29654	0.00169	0.18296	0.00196	0.7466	0.0119	30.527	0.539	104	3452	9
w98-19.1	75	70	74	0.015	0.29881	0.00146	0.24495	0.00175	0.7369	0.0116	30.360	0.517	103	3464	8
w98-20.1	77	77	77	0.117	0.29766	0.00147	0.26660	0.00207	0.7411	0.0117	30.414	0.519	103	3458	8
w98-21.1	61	40	57	0.118	0.30048	0.00165	0.17628	0.00192	0.7329	0.0117	30.365	0.530	102	3473	8
w98-22.1	83	92	82	0.069	0.29712	0.00139	0.29123	0.00195	0.7266	0.0113	29.766	0.501	102	3455	7
w98-23.1	66	51	62	0.096	0.29926	0.00155	0.20596	0.00188	0.7253	0.0114	29.929	0.515	101	3466	8
w98-24.1	80	79	75	0.099	0.29604	0.00144	0.26216	0.00198	0.6916	0.0107	28.230	0.473	98	3450	8
w98-25.1	101	114	102	-0.012	0.30116	0.00134	0.30044	0.00189	0.7350	0.0114	30.521	0.509	102	3476	7
w98-26.1	92	97	92	0.015	0.29891	0.00132	0.27981	0.00170	0.7291	0.0113	30.049	0.502	102	3465	7
w98-27.1	82	68	78	0.054	0.29711	0.00140	0.22115	0.00173	0.7257	0.0113	29.728	0.501	102	3455	7
w98-28.1	93	96	92	0.115	0.29780	0.00133	0.27700	0.00180	0.7221	0.0112	29.652	0.495	101	3459	7
w98-29.1	66	51	64	0.081	0.29936	0.00162	0.20904	0.00206	0.7470	0.0119	30.831	0.537	104	3467	8
w98-30.1	139	141	140	0.048	0.29923	0.00108	0.27369	0.00139	0.7460	0.0114	30.777	0.497	104	3466	6

Table B3: Ion microprobe analytical results for sample C (original number W98-5)

Grain .spot	U (ppm)	Th (ppm)	Pb (ppm)	f206%	$^{207}Pb/^{206}Pb$	±1σ	$^{208}Pb/^{206}Pb$	±1σ	$^{206}Pb/^{238}U$	±1σ	$^{207}Pb/^{235}U$	±1σ	% concordance	$^{207}Pb/^{206}Pb$ Age	±1σ
124-1.1	250	207	226	0.123	0.29945	0.00068	0.22255	0.00086	0.6880	0.0071	28.407	0.307	97	3467	4
124-2.1	142	91	129	0.099	0.29862	0.00091	0.16987	0.00102	0.7169	0.0076	29.520	0.336	101	3463	5
124-3.1	321	384	307	0.120	0.29740	0.00058	0.31472	0.00082	0.6860	0.0070	28.127	0.300	97	3457	3
124-4.1	171	120	152	0.124	0.29944	0.00084	0.18678	0.00097	0.6888	0.0072	28.440	0.319	97	3467	4
124-5.1	211	168	196	0.101	0.29665	0.00091	0.20945	0.00104	0.7128	0.0109	29.157	0.464	100	3453	5
124-6.1	152	109	140	0.177	0.29751	0.00112	0.19007	0.00138	0.7160	0.0110	29.370	0.478	101	3457	6
124-7.1	246	174	210	0.060	0.29496	0.00079	0.18622	0.00089	0.6694	0.0101	27.226	0.426	96	3444	4
124-8.1	515	800	443	0.135	0.28157	0.00046	0.41481	0.00079	0.5870	0.0087	22.791	0.346	88	3372	3
124-9.1	179	118	162	0.059	0.29779	0.00079	0.17549	0.00083	0.7120	0.0108	29.236	0.458	100	3459	4
124-10.1	326	297	257	0.120	0.28479	0.00064	0.20701	0.00078	0.6103	0.0091	23.965	0.369	91	3389	3
124-11.1	244	306	244	0.106	0.29656	0.00088	0.32662	0.00130	0.7139	0.0109	29.190	0.463	101	3452	5
124-12.1	376	321	299	0.121	0.29110	0.00079	0.21466	0.00098	0.6115	0.0092	24.545	0.383	90	3423	4
124-13.1	278	215	253	0.429	0.29737	0.00092	0.19805	0.00128	0.6974	0.0106	28.595	0.453	99	3457	5
124-14.1	534	842	470	0.115	0.28723	0.00065	0.41988	0.00110	0.5963	0.0089	23.617	0.364	89	3403	4
124-15.1	218	226	207	0.030	0.29922	0.00091	0.26879	0.00116	0.7020	0.0107	28.961	0.461	99	3466	5
124-16.1	211	143	187	0.138	0.29754	0.00096	0.18453	0.00112	0.6930	0.0106	28.432	0.455	98	3457	5
124-17.1	160	118	145	0.437	0.29471	0.00123	0.20223	0.00180	0.6974	0.0107	28.340	0.467	99	3443	6
124-18.1	295	418	290	0.094	0.29915	0.00081	0.35916	0.00122	0.6865	0.0104	28.315	0.444	97	3466	4
124-19.1	592	524	549	0.026	0.29759	0.00049	0.23278	0.00055	0.7033	0.0105	28.858	0.439	99	3458	3
124-20.1	358	247	315	0.143	0.29656	0.00065	0.19730	0.00078	0.6811	0.0102	27.850	0.430	97	3452	3
124-21.1	263	230	248	0.100	0.29752	0.00077	0.23691	0.00100	0.7108	0.0107	29.157	0.456	100	3457	4
124-22.1	244	179	220	0.039	0.29810	0.00078	0.19347	0.00084	0.7029	0.0106	28.890	0.452	99	3460	4
124-23.1	246	183	220	0.063	0.29774	0.00079	0.19031	0.00085	0.6961	0.0105	28.577	0.448	98	3459	4
124-24.1	176	109	156	0.063	0.29767	0.00092	0.16327	0.00095	0.7041	0.0107	28.898	0.460	99	3458	5
124-25.1	755	776	504	0.100	0.27057	0.00052	0.26710	0.00072	0.5028	0.0075	18.756	0.286	79	3309	3
124-26.1	1196	2196	697	0.053	0.24871	0.00046	0.45642	0.00088	0.3962	0.0059	13.586	0.207	68	3177	3
124-27.1	306	245	280	0.140	0.29775	0.00078	0.22764	0.00098	0.6937	0.0105	28.479	0.445	98	3459	4
124-22.2	261	229	241	0.117	0.29826	0.00078	0.22955	0.00096	0.7003	0.0106	28.800	0.450	99	3461	4
124-16.2	2023	4061	1538	0.060	0.25426	0.00031	0.53995	0.00065	0.4905	0.0073	17.196	0.259	80	3211	2
124-17.2	162	96	144	0.157	0.29827	0.00101	0.16319	0.00113	0.7063	0.0108	29.049	0.468	100	3461	5

Table B4: Ion microprobe analytical results for sample D (original number VM00-124)

Grain .spot	U (ppm)	Th (ppm)	Pb (ppm)	f206%	$^{207}Pb/^{206}Pb$	±1σ	$^{208}Pb/^{206}Pb$	±1σ	$^{206}Pb/^{238}U$	±1σ	$^{207}Pb/^{235}U$	±1σ	% concordance	$^{207}Pb/^{206}Pb$ Age	±1σ
96001-1	140	78	121	0.271	0.29580	0.00129	0.14499	0.00154	0.6934	0.0087	28.278	0.391	98	3448	7
96001-2	147	108	132	0.271	0.29680	0.00122	0.19239	0.00158	0.6971	0.0087	28.527	0.389	99	3454	6
96001-3	147	183	148	0.239	0.30055	0.00125	0.33068	0.00192	0.7126	0.0090	29.531	0.405	100	3473	6
96001-4	185	141	169	0.145	0.29495	0.00105	0.19986	0.00129	0.7065	0.0087	28.731	0.380	100	3444	6
96001-5	217	191	206	0.101	0.29517	0.00094	0.23338	0.00113	0.7186	0.0087	29.245	0.378	101	3445	5
96001-6	45	27	44	1.338	0.30099	0.00283	0.14695	0.00478	0.7418	0.0111	30.787	0.575	103	3475	15
96001-7	165	126	151	0.378	0.29600	0.00114	0.20434	0.00156	0.6985	0.0086	28.506	0.381	99	3449	6
96001-8	92	52	84	1.260	0.29430	0.00183	0.14394	0.00300	0.7108	0.0093	28.843	0.438	101	3440	10
96001-9	135	96	122	0.423	0.29421	0.00118	0.18610	0.00161	0.7007	0.0088	28.425	0.387	100	3440	6
96001-10	259	114	224	0.213	0.29507	0.00084	0.11681	0.00090	0.7095	0.0085	28.864	0.365	100	3445	4

Table B5: Ion microprobe analytical results for sample E (original number JW95-001)

Grain .spot	U (ppm)	Th (ppm)	Pb (ppm)	ƒ206%	$^{207}Pb/^{206}Pb$	±1σ	$^{208}Pb/^{206}Pb$	±1σ	$^{206}Pb/^{238}U$	±1σ	$^{207}Pb/^{235}U$	±1σ	% concordance	$^{207}Pb/^{206}Pb$ Age	±1σ
w94-1.1*	300	310	145	4.078	0.29604	0.00236	0.16414	0.00469	0.3360	0.0036	13.714	0.193	54	3450	12
w94-2.1	172	84	41	0.311	0.08427	0.00135	0.14664	0.00289	0.2250	0.0024	2.614	0.053	101	1299	31
w94-3.1	42	159	17	3.834	0.08223	0.00686	1.14164	0.02125	0.1999	0.0027	2.266	0.195	94	1251	164
w94-4.1	212	167	202	0.116	0.29784	0.00096	0.20910	0.00112	0.7323	0.0079	30.072	0.349	102	3459	5
w94-5.1	165	31	119	0.394	0.29712	0.00129	0.04400	0.00150	0.6179	0.0068	25.314	0.310	90	3455	7
w94-6.1	173	115	121	0.384	0.26549	0.00122	0.19077	0.00173	0.5505	0.0060	20.151	0.248	86	3280	7
w94-7.1	195	150	180	0.082	0.29955	0.00101	0.20653	0.00114	0.7113	0.0077	29.380	0.345	100	3468	5
w94-8.1*	1127	431	503	0.390	0.18886	0.00049	0.09879	0.00073	0.3975	0.0040	10.350	0.112	79	2732	4
w94-9.1	355	311	337	0.179	0.29813	0.00082	0.23005	0.00105	0.7178	0.0075	29.505	0.330	101	3461	4
w94-10.1*	569	227	306	0.478	0.22299	0.00071	0.10088	0.00107	0.4639	0.0048	14.263	0.158	82	3002	5
w94-11.1	273	219	184	0.095	0.19254	0.00080	0.22144	0.00129	0.5524	0.0059	14.666	0.174	103	2764	7
w94-12.1	282	98	94	0.214	0.10726	0.00077	0.10265	0.00131	0.3176	0.0033	4.697	0.063	101	1753	13
w94-13.1*	426	625	243	0.620	0.26703	0.00131	0.25965	0.00220	0.4246	0.0064	15.631	0.257	69	3289	8
w94-4.2	187	138	180	0.411	0.29818	0.00111	0.19969	0.00155	0.7377	0.0112	30.328	0.488	103	3461	6
w94-7.2	269	245	263	0.123	0.29792	0.00090	0.23874	0.00112	0.7370	0.0111	30.274	0.476	103	3459	5
w94-1.2*	137	73	109	1.196	0.29532	0.00173	0.12631	0.00283	0.6284	0.0097	25.587	0.438	91	3446	9
w94-5.2*	773	153	582	0.510	0.29397	0.00061	0.05282	0.00076	0.6377	0.0095	25.846	0.394	92	3439	3
w94-14.1	176	106	154	0.102	0.27787	0.00099	0.16118	0.00112	0.7046	0.0107	26.996	0.433	103	3351	6
w94-15.1	258	198	254	0.131	0.29625	0.00093	0.20135	0.00109	0.7622	0.0115	31.132	0.492	106	3451	5
w94-7.3	219	166	214	0.080	0.29918	0.00095	0.19795	0.00108	0.7576	0.0115	31.251	0.496	105	3466	5
w94-16.1*	269	107	232	1.081	0.26533	0.00122	0.12447	0.00203	0.6965	0.0105	25.482	0.417	104	3279	7
w94-5.3	246	48	142	0.330	0.27835	0.00107	0.05166	0.00126	0.4991	0.0075	19.155	0.305	78	3354	6
w94-5.4	455	172	329	0.165	0.29174	0.00076	0.08860	0.00078	0.6054	0.0090	24.352	0.377	89	3427	4
w94-5.5*	477	115	326	0.547	0.29119	0.00082	0.05733	0.00106	0.5771	0.0086	23.169	0.360	86	3424	4
w94-17.1*	266	195	99	1.784	0.26333	0.00173	0.20896	0.00323	0.2770	0.0042	10.059	0.172	48	3267	10

Table B6: Ion microprobe analytical results for sample F (original number W94-22.3)

Grain .spot	U (ppm)	Th (ppm)	Pb (ppm)	ƒ206%	$^{207}Pb/^{206}Pb$	±1σ	$^{208}Pb/^{206}Pb$	±1σ	$^{206}Pb/^{238}U$	±1σ	$^{207}Pb/^{235}U$	±1σ	% concordance	$^{207}Pb/^{206}Pb$ Age	±1σ
9536-1	112	36	80	0.028	0.27308	0.00075	0.08863	0.00072	0.6108	0.0296	22.997	1.124	92	3324	4
9536-2	121	41	93	0.046	0.27201	0.00073	0.08753	0.00067	0.6514	0.0316	24.433	1.194	97	3318	4
9536-3	179	78	135	0.040	0.27072	0.00057	0.11600	0.00052	0.6288	0.0304	23.471	1.143	95	3310	3
9536-4	148	65	117	-0.005	0.27263	0.00068	0.11862	0.00083	0.6621	0.0321	24.888	1.215	99	3321	4
9536-5	240	105	172	0.254	0.26339	0.00051	0.10859	0.00061	0.6022	0.0291	21.869	1.065	93	3267	3
9536-6	116	40	83	1.402	0.26061	0.00099	0.08489	0.00180	0.5925	0.0287	21.292	1.045	92	3250	6
9536-7	180	60	138	0.100	0.27245	0.00092	0.08876	0.00084	0.6508	0.0079	24.447	0.317	97	3320	5
9536-8	243	131	196	0.057	0.27181	0.00078	0.14475	0.00081	0.6625	0.0079	24.828	0.313	99	3316	4
9536-9	205	77	158	0.065	0.27331	0.00087	0.09904	0.00078	0.6523	0.0078	24.583	0.315	97	3325	5
9536-10	164	75	129	0.099	0.27110	0.00101	0.12209	0.00104	0.6543	0.0080	24.457	0.323	98	3312	6
9536-11	290	145	162	0.330	0.27423	0.00088	0.14582	0.00111	0.4514	0.0053	17.068	0.216	72	3330	5
9536-12	151	79	123	0.157	0.27184	0.00108	0.13869	0.00124	0.6666	0.0083	24.985	0.338	99	3317	6
95366-1	193	82	138	0.182	0.26742	0.00099	0.11168	0.00112	0.6014	0.0073	22.175	0.291	92	3291	6
95366-2	105	92	95	0.219	0.29409	0.00150	0.23095	0.00201	0.6847	0.0089	27.764	0.403	98	3439	8
95366-3	123	72	102		0.27249	0.00124	0.15870	0.00145	0.6705	0.0085	25.192	0.353	100	3320	7
95366-4	133	182	86		0.26871	0.00136	0.09698	0.00160	0.5442	0.0068	20.161	0.285	85	3298	8

Table B7: Ion microprobe analytical results for sample G (original number W95-36)

References

Appel, P.W.U., Rollinson, H.R. and Touret, J.L.R., 2001. Remnants of an Early Archaean (>3.75 Ga) sea-floor, hydrothermal system in the Isua Greenstone Belt. *Precambrian Research,* **112:** 27-49.

Armstrong, R.A., Compston, W., De Wit, M.J. and Williams, I.S., 1990. The stratigraphy of the 3.5-3.2 Ga Barberton Greenstone Belt revisited: a single zircon ion microprobe study. *Earth and Planetary Science Letters,* **101:** 90-106.

Bailey, R.A., 1976. Volcanism, Structure, and Geochronology of Long Valley Caldera, Mono County, California. *Journal of Geophysical Research,* **81:** 725-744.

Barley, M.E., 1984. Volcanism and hydrothermal alteration, Warrawoona Group, East Pilbara. In: J.R. Muhling, D.I. Groves and T.S. Blake (Editors), Archaean and Proterozoic Basins of the Pilbara, Western Australia: Evolution, and Mineralization Potential. University of Western Australia, *Geology Department & University Extension Publ.,* **9**: 23-36.

Barley, M.E., 1993. Volcanic, sedimentary and tectonostratigraphic environments of the ~3.46 Ga Warrawoona Megasequence: a review. *Precambrian Research,* **60:** 47-67.

Barley, M.E., Dunlop, J.S.R., Glover, J.E. and Groves, D.I., 1979. Sedimentary evidence for an Archaean shallow-water volcanic-sedimentary facies, Eastern Pilbara Block, Western Australia. *Earth and Planetary Science Letters,* **43:** 74-84.

Barley, M.E., Loader, S.E. and McNaughton, N.J., 1998. 3430 to 3417 Ma calc-alkaline volcanism in the McPhee Dome and Kelly Belt, and growth of the eastern Pilbara Craton. *Precambrian Research,* **88:** 3-23.

Bathurst, R.G.C., 1971. Carbonate sediments and their diagenesis. *Developments in Sedimentology,* **12.** Elsevier, 620 pp.

Beintema, K.A., 2003. Geodynamic evolution of the West and Central Pilbara Craton in Western Australia: a mid-Archaean active continental margin. *Geologica Ultraiectina,* **232:** 248 pp.

Bodnar, R.J. and Vityk, M.O., 1994. Interpretation of microthermometric data for H_2O-NaCl fluid inclusions. In: B. De Vivo and M.L. Frezzotti (Editors), Fluid inclusions in minerals: methods and applications. Virginia Polytechnic Institute and State University, pp. 117-130.

Brandl, G. and De Wit, M.J., 1997. The Kaapvaal Craton, South Africa. In: M.J. de Wit and L.D. Ashwal (Editors), Greenstone Belts. Clarendon Press, Oxford, pp. 581-608.

Brauhart, C.W., Groves, D.I. and Morant, P., 1998. Regional alteration systems associated with volcanogenic massive sulfide mineralization at Panorama, Pilbara, Western Australia. *Economic Geology,* **93:** 292-302.

Buick, R. and Barnes, K.R., 1984. Cherts in the Warrawoona Group: Early Archaean silicified sediments deposited in shallow-water environments. In: J.R. Muhling, D.I. Groves and T.S. Blake (Editors), Archaean and Proterozoic Basins of the Pilbara, Western Australia: Evolution, and Mineralization Potential. University of Western Australia, *Geology Department & University Extension Publ.,* **9:** 37-53.

Buick, R. and Dunlop, J.S.R., 1990. Evaporitic sediments of Early Archaean age from the Warrawoona Group, North Pole, Western Australia. *Sedimentology,* **37:** 247-277.

Buick, R. et al., 1995. Record of emergent continental crust ~3.5 billion years ago in the Pilbara craton of Australia. *Nature,* **375:** 574-577.

Byerly, G.R., Kröner, A., Lowe, D.R., Todt, W. and Walsh, M.M., 1996. Prolonged magmatism and time constraints for sediment deposition in the early Archean Barberton greenstone belt: evidence from the Upper Onverwacht and Fig Tree groups. *Precambrian Research,* **78:** 125-138.

Byerly, G.R., Lowe, D.R., Wooden, J.L. and Xie, X., 2002. An Archean Impact Layer from the Pilbara and Kaapvaal Cratons. *Science,* **297:** 1325-1327.

Cas, R.A.F. and Wright, J.V., 1987. Volcanic successions: modern and ancient. Allen & Unwin, London, 528 pp.

Cathelineau, M., Izquierdo, G. and Nieva, D., 1989. Thermobarometry of hydrothermal alteration in the Los Azufres geothermal system (Michoacan,

Mexico): Significance of fluid-inclusion data. *Chemical Geology,* **76:** 229-238.

Chesner, C.A. and Rose, W.I., 1991. Stratigraphy of the Toba Tuffs and the evolution of the Toba-Caldera Complex, Sumatra, Indonesia. *Bulletin of Volcanology,* **53:** 343-356.

Claoué-Long, J.C., Compston, W., Roberts, J. and Fanning, C.M., 1995. Two Carboniferous ages: a comparison of SHRIMP zircon dating with conventional zircon ages and $^{40}Ar/^{39}Ar$ analysis, Geochronology Time Scales and Global Stratigraphic Correlation. *SEPM Special Publication,* **54**: 3-21.

Collins, W.J., 1989. Polydiapirism of the Archean Mount Edgar batholith, Pilbara block, Western Australia. *Precambrian Research,* **43:** 41-62.

Compston, W., Williams, I.S., Kirschvink, J.L., Zhang, Z. and Ma, G., 1992. Zircon U-Pb ages for the Early Cambrian timescale. *Journal of the Geological Society of London,* **149:** 171-184.

Condie, K.C. and Hunter, D.R., 1976. Trace element geochemistry of Archean granitic rocks from the Barberton region, South Africa. *Earth and Planetary Science Letters,* **29:** 389-400.

Cumming, G.L. and Richards, J.R., 1975. Ore lead isotopic ratios in a continuously changing Earth. *Earth and Planetary Science Letters,* **28:** 155-171.

Dann, J.C., 2000. The 3.5 Ga Komati Formation, Barberton Greenstone Belt, South Africa, Part I: New maps and magmatic architecture. *Journal of South African Geology,* **103:** 47-68.

De Ronde, C.E.J., Channer, D.M.d., Faure, K., Bray, C.J. and Spooner, E.T.C., 1997a. Fluid chemistry of Archean seafloor hydrothermal vents: Implications for the composition of circa 3.2 Ga seawater. *Geochimica et Cosmochimica Acta*, **61:** 4025-4042.

De Ronde, C.E.J., Channer, D.M.d. and Spooner, E.T.C., 1997b. Archaean Fluids. In: M.J. de Wit and L.D. Ashwal (Editors), Greenstone Belts. Oxford monographs on geology and geophysics. Clarendon Press, Oxford, pp. 309-335.

De Ronde, C.E.J. and De Wit, M.J., 1994. Tectonic history of the Barberton greenstone belt, South Africa: 490 million years of Archean crustal evolution. *Tectonics,* **13:** 983-1005.

De Ronde, C.E.J., De Wit, M.J. and Spooner, E.T.C., 1994. Early Archean (> 3.2 Ga) Fe-oxide-rich, hydrothermal discharge vents in the Barberton Greenstone Belt, South Africa. *Geological Society of America Bulletin,* **106:** 86-104.

De Ronde, C.E.J., De Wit, M.J., Spooner, E.T.C., Channer, D.M.d. and Christenson, B.W., 2004. Ironstone pods in the Archean Barberton greenstone belt, South Africa: Earth's oldest seafloor hydrothermal vents reinterpreted as Quaternary subaerial hotsprings: Comment. *Geology,* accepted for publication.

De Ronde, C.E.J. and Ebbesen, T.W., 1996. 3.2 b.y. of organic compound formation near sea-floor hot springs. *Geology,* **24:** 791-794,

De Ronde, C.E.J. and Kamo, S., 2000. An Archaean arc-arc collisional event: a short-lived (ca 3 Myr) episode, Weltevreden area, Barberton greenstone belt, South Africa. *Journal of African Earth Sciences*, **30:** 219-248.

De Ronde, C.E.J., Kamo, S., Davis, D.W., De Wit, M.J. and Spooner, E.T.C., 1991. Field, geochemical and U-Pb isotopic constraints from hypabyssal felsic intrusions within the Barberton greenstone belt, South Africa: Implications for tectonics and the timing of gold mineralization. *Precambrian Research,* **49:** 261-280.

De Vries, S.T., 1999. Sedimentology, deformation and felsic volcanism of the Early Archaean Buck Ridge Chert Complex, Upper Onverwacht Group, Barberton Greenstone Belt, South Africa. Unpublished MSc Thesis, Utrecht University, Utrecht, 50 pp. (+ 52 figures)

De Wit, M.J., 1982. Gliding and overthrust nappe tectonics in the Barberton greenstone belt. *Journal of Structural Geology,* **4:** 117-136.

De Wit, M.J., 1983. Notes on a preliminary 1:25000 geological map of the southern part of the Barberton greenstone belt. In: C.R. Anhaeusser (Editor), Contributions to the Geology of the Barberton Mountain Land. *Special Publication Geological Society of South Africa,* **9:** 185-187 and map.

De Wit, M.J., 1986. Extensional tectonics during the igneous emplacement of the mafic-ultramafic rocks

of the Barberton greenstone belt (abstract). *Tech. Rep. Lunar Planet. Inst.,* **86-10:** 84-85.

De Wit, M.J., 1998. On Archean granites, greenstones, cratons and tectonics: does the evidence demand a verdict? *Precambrian Research,* **91:** 181-226.

De Wit, M.J., Armstrong, R., Hart, R.J. and Wilson, A.H., 1987a. Felsic igneous rocks within the 3.3 to 3.5 Ga Barberton Greenstone Belt: high crustal level equivalents of the surrounding Tonalite-Trondhjemite terrain, emplaced during thrusting. *Tectonics,* **6:** 529-549.

De Wit, M.J. and Ashwal, L.D. (Editors), 1997. Greenstone Belts. *Oxford monographs on geology and geophysics,* **35**. Clarendon Press, Oxford, 809 pp.

De Wit, M.J., Fripp, R.E.P. and Stanistreet, I.G., 1983. Tectonic and stratigraphic implications of new field observations along the southern part of the Barberton greenstone belt. In: C.R. Anhaeusser (Editor), Contributions to the geology of the Barberton Mountain Land. *Special Publication Geological Society of South Africa,* **9:** 21-29.

De Wit, M.J., Hart, R., Martin, A. and Abbott, P., 1982. Archaean Abiogenic and Probable Biogenic Structures Associated with Mineralized Hydrothermal Vent Systems and Regional Metasomatism, with Implications for Greenstone Belt Studies. *Economic Geology,* **77:** 1783-1801.

De Wit, M.J., Hart, R.A. and Hart, R.J., 1987b. The Jamestown ophiolite complex, Barberton mountain belt: A section through 3.5 Ga oceanic crust. *Journal of African Earth Sciences,* **6:** 681-730.

Diamond, L.W., 2001. Review of the systematics of CO_2-H_2O fluid inclusions. *Lithos,* **55:** 69-99.

DiMarco, M.J. and Lowe, D.R., 1989a. Shallow-water volcaniclastic deposition in the Early Archean Panorama Formation, Warrawoona Group, eastern Pilbara Block, Western Australia. *Sedimentary Geology,* **64:** 43-63.

DiMarco, M.J. and Lowe, D.R., 1989b. Stratigraphy and Sedimentology of an Early Archean Felsic Volcanic Sequence, Eastern Pilbara Block, Western Australia, with Special Reference to the Duffer Formation and Implications for Crustal Evolution. *Precambrian Research,* **44:** 147-169.

Dunlop, J.S.R., 1978. Shallow-water sedimentation at North Pole, Pilbara Block, Western Australia. University of Western Australia, *Geology Department & University Extension Publ.,* **2:** 30-38.

Dunlop, J.S.R. and Buick, R., 1981. Archaean epiclastic sediments derived from mafic volcanics, North Pole, Pilbara Block, Western Australia. *Spec. Publications geol. Soc. Aust.,* **7:** 225-233.

Dunlop, J.S.R., Muir, M.D., Milne, V.A. and Groves, D.I., 1978. A new microfossil assemblage from the Archaean of Western Australia. *Nature,* **274:** 676-678.

Eriksson, K.A., 1980a. Hydrodynamic and paleogeographic interpretation of turbidite deposits from the Archean Fig Tree Group of the Barberton Mountain Land, South Africa. *Geological Society of America Bulletin,* **Part I, 91:** 21-26.

Eriksson, K.A., 1980b. Transitional sedimentation styles in the Moodies and Fig Tree Groups, Barberton Mountain Land, South Africa: Evidence favouring an Archean continental margin. *Precambrian Research,* **12:** 141-160.

Eriksson, K.A., 1981. Archaean platform-to-trough sedimentation, East Pilbara block, Australia. *Special Publ. Geol. Soc. Australia,* **7:** 235-244.

Eriksson, K.A., 1982. Geometry and internal characteristics of Archaean submarine channel deposits, Pilbara Block, Western Australia. *Journal of Sedimentary Petrology,* **52:** 383-393.

Eriksson, K.A., Krapez, B. and Fralick, P.W., 1994. Sedimentology of Archean greenstone belts: signatures of tectonic evolution. *Earth-Science Reviews,* **37:** 1-88.

Farmer, J.D., 1996. Hydrothermal systems on Mars: an assessment of present evidence. In: G.R. Bock and J.A. Goode (Editors), Evolution of hydrothermal ecosystems on Earth (and Mars?). Wiley, Chichester, Ciba Foundation Symposium 202, pp. 273-299.

Farmer, J.D., 2000. Hydrothermal Systems: Doorways to Early Biosphere Evolution. *GSA Today,* **10:** 1-9.

Fisher, A.G., 1964. The Lofer Cyclothems of the Alpine Triassic. *Kansas Geological Survey Bulletin,* **169:** 107-149.

Fisher, R.V. and Schmincke, H.-U., 1984. Pyroclastic Rocks. Springer-Verlag, Berlin, 471 pp.

Francis, P., 1993. Volcanoes: a planetary perspective. Oxford University Press, 443 pp.

French, B.M., 1998. Traces of Catastrophe: A Handbook of Shock-Metamorphic Effects in Terrestrial Meteorite Impact Structures. *LPI Contribution,* **954.** Lunar and Planetary Institute, Houston, 120 pp.

Glikson, A.Y., 2001. The astronomical connection of terrestrial evolution: crustal effects of post-3.8 Ga mega-impact clusters and evidence for major 3.2±0.1 Ga bombardment of the Earth-Moon system. *Journal of Geodynamics,* **32:** 205-229.

Green, M.G., Sylvester, P.J. and Buick, R., 2000. Growth and recycling of early Archaean continental crust: geochemical evidence from the Coonterunah and Warrawoona Groups, Pilbara Craton, Australia. *Tectonophysics,* **322:** 69-88.

Hamilton, W.B., 1998. Archean magmatism and deformation were not products of plate tectonics. *Precambrian Research,* **91:** 143-179.

Hanor, J.S. and Duchač, K., 1990. Isovolumetric silicification of early Archean komatiites: geochemical mass balances and constraints on origin. *Journal of Geology,* **98:** 863-877.

Heinrichs, T., 1984. The Umsoli Chert, turbidite testament for a major phreatoplinian event at the Onverwacht/ Fig Tree transition (Swaziland Supergroup, Archaean, South Africa). *Precambrian Research,* **24:** 237-283.

Heubeck, C. and Lowe, D.R., 1994. Depositional and tectonic setting of the Archean Moodies Group, Barberton Greenstone Belt, South Africa. *Precambrian Research,* **68:** 257-290.

Heubeck, C. and Lowe, D.R., 1999. Sedimentary petrography and provenance of the Archean Moodies Group, Barberton Greenstone Belt. In: D.R. Lowe and G.R. Byerly (Editors), Geologic Evolution of the Barberton Greenstone Belt, South Africa. *Geological Society of America Special Paper,* **329:** 259-286.

Hickman, A.H., 1983. Geology of the Pilbara Block and its environs. *Western Australia Geological Survey Bulletin,* **127,** 268 pp.

Hofmann, A., Dirks, P.H.G.M. and Jelsma, H.A., 2001. Late Archaean foreland basin deposits, Belingwe greenstone belt, Zimbabwe. *Sedimentary Geology,* **141-142:** 131-168.

Holland, H.D., 1972. The geologic history of sea water - an attempt to solve the problem. *Geochimica et Cosmochimica Acta,* **36:** 637-651.

Hulen, J.B. and Nielson, D.L., 1988. Hydrothermal brecciation in the Jemez Fault Zone, Valles Caldera, New Mexico: Results from continental scientific drilling program core hole VC-1. *Journal of Geophysical Research,* **93:** 6077-6089.

Humphris, S.E., Fornari, D.J., Scheirer, D.S., German, C.R. and Parson, L.M., 2002. Geotectonic setting of hydrothermal activity on the summit of Lucky Strike Seamount (37°17'N, Mid-Atlantic Ridge). *Geochemistry Geophysics Geosystems,* **3:** doi: 10.1029/2001GC000284.

Isozaki, Y., Ueno, Y., Kitajima, K., Kabashima, T. and Maruyama, S., 1998. Early Archean mid-oceanic ridge sediments and the oldest bacteria from the Pilbara Craton, W. Australia. *GSA Abstracts,* **30:** A98.

Isozaki, Y., Ueno, Y., Yurimoto, H. and Maruyama, S., 1999. 3.5 Ga Kerogen-rich silica dikes from North Pole area, Western Australia: Subseafloor biosphere in the Archean? *Eos Trans.,* **80:** 88.

Kamo, S.L. and Davis, D.W., 1994. Reassessment of Archean crustal development in the Barberton Mountain Land, South Africa, based on U-Pb dating. *Tectonics,* **13:** 167-192.

Kisch, H.J. and Nijman, W., 2004. Metamorphic grade from K-micas in the metasediments of the Pilbara and Barberton Greenstone Belts. In: W.U. Reimold and A. Hofmann (Comp.), Abstract volume, Field Forum on Processes on the Early Earth, Kaapvaal Craton, South Africa, 4-9 July 2004, pp. 47-48.

Kisters, A.F.M., Stevens, G., Dziggel, A. and Armstrong, R.A., 2003. Extensional detachment faulting and core-complex formation in the southern Barberton granite-greenstone terrain, South

Africa: evidence for a 3.2 Ga orogenic collapse. *Precambrian Research,* **127:** 355-378.

Kitajima, K., Kabashima, T., Ueno, Y., Terabayashi, M. and Maruyama, S., 2001a. Archaean seafloor hydrothermal system in the North Pole of the Pilbara Craton, Western Australia. In: K.F. Cassidy, J.M. Dunphy and M.J. Van Kranendonk (Editors), 4th International Archaean Symposium. AGSO - Geoscience Australia, Perth, pp. 51-53.

Kitajima, K., Maruyama, S., Utsunomiya, S. and Liou, J.G., 2001b. Seafloor hydrothermal alteration at an Archaean mid-ocean ridge. *Journal of Metamorphic Geology,* **19:** 583-599.

Kloppenburg, A., 2003. Structural evolution of the Marble Bar Domain, Pilbara granite-greenstone terrain, Australia: the role of Archaean mid-crustal detachments. *Geologica Ultraiectina,* **237:** 256 pp.

Krapez, B., 1993. Sequence stratigraphy of the Archaean supracrustal belts of the Pilbara Block, Western Australia. *Precambrian Research,* **60:** 1-45.

Krapez, B. and Barley, M.E., 1987. Archaean strike-slip faulting and related ensialic basins: evidence from the Pilbara Block, Australia. *Geological Magazine,* **124:** 555-567.

Kröner, A., Byerly, G.R. and Lowe, D.R., 1991. Chronology of early Archaean granite-greenstone evolution in the Barberton Mountain Land, South Africa, based on precise dating by single zircon evaporation. *Earth and Planetary Science Letters,* **103:** 41-54.

Kröner, A. and Todt, W., 1988. Single Zircon Dating Constraining the Maximum Age of the Barberton Greenstone Belt, Southern Africa. *Journal of Geophysical Research,* **93:** 15329-15337.

Lamb, S.H. and Paris, I., 1988. Post-Onverwacht Group stratigraphy in the SE part of the Archaean Barberton greenstone belt. *Journal of African Earth Sciences,* **7:** 285-306.

Langmuir, C.H. et al., 1997. Hydrothermal vents near a mantle hot spot: the Lucky Strike vent field at 37°N on the Mid-Atlantic Ridge. *Earth and Planetary Science Letters,* **148:** 69-91.

Lanier, W.P. and Lowe, D.R., 1982. Sedimentology of the Middle Marker (3.4 Ga), Onverwacht Group, Transvaal, South Africa. *Precambrian Research*, **18:** 237-260.

Lowe, D.R., 1982. Comparative sedimentology of the principal volcanic sequences of Archean greenstone belts in South Africa, Western Australia and Canada: implications for crustal evolution. *Precambrian Research,* **17:** 1-29.

Lowe, D.R., 1983. Restricted shallow-water sedimentation of early Archean stromatolitic and evaporitic strata of the Strelley Pool Chert, Pilbara Block, Western Australia. *Precambrian Research,* **19:** 239-283.

Lowe, D.R., 1999a. Petrology and sedimentology of cherts and related silicified sedimentary rocks in the Swaziland Supergroup. In: D.R. Lowe and G.R. Byerly (Editors), Geologic Evolution of the Barberton Greenstone Belt, South Africa. *Geological Society of America Special Paper,* **329:** 83-114.

Lowe, D.R., 1999b. Shallow-water sedimentation of accretionary lapilli-bearing strata of the Msauli Chert: Evidence of explosive hydromagmatic komatiitic volcanism. In: D.R. Lowe and G.R. Byerly (Editors), Geologic Evolution of the Barberton Greenstone Belt, South Africa. *Geological Society of America Special Paper,* **329:** 213-323.

Lowe, D.R. and Byerly, G.R. (Editors), 1999a. Geologic Evolution of the Barberton Greenstone Belt, South Africa. *Geological Society of America Special Paper,* **329:** 319 pp.

Lowe, D.R. and Byerly, G.R., 1999b. Stratigraphy of the west-central part of the Barberton Greenstone Belt, South Africa. In: D.R. Lowe and G.R. Byerly (Editors), Geologic Evolution of the Barberton Greenstone Belt, South Africa. *Geological Society of America Special Paper,* **329:** 1-36.

Lowe, D.R. and Byerly, G.R., 2003. Ironstone pods in the Archean Barberton greenstone belt, South Africa: Earth's oldest seafloor hydrothermal vents reinterpreted as Quaternary subaerial springs. *Geology,* **31:** 909-912.

Lowe, D.R., Byerly, G.R. and Heubeck, C., 1999. Structural divisions and development of the west-central part of the Barberton Greenstone Belt. In: D.R. Lowe and G.R. Byerly (Editors), Geologic Evolution of the Barberton Greenstone Belt, South

Africa. *Geological Society of America Special Paper,* **329:** 37-82.

Lowe, D.R., Byerly, G.R., Ransom, B.L. and Nocita, B.W., 1985. Stratigraphic and sedimentological evidence bearing on structural repetition in early Archean rocks of the Barberton Greenstone Belt, South Africa. *Precambrian Research,* **27:** 165-186.

Lowe, D.R. and Fisher Worrell, G., 1999. Sedimentology, mineralogy, and implications of silicified evaporites in the Kromberg Formation, Barberton Greenstone Belt, South Africa. In: D.R. Lowe and G.R. Byerly (Editors), Geologic Evolution of the Barberton Greenstone Belt, South Africa. *Geological Society of America Special Paper,* **329:** 167-188.

Lowe, D.R. and Knauth, L.P., 1977. Sedimentology of the Onverwacht Group (3.4 b.y.), Transvaal, South Africa, and its bearing on characteristics and evolution of the early Earth. *Journal of Geology,* **85:** 699-723.

Lowe, D.R. and Nocita, B.W., 1999. Foreland basin sedimentation in the Mapepe Formation, southern-facies Fig Tree Group. In: D.R. Lowe and G.R. Byerly (Editors), Geologic Evolution of the Barberton Greenstone Belt, South Africa. *Geological Society of America Special Paper,* **329:** 233-258.

Ludwig, K.R., 1999. Isoplot/Ex version 2.00: A Geochronological Toolkit for Microsoft Excel. *Berkeley Geochronological Center Special Publication,* **1a:** 46 pp.

Maliva, R.G. and Siever, R., 1988. Diagenetic replacement controlled by force of crystallization. *Geology,* **16:** 688-691.

Mandl, G. and Crans, W., 1981. Gravitational gliding in deltas. In: K.R. McClay and N.J. Price (Editors), Thrust and Nappe Tectonics. *Geol. Soc. of London Spec. Publ.,* **82:** 41-54.

Maruyama, S., Isozaki, Y. and Kimura, G., 1991. Is the Mid-Archean barite formation from the Pilbara Craton, Australia, under the deep-sea environment? *Eos Trans.,* **72:** 532.

McNaughton, N.J., Compston, W. and Barley, M.E., 1993. Constraints on the age of the Warrawoona Group, eastern Pilbara Block, Western Australia. *Precambrian Research,* **60:** 69-98.

Mercolli, I., 1979. Le inclusioni fluide nei noduli di quarzo dei marmi dolomitici della regione del Campolungo (Ticino). PhD Thesis, ETH, Zürich, 138 pp.

Minami, M., Shimizu, H., Masuda, A. and Adachi, M., 1995. Two Archean Sm-Nd ages of 3.2 and 2.5 Ga for the Marble Bar Chert, Warrawoona Group, Pilbara Block, Western Australia. *Geochemical Journal,* **29:** 347-362.

Nakamura, N., 1974. Determination of REE, Ba, Fe, Mg, Na and K in carbonaceous and ordinary chondrites. *Geochimica et Cosmochimica Acta,* **38:** 757-775.

Naumov, V.B. and Malinin, S.D., 1968. A new method for determining pressure by means of gas-liquid inclusions. *Geochemistry International,* **5:** 382-391.

Nelson, D.R., 1997. Compilation of SHRIMP U-Pb zircon geochronology data, 1996. Western Australia Geological Survey, Record 1997/2: 189 pp.

Nelson, D.R., 1999. Compilation of geochronology data, 1998. Western Australia Geological Survey, Record 1999/2: 222 pp.

Nelson, D.R., 2000. Compilation of geochronology data, 1999. Western Australia Geological Survey, Record 2000/2: 251 pp.

Nelson, D.R., 2001. Compilation of geochronology data, 2000. Geological Survey of Western Australia, Record 2001/2: 205 pp.

Nijman, W., De Bruijne, C.H. and Valkering, M.E., 1998a. Growth fault control of Early Archaean cherts, barite mounds and chert-barite veins, North Pole Dome, Eastern Pilbara, Western Australia. *Precambrian Research, 88: 25-52. (Re-edition in Precambrian Research, 1999,* **95:** 247-274)

Nijman, W. and De Vries, S.T., 2004. Early Archaean crustal collapse structures and sedimentary basin dynamics. In: P.G. Eriksson, W. Altermann, D.R. Nelson, W.U. Mueller and O. Catuneanu (Editors), The Precambrian Earth: Tempos and Events. *Developments in Precambrian Geology,* **12.** Elsevier, pp. 139-155.

Nijman, W., De Vries, S.T., Vos, I. and Louzada, K.L., 2001. Synsedimentary collapse structures in the

Warrawoona Group, Coppin Gap greenstone belt. In: M.J. Van Kranendonk, A.H. Hickman, I.R. Williams and W. Nijman (Editors), Archaean geology of the East Pilbara granite-greenstone terrane, Western Australia - a field guide. Western Australia Geological Survey, pp. 77-83.

Nijman, W., Willigers, B.A. and Krikke, A., 1998b. Tensile and compressive growth structures: relationships between sedimentation, deformation and granite intrusion in the Archaean Coppin Gap greenstone belt, Eastern Pilbara, Western Australia. *Precambrian Research, 88: 83-107. (Re-edition in Precambrian Research, 1999,* **95:** 277-302)

Nocita, B.W. and Lowe, D.R., 1990. Fan-delta sequence in the Archean Fig Tree Group, Barberton Greenstone Belt, South Africa. *Precambrian Research,* **48:** 375-393.

Nutman, A.P., 1997. The Greenland Sector of the North Atlantic Craton. In: M.J. De Wit and L.D. Ashwal (Editors), Greenstone Belts. Clarendon Press, Oxford, pp. 665-674.

Oliver, N.H.S. and Cawood, P.A., 2001. Early tectonic dewatering and brecciation on the overturned sequence at Marble Bar, Pilbara Craton, Western Australia: dome-related or not? *Precambrian Research,* **105:** 1-15.

Paces, J.B. and Miller, J.D., 1993. Precise U-Pb Ages of Duluth Complex and Related Mafic Intrusions, Northeastern Minnesota: Geochronological Insights to Physical, Petrogenetic, Paleomagnetic, and Tectonomagmatic Processes Associated with the 1.1 Ga Midcontinent Rift System. *Journal of Geophysical Research,* **98:** 13 997-14 013.

Paris, I.A., 1990. Depositional environment of the Onverwacht sedimentary rocks Barberton greenstone belt, South Africa. *Journal of African Earth Sciences,* **10:** 509-518.

Paris, I.A., Stanistreet, I.G. and Hughes, M.J., 1985. Cherts of the Barberton greenstone belt interpreted as products of submarine exhalative activity. *Journal of Geology,* **93:** 111-129.

Phillips, R.J. and Hansen, V.L., 1994. Tectonic and magmatic evolution of Venus. *Annual Reviews Earth and Planetary Sci.,* **22:** 597-654.

Pidgeon, R.T., Furfaro, D., Kennedy, A.K., Nemchin, A.A. and Van Bronswijk, W., 1994. Calibration of zircon standards for the Curtin SHRIMP II, 8th International Conference on Geochronology. USGS Circular, Berkeley, USA, pp. 251.

Pilkington, M. and Grieve, R.A.F., 1992. The Geophysical Signature of Terrestrial Impact Craters. *Reviews of Geophysics,* **30:** 161-181.

Prinz, T., 1996. Multispectral remote sensing of the Gosses Bluff impact crater, central Australia (N.T.) by using Landsat-TM and ERS-1 data. *ISPRS Journal of Photogrammetry & Remote Sensing,* **51:** 137-149.

Ransom, B., Byerly, G.R. and Lowe, D.R., 1999. Subaqueous to subaerial Archean ultramafic phreatomagmatic volcanism, Kromberg Formation, Barberton Greenstone Belt, South Africa. In: D.R. Lowe and G.R. Byerly (Editors), Geologic Evolution of the Barberton Greenstone Belt, South Africa. *Geological Society of America Special Paper,* **329:** 151-166.

Richards, J.R., Fletcher, I.R. and Blockley, J.G., 1981. Pilbara Galenas: Precise Isotopic Assay of the Oldest Australian Leads; Model Ages and Growth-Curve Implications. *Mineralium Deposita,* **16:** 7-30.

Robb, L.J. and Anhaeusser, C.R., 1983. Chemical and petrogenetic characteristics of Archaean tonalite-trondhjemite gneiss plutons in the Barberton Mountain Land. In: C.R. Anhaeusser (Editor), Contributions to the Geology of the Barberton Mountain Land. *Special Publication of the Geological Society of South Africa,* **9:** 103-116.

Roedder, E., 1984. Fluid Inclusions. *Reviews in Mineralogy,* **12,** 644 pp.

Rosing, M.T. and Frei, R., 2004. U-rich Archaean sea-floor sediments from Greenland - indications of >3700 Ma oxygenic photosynthesis. *Earth and Planetary Science Letters,* **217:** 237-244.

Runnegar, B., 2001. Archean sulfates from Western Australia: implications for Earth's early atmosphere

and ocean. 11th Goldschmidt Conference, Virginia, USA, abstract no. 3859.

Seyfried, W.E.J., Ding, K., Berndt, M.E. and Chen, X., 1999. Experimental and theoretical controls on the composition of mid-ocean ridge hydrothermal fluids. In: C.T. Barrie and M.D. Hannington (Eds), Volcanic-Associated Massive Sulfide Deposits: Processes and Examples in Modern and Ancient Settings. Rev. *Economic Geology,* **8:** 181-200.

Siever, R., 1992. The silica cycle in the Precambrian. *Geochimica et Cosmochimica Acta,* **56:** 2165-2172.

Smith, R.B. and Braile, L.W., 1984. Crustal Structure and Evolution of an Explosive Silicic Volcanic System at Yellowstone National Park. In: Explosive Volcanism: Inception, Evolution, and Hazards. Studies in Geophysics. National Academy Press, Washington D.C., pp. 96-109.

Smithies, R.H., Hickman, A.H. and Nelson, D.R., 1999. New constraints on the evolution of the Mallina Basin, and their bearing on relationships between the contrasting eastern and western granite-greenstone terranes of the Archaean Pilbara Craton, Western Australia. *Precambrian Research,* **94:** 11-28.

Smithies, R.H., Nelson, D.R. and Pike, G., 2001. Development of the Archaean Mallina Basin, Pilbara Craton, northwestern Australia; a study of detrital and inherited zircon ages. *Sedimentary Geology,* **141-142:** 79-94.

Smrekar, S.E. and Stofan, E.R., 1997. Corona Formation and Heat Loss on Venus by Coupled Upwelling and Delamination. *Science,* **277:** 1289-1294.

Smrekar, S.E. and Stofan, E.R., 1999. Origin of Corona-Dominated Topographic Rises on Venus. *Icarus,* **139:** 100-115.

Solomon, S.C. et al., 1992. Venus tectonics - an overview of Magellan observations. *Journal of Geophysical Research,* **97:** 13199-13255.

Spooner, E.T.C. and Fyfe, W.S., 1973. Sub-sea-floor metamorphism, heat and mass transfer. *Contr. Mineral. and Petrol.,* **42:** 287-304.

Stanistreet, I.G. and Hughes, M.J., 1984. Pseudoconglomerate and a re-examination of some paleoenvironmental controversies. *Geology,* **12:** 717-719.

Stoffers, P. et al., 1999. Little-studied Arc-Backarc System in the Spotlight. *Eos, Trans.,* **80:** 356, 359.

Sugitani, K., 1992. Geochemical characteristics of Archaean cherts and other sedimentary rocks in the Pilbara Block, Western Australia: evidence for Archaean seawater enriched in hydrothermally-derived iron and silica. *Precambrian Research,* **57:** 21-47.

Thorpe, R.I., Hickman, A.H., Davis, D.W., Mortensen, J.K. and Trendall, A.F., 1992a. Constraints to models for Archaean lead evolution from precise zircon U-Pb geochronology for the Marble Bar region, Pilbara Craton, Western Australia. In: J.E. Glover and S.E. Ho (Editors), The Archaean: Terrains, processes and metallogeny. Geology Dept (Key Centre) & University Extension, The University of Western Australia, pp. 395-407.

Thorpe, R.I., Hickman, A.H., Davis, D.W., Mortensen, J.K. and Trendall, A.F., 1992b. U-Pb zircon geochronology of Archaean felsic units in the Marble Bar region, Pilbara Craton, Western Australia. *Precambrian Research,* **56:** 169-189.

Toulkeridis, T., Clauer, N., Kröner, A., Reimer, T. and Todt, W., 1999. Characterization, provenance, and tectonic setting of Fig Tree greywackes from the Archaean Barberton Greenstone Belt, South Africa. *Sedimentary Geology,* **124:** 113-129.

Touret, J., 1977. The significance of fluid inclusions in metamorphic rocks. In: D.G. Fraser (Editor), Thermodynamics in Geology. D. Reidel Publishing Company, Dordrecht-Holland, pp. 203-227.

Touret, J.L.R., 2003. Remnants of early Archaean hydrothermal methane and brines in pillow-breccia from the Isua Greenstone Belt, West Greenland. *Precambrian Research,* **126:** 219-233.

Van Haaften, W.M. and White, S.H., 1998. Evidence for multiphase deformation in the Archean basal Warrawoona Group in the Marble Bar area, East Pilbara, Western Australia. *Precambrian Research,* **88:** 53-66.

Van Haaften, W.M. and White, S.H., 2001. Reply to comment on ''Evidence for multiphase deformation in the Archaean basal Warrawoona group in the

Marble Bar area, East Pilbara, Western Australia'' (van Haaften, W.M., White, S.H., 1998. Precambrian Research 88, 53–66) by M.J., Van Kranendonk, A.H. Hickman, W.J., Collins. *Precambrian Research,* **105:** 79-84.

Van Kranendonk, M.J., 1998. Litho-tectonic and structural components of the North Shaw 1:100000 sheet, Archaean Pilbara Craton. GSWA Annual Review, 1997-1998: 63-70.

Van Kranendonk, M.J., 2000. Geology of the North Shaw 1:100000 sheet: Western Australia Geological Survey, 1:100000 Geological Series Explanatory Notes, 86 pp.

Van Kranendonk, M.J., 2004. Archaean Tectonics 2004: A review - Preface. *Precambrian Research,* **131:** 143-151.

Van Kranendonk, M.J., Hickman, A.H. and Collins, W.J., 2001a. Comment on "Evidence for multiphase deformation in the Archaean basal Warrawoona group in the Marble Bar area, East Pilbara, Western Australia" by van Haaften, W.M., White, S.H., 1998. *Precambrian Research,* **105:** 73-78.

Van Kranendonk, M.J., Hickman, A.H., Smithies, R.H., Nelson, D.R. and Pike, G., 2002. Geology and Tectonic Evolution of the Archean North Pilbara Terrain, Pilbara Craton, Western Australia. *Economic Geology,* **97:** 695-732.

Van Kranendonk, M.J., Hickman, A.H., Williams, I.R. and Nijman, W., 2001b. Archaean geology of the East Pilbara granite-greenstone terrane, Western Australia - a field guide, Record 2001/9. Western Australia Geological Survey, 134 pp.

Varghese, G. and George, J., 2004. Pattern Formation in Reaction Diffusion Systems: A Moving Boundary Model. *Solid State Phenomena,* **97-98:** 125-132.

Vearncombe, S. et al., 1995. 3.26 Ga Black Smoker-Type Mineralization in the Strelley Belt, Pilbara-Craton, Western-Australia. *Journal of the Geological Society,* **152:** 587-590.

Vearncombe, S. and Kerrich, R., 1999. Geochemistry and geodynamic setting of volcanic and plutonic rocks associated with Early Archaean volcanogenic massive sulphide mineralization, Pilbara Craton. *Precambrian Research,* **98:** 243-270.

Vearncombe, S., Vearncombe, J.R. and Barley, M.E., 1998. Fault and stratigraphic controls on volcanogenic massive sulphide deposits in the Strelley Belt, Pilbara Craton, Western Australia. *Precambrian Research,* **88:** 67-82.

Viljoen, M.J. and Viljoen, R.P., 1969. The Geological and Geochemical Significance of the Upper Formations of the Onverwacht Group, Upper Mantle Project. *Special Publication Geological Society of South Africa,* **2:** 113-151.

Von Damm, K.L., 1995. Controls on the Chemistry and Temporal Variability of Seafloor Hydrothermal Fluids. In: S.E. Humphris, R.A. Zierenberg, L.S. Mullineaux and R.E. Thomson (Editors), Seafloor Hydrothermal Systems: Physical, Chemical, Biological, and Geological Interactions. *Geophysical Monograph,* **91.** American Geophysical Union, pp. 222-247.

Walsh, M.M., 1992. Microfossils and possible microfossils from the early Archean Onverwacht Group, Barberton Mountain Land, South Africa. *Precambrian Research,* **54:** 271-293.

Walsh, M.M. and Lowe, D.R., 1985. Filamentous microfossils from the 3,500-Myr-old Onverwacht Group, Barberton Mountain Land, South Africa. *Nature,* **314:** 530-532.

Walsh, M.M. and Lowe, D.R., 1999. Modes of accumulation of carbonaceous matter in the Early Archean: A petrographic and geochemical study of the carbonaceous cherts of the Swaziland Supergroup. In: D.R. Lowe and G.R. Byerly (Editors), Geologic Evolution of the Barberton Greenstone Belt, South Africa. *Geological Society of America Special Paper,* **329:** 115-132.

Watters, T.R. and Janes, D.M., 1995. Coronae on Venus and Mars: Implications for similar structures on Earth. *Geology,* **23:** 200-204.

Westall, F., 2004. Precambrian Geology and Exobiology. In: P.G. Eriksson, W. Altermann, D.R. Nelson, W.U. Mueller and O. Catuneanu (Editors), The Precambrian Earth: Tempos and Events. *Developments in Precambrian Geology,* **12.** Elsevier, pp. 575-587.

Westall, F. et al., 2001. Early Archean fossil bacteria and biofilms in hydrothermally-influenced sediments from the Barberton greenstone belt, South Africa. *Precambrian Research,* **106:** 93-116.

Westall, F., Orberger, B., Rouchon, V., Rouzaud, J.-N. and Wright, I., 2004. On the identification of early Archaean microfossils in cherts from Barberton and the Pilbara. In: W.U. Reimold and A. Hofmann (Comp.), Abstract volume, Field Forum on Processes on the Early Earth, Kaapvaal Craton, South Africa, 4-9 July 2004, pp. 94-97.

Williams, D.A.C. and Furnell, R.G., 1979. Reassessment of part of the Barberton type area, South Africa. *Precambrian Research,* **9:** 325-347.

Williams, I.R., 1999. Geology of the Muccan 1:100000 sheet: Western Australia Geological Survey. 1:100000 Geological Series Explanatory Notes, 39 pp.

Williams, I.S. and Claesson, S., 1987. Isotopic evidence for the Precambrian provenance and Caledonian metamorphism of high-grade paragneisses from the Seve Nappes, Scandinavian Caledonides. II. Ion microprobe zircon U-Th-Pb. *Contrib Mineral Petrol,* **97:** 205-217.

Williams, I.S. and Collins, W.J., 1990. Granite-greenstone terranes in the Pilbara Block, Australia, as coeval volcano-putonic complexes; evidence from U-Pb zircon dating of the Mount Edgar Batholith. *Earth and Planetary Science Letters,* **97:** 41-53.

Wilson, J.L., 1975. Carbonate Facies in Geological History. Springer Verlag, Berlin-Heidelberg, 471 pp.

Worthington, T.J., Gregory, M.R. and Bondarenko, V., 1999. The Denham Caldera on Raoul Volcano: dacitic volcanism in the Tonga-Kermadec arc. *Journal of Volcanology and Geothermal Research,* **90:** 29-48.

Wright, I.C. and Gamble, J.A., 1999. Southern Kermadec submarine caldera arc volcanoes (SW Pacific): caldera formation by effusive and pyroclastic eruption. *Marine Geology,* **161:** 207-227.

Zegers, T.E., 1996. Structural, kinematic and metallogenic evolution of selected domains of the Pilbara granitoid-greenstone terrain. *Geologica Ultraiectina,* **146:** 208 pp.

Zegers, T.E., Barley, M.E., Groves, D.I., McNaughton, N.J. and White, S.H., 2002. Oldest Gold: Deformation and Hydrothermal Alteration in the Early Archean Shear Zone-Hosted Bamboo Creek Deposit, Pilbara, Western Australia. *Economic Geology,* **97:** 757-773.

Zegers, T.E., De Wit, M.J., Dann, J. and White, S.H., 1998. Vaalbara, Earth's oldest assembled continent? A combined structural, geochronologic and paleomagnetic test. *Terra Nova,* **10:** 250-259.

Zegers, T.E., White, S.H., De Keijzer, M. and Dirks, P., 1996. Extensional structures during deposition of the 3460 Ma Warrawoona Group in the eastern Pilbara Craton, Western Australia. *Precambrian Research,* **80:** 89-105.

Samenvatting in het Nederlands (Summary in Dutch)

Inleiding

Het vroeg-Archeïcum beslaat de periode van ongeveer 3,8 tot 3,3 miljard jaar geleden. De Aarde zag er toen anders uit dan tegenwoordig; er waren nog geen macroscopische levensvormen en mogelijk bestond er nog geen plaattektoniek (het proces van over de Aarde schuivende schollen) of plaattektoniek bestond in een andere vorm dan op dit moment. Er zijn nog maar weinig overblijfselen uit de periode van 3,8 tot 3,3 miljard jaar geleden die op dit moment aan het aardoppervlak kunnen worden onderzocht. Gesteenten van deze ouderdom worden gevonden in Australië, Canada, Groenland en Zuid-Afrika. De oudste hiervan bevinden zich in Canada en Groenland. Deze twee gebieden hebben middelmatige tot hooggradige metamorfose ondergaan, dat wil zeggen ze zijn veranderd onder invloed van hoge temperatuur en druk. Sedimentaire gesteenten in deze gebieden zijn daardoor niet meer geschikt voor onderzoek. De Barberton Groensteengordel in Zuid-Afrika en het Pilbara Graniet-Groensteengebied in West-Australië hebben relatief weinig te lijden gehad onder deformatie (vervorming) en metamorfose. Deze studie concentreert zich daarom op delen van deze twee gebieden.

Tot nu toe waren studies aan vroeg-Archeïsche afzettingen voornamelijk gericht op één of twee aspecten van de gesteenteopeenvolging, zoals het afzettingsmilieu, de geochemie, de structurele geologie, vloeistofinsluitsels of de mogelijke ontwikkeling van het leven in de tijd dat deze sedimenten werden afgezet. De verschillende studies werden uitgevoerd in vergelijkbare, maar meestal door tijd of plaats gescheiden (delen van) groensteengordels, waardoor ze moeilijk te correleren en te vergelijken zijn. Als gevolg daarvan is er slechts beperkt inzicht in de geometrie van vroeg-Archeïsche sedimentaire bekkens en de omstandigheden waaronder deze bekkens werden gevormd en gevuld.

Deze studie heeft tot doel om beter inzicht te krijgen in de geometrie van vroeg-Archeïsche bekkens en eventuele syndepositionele deformatie (deformatie tijdens de afzetting). Syndepositionele, extensionele (rek) deformatie is beschreven voor de Coongan Groensteengordel (Pilbara, Australië) door Zegers et al. (1996), voor het North Pole Dome gebied (Pilbara) door Nijman et al. (1998a) en voor de Barberton Groensteengordel (Zuid-Afrika) door De Vries (1999). In deze studie wordt onderzocht hoe wijd verbreid deze extensionele structurele controle was. Ook wordt beoogd beter inzicht te krijgen in de sedimentologische en diagenetische processen in vroeg-Archeïsche sedimentaire bekkens, evenals in de locatie van hydrothermale systemen binnen deze bekkens. De hydrothermale systemen en hun effecten op de sedimenten en temperatuurverdeling in de bekkens zijn met name van belang in relatie tot de ontwikkeling van het leven op Aarde.

In deze studie is gekozen voor een multidisciplinaire aanpak, waarbij de nadruk ligt op het relateren van informatie op basis van verschillende disciplines. Grootschalige kartering, waarin sedimentaire, structurele en vulkanische data worden gecombineerd, is aangevuld met gedetailleerde (10-100 meter schaal) kartering, de opname van gedetailleerde sedimentaire secties, geochemie en geochronologie (ouderdomsbepaling).

Uiteindelijk leidt een dergelijke geïntegreerde studie naar verwachting niet alleen tot conclusies met betrekking tot de schaal, vorm en omgeving van de bekkens, maar de conclusies kunnen ook inzicht geven in bijvoorbeeld plaattektoniek en lithosfeer/korst ontwikkeling van de vroege Aarde. De vorm en vulling van sedimentaire bekkens kan bijvoorbeeld informatie geven over het tektonische regime waaronder deze bekkens werden gevormd. De aard van het tektonische regime is voor een groot deel van het Archeïcum nog steeds controversieel (zie bijvoorbeeld De Wit, 1998; Hamilton, 1998; Hofmann et al., 2001; Van Kranendonk et al., 2002 en daarin genoemde referenties).

De studiegebieden

Oost-Pilbara

Het Pilbara Graniet-Groensteengebied is ontsloten over een oppervlakte van ca 480 bij 230 km in het noorden van West-Australië. Het heeft een ouderdom van ca 3,72-2,85 miljard jaar. Het meest oostelijke deel van de Pilbara, het Oost-Pilbara Graniet-Groensteengebied is het oudst en bestaat uit gesteenten met een ouderdom van meer dan 3,3 miljard jaar. Het gebied wordt gekenmerkt door grote, ovaalvormige granitoïd complexen die worden omgeven door flauw tot steil hellende groensteengordels. De groensteengordels bestaan voornamelijk uit ultramafische en mafische gesteenten (basische gesteenten met < 53 gewichtsprocent SiO_2) en kleinere volumes intermediaire-felsische gesteenten (zure gesteenten met > 53 gewichtsprocent SiO_2) en sedimenten. De Coppin Gap Groensteengordel, tussen de Mt Edgar en Muccan Granitoïd Complexen, is gekozen als studiegebied. Het zuidelijke deel van deze groensteengordel vormt een goed bewaarde doorsnede door een stukje van de vroeg-Archeïsche korst. Het grootste gedeelte van de gesteenten in het studiegebied behoort tot de ca 3,49-3,31 miljard jaar oude Warrawoona Groep.

Barberton

De Barberton Graniet-Groensteengordel (Zuid-Afrika) is ontsloten in het oostelijke deel van het ca 1750 bij 1650 km grote Kaapvaal Kraton. De ca 3,5-3,1 miljard jaar oude Barberton Groensteengordel beslaat een oppervlakte van ongeveer 130 bij 70 km. De groensteengordel is dicht geplooid en wordt omgeven door trondhjemiet-tonaliet en granodioriet-intrusies. De groensteen-gordel bestaat uit twee verschillende delen, die rond 3,23 miljard jaar geleden in botsing kwamen. De delen worden nu gescheiden door het Saddleback-Inyoka breuksysteem (o.a. beschreven door De Ronde en Kamo, 2000). De gesteenten in de Barberton Groensteengordel worden verdeeld in drie groepen. Van oud naar jong zijn dit de Onverwacht, Fig Tree en Moodies Groepen. Het ca 3,45-3,42 miljard jaar oude studiegebied bevindt zich in het zuidelijke deel van de groensteengordel en maakt deel uit van de boven-Onverwacht Groep. Het bevat onder meer de Buck Ridge Chert, de dikste (ca 400 meter) sedimentaire opeenvolging in de Barberton Groensteengordel onder de midden-Archeïsche Fig Tree Groep.

De hoofdstukken van dit proefschrift

In Hoofdstuk 2 en 3 wordt de algemene geologie van de boven-Hooggenoeg Formatie in de Barberton Groensteengordel in Zuid-Afrika en van de Warrawoona Groep in Coppin Gap Groensteengordel in de Pilbara, Australië beschreven. Deze hoofdstukken vormen een raamwerk voor de studies aan het Buck Ridge vulkano-sedimentaire complex (**BR-vsc**, in de Barberton

Groensteengordel) en het Kittys Gap vulkano-sedimentaire complex (**KG-vsc**, in de Coppin Gap Groensteengordel) in Hoofdstuk 4 tot en met 6. De BR-vsc en de KG-vsc hebben een vergelijkbare algemene geologie en zijn ongeveer even oud (ca 3,45 miljard jaar).

Hoofdstuk 2

Het 3,45 – 3,42 miljard jaar oude BR-vsc maakt deel uit van de bovenste Hooggenoeg Formatie. Het complex werd afgezet in een extensioneel regime, wat heeft geresulteerd in grootschalige, syndepositionele afschuivingsbreuken die het complex doorsnijden. De BR-vsc is een bimodaal vulkanisch complex dat voornamelijk bestaat uit massieve en kussenbasalten en felsische, kwarts-plagioklaas porfierische gesteenten. De laatstgenoemde nemen in volume toe richting de top van het complex. De basalten en porfierische gesteenten worden afgedekt door felsische vulkaniklastische afzettingen en andere, voornamelijk gesilicificeerde sedimenten. Afzetting van deze vulkaniklastica en andere sedimenten vond plaats in ondiep water. De BR-vsc werd geïntrudeerd door ongeveer even oude, ondiepe felsische porfieren, die de breukvlakken van de afschuivingsbreuken verbergen. De extensie creëerde ook ruimte voor de intrusie van ongeveer loodrecht op de gelaagdheid staande felsische en mafische aders en zwarte chert(vuursteen)-aders. Observaties in het gebied onmiddellijk ten noorden van de BR-vsc suggereren de aanwezigheid van een plooipatroon met ongeveer noordwest-zuidoost strekkende plooiassen. Uraan-lood datering van een felsisch gesteente uit dit gebied toont aan dat dit gesteente ongeveer even oud is als de felsisch-vulkanische gesteenten in de BR-vsc. Dit impliceert dat de plooiing heeft geleid tot verdubbeling van de BR-vsc, of delen daarvan, en dat het gebied ten noorden van de Buck Ridge niet uitsluitend jonger is dan de BR-vsc, zoals tot nu toe werd gedacht.

Hoofdstuk 3

In Hoofdstuk 3 ligt de nadruk op de vroegste fase van deformatie en de stratigrafische continuïteit van de Warrawoona Groep in de Coppin Gap Groensteengordel. In deze groensteengordel bestaat de Warrawoona Groep uit ultramafische, mafische, intermediaire en felsische gesteenten en in mindere mate uit gelaagde ijzerrijke afzettingen (zgn. 'banded iron formations') en gesilicificeerde sedimenten. Een groot deel van de gesteenteopeenvolging bestaat uit felsisch-vulkanische gesteenten van de Duffer en Panorama Formaties. De gesteenten vormen op geen enkele plaats in het studiegebied een continue stratigrafische opeenvolging. In plaats daarvan bestaat de Warrawoona Groep uit delen stratigrafie die worden begrensd door deformatiezones (meestal schuifzones). Ondanks de aanwezigheid van zulke zones, tonen nieuwe uraan-lood zirkoon dateringen aan dat de chronostratigrafische opeenvolging in de Coppin Gap Groensteengordel niet fundamenteel is verstoord. De precisie van de uraan-lood dateringen is echter onvoldoende om kleine hiaten of verdubbelingen in de stratigrafische opeenvolging, in de orde van een paar miljoen jaar, uit te sluiten.

De Coppin Gap Groensteengordel wordt doorsneden door een aantal afschuivingsbreuken, waarbij het westelijke blok naar beneden is gezakt. Ze komen voor op de schaal van de hele groensteengordel en op kleinere schaal als aparte series in verschillende niveaus in de Warrawoona Groep. Een gedeelte van deze series met afschuivingsbreuken was syndepositioneel. Vroege inzakking onder invloed van de zwaartekracht van een groot deel van de Duffer Formatie in het studiegebied suggereert ook gravitatief transport waarbij het bovenblok naar het westen bewoog. Syndepositionele extensie van Warrawoona Group afzettingen vond plaats in de hele Oost-Pilbara en wordt daarom

geïnterpreteerd als het dominante tektonische regime in die periode. De extensie in de Coppin Gap Groensteengordel had een consistente west-blok-naar-beneden oriëntatie gedurende een periode van minstens 20 miljoen jaar.

Hoofdstuk 4

Aan de top van zowel de BR-vsc in de Barberton Groensteengordel als de KG-vsc in de Coppin Gap Groensteengordel werden sedimenten afgezet. Deze sedimenten zijn bestudeerd door middel van een combinatie van kartering en de opname van gedetailleerde sedimentaire secties. De afzetting van de sedimenten in beide complexen werd beïnvloed door de activiteit van afschuivingsbreuken. Beide sedimentaire opeenvolgingen ondergingen vrijwel volledige, vroeg-diagenetische silicificatie, hetgeen op veel plaatsen heeft geleid tot een excellente preservatie van sedimentaire structuren, terwijl het op andere plaatsen heeft geresulteerd in complicatie en verlies van de sedimentaire texturen en structuren. De sedimenten in beide complexen bestaan uit vulkanisch afbraakmateriaal van lokale herkomst. Er zijn geen aanwijzingen voor de grootschalige afbraak van (onderliggende) oudere gesteenten of voor lange-afstand transport van het afbraakmateriaal. Ondanks de overeenkomsten in de geologie en de ouderdom van beide complexen zijn er kleine verschillen in de sedimentaire opeenvolging tussen beide gebieden. De sedimenten van de BR-vsc laten een regressieve-transgressieve opeenvolging zien, die werd gevormd in de buurt van het nulniveau ('zeeniveau') en zo af en toe boven water kwam. De sedimenten van de KG-vsc zijn voornamelijk gerecycled en werden onder water afgezet, eveneens in de buurt van het nulniveau. De sedimenten van de KG-vsc werden mogelijk afgezet onder invloed van getijdenwerking.

Hoofdstuk 5

In Hoofdstuk 5 worden de veldrelaties tussen breuken, aders en breccies in de felsisch-vulkanische afzettingen en bovenliggende sedimenten van de BR-vsc en de KG-vsc in detail beschreven. Dit heeft tot doel inzicht te geven in de algemene geologie van vroeg-Archeïsche hydrothermale systemen en om de geometrie van dergelijke systemen en de locaties waar deze systemen aan de oppervlakte exhaleerden te reconstrueren. In beide complexen komen meters-brede chert(vuursteen)-aders voor in de top van de vulkanische opeenvolging, dicht onder de sedimenten. De aders komen vooral voor in de omgeving van de syndepositionele afschuivingsbreuken. Ze worden geïnterpreteerd als overblijfselen van vroeg-Archeïsche hydrothermale systemen. De hydrothermale systemen waren actief gedurende of kort na afzetting van de sedimenten en veroorzaakten vroege en multi-fase silicificatie, veradering en brecciëring van de sedimenten. De hydrothermale systemen van de BR-vsc en KG-vsc kwamen aan de oppervlakte in ondiep water, rond het nulniveau. Ze werden niet gevormd in een diepzeemilieu of in de omgeving van een midden-oceanische rug, zoals is gesuggereerd voor sommige andere vroeg- tot midden-Archeïsche hydrothermale systemen.

Hoofdstuk 6

Kwartskristallen in (i.) het cement van breccies, in (ii.) aan de gelaagdheid gebonden netwerken van centimeter-schaal kwartsaders en in (iii.) holtevullingen onder gestapelde keien - drie typen structuren die in het vorige hoofdstuk werden geïnterpreteerd als gerelateerd aan hydrothermale activiteit - bevatten grote aantallen vloeistofinsluitseltjes. De insluitseltjes blijken te bestaan uit een twee fasen waterige vloeistof of uit een water-kooldioxide mengsel. De waterige insluitsels worden

verdeeld in drie verschillende groepen, op basis van hun micro-thermometrische karakteristieken. Type H_A (hoge saliniteit, hoge homogenisatie temperatuur), type M_A (gemiddelde saliniteit en homogenisatie temperatuur) en type L_A (lage saliniteit, uiteenlopende homogenisatie temperatuur). De vierde groep wordt gevormd door de water-kooldioxide insluitsels (type C). De optische en microthermometrische karakteristieken van deze insluitsels geven aan dat de vloeistof homogeen was op het moment dat deze werd ingesloten. Vloeistoftypen H_A en C waren niet mengbaar op het moment van insluiting. De minimum insluitingstemperatuur was ongeveer 150°C voor type H_A en minimaal 255°C voor type C insluitsels. Fase-relaties in het H_2O-CO_2 systeem voorspellen een bijbehorende druk van 2,2 kilobar. De ontmenging van de originele vloeistof in deze twee types hing mogelijk samen met de opening van de hydrothermale aders. Vloeistoftype M_A kan zijn ontstaan als gevolg van menging van vloeistoftype H_A met een vloeistof met een lagere saliniteit, bij een lagere temperatuur. Vloeistoftype L_A kan zijn gevormd uit een tweede ontmenging van vloeistoftype C.

Hoofdstuk 7

In Hoofdstuk 7 worden het mechanisme van bekkenvorming en de grootte en vorm van de bewaard gebleven ca. 3,5-3,4 miljard jaar oude bekkens behandeld, gebaseerd op de gegevens en conclusies uit de Barberton en Pilbara Groensteengordels in de voorgaande hoofdstukken. De bestudeerde vroeg-Archeïsche, door afschuivingsbreuken gecontroleerde, sedimentaire bekkens hadden een doorsnede van minimaal 30-140 km. Ze waren niet gerelateerd aan een lineair tektonisch regime en evenmin aan het omhoog komen van de granitoïd complexen zoals die voorkomen in de Pilbara. De bekkens hadden een voornamelijk vulkanische vulling, en de bekkenafzettingen werden beïnvloed door hydrothermale systemen die ontluchtten rond het nulniveau. Noch inslagstructuren van meteorieten, noch vulkanische structuren op de hedendaagse Aarde zijn echt te vergelijken met de vroeg-Archeïsche bekkenstructuren zoals deze bewaard zijn gebleven in de Barberton en Pilbara Groensteengordels. Wel zijn deze bekkens in een aantal opzichten vergelijkbaar met bijvoorbeeld de grootste caldera-structuren op Aarde, en met vulkanen in 'back-arc' gebieden. Mogelijk waren het geodynamische regime van de vroege Aarde en/of de vroeg-Archeïsche korst dusdanig verschillend dat er destijds een ander type vulkanisme-gerelateerde bekkens werd gevormd. Mars en Venus laten zien wat voor bekkens kunnen worden gevormd wanneer plaattektoniek afwezig is. Met name de corona-structuren op Venus zijn in een aantal opzichten vergelijkbaar met de vroeg-Archeïsche bekkenstructuren in de Barberton en Pilbara Groensteengordels. Door het ontbreken van gedetailleerde gegevens over de structuren op Mars en Venus blijft de vergelijking met zulke structuren vooralsnog oppervlakkig.

Dankwoord (Acknowledgements)

Velen hebben op één of andere manier bijgedragen aan de totstandkoming van dit proefschrift. Allereerst bedank ik mijn begeleider Wout Nijman en mijn promotoren Poppe de Boer en Maarten de Wit. Gedurende mijn promotietijd waren zij op verschillende manieren betrokken bij het onderzoek. Als initiatiefnemer van het project Earth's Earliest Sedimentary Basins, waar dit promotie onderzoek deel van uitmaakte, en daarna als 'dagelijks' begeleider, was de rol van Wout Nijman in dit onderzoek het grootst. Wout was altijd een gedeelte van de tijd aanwezig bij de veldwerken, waar ik zijn ruime veldervaring in het algemeen en met het Archeïcum van de Oost-Pilbara in het bijzonder, als zeer waardevol heb ervaren. Poppe de Boer ging ook twee keer mee op veldwerk en was afgezien daarvan altijd betrokken bij dit onderzoek vanuit Utrecht. Maarten de Wit was medeinitiatiefnemer van het project Earth's Earliest Sedimentary Basins. Op zijn uitnodiging werd ook de Barberton Groensteengordel in Zuid-Afrika in het Archeïcum onderzoek vanuit de Universiteit Utrecht betrokken. Ik dank hen alle drie voor hun kritische commentaren op eerdere versies van dit proefschrift, die hebben geleid tot een belangrijke verbetering van het manuscript. Voor afzonderlijke onderdelen van het proefschrift was de begeleiding van Manfred van Bergen (met betrekking tot de vulkanologie en de geochemie) en Jacques Touret (op het gebied van de vloeistofinsluitsels) erg waardevol.

Direct betrokken bij het onderzoek waren ook de studenten die mee gingen op veldwerk. Sommigen als veldassistent, anderen om een eigen (deel)onderzoek te doen. In chronologische volgorde waren dit Onno Houtzager, Ivo Vos, Juliette van der Meer, Karin Louzada, Tjirk Benedictus en Sander van der Boorn. Karin Louzada ging zelfs drie keer mee, twee keer naar Australië en één keer naar Zuid-Afrika. Bedankt allemaal voor jullie bijdragen aan het onderzoek en natuurlijk voor de gezelligheid tijdens de veldwerken!

Ik heb veel geleerd van de discussies met leden van de Old Rock Literature Club (ORLC), een initiatief van Tanja Zegers. Zij hebben mijn kennis over het Archeïcum en de geologie in het algemeen enorm verbreed.

My thesis also benefited from discussions with collegues from outside Utrecht University during fieldworks and excursions, conferences, workshops, and visits to other institutes. I would like to thank Cornel de Ronde for his hospitality and his advice in the initial stages of my thesis, during my visit to the Institute of Geological and Nuclear Sciences in New Zealand. I thank Frances Westall for introducing me in the topic of early life on Earth, and for giving me the opportunity to visit NASA / the Lunar and Planetary Institute in Houston and to attend the workshop on Early Earth and Early Life in Les Treilles, France. I would like to thank Dave Nelson for his efforts to provide me with time on the SHRIMP at Curtin University of Technology in Perth, Australia, and for his help and advice during my three-week visit in September 2002. I am grateful to Richard Armstrong for the very efficient way in which we could do the sample preparation and dating of my samples from the Barberton Greenstone Belt at the Australian National University in Canberra, Australia.

I would like to thank the members of the dissertation committee: Cornel de Ronde, Jan Smit, Jacques Touret, Frances Westall and Bert van der Zwaan for reading the manuscript and for their suggestions that helped to improve this thesis.

Op de Faculteit / het Departement Aardwetenschappen in Utrecht bedank ik de medewerkers van de ondersteunende diensten, waaronder de laboranten van de projectgroep Sedimentologie, de slijpkamer en de audio-visuele dienst, voor hun hulp bij het werk voor dit proefschrift.

Daarnaast bedank ik mijn oud-kamergenoten, de leden van de projectgroep Sedimentologie, collega-promovendi en postdocs bij Aardwetenschappen en bij de overkoepelende promovendi-organisatie van de Universiteit Utrecht. Zij allen zorgden ervoor dat mijn promotietijd in Utrecht niet alleen leerzaam, maar vooral ook gezellig was. Mijn vriendinnen, vrienden, familieleden en 'schoon'-familieleden bedank ik voor hun belangstelling voor mijn werk en de onmisbare afleiding daarvan.

Ten slotte ben ik Auke enorm dankbaar voor al zijn praktische en vooral ook mentale steun gedurende de afgelopen vijf jaar.

Curriculum Vitae

Sjoukje Tsjitske de Vries werd geboren op 31 oktober 1975 in Leeuwarden. Na in 1988-1989 een jaar op het Stedelijk Gymnasium in Leeuwarden te hebben gezeten, verhuisde zij met haar ouders naar Texel. Daar doorliep zij van 1989-1994 het VWO op Scholengemeenschap De Hoge Berg in Den Burg. In september 1994 begon zij met de studie Geologie aan de Universiteit Utrecht. Tijdens haar specialisatie in de richting Structurele Geologie / Tektoniek liep zij stage bij Shell International Exploration and Production in Rijswijk en deed zij veldwerk in West-Australië en Zuid-Afrika. In 1999 behaalde zij het doctoraal diploma met het judicium cum laude. In augustus 1999 begon zij aan dezelfde universiteit met haar promotie, waarvan de resultaten in dit proefschrift worden beschreven.

Sjoukje Tsjitske de Vries was born on 31 October 1975 in Leeuwarden, The Netherlands. She received her secondary education in Leeuwarden and Den Burg. After one year at the Stedelijk Gymnasium in Leeuwarden in 1988-1989, her parents and she moved to the island of Texel. There she attended the Scholengemeenshap De Hoge Berg in Den Burg, from which she graduated in 1994. From September 1994 on she studied Geology at Utrecht University in the Netherlands. During her studies, she did an internship with Shell International Exploration and Production in Rijswijk, and went on fieldwork to Western Australia and South Africa. Specialising in Structural Geology and Tectonics, she graduated cum laude (with the highest distinction) in 1999. Immediately after that, she started her PhD study at the same university. The results of that study have been described in this thesis.